Chemoselective conjugation of biological active peptides to functional scaffolds

Dissertation

zur Erlangung des akademischen Grades

doctor rerum naturalium (Dr. rer. nat)

im Fach: Chemie

Spezialisierung: Organische und Bioorganische Chemie

eingereicht an der

Mathematisch-Naturwissenschaftlichen Fakultät der Humboldt-Universität zu Berlin

von

M. Sc. Maria Glanz

Präsidentin der Humboldt-Universität zu Berlin

Prof. Dr.-Ing. Dr. Sabine Kunst

Dekan der Mathematischen-Naturwissenschaftlichen Fakultät

Prof. Dr. Elmar Kulke

Berlin, Januar 2019

Gutachter:

1. Prof. Dr. Christian P. R. Hackenberger
2. Prof. Dr. Hans Börner
3. Prof. Dr. Nediljko Budisa

Tag der mündlichen Prüfung: 03.07.2019

Diese Arbeit wurde im Zeitraum vom 01.12.2013 zum 30.06.2018 unter der Leitung von Prof. Dr. Christian P.R. Hackenberger am Leibniz-Forschungsinstitut für Molekulare Pharmakologie angefertigt.

1. Gutachter: Prof. Dr. Christian P. R. Hackenberger
Chemische Biologie II
Leibniz-Forschungsinstitut für Molekulare Pharmakologie, Berlin

2. Gutachter: Prof. Dr. Hans Börner
Institut für Chemie
Humboldt-Universität zu Berlin

3. Gutachter: Prof. Dr. Nediljko Budisa
Institut für Chemie
Technische Universität Berlin

Declaration

I hereby declare, that I have completed the thesis independently using only the aids and tools specified. I have not applied for a doctors's degree in the doctoral subject elsewhere and do not hold a corresponding doctor's degree. I have take due note of the Faculty of Mathematics and Natural Sciences PhD Regulations, published in the Official Gazette of Humboldt-University zu Berlin no. 42 on July 11 2018.
Berlin,

Maria Glanz

Hiermit erkläre ich, die Dissertation selbstständig und nur unter Verwendung der angegebenen Hilfen und Hilfsmittel angefertigt zu haben. Ich habe mich nicht anderwärts um einen Doktorgrad in dem Promotionsfach beworben und besitze keinen entsprechenden Doktorgrad. Die Promotionsordnung der Mathematisch-Naturwissenschaftlichen Fakultät, veröffentlicht im Amtlichen Mitteilungsblatt der Humboldt-Universität zu Berlin Nr. 42 am 11.Juli 2018, habe ich zur Kenntnis genommen.
Berlin,

Maria Glanz

This dissertation resulted so far in the following publication, patent, posters and talks.

Publication

Daniel Lauster*, Maria Glanz*, Markus Bardua, Kai Ludwig, Markus Hellmund, Ute Hoffmann, Alf Hamann, Christoph Böttcher, Rainer Haag, Christian P.R. Hackenberger

*shared contribution

Angew. Chem. Int. Ed. **2017**, *56,* 5931 – 5936.

Multivalent Peptide-Nanoparticle Conjugates for Influenza-Virus Inhibition.

Angew. Chem. **2017**, *129*, 6025-6030. (deutsche Version)

Multivalente Peptid-Nanopartikel-Konjugate zur Hemmung des Influenzavirus

Patent

Marc-André Kasper, Maria Glanz, D. Schumacher, T. Sauer, C.P.R. Hackenberger

EP 16001917.0 , 09/2016

Chemoselective thiol-conjugation with alkene or alkyne-phosphonamidates

Posters

1) Maria Glanz, Daniel Lauster, Nina Bohlke, Markus Hellmund, Rainer Haag, Nediljko Budisa, Andreas Hermann, Christian P.R. Hackenberger

3rd International SFB 765 - Symposium, 23. - 24.10.2014 Berlin

„Multivalent Peptide-Conjugates for viral interaction“

2) Maria Glanz, Daniel Lauster, Markus Hellmund, Kai Ludwig, Christoph Böttcher, Rainer Haag, Andreas Herrmann, Christian P.R. Hackenberger

10th Status Seminar Chemical Biology, 20. - 21.01. 2015 Frankfurt /M.

„Multivalent peptide-conjugates to address viral interactions“

*poster selected for speed lecture

3) Simon Klenk*, Maria Glanz*, Saba Nojoumi, Daniel Lauster, Sandra Behren, Andreas Herrmann, Nediljko Budisa, Christian P. R. Hackenberger
ECBS & ICBS Joint Meeting 2015, 07. - 09. 10. 2015 Berlin
„Multivalent peptide- and protein-based scaffolds for inhibition of influenza virus binding to host cells“
**shared contribution*

4) Maria Glanz, Daniel Lauster, Markus Hellmund, Kai Ludwig, Christoph Böttcher, Rainer Haag, Andreas Herrmann, Christian P.R. Hackenberger
34th European Peptide Symposium, 04. - 09. 2016 Leipzig
„Multivalent Peptide-Polymer-conjugates to adress viral interactions“

5) Maria Glanz, Daniel Lauster, Markus Bardua, Markus Hellmund, Kai Ludwig, Ute Hoffmann, Alf Hamann, Christoph Böttcher, Rainer Haag, Andreas Herrmann, Christian P. R. Hackenberger
International Symposium on functional Biointerfaces, 04.10.2016 - 05.10.2016
„Multivalent Peptide-Conjugates to address viral interaction“

6) Maria Glanz, Marc-André Kasper, Jordi Bertran-Vicente, Christian P. R. Hackenberger
7th Chemical Protein Synthesis Meeting, 04. - 07.09.2017 Haifa, Israel
„Development of New Cysteine-Selective Bioconjugation Methods Based on Electrophilic Phosphorous(V) Compounds“

7) Maria Glanz*, Simon Klenk*, Daniel Lauster, Saba Nojoumi, Sandra Behren, Kai Ludwig, Christoph Böttcher, Rainer Haag, Nediljko Budisa, Andreas Herrmann, Christian P. R. Hackenberger
GDCh-Wissenschaftsforum Chemie 2017, 14.09. 2017
„Multivalent peptide- and protein-based scaffolds for inhibition of influenza virus binding to host cells“
*shared contribution

8) Maria Glanz*, Simon Klenk*, Daniel Lauster, Saba Nojoumi, Sandra Behren, Kai Ludwig, Christoph Böttcher, Rainer Haag, Nediljko Budisa, Andreas Herrmann, Christian P. R. Hackenberger

4th International SFB 765 – Symposium, 04. - 06.10.2014 Berlin

„Multivalent peptide- and protein-based scaffolds for inhibition of influenza virus binding to host cells“

*shared contribution

Talks

Maria Glanz, Daniel Lauster, Markus Hellmund, Kai Ludwig, Christoph Böttcher, Rainer Haag, Andreas Herrmann, Christian P.R. Hackenberger

10th Status Seminar Chemical Biology, 20. - 21.01. 2015 Frankfurt /M. – Speed lecture

„Multivalent peptide-conjugates to address viral interactions“

Maria Glanz*, Simon Klenk*, Christian P.R. Hackenberger

SFB765 „Disziplinforum“, 13.10.2016

„Protein Conjugations: A versatile tool for Chemical Biology Research“

*shared contribution

Acknowledgements

First, I would like to thank my supervisor Prof. Dr. Christian Hackenberger for the opportunity to carry out my PhD work in the highly interesting and interdisciplinary field of chemical biology. I highly appreciated his support and the freedom that was given to me in exploring diverse techniques and aspects connected to this field.

I also would like to thank Prof. Dr. Hans Börner and Prof. Dr. Nediljko Budisa for taking the time and interest to review this thesis.

I am very thankful to the great scientist I was able to work with over the years and who made working on mostly interdisciplinary projects possible. In this context special thanks go to Daniel Lauster, Kalie Mix, Kai Licha, Andreas Oder and Henry D. Herce.

Also I want to acknowledge the FMP as work place as such, giving me the best resources for conducting my work and also all the knowledgeable advisees at the FMP helping me to understand numerous techniques and taking care of all the equipment. In names this would be, Dagmar Krause, Ines Kretzschmar, Heike Nikolenko, Oxana Krylova, Martin Lehmann, Jenny Eichhorst, Peter Schmieder, Brigitte Schlegel, Eberhard Krause, Heike Stephanowitz and Burkhard Wiesner.

Special thanks go to the former and current members of the Hackenberger Lab. It was great working and spending time with you all. Thanks you so much Olaia Nieto-Garcia, Jordi Bertran-Vicente, Debasish Bhowmick, Andrew Grimes, Paul Majkut, Robert Vallee, Simon Reiske, Tom Sauer, Lukas Artner, Divya Agrawal, Vera Martos, Alec Michels, Lutz Adam, Phillip Ochtrop, Antoine Wallabreque, Nicole Nischan, Wenyi Li, Dominik Schumacher, Sergej Schwagerus, Marianne Dreißigacker, Katrin Wittig, Kristin Kemnitz-Hassanin, Anett Hauser and Anselm Schneider
Thanks for all the Christmas dinners and advice to Michaela Mühlberg. Thank you for the best conference trip to Israel and the always kind words Alice Baumann.
Thank you Oliver Reimann for introducing me to all the peptide-synthesis basics during the internship that made me come back to the Hackenberger lab. Thank you Marc-André Kasper and Simon Klenk for being amazing office mates and making the days there so much fun. A huge thank you goes to Kristina Siebertz for all the time shared in our small lab and the office, the proof reading of the thesis and sharing the first day at the FMP together. Also thank you Karolina Walker for making study chemistry much more fun.

I would also like to thank all the people outside chemical biology. Especially Jackie, Malte, Barry, Caro, Luise, Josef, Theresa, Lisbeth, Claudia, Dirq, Heike, Astrid, Basti, Milla, Nina and of course my whole family.

The biggest of all thank you’s goes to Robert Hillebrand.

1 Table of Contents

2 Abbreviations

ADC	antibody-drug-conjugates
AU	absorbance unit
CD	circular dichroism
cDNA	complementary deoxyribonucleic acid
CDR	complementary determining region
CPP	cell penetrating peptide
cCPP	cyclic cell penetrating peptides
CuAAC	cupper catalyzed alkyne azide cycloaddition
Cy3	cyanine 3
DCM	dichloromethane
DIPEA	*N,N*-diisopropylethylamine
DMEM	Dulbecco modified eagle medium
DMF	dimethylforamide
DMSO	dimethylsulfoxide
dNTP	deoxynucleoside triphosphate
DTT	dithiotreitol
eGFP	enhanced green fluorescent protein
FACS	fluorescence activated cell sorting
Fmoc-	fluorenylmethyloxycarbonyl
FRET	Förster resonance energy transfer
GST	glutathione-S-transferase
HA	hemagglutinin
HATU	1-[Bis(dimethylamino)methylene]-1H-1,2,3-triazolo[4,5-b]pyridinium 3-oxid hexafluorophosphate
HEPES	4-(2-hydroxyethyl)-1-piperazineethanesulfonic acid
HIV	human immunodeficiency virus
HPLC	high performance liquid chromatography
HRMS	high resolution mass spectrometry
HTRF	homogeneous time resolved fluorescence
IC_{50}	inhibitory concentration
IEDDA	inverse electron demand diels-alder
kDa	kilodalton
LRMS	low resolution mass spectrometry

Abbreviations

m/z	mass over charge
MALDI-TOF	matrix assisted laser
MeCN	acetonitrile
MesNa	methanethiolate
mRNA	messenger ribonucleic acid
MWCO	mass weight cut off
NHS	*N*-hydroxysuccinimide
Ni-NTA	nickel – nitrilotriacetic acid
NMM	*N*-methylmorpholine
OD_{600}	optical density at 600 nm
PBS	phosphate bufferes saline
PCR	polymerase chain reaction
PEG	polyethylene glycol
PG	protecting group
PLI	protein – ligand interaction
PPI	protein – protein interaction
PTM	posttranslational modification
quant.	quantitative
RCM	ring closing metathesis
RP	reverse phase
SA	sialic acid
SDS	sodium dodecyl sulfate
SEC	size exclusion chromatography
shRNA	short hairpin ribonucleic acid
SPAAC	strain – promoted alkyne azide cycloaddition
SPANC	strain – promoted azide nitrone cycloaddition
SPPS	solid phase peptide synthesis
TAMRA	Carboxytetramethylrhodamine
TFA	trifluoroacetic acid
THF	tetrahydrofurane
TIS	triisopropylsilane
UPLC	ultra performance liquid chromatography

3 Abstract

3.1 English

Synthetic peptides are a unique and versatile class of biomolecules. Due to their complex structure they can bind targets in a highly specific manner and furthermore exhibit unique biological active properties. Even though they are complex in structure, they are straightforward synthetically accessible, due to many advances made in the field of peptide synthesis throughout the last decades. Concerning functional peptides the discovery of cell penetrating peptide (CPP) sequences derived from full-length proteins highlighted the great potential to transfer peptidic properties to any cargo by using bioconjugation methods that can link both entities. This thesis evolves around the many different aspects, in which biological active peptides can be used, from specific binders to cell penetration tags. Furthermore, the site specific and chemoselective conjugation of an unprotected peptide to a functional scaffold has been addressed throughout this thesis.

In the first project the synthesis of a peptide – polymer – nanoparticle was shown to yield a highly potent virus entry blocker. Here, a viral-membrane-protein binding peptide was displayed multiply on a polymeric nanoparticle *via* a chemoselective reaction, upon which its binding affinity and therefore antiviral activity could be enhanced drastically throughout the multivalent effect. This project highlighted the synthesis of a highly potent and target-specific inhibitor by the use of bioactive peptides and their convenient synthesis.

In the second project the conjugation of unprotected peptides to a functional scaffold was addressed. Here a novel bioconjugation technique was developed for the covalent linkage between an unprotected azido-containing peptide and a thiol-bearing biomolecule. The connecting linker herein used, was an alkyne-phosphonite, which proofed to be highly versatile. The electron rich alkyne-phosphonite was first reacted in a Staudinger phosphonite reaction with the unprotected azido-peptide yielding an alkyne-phosphonamidate-peptide. In this phosphonamidate the alkyne is turned to be electron poor, making a selective thiol addition to the alkyne possible. This reaction cascade was probed for tagging eGFP with cyclic cell penetrating peptides (cCPP) and their *in vitro* application in HeLa cells was assessed. Here, we could verify that upon covalent conjugation of eGFP with the peptidic tag *via* this new bioconjugation technique, the full-length eGFP protein was rapidly transduced into the cytosol of cells.

This novel Staudinger induced thiol addition reaction was further used in a third project, in which a certain biologic function was induced by macrocyclizing synthetic peptides intramolecularly. Here CPPs were macrocyclized by conjugating azido and sulfhydryl functionality in the peptide structure throughout an alkene-phosphonite. Thereby, the

remarkable transduction properties of cCPPs were induced and could be verified by *in vitro* studies. In the same fashion a peptide taken out of a protein structure was stabilized in its native α-helix, upon which the peptide is able to pose as remarkable protein-protein-interaction (PPI) inhibitor.

In the fourth project a different chemoselective reaction was explored to conjugate cCPPs to eGFP. Here carboxylic acids in the protein structure were esterified successfully utilizing a diazo moiety, which was either directly incorporated into the cCPP or the cCPP was conjugated to an alkyne-diazo tag, post-esterification on protein level. The ester linkage was hypothesized to be cleaved inside cells upon cellular transduction to give the native protein, but unfortunately this could not be quantified or verified, due to an inherent toxicity observed for the conjugation product when applied on HeLa cells.

3.2 Deutsch

Synthetische Peptide bilden eine einzigartige und vielseitige Klasse von Biomolekülen. Aufgrund ihrer komplexen Struktur sind sie in der Lage hochspezifisch an Zielmoleküle zu binden und können darüber hinaus biologisch aktive Eigenschaften aufweisen. Obwohl sie in ihrer Struktur komplex sind, können sie durch die Fortschritte, die auf dem Gebiet der Peptidsynthese in den letzten Jahrzehnten erzielt wurden einfach synthetisiert werden. Im Bezug auf biologisch aktive Peptide zeigte zum Beispiel die Entdeckung von zellpenetrierenden Peptidsequenzen, die aus nativen Proteinen abgeleitet wurden, dass bestimmte Proteineigenschaften in ihrer reduzierten peptidischen Struktur, durch die Verwendung von Biokonjugationsverfahren auf Cargos übertragen werden können. In dieser Dissertation wurden verschiedenen Anwendungen, für die biologisch aktive Peptide verwendet werden können, zum Beispiel in Form spezifischer Binder bis hin zu zellulären Aufnahme-Markern untersucht. In Zuge dessen wurde in dieser Arbeit die ortsspezifische und chemoselektive Konjugation ungeschützter Peptide an funktionelle Gerüstmoleküle betrachtet.

Im ersten Projekt wurde gezeigt, dass multivalente Peptid – Polymer – Nanopartikel synthetisiert und als hochpotente Viruseintrittsblocker eingesetzt werden können. Ein Virus-Membranprotein bindendes Peptid wurde durch eine chemoselektive Reaktion multivalent an einen polymeren Nanopartikel konjugiert. Dadurch konnten dessen Bindungsaffinität und damit auch das antivirale Potential über einen multivalenten Effekt drastisch gesteigert werden. Dieses Projekt zeigt die erfolgreiche Synthese eines hochpotenten Virus-Inhibitors auf Grundlage eines spezifisch bindenden Peptids welches einfach und schnell synthetisiert werden kann.

Im zweiten Projekt wurde eine Methode zur Konjugation eines ungeschützten Peptids an ein funktionelles Protein untersucht. Konkret wurde eine neuartige Biokonjugationstechnik für die Konjugation zwischen einem ungeschützten Azido-Peptid und einem Thiol-tragenden Biomolekül entwickelt. Der hier verwendete Linker ist ein Alkinphosphonit, welches sich als vielseitiges Molekül erwiesen hat. Das elektronenreiche Alkinphosphonit wurde zunächst in einer Staudinger-Phosphonit-Reaktion mit einem ungeschützten Azido-Peptid zu einem Alkin-Phosphonamidat-Peptid umgesetzt. Im entstandenen Phosphonamidat ist das Alkin elektronenarm und lässt so eine selektive Thioladdition zu. Diese Reaktionskaskade wurde zur Markierung von eGFP mit zyklischen zellpenetrierenden Peptiden (cCPP) verwendet. Die cCPP vermittelte Transduktion des markierten eGFP konnte anschließend in HeLa-Zellen beobachtet werden.

Die Staudinger-induzierte Thiol Additionsreaktion wurde in einem dritten Projekt als intramolekulare Makrozyklisierungsstrategie angewendet. Durch die intramolekulare Verbrückung einer Peptidstruktur, sollte eine biologische Funktion im Peptid erzeugt werden. Konkret wurde ein CPP durch Konjugation von Azido- und Sulfhydrylfunktionen in der Peptid Struktur makrozyklisiert, wodurch die Transduktionseigenschaften des CPP verstärkt und auch in *in-vitro* Studien verifiziert werden konnten. Auf die gleiche Weise konnte ein kurzes Peptid, das aus einer Proteinstruktur abgeleitet wurde in seiner nativen α-Helix, stabilisiert werden und somit als Protein-Protein-Interaktion (PPI) Inhibitor fungieren.
Im vierten Projekt wurde eine weitere chemoselektive Reaktion angewendet, um cCPPs an eGFP zu konjugieren. Hierbei konnten Carbonsäuren in der Proteinstruktur erfolgreich mit einer Diazoeinheit verestert werden. Die Diazogruppe wurde entweder direkt in die cCPP Struktur integriert oder als Alkin-Diazo-Linker mit dem eGFP verestert, sodass anschließend ein Azido-cCPP über CuAAC an diesen Alkinlinker im Protein konjugiert werden konnte.
Die Grundidee war, dass die Esterbindung nach der Transduktion im Cytosol durch Esterasen gespalten und so das native Protein nach der Aufnahme in der Zelle vorliegt. Auf Grund der inhärenten Toxizität gegenüber HeLa Zellen, die für diese Konjugationsprodukte beobachtet wurden, konnte dies jedoch weder verifiziert noch quantifiziert werden.

4 Introduction

4.1 Motivation

Proteins are the main players in biological processes and are covering a huge number of different functions inside and outside cells.[1] There are structural proteins, maintaining cell shape and composing structural elements in connecting tissues. Enzymes catalyze chemical reactions and further play an essential role in signal transduction and cell regulation.[2] Proteins are also involved in metabolic pathways and the regulation of disease processes. Furthermore cell signaling is controlled e.g. by proteins in form of receptors, ion channels or anchoring structures on cellular membranes. Proteins can also accomplish transportation of certain molecules and are even moving along surfaces.

The underlying main characteristic of their numerous functions is their ability to bind in a specific and highly affine manner to other proteins, biomolecules or even small molecules.[3] The recognition of its binding partner is a result of the protein structure itself. The diversity of the different amino acid side chain functionalities are resulting in hydrogen binding, electrostatic and hydrophobic interaction, which form the protein's 3D structural features that allow for a precise recognition of two binding partners like lock and key. Because they are involved in these many regulatory processes, the structural features of protein-protein interaction (PPI) and protein-ligand interaction (PLI) sites are highly interesting to researchers. Understanding the binding or function in structural detail allows the remodeling and usage of those core motifs as diagnostic and therapeutic tools. The reduction of a protein to its short bioactive peptide motif is furthermore the underlying rational of many peptide therapeutics that are chemically complex but still synthetic well reachable active compounds.[4,5]

The chemical complexity of peptide therapeutics has the advantage of preserving the specific recognition and its synthesis works *via* well-established protocols.[6] Further modification though comes with challenges. To label or modulate proteins and bioactive peptides in order to use them as tools in research, diagnostic settings or therapies, one encounters challenging chemical endeavors that formed the field of chemical biology. Here, chemoselective reactions have been developed that are fast and can be carried out in presence of all other naturally occurring functionalities in an aqueous environment at ambient temperatures.[7]

This thesis evolves around the development of a chemoselective reaction that allows the connection of a bioactive peptide to a protein as well as the modulation of a bioactive peptide structure derived from a proteins core binding motif. Further it is shown how the specificity of a bioactive peptide can be used for the inhibition of viral infections.

4.2 Bioactive peptides

Cellular processes are orchestrated through a dense network of proteins. They interact with ligands or other proteins and thereby regulate cellular function. This molecular machinery is build upon the specific recognition of a protein by its binding partner and the ability of them to discriminate between those. Interactions can either be transient or stable, but are usually highly specific and noncovalent. These binding characteristics can be recreated in short synthetic peptides. Once exhibiting distinct functions in a biological setting, inspired from their protein lead structure they are termed “bioactive peptides”.

4.2.1 Protein binding site mimicking peptides

Peptides are a special class of bioactive molecules, because they are neither small molecules nor big proteins but combine many advantageous characteristics of these two groups. They offer a high selectivity and potency for their destined target, similar to proteins, but their synthesis is more feasible, controllable and can be scaled up. In contrast to small molecules they have a predictable and natural metabolism, which makes them mostly well-tolerated *in vivo*.[4,5] The easy synthesis of peptides by solid phase supported standard protocols, allow introduction of unnatural amino acids, which can be used to incorporate a number of complex modifications by chemoselective reactions. Those reactions have been under intense investigation in recent years (see chapter 4.3).[7] They make it easy to mimic a structural element found in nature[8], modify the biomolecule of interest to the researchers need or apply it in a diagnostic or therapeutic set up in a variable manner. Still some drawbacks of bioactive peptides can be their rapid digestion by proteases and their fast elimination. Also the threat of an inherent immunogenicity is concerning when thinking of a therapeutic application. Still there are over 60 peptide drugs approved in the US and other major markets around the world with numerous being evaluated in clinical trials, because their advantages can often outweigh their drawbacks. Improvements on stability and half-life’s has been made over the years.[9] Peptide drugs are targeting receptors, enzymes and are also used to disrupt Protein-Protein-Interactions. Currently some of the most relevant peptidic drugs are used for treatment of osteoporosis (Teriparatide)[10], diabetes (Exenatide, Liraglutide)[11], growth disorder (Lanreotide), HIV (Enfuvirtid) and pain (Ziconotide)[12] with structures derived from native proteins.

Recent developments in the peptide therapeutic field are results of improved ways of target identification. For one, structural biology methods have rapidly improved over the last years giving rise to more structural insides into binding events of proteins and hence allow better

rational lead development.[13] Further improvement was also made in the library based screening technologies, allowing the systematic *de novo* target-directed lead creation.

For the later especially the emergence and evolution of focused library screening approaches makes it easy nowadays to generate highly affine peptidic binders. The big advantage of library-based screening technologies is its big variance of binders tested. Essential for the process that usually consists of library construction, selection of this library for a specific target in several rounds and a final analysis step is the compartmentalization and/or covalent linkage between pheno- and genotype of the binder. Phage display is most commonly used to achieve this linkage.[14] Here filamentous phages are expressing multiple copies of a peptide or protein on their coat protein, with the cDNA encoding these peptides/proteins compartmentalized inside the phage itself (Figure 1A).[15] After phage expression and affinity panning the library of binders against an immobilized target, the unbound phages are washed off and another round of selection is started. After several rounds only highly affine binders are left and their amino acid sequence can be conveniently analyzed throughout their compartmentalized cDNA. This process is limited by the usage of *in vivo* and *in vitro* steps to a library size in the order of 10^9 consisting mainly of peptides composed of native amino acids. The phage display system gives the opportunity to incorporate a chemically or enzymatic post-translational modification step to the selection, which hence widens its structural variety to some extend.[16,17] The Heinis group also reported on the post-translational intramolecular alkylation of cysteines in the peptide structure, to generate constraint bicyclic peptides for even higher affinity and selectivity.[18–20]

To significantly maximizing the used focused libraries, new pure *in vitro* technologies have been developed recently and give access to rare sequences. Especially mRNA display techniques combined with next generation sequencing gave rise to a huge number of new peptidic binders.[21–25] In mRNA-display the covalent linkage between the encoding mRNA and the to be screened peptide binder is enabled by puromycin (Figure 1B).[26] Puromycin resembles the structure of a tyrosine covalently linked to the 3'carbon of an adenine nucleoside *via* an amide linkage. When puromycin modified mRNA-strands are translated, the translation is finished at the 3' end with the transfer of the nascent peptide to the free amine of puromycin. This is only possible due to the inherent similarity of puromycine to tyrosine, which cannot be distinguished by the peptidyl transfer center of the ribosome, resulting in a covalent mRNA-peptide fusion library. After reverse transcription of the mRNA to a RNA/DNA hybrid, the peptidic library is screened for its affinity towards an immobilized target. The immobilization makes it easy to wash of all non-binding biomolecules. The RNA/DNA hybrid of the first round selection binders can then be amplified by PCR and conveniently analyzed by DNA sequencing. Binders of the first round can then again be

transcribed and affinity panned in another selection round. The realization of this process to be fully *in vitro,* also posed the opportunity to explore the usage of non-native amino acids. In an *in vitro* system one can simply add tRNAs loaded with unnatural amino acids by natural or modified aminoacyl tRNA synthetases (ARS) in the translation process.[27]

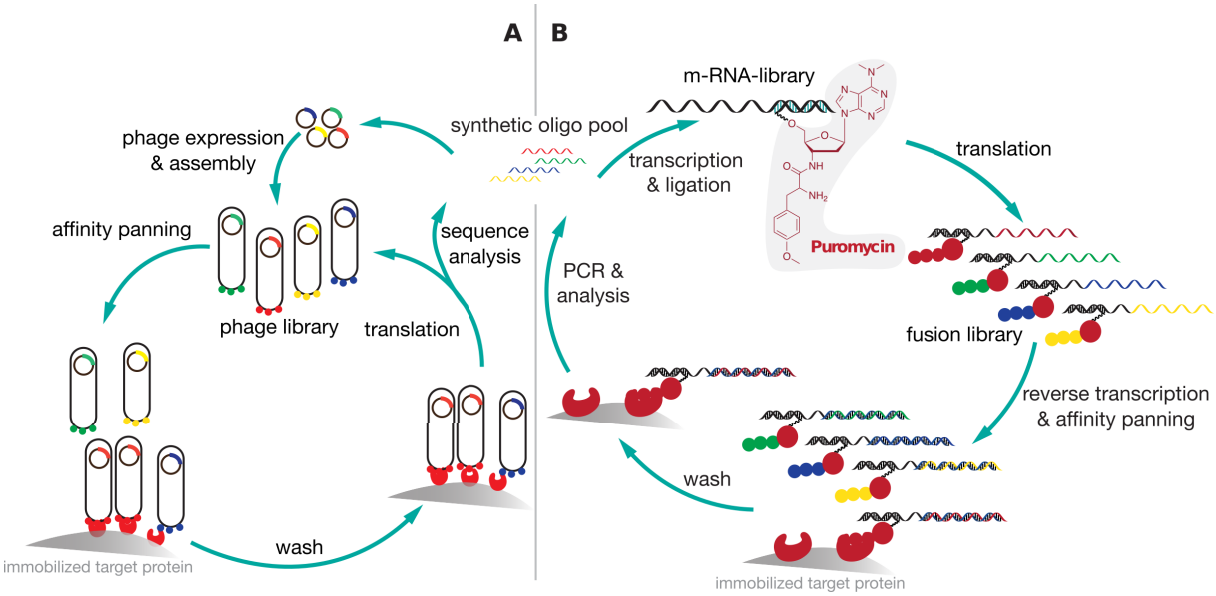

Figure 1: Overview of library screening technologies A) Phage display and B) mRNA display.

For this purpose the Suga lab developed promiscuous aminoacylating ribozymes, so called flexizymes, which can load a wide variety of unnatural amino acids onto tRNA and hence give rise to an extensive gene code reprogramming for the expression of complex non native peptides.[28] The combination of the flexible *in vitro* translation (FIT) method with mRNA display, first demonstrated also by the Suga lab[29], witnessed the breakthrough of library-based screening methods to the pharmaceutical industry.

A less systematic approach towards finding highly specific peptidic binders is the inspiration from nature itself. With the emergence of improved and highly precise protein structure analysis methods, shown with the advances in electron microscopy lately, this rational approach might even gain more attention in the future. The idea of taking *e.g.* complementarity determining regions (CDR) of antibodies and use their structural information for the development of peptide binders was first reported on in the early 90s.[30–32] Either linear peptide sequences or important structural features, which were fused covalently into a peptidic structure were shown to create potent peptidic inhibitors.[31,33–35] An example of simply using a linear peptidic sequence from a CDR domain for the creation of a peptidic hemagglutinin binding ligand, was reported by Memczak *et al.*. Here they reported the finding of a peptidic binder with micromolar affinity directly from the native CDR-structure, which could even be improved by peptide microarray.[33] Just recently a paper gained much attention in which the structural knowledge of the binding between

hemagglutinin (HA) and its complementary antibody was used to generate a peptidic infection inhibitor, that can bind HA with nanomolar affinity at the highly conserved stem region of the membrane protein and block the low pH conformational change that is associated with cellular membrane fusion.[36] These examples are highlighting impressively the possibilities when combining structural information and peptide based inhibitor development.

4.2.2 Solid-Phase peptide synthesis

The groundwork for the easy synthesis of bioactive peptides was laid in the 20th century. Emil Fischer could accomplish the first dipeptide synthesis over 100 years ago.[37] Max Bergmann showed the effective amine protection of an amino acid with a carbobenzoxy group[38] and finally Bruce Merrifield revolutionized the synthesis of peptides with inventing the solid-phase peptide synthesis (SPPS).[39,40] Merrifield reported the synthesis of longer peptide fragments by attaching the amino acid's C-terminus covalently to an insoluble resin. This approach gave the advantages of carrying out all reactions in one flask and without the purification of each coupling product, because one can easily filter off any excess reagent. From this report onwards researchers devoted a lot of time to developing better resins, linkers, protecting group strategies and monitoring of the individual steps.[41,42] The general synthesis route is started by attaching the C-terminal residue to the solid support *via* its carboxyl group. In all resin bound synthesis steps the amino acids are protected with a temporary amine protecting group and a permanent side chain protecting group if needed. The key feature here is that the two different protecting groups have to be orthogonally cleavable. After immobilization of the first amino acid building block leftover reagents are washed off by simple filtration. After deprotection of the terminal amine the following activated fully protected amino acid can be coupled to the free amine.

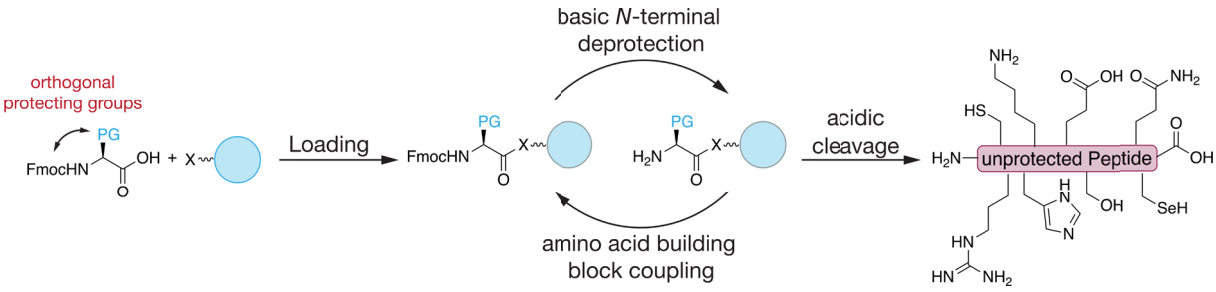

Figure 2: Principle of solid-phase peptide synthesis using the Fmoc-strategy.

After another washing step the protected amine is deprotected and another amino acid can be added. This reaction scheme results in a C to N-term synthesis direction of the peptide. After the full stepwise addition of all amino acids, the protected peptide can be cleaved off from the resin with the same conditions the permanent side chain protecting groups are cleaved off to yield the unprotected peptide in solution (Figure 2). Nowadays, the most commonly used protecting group strategy is Fmoc-chemistry. Here the permanent side chain protecting groups are acid labile and the *N*-terminal temporary protecting group (Fmoc) is cleaved under basic conditions. For this strategy all natural amino acids are commercially available with appropriate protection. Furthermore there are many unnatural amino acids or ones that bear a post translational modification as well as non-peptidic building blocks available for the generation of a wide variety of peptides and peptidomimetics, which makes peptides very attractive from a pharmaceutical and an academic point of view.

4.2.3 Stabilizing peptides in structure and function

Because protein-protein interactions (PPI)s are regulating the vast majority of cellular processes their inhibition represents a major therapeutic goal. However, as PPIs have planar and large surface areas this goal is difficult to span with small molecule inhibitors. In addition does the development of small molecule inhibitors lack a rational starting point due to the absence of ligands in PPIs. Mostly one can only lean on the identification of “hot spots” involved in the interaction for the rational design of an inhibitor. These are amino acids that are contributing most to the interaction and are found in the structurally conserved region of the protein-protein interface.

In the last years the possibility of using protein inspired inhibitors became more popular.[43] Here one of the interacting proteins is reduced to the size of its binding epitope, which is the starting point for the design of the inhibitor. It must be noted that the structural integrity of the binding epitopes is highly connected to the surrounding protein structure and most short peptidic sequences loose this structure when excised from the full-length protein. In addition to that, they also become more prone to degradation by proteases. Therefore, the demand for tools to mimic or stabilize these secondary structures, which not only provide the function embedded into the proteins structures, but also shield the peptide to a certain extend towards proteases is high. As α-helices are found to be contributing to 62% of all PPI interfaces[44] and make up 40% of secondary structural motifs in proteins, it is of special interest to stabilize or induce this specific structural motif.

An α-helix is characterized by intramolecular hydrogen bonds between the amide proton of an amino acid with the carbonyl group of the amino acid four residues earlier (i, i + 4) (see Figure 3A). Salt bridges between side chain residues can achieve further stabilization. Since the 1980s researchers tried to stabilize or induce α-helicity by organic synthesis tools. The method of choice was to covalently link amino acid side chains in specific positions in the peptide structure. If length and position of this macrocyclization linkage was positioned right, helicity could be restored or induced, often rendering the peptide more stable towards proteases and in some cases also improving cell penetration properties.[45]

One of the first side chain macrocyclization techniques was the covalent formation of a lactam between lysine and glutamic/aspartic acid residues (Figure 4a) and revealed preservation of helicity and activity of a cyclized growth hormone.[46] From there onwards different length of side chains and position were investigated for the helical stabilization with lactam linkages and were successfully applied in stabilizing peptidic hormones, viral fusion inhibitors[47,48], anti bacterials[49], receptor agonists and antagonist[50] and many more.[51–57] Also early on, thiol-based cross-linking strategies have been employed for inducing helicity. Disulfide formation between a 2-amino-6-mercaptohexanoic acid and D-Cys at *i, i*+7 position (Figure 3C and Figure 4b) yielded one of the first artificially constrained helical peptides.[58]

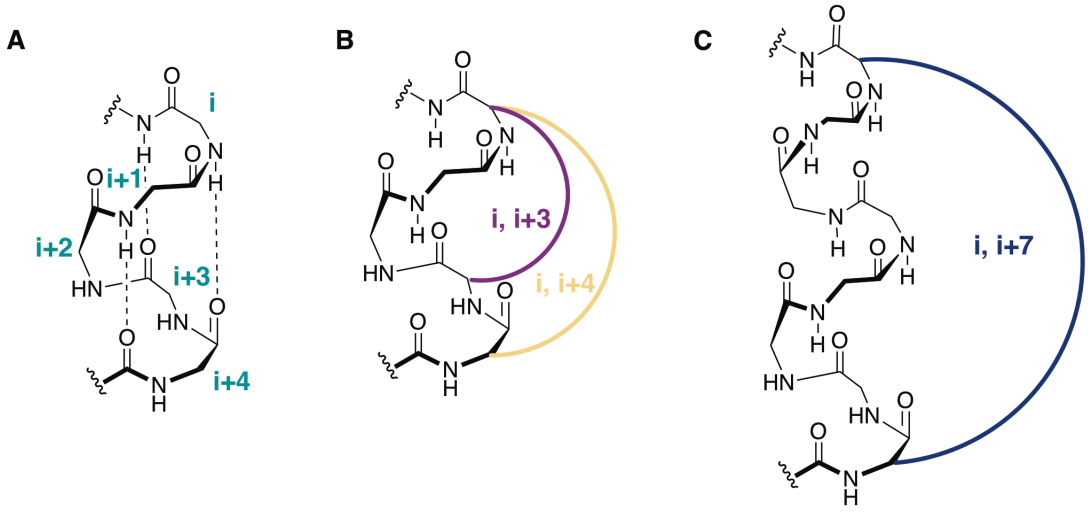

Figure 3: Schematic structure of a α-helix A) hydrogen bonding in an α-helix B) stabilization of one turn by i, i+3 or i, i+4 side chain linkage C) stabilization of two turns by i, i+7 side chain linkage.

There were further reports on crosslinking L- and D-cysteine in i,i+3 position (Figure 3B and 4c) and also on varying the linker length by employment of homocysteine.[55,59] In order to gain more durable cross-linkers that withstands reductive conditions, thioether bonds were introduced for crosslinking (Figure 4d) and even developed for macrocyclization on protein level *via* genetic encoding.[60,61] The lactamisation and the disulfide side chain linkage

strategies were so vastly used because the linkage could consists of proteogenic amino acids, which are cheap and easy to incorporate. Nevertheless one of the major drawbacks is an additional orthogonal protecting group strategy that is needed during the solid phase peptide synthesis and the inherent lability towards proteases or reductive conditions. A huge impact on the helical peptide cyclization field had the development of the "hydrocarbon peptide stapling technique" in 2000 by the Verdine lab.[62] They published a linker in which olefinic α,α,-di-substituted amino acids were cross linked by ring closing metathesis. Here they combined methylation of the α-carbon of the amino acid, which is known to increase the helical predisposition and the covalent cross link of two unnatural olefinic amino acids by ring closing metathesis. The metathesis between two olefinic amino acids in a peptide was published before by Blackwell and Grubbs, for the crosslinking of adjacent *O*-allyl serine residues (Figure 4e).[63]

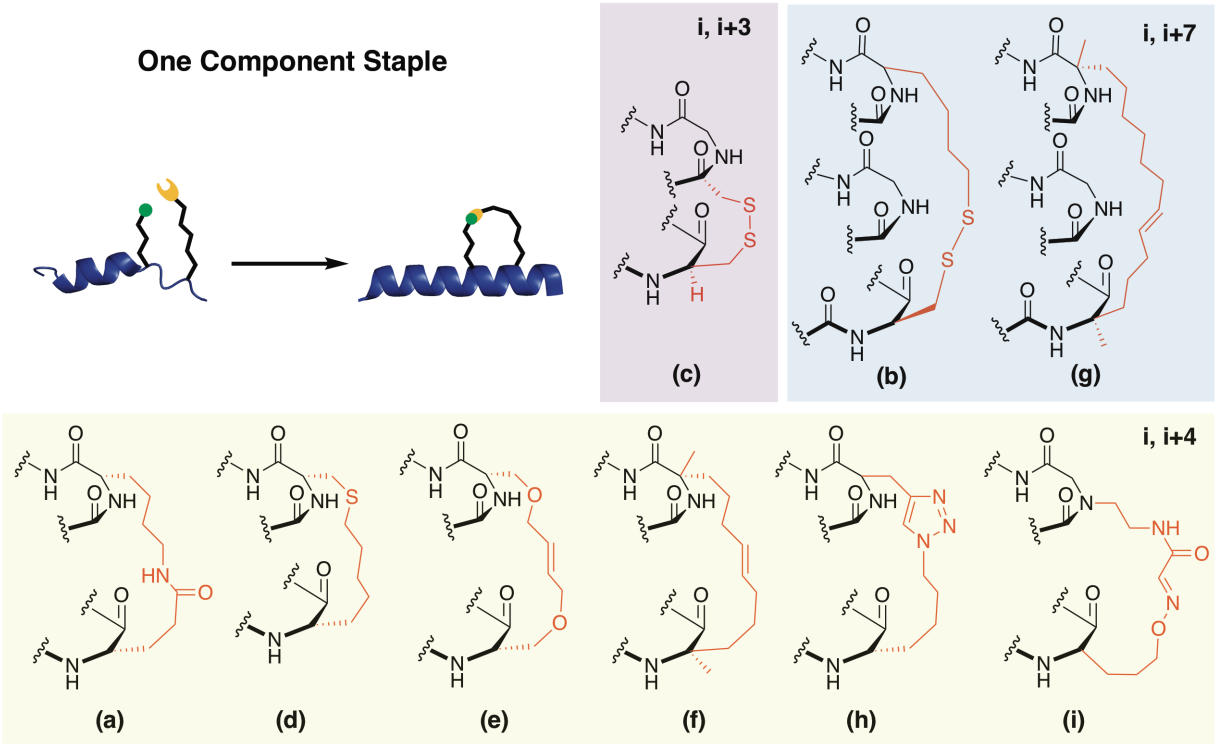

Figure 4: Overview of different macrocyclization techniques for one component staples.

The olefinic α,α,-di-substituted amino acids were incorporated at i, i + 3; i, i + 4 and i, i + 7 positions in a peptide (Figure 3 and 5). For each position the stereochemistry on the α,α,-disubstituted olefinic amino acids needed to be adjusted to generate the desired staple of one turn for the incorporation in i,i+3 and i,i+4 (Figure 4f) position and for two turns when the covalent linker was formed in i,i+7 position (Figure 4g and 5). [62,64,65] An even further enhancement of helicity and notably also cell permeability, was gained by combining two or more separate staples in one peptide[45] or even using an amino acid, which enables a dual

hydrocarbon staple for the creation of a double staple, which was termed “stitched peptide”.[66] The all-hydrocarbon staple has since been used in addressing many different targets, one of the most recognized study showed the activation of apoptosis *in vivo* by an all-hydrocarbon stapled BH3 peptide.[67] Just recently, chemically orthogonal ring-closing reactions have been reported, which allow formation of a defined double stapling of peptides. It was shown that ring closing olefin (RCM) and alkyne metathesis (RCAM) can be carried out consecutively on peptide resin to yield a bicyclic peptide.[68]

The big advantage of covalently linking two functional groups that are not found in natural amino acids in a chemoselective fashion, is that one does not need to strategize about orthogonal protecting groups throughout SPPS. Hence more chemoselective reactions were explored for the intramolecular macrocyclization of peptides (see also Chapter 4.3). It was shown that copper catalyzed alkyne azide cycloaddition (CuAAC) (Figure 4h) and also oxime formation (Figure 4i) could achieve the same structure stabilizing effect as the lactam or hydrogencarbon linker could.[69–71]

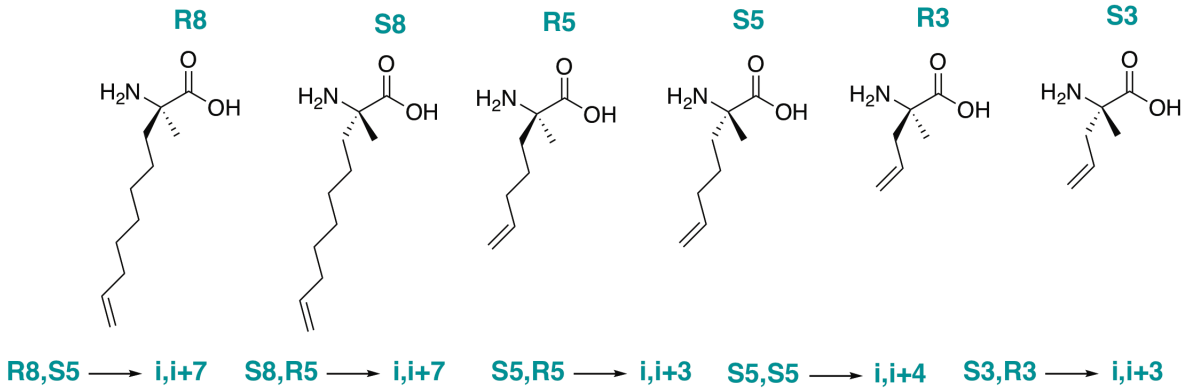

Figure 5: The α,α,-disubstituted olefinic amino acids used for creation of staples.

While more chemical reactions were being used for the intramolecular staple, also more complex staple strategies with even further functionalization opportunities were introduced in form of two component staples (Figure 6).

A two component staple, is a linker formed between two amino acids, which are bridged by a bifunctional linker, that is not part of the peptide itself.[72] Its major advantage lays in the fact, that there can be complex moieties introduced into the peptide without the need of lengthy non-native amino acid synthesis. One of the first two-component staples was a photo switchable linker based on azobenzene (Figure 6a).[73,74] By using a photoisomerizable crosslinker the α-helical structure was inducible upon irradiation. Furthermore the group of David Spring used *e.g.* a clickable linker that can be first functionalized with any tag of interest and then conjugated to a synthetic peptide (Figure 6b). In their study they report on the improved cellular uptake and hence improved activity by incorporating solubilizing poly-

Arginine tags into the linker or using this technique for functionalization of a peptide generated from the p53 protein with TAMRA.[75] To understand the linker's influence on a broader spectrum the easy handling and incorporation of two-component linkers was used for different screens. The Inouye lab wanted to find the optimal length and rigidity for maximal helicity and therefore screened disuccinimidyl-linkers with alkylamine side chains (Figure 6c).[76] The Greenbaum lab did a similar study with bis-electrophilic systems, which they reacted with cysteines (Figure 6d;e)[77]. Bis-arylation of two cysteines was also probed in i,i+4 position with hexafluorobenzene (Figure 6f) and could stabilize the helical character of a HIV-1 capsid binder.[78]

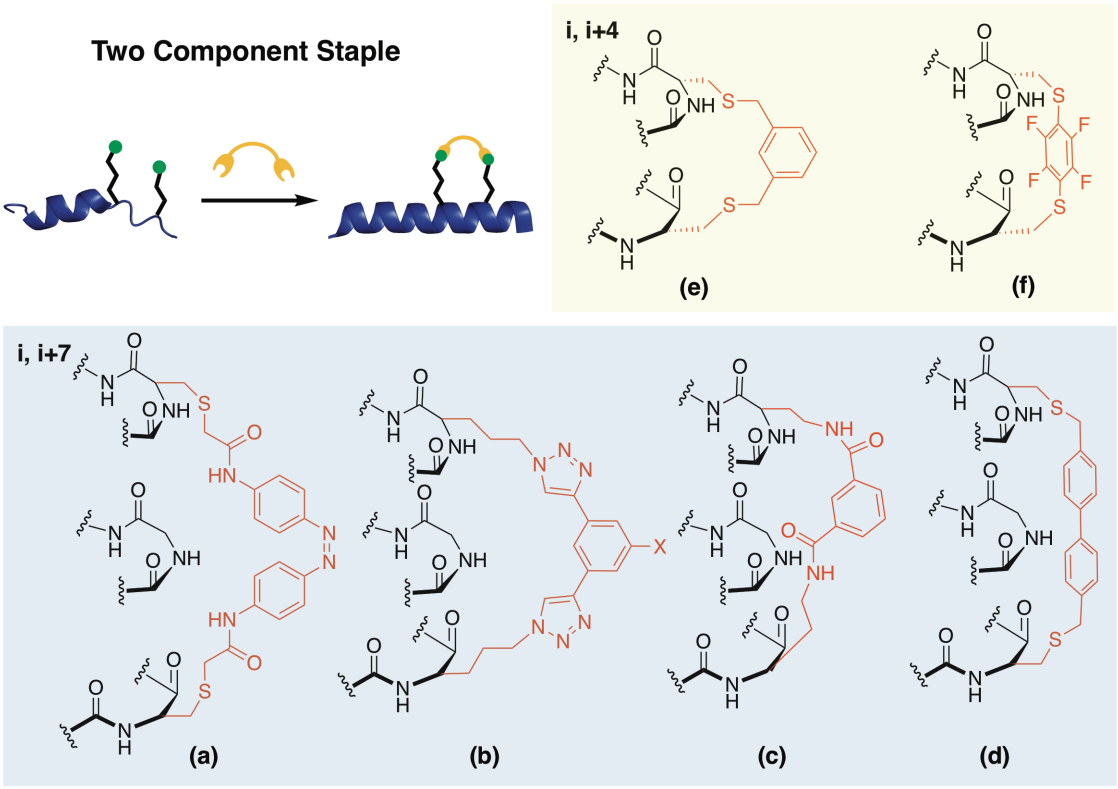

Figure 6: Overview of different macrocyclization techniques for two component staples.

Throughout those studies it was shown that helicity could be stabilized and induced by a wide variety of linkers. Furthermore, upon covalent macrocyclization the binding affinity towards the target was improved, which is correlating to the secondary peptide structure stabilization. But when some of the peptidic binders were tested *in vitro* it could be observed that the inhibitory efficiency was highly context dependent and an overall underlying rule for the potency of a peptidic inhibitor could not be deduced. A reason for this is that helicity seems to not be the most important factor in the success of a peptidic inhibitor. In order to be able to interfere with the PPI one critical characteristic is also the cell penetrating properties of the helical peptides when working *in vivo*. In the beginning of peptide stapling it was believed that cellular uptake is solely facilitated by a perfect helix,

which is supposed to enhance uptake by burying the hydrophilic amide backbone inside the peptide conformation and therefore masks the hydrophilicity of the peptide and enhance the interaction with the hydrophobic interior of cellular membrane. But because the cellular uptake mechanism was not well understood and most studies relied on a trial and error basis, more systematic studies were just undertaken recently to determine what makes a stapled peptide cell permeable and what hinders it cellular entry.

For all-hydrocarbon stapled peptides the Verdine lab did a broad screen of about 200 peptides, which proofed that helicity is not the only important characteristic for cellular uptake. Another essential factor is the formal charge of the peptide. They found the best cellular uptake for peptides with a formal charge of +3 to +5 and also very good uptake for +1 to +3 and +5 to +7 charged peptides.[79] Further studies on the criteria for cell penetration manifested the interplay between positive charge and hydrophobicity. The Walensky lab looked into the importance of staple position, pI of the peptide and hydrophobicity.[80] They could show similarly, that the hydrophobicity plays a huge role in cellular uptake, and that if the staple is positioned at the hydrophobic-hydrophilic boundary in the peptide and thereby is extending the hydrophobic space, the penetration properties are improved. They also found that a helicity between 60 – 89% is most optimal for cellular uptake. Contrary to what is often reported they could show that a hydrophobic peptide with lower pI values (8.8 – 9.34) gave as good cell penetration as peptides with higher pIs. Moreover, they found that hydrophobic peptides with higher pI (9.76 – 10.3) were more likely to enhance cell lysis, which renders them inappropriate for cellular assays.[81,82] Recently, also a systematical cellular uptake study for a variety of different staple linkers concluded that cell permeability could be greatly correlated to the relative hydrophobicity of a macrocyclized peptide which is also determined by the nature of its linker.[83]

These complex studies show that not only affinity towards a target is important for creating a promising functional binder, but also its behavior in biological processes is crucial and needs to be understood on a broader level in order to be able to interfere or analyze the highly complex interplay of biological mechanisms.

4.2.4 Cell Penetrating Peptides

Cell penetrating peptides (CPP) have the ability to cross cell membranes effectively without the involvement of receptors. It was shown that the cell penetrating property of peptides can even be transferred to an attached cargo, which gets dragged into cells by the CPP. This fact makes them one of the most promising strategies for cellular delivery of therapeutic moieties like nucleic acids, drugs, imaging agents and biomolecules not only in

a pharmaceutical setting but also for basic academic research.[84] There are different classes of cell penetrating peptides ranging from protein-derived to chimeric or synthetic short peptides sequences, with either amphipathic or cationic characteristics. Two of the most intensively studied cationic CPPs are discussed here, the TAT-peptide, which is derived from the RNA-binding domain of the HIV-1 protein and Oligoarginine peptides, which are synthetic derivations of TAT.

In 1988 two groups reported that, the HIV TAT transactivation factor protein can cross cellular membranes efficiently and localizes to the nucleus.[85,86] From there on different studies showed that only a short fraction of the protein is responsible for this behavior. When reduced to this short peptidic fraction, it is able to facilitate cellular uptake of biomolecules upon covalent conjugation.[87–89] Lebleu and co-workers showed that the basic sequence within this fragment is the actual driving force of cellular internalization, contrary to initial hypothesis that the helical structure of the TAT-protein is responsible. Hence they could show that using solely this basic 9-mer sequence was enough to facilitate cellular uptake of a cargo.[90] Dowdy *et al.* even reported that the tat-peptide can deliver β-galactosidase across the blood brain barrier.[89]

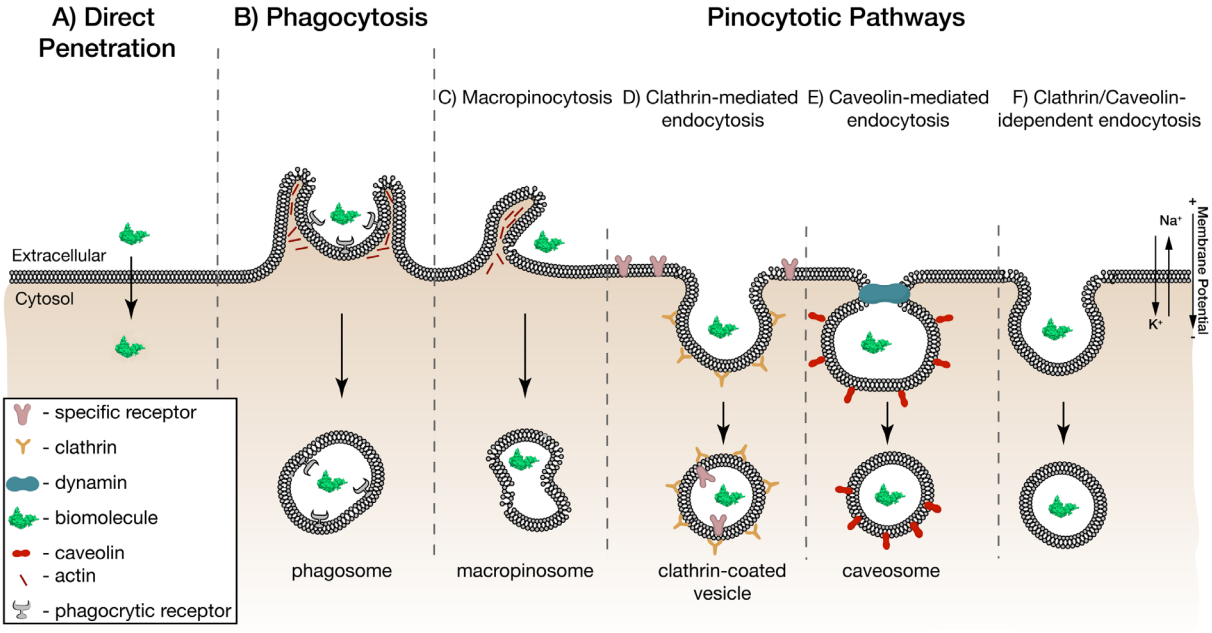

Figure 7: Overview of different cellular uptake mechanisms. Figure adapted from Zhu *et al.*[91].

In an undertaking to elucidate the driving force of this uptake behavior the 9-mer TAT-sequence (RKKRRQRRR) itself was under investigation.[92–94] The TAT - RNA binding domain of HIV underwent an alanine scan, which sowed that any substitution of a basic amino acid resulted in reduced cellular uptake. Synthesis of an all D-amino acids peptide or replacing all non-arginines by arginines, resulted in cellular uptake. This proofed the peptide

sequence to be non-specific for any sort of receptor. Also it was observed that an all-arginine peptide exhibits an even superior uptake behavior than TAT itself.[92–94] Because simple passive diffusion does not seem to be possible for the highly polar CPPs unraveling the cellular uptake mechanism was pressing, in order to be able to translate this remarkable behavior to improve cellular uptake of drugs, dyes, proteins and peptides. Early on it was reported that cellular uptake of CPPs is an energy independent pathway that is not sensitive towards endocytosis inhibitors and delivers the peptide directly into the cytosol.[90,94] However these findings were retracted and found to be mainly artifacts resulting from cellular fixation.[95] In following studies the involvement of almost all endocytotic pathways in the cellular uptake, including macropinocytosis (Figure 7C)[96], clathrin-mediated endocytosis (Figure 7D)[97] and caveolae/lipid-raft-mediated endocytosis (Figure 7E)[96,98,99] was implemented.

But also in total contrast, there were still observations of direct translocation (Figure 7A) of labeled Tat-peptides in live cells, which could not emerge from fixation artifacts.[100,101] It was shown that these contradictive findings are actually all valid next to each other, because the cellular uptake mechanism for CPP-Cargo-conjugates is highly dependent on transporter type, cargo type and size, cell type, concentration and also the method of uptake analysis. Especially big cargos, like proteins, are mainly taken up throughout endocytosis when linear arginine-rich peptides are conjugated.[101,102] It was difficult to determine the exact classification of uptake mechanism, as it was observed that most of the times there is a co-occurrence of competing uptake pathways and hence no universal uptake mechanism could be deduced.[103–106] When using CPPs for the delivery of biomolecules into cells, the preferred uptake mechanism would be the direct penetration (Figure 7A) into cytosol. This would ensure that biomolecules would be able to reach their intracellular targets without the possibility to be rendered ineffective by being trapped in endosomes (Figure 7B-F). Therefore understanding the factors favoring direct membrane penetration is crucial.

For a predominately direct penetration it is important to achieve a high cell surface adsorption. The Wender and Futaki labs demonstrated that the guanidinium head groups are highly important for cellular uptake, as they are forming bidentate hydrogen bonds with negatively charged cellular surface groups (phosphates, carboxylates, sulfates) and uptake was increased by a high number of guanidinium head groups (6-12 arginines) (Figure 8A).[84,94,107] The high attraction of arginines toward negatively charged cellular surfaces is hence the underlying rational of all proposed mechanisms in a direct transduction into cells. A possible pore formation was evaluated in molecular dynamic simulations and electrophysiological experiments.[108,109] They show that by increasing the peptide concentration on the cellular surface and subsequent interaction, the lipid

arrangement gets distorted and thinned out. Hence arginine side chains can interact with the distal bilayer, whereby the nucleation of a water pore is induced, resulting in the translocation of peptides through this pore (Figure 8B). Here pH was shown to have major influence on peptide binding to the lipids extracellularly and release from the lipid intracellularly, as the peptide binding to deprotonated lipids is observed in lower pH and its release at slightly higher pH.[110] Another proposed mechanism for the transduction is the formation of a lipophilic ion pair, which is masking the polarity of the guanidinium group, making it possible to diffuse into the membrane. This concept was termed adaptive translocation (Figure 8C). Here the membrane potential is also important for the diffusion of peptides through the membrane, because highly charged peptides are driven to the inside of the cell by the intracellular lower voltage.[107] It was shown that more curved membranes seem to be better penetrable, due to more intrinsic membrane defects, making it easier to interact with the lipid interior.[104,111]

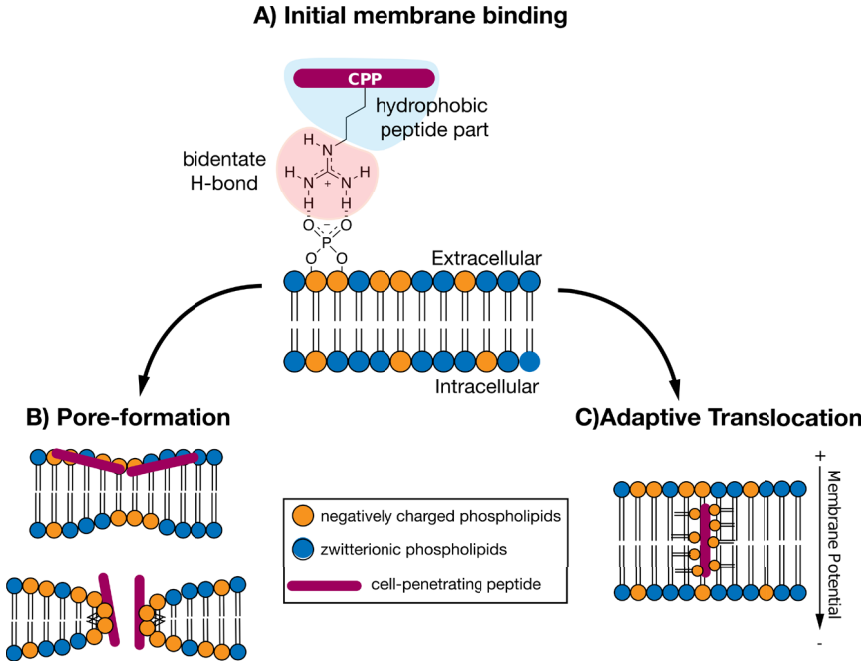

Figure 8: Proposed mechanisms for direct translocation of Arginine-rich cell penetrating peptides. Graphic adapted from Bechara *et al*.[12]

Looking on improving the direct uptake into the cytosol, the facts known about the internalization were exploited. Building upon the theory of adaptive translocation and the observation that R8 could be extracted into the octanol phase in presence of sodium laurate, the Futaki and Matile labs showed that a direct translocation of smaller and bigger cargos with R8-peptides is possible in the presence of the hydrophobic counteranion pyrenebutyrate (PyB).[113–115] Further a membrane curvature inducing peptide (EpN18) was

co-administered with the CPP-cargo and resulted in direct cell penetration.[116] The Futaki lab could pinpoint the effect of the PyB and EpN18 towards a loosening of the lipid packing, which allowed for a better interaction of hydrophobic peptide backbone with the hydrophobic lipid core.[117] A totally different approach toward the improvement of direct cellular penetration was achieved by the Cardoso Lab. They investigated the influence of backbone rigidity and static presentation of the guanidinium groups on cell penetration and found that by cyclizing the peptide backbone they could achieve higher cellular uptake mainly into the cytosol and nucleolus for TAT and R10 without the need of any additives.[118] The increased uptake was explained by the larger distance between guanidine head groups, which was already observed to positively influence the direct cell penetration in a linear model and was recently also proven for rigid oligoprolines bearing guanidinium groups.[119,120] The improved efficiency of cyclized TAT and R10 peptides could even achieve the cellular delivery of bigger cargos, like proteins and nanobodies, directly into the cytosol, which is referred to as transduction in the following chapters.[121,122]

4.3 Bioconjugation Reactions

The selective modification of a biomolecule with any given other functional moiety, like drugs, fluorophores, peptidic tags, post translational modifications, PEG, biotin etc. is a crucial task of chemical biology.[123] Stable and defined conjugates are ideal in the creation of therapeutics, like antibody – drug – conjugates and protein or nanoparticle based materials. The requirements for bioconjugation reactions are numerous and complex. First of all bioconjugation reactions should be carried out under physiological pH, at moderate temperatures (20 – 37°C) and in aqueous buffered environment, in order to preserve structural and functional integrity of the conjugate. Furthermore, one seeks for site-specific reactions to be able to create a homogenous and structurally defined product. Hence chemoselective reactions are employed on native amino acid residues or even bioorthogonal reactions on non-native amino acids introduced into the biomolecule for the covalent functionalization.[124,125] Throughout the combination of purely biochemical methods with organic chemistry new strategic approaches are created for studying and therefore understanding protein functions.

4.3.1 Bioconjugation on native amino acids

Nature provides us with a big variety of functional groups in protein structures, which are posing the opportunity of being used in diverse bioconjugation reactions. Solvent exposed amino acids have been used conveniently for the modification of proteins for decades, in numerous types of reactions. But as the big number of different reactive groups in the protein structure can be seen as an advantage, it can also be a major drawback.

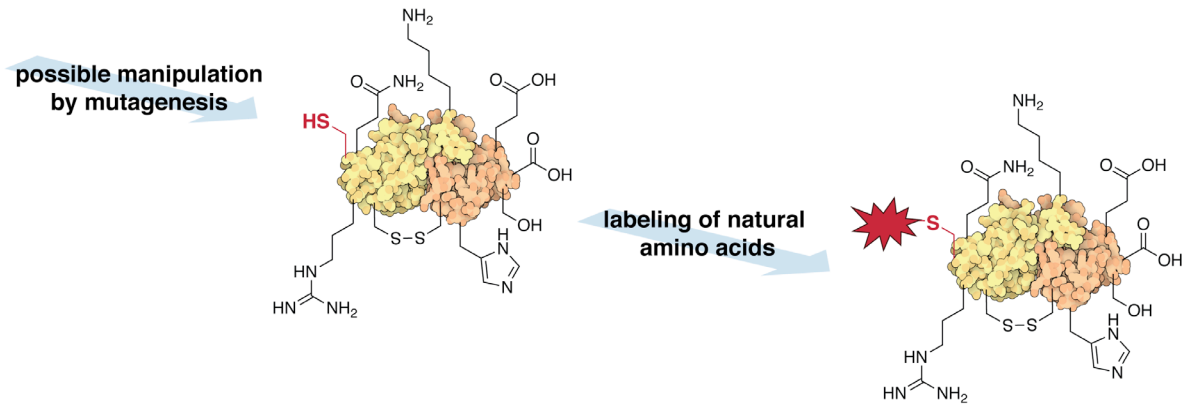

Figure 9: General principle of labeling natural amino acids for the incorporation of chemical tags.

Often the precise and selective labeling is not possible when using native side chain functionalities due to their multiple occurrences in the protein structure. To ensure selectivity, the protein structure and amino acid composition as such, have to be evaluated for each given experiment. Furthermore, also the desired reaction has to be validated for its purpose. However, if one chooses a reaction wisely and knows about their advantages and drawbacks, chemoselective reactions on natural residues are powerful tools for the modification of biomolecules without the need of lengthy biochemical protein modifications (Figure 9).

4.3.1.1 Reactions with native cysteines

Cysteine modifying reactions are widely favored over other native functionalities, because of the inherent high nucleophilicity of the sulfhydryl side chain, which is much more reactive than other nucleophiles found in the protein structure, rendering most reactions with cysteines chemoselective when done under appropriate conditions (Figure 10).[126,127] Moreover cysteines are of low abundance or found masked in disulfide bridges in proteins.[128] Hence one can either introduce addressable cysteines by standard biochemical point mutations, leading to defined positions of the to be functionalized handle. Or one can reduce disulfide bridges and use the generated cysteines for conjugations, also at mostly defined position.[129] One of the oldest methods for the modification of cysteines is the use of α-halocarbonyls, which are known for their fast and clean reaction with sulfhydryls since 1935.[130] Iodoacetyl-functionalized crosslinkers, biotinylation reagents, mass spectrometry tags etc. are commercially available and are used in many biological studies because of the ease and speed of this reaction. A major advantage is the stable and compact linkage that is formed. But it is also known, that the iodoacetylgroup is reacting in a low occurrence with other side chain functionalities, like amines from lysine or thiothers in methionines, when no cysteine is present or at a high excess of the reagent. One can circumvent these side reactions by using equimolar amounts or just slight excess of the compound and performing the conjugation reaction at pH 8.3, at which the reaction is the most specific for sulfhydryl groups.

Vinylsulfones have also been described for labeling of proteins, especially for PEGylation. They react in a Michael-type addition selectively with cysteines at pH 7-8. Going to higher pH the reaction rate is increased but cysteine selectivity is lost and lysine conjugation byproducts observed. Even though the conjugation products are highly stable in aqueous systems and in presence of other nucleophiles this reaction is not the most popular choice, due to its slow kinetics compared to *e.g* maleimides.

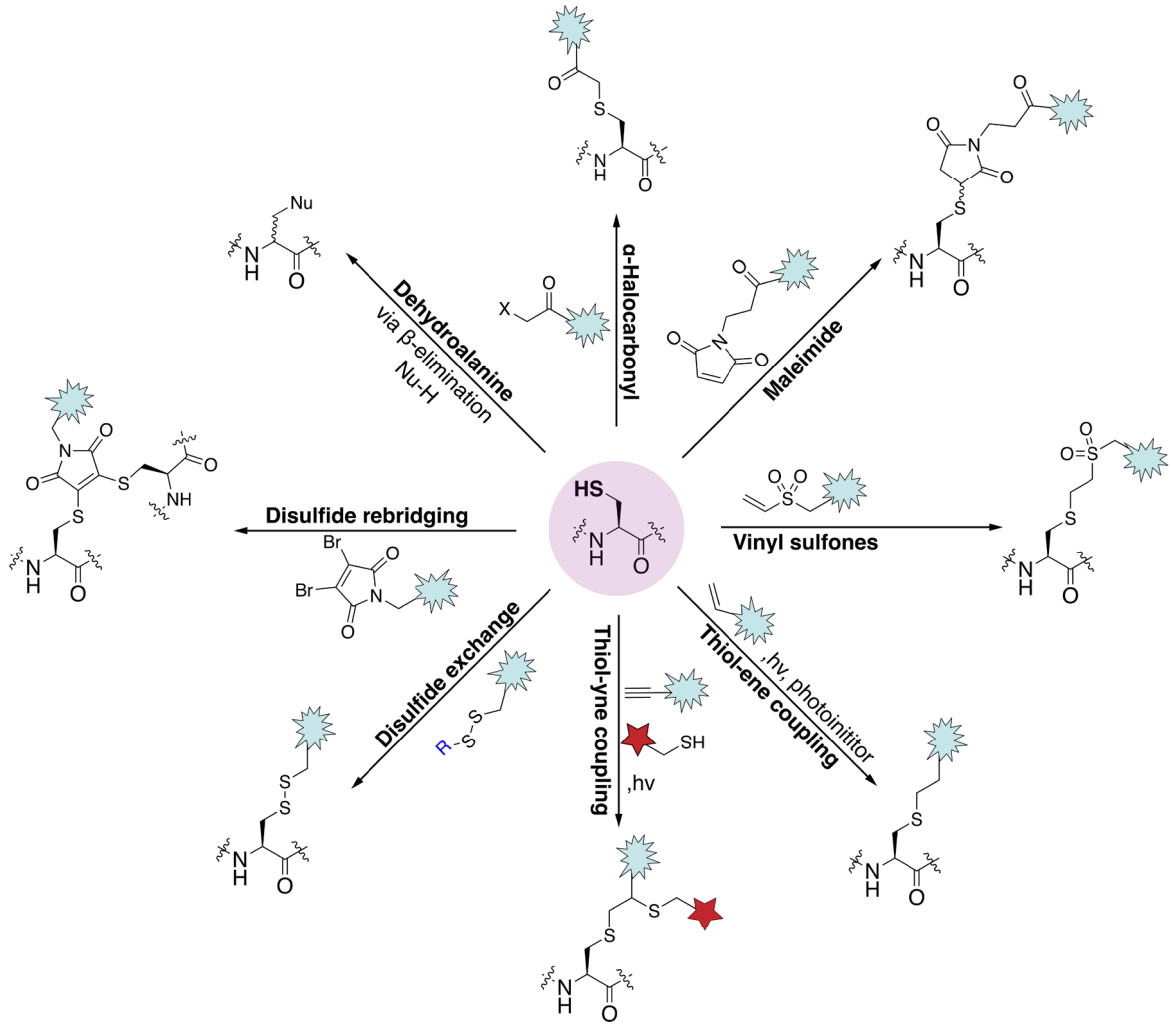

Figure 10: Overview of well-known bioconjugation reactions on cysteine.

Next to michael-type reactions, sulfhydryl-groups are also known to react under radical conditions. This has been utilized for bioconjugation reactions with terminal alkenes or alkynes in thiol-ene (TEC) or thiol-yne couplings (TYC) (Figure 10). The TEC starts with the formation of a thiyl radical by light and/or an initiator induction. The addition to the alkene occurs in an anti-Markovnikov fashion and is quenched by the abstraction of hydrogen from another sulfhydryl. The reaction was first used for the glycosylation of a viral capsid by the Davis group at rather low pH (pH4-6).[131] TYC is conducted in a similar free-radical fashion, in which two thiol containing fragments are added to the alkyne, with the first step being again an anti-Markovnikov addition of a thiyl radical to the triple bond generating a vinyl thioether, which can undergo then a subsequent TEC reaction with a second thiol functionalized fragment. The limitation of these reactions however is the formation of thiyl radical, which could damage the protein.

Employing disulfide formation of cysteines with a thiol containing tag was developed as another bioconjugation reaction. For this purpose it is essential to work with an activated

thiol otherwise the thermodynamic preference to undergo a thiol exchange is not given. An activated thiol is a disulfide-masked thiol with a good leaving group, which results in an unreactive thiol after the reaction. Commonly known activating groups are pyridyl disulfides, thiosulphonates, thiosulphates or 5-thio-2-nitrobenzoic acid (TNB)-like disulfides. Tags like fluorophores, biotinylation or PEGylation reagents are commercially available functionalized with those activating groups. Disulfide forming reactions have also been used for the generation of antibody – drug – conjugates (ADCs)[132] and nanobody-CPP conjugates[122] exhibiting the advantage that the functional moiety is cleaved from its cargo inside cells due to the reductive conditions found there. But this feasible intracellular liberation strategy can also be the source of major inherent lability making it crucial to assess the compatibility of assay and conjugation technique.

The most prominently used method for cysteine labeling to date is the coupling of a maleimide-containing molecule to cysteines. This reaction exhibits particularly fast kinetics and high selectivity under near neutral conditions (pH 6.4 – 7.4) (Scheme 1A).[133] Maleimide chemistry is one of the main choices for the generation of ADCs and used in both ADCs on the market. Further it is part of 24 out of 34 ADCs in clinical trials and standardly used for protein labeling with affinity tags, fluorophores and conjugations to nanoparticles, which is highlighting its comfortable application.

However, one major limitation of this chemistry has been addressed lately, i.e. the inherent lability of the formed thiosuccinimidyl adduct. Highly solvent-accessible conjugation sites were shown to undergo rapid thiol exchange with other reactive thiols in biologic environments, lowering the actual concentration of the effector molecule at the target site (Scheme 1A).[134] To circumvent this loss of effector molecule, an exocyclic olefinic maleimide has been described recently, that allows the stable thiol addition to the maleimide (Scheme 1B).[135] Thiol exchange reactions can also be prevented when the maleimide undergoes hydrolysis to thiomaleamic acid, which is rather slow process that only goes to completion after one month at 37°C. Hence efforts have been made to increase the velocity of this hydrolysis step (Scheme 1C). Researchers could achieve the complete hydrolysis after one hour incubation on ice.[136,137] Still the hydrolysis is giving heterogeneous products and also the possibility of starting material undergoing hydrolysis, is reason enough to further engineer new reactions with the hope of finding new fast, selective and yet stable alternatives.

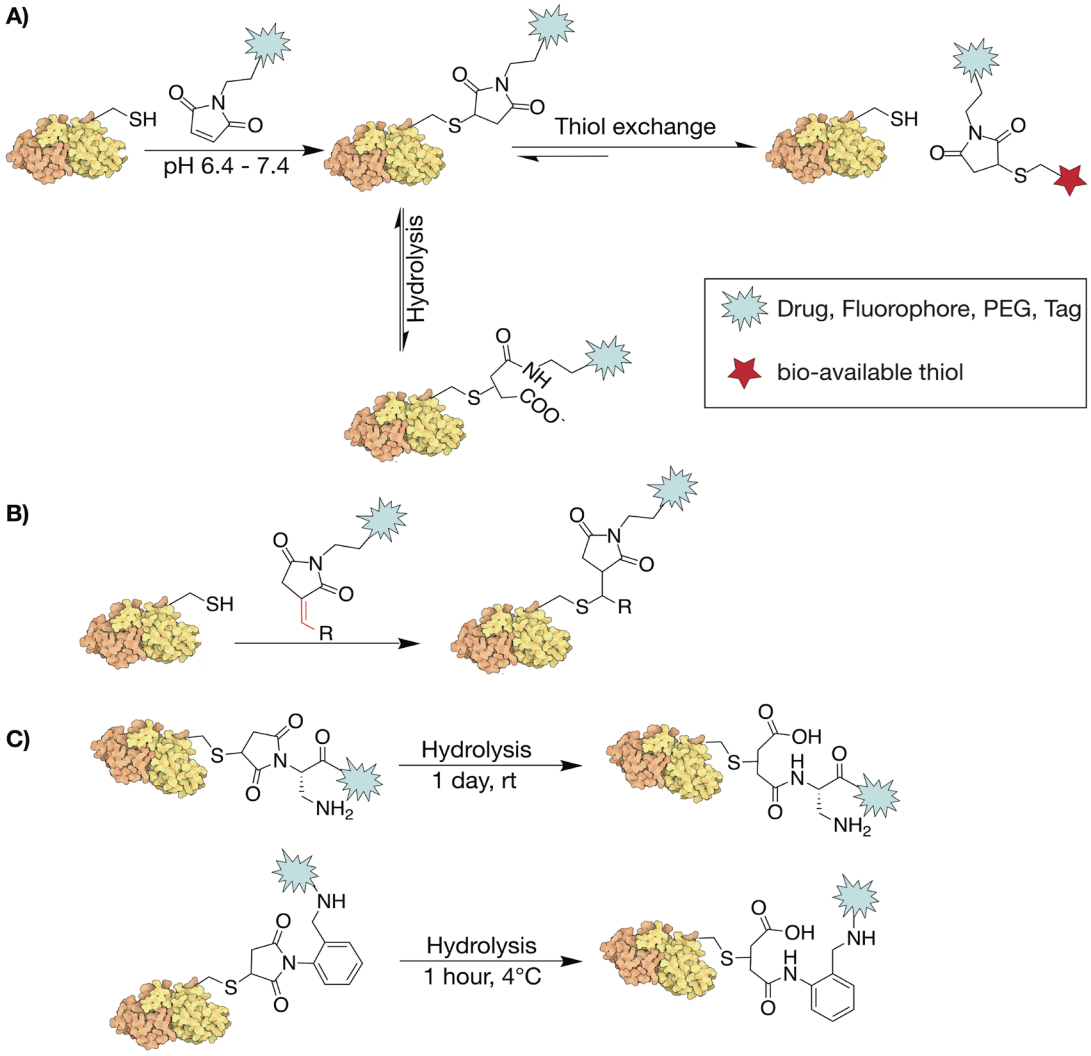

Scheme 1: Maleimide chemistry as bioconjugation method A) conventional maleimide labeling B) exocyclic olefinic maleimides give stable product resistant to thiol exchange C) strategies for fast maleimide hydrolysis[136,137].

In some cases, structure-stabilizing disulfides are being reduced and used in the conjugation with cysteine reactive labels, as seen prominently in ADCs. Hereby, the integrity of the protein can be at risk. To circumvent this, methods have been developed in which the disulfide is rebridged by the labeling technique itself. This methodology was reported for dibromomaleimides (Figure 11A)[138], dithiophenolmaleimide (Figure 11A)[139], bis-sulfone reagents (Figure 11B)[140] or dibromopyridazinediones (Figure 11C)[141]. For a more stable conjugate a rapid maleimide hydrolysis was also developed for the dibromomaleimides recently.[142] Dibromopyridazones were created as handle that can not only react with two cysteines, but are further bearing an alkyne and a strained alkyne handle, which can undergo bioorthogonal reactions with azides and were used to prepare antibodies conjugated with drugs, fluorophores and/or PEG modularly to the assays need (Figure 11C).

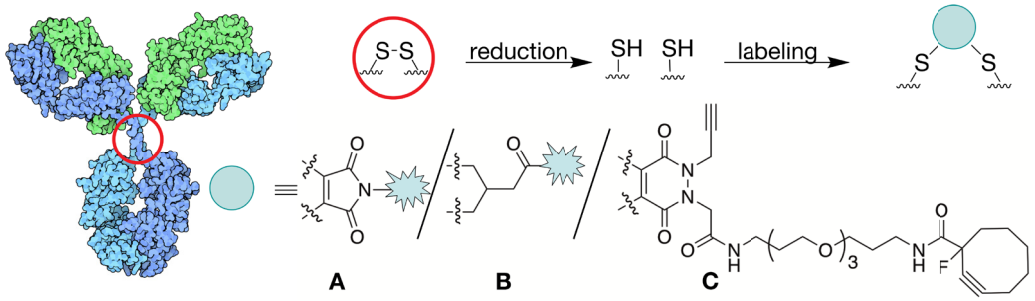

Figure 11: Disulfide rebridging approach with A) dibromo-or dithiophenolmaleimide B) bis-sulfone reagents and C) dibromopyridazones.

Another cysteine employing reaction, which is not using the nucleophilicity of the sulfhydryl group, is the generation of an electrophilic center in form of a dehydroalanine, throughout a β-elimination of thiolate from the cysteine moiety. The dehydroalanine can then further be used for the addition of a wide variety of tags (Scheme 2A). There are different ways described in literature to achieve the β-elimination of thiolate ranging from oxidative- and reduction-elimination to base mediated eliminations to bis-alkylation-eliminations (Scheme 2B). Base mediated elimination of disulfides can be used on peptide level in organic solvents by strong bases but could not achieve dehydroalanine formation on protein level. Also reduction-elimination is used successfully on peptide level in organic solvents with strong bases, but could only be transfer to a protein substrate to some extend if this is stable to high pH. For proteins the most feasible procedures are oxidative-elimination or bis-alkylation-elimination.[143] Recent studies showed that the oxidative elimination of cysteines to dehydroalanine could be achieved under relatively mild conditions, which are compatible with protein substrates. Here *o*-mesitylenesulfonylhydroxylamine (MSH, Scheme 2C) was used to selectively amidate cysteine followed by a fast elimination to dehydroalanine.[144]

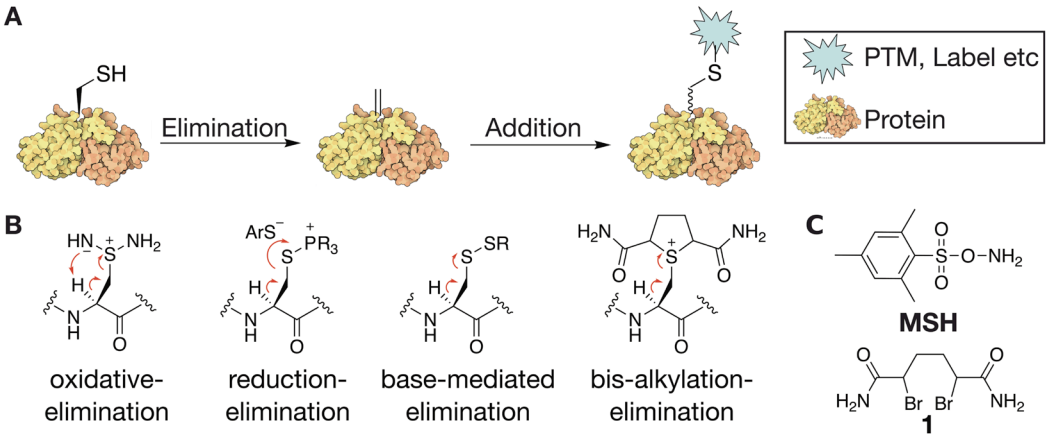

Scheme 2: A) Cysteine labeling *via* dehydroalanine generation B) Different β-elimination strategies C) Reagents used in oxidative-elimination and bis-alkylation-elimination.

In addition to this, the Davis group reported in a comprehensive study of dehydroalanine formation *via* different pathways, that the use of MSH on a more complex protein substrate resulted in non-selective amination. In contrast bis-alkylation-elimination could be evolved to work under mild conditions.[143] Here, the Davis group reported that the water soluble α,α'-dibromoadipic-bis-amide **1** (Scheme 2C) can yield the dehydroalanine after one hour at 37°C at pH 7 - 8 for different protein substrates. After creation of dehydroalanine, the electrophilic center can be used for nucleophilic thiol addition reactions with labels or posttranslational modification analogues and could be shown on a number of model peptides and proteins. [140,143,145–147] However, the drawback of this method is the generation of a racemic mixture upon addition to the dehydroalanine.

Despite the high number of cysteine modifiying methods still new reactions for thiol functionalization are developed, due to the undeniable power of the sulfhydryl moiety. A very impressive approach towards thiol functionalization was reported first in 2015 by the Buchwald and Pentelute labs. They used organometallic palladium reagents to arylate cysteine moieties in peptides and proteins.[148] *Via* the aryl moiety they could introduce affinity tags, fluorophores, bioconjugation handles and even drugs, chemoselectively into proteins (Scheme 3A).

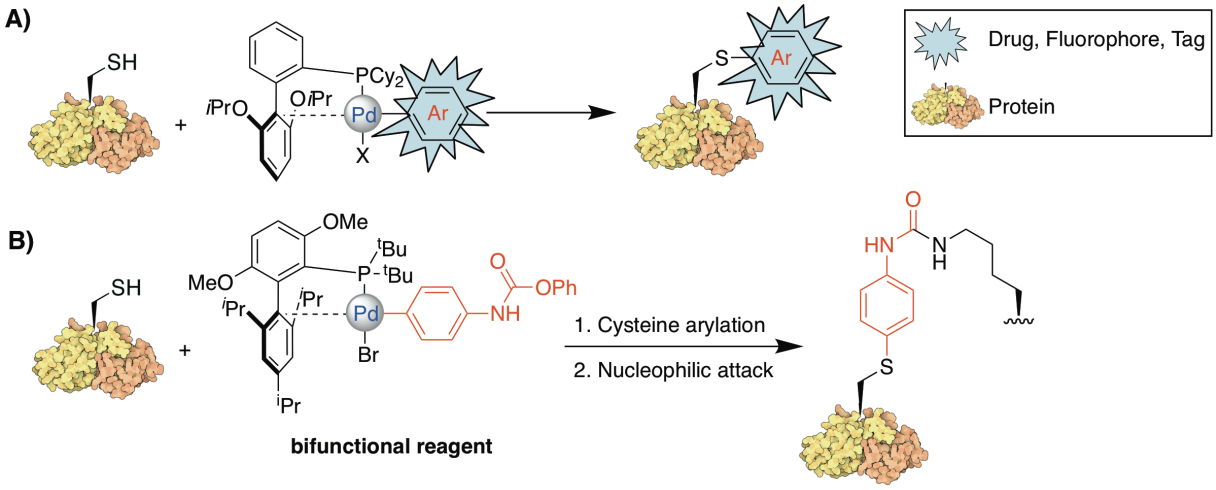

Scheme 3: Organometallic reagents for cysteine bioconjugation. A) Palladium mediated arylation of cysteine. B) Cross-linking of cysteine and lysine carrying proteins.

They also showed the crosslinking capability in peptides containing two cysteines of the palladium oxidative addition. In 2018 thy furthermore showed the usage of their palladium complex in a crosslinking approach between cysteines and lysine side chains.[149] by introducing an electrophilic group into the palladium complex they created a bifunctional reagent, which is able to first undergo palladium mediated cysteine arylation followed by reaction with a neighboring nucleophile at the aryl moiety (Scheme 3B). Throughout this

bifunctional reagent they achieved peptide as well as protein crosslinking in an intra- or intermolecular fashion.

4.3.1.2 Reactions on aspartic and glutamic acids

Carboxylic acid side chains from aspartic and glutamic acids are not often targeted for bioconjugation, due to the carboxylates low reactivity in water, which demands activation in order to be used as good electrophile. When activating carboxylates with *e.g.* carbodiimides, the resulting activated acylisoureas is prone to hydrolyze with solvent water or react with different nucleophiles found in the protein structure itself, rendering them not chemoselective.[150,151] Lately the Raines lab made use of carboxylates for bioconjugation by *O*-alkylating them with diazo compounds, which is yielding covalent ester bonds. These esters can be cleaved by naturally occurring esterases, making this conjugation especially interesting for a pro-drug inspired approach to bioconjugation.[152]

The groundwork for their studies was laid in the 1960s. Back then stabilizing α-diazo amides was found to be limiting their promiscuity to a certain extend, showing that they are mainly reacting with carboxylic acids in aqueous environment. However, this reaction was also not fully chemoselective because S-alkylation, N-alkylation and phenol alkylation was found to a certain extend.[153] With this observation even more stabilized diazo-compounds were explored and used in protein-based studies, especially for the mapping of reactive carboxylic acids in a protein structure. Nonetheless, a chemoselective and hydrolysis stable compound could never be generated and made the use of the O-alkylation by diazo-compounds rather unpopular.[154] Inspired by the overall versatility of diazo-compounds (also see chapter 4.3.2.2.) the Raines Lab set out to accomplish the task of tuning a diazo-compound towards selectivity and stability. They achieved this throughout the basicity of either 9-diazofluorene or α-diazo (*p*-methylphenyl) glycin derivatives, which enable an efficient esterification of carboxylates in water that can further be cleaved by esterases (Scheme 4).[155,156] Even though the diazo-compound is still prone to hydrolysis this side reaction was tuned to be a slow process, by balancing the basicity of the diazo compound, between being too low to not react and too high to lead to hydrolysis.

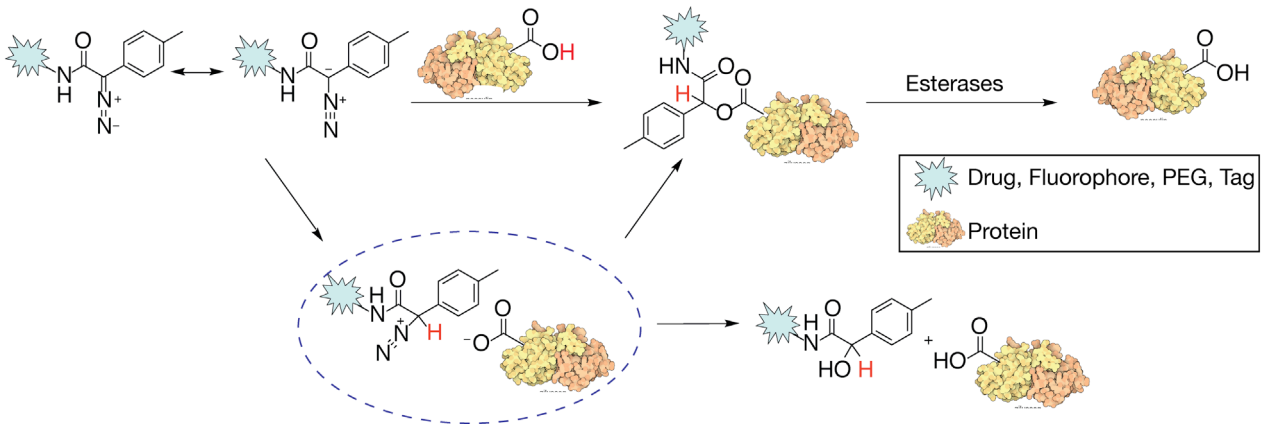

Scheme 4: Bioreversible esterification of carboxylic acids on proteins using diazo-compounds. Presumptive mechanism according to Roberts et al..[157]

4.3.2 Bioconjugation reactions on unnatural amino acids

When carrying out bioconjugations in a more complex environment, for example in a cell, in a complex protein mixture or on a multifunctional peptide, one can still aim for a truly site specific and defined labeling. For this purpose it is inevitable to employ bioorthogonal reactions. These are reactions, which can only occur between two unnatural moieties that are not found in a native protein or cellular environment.[125]

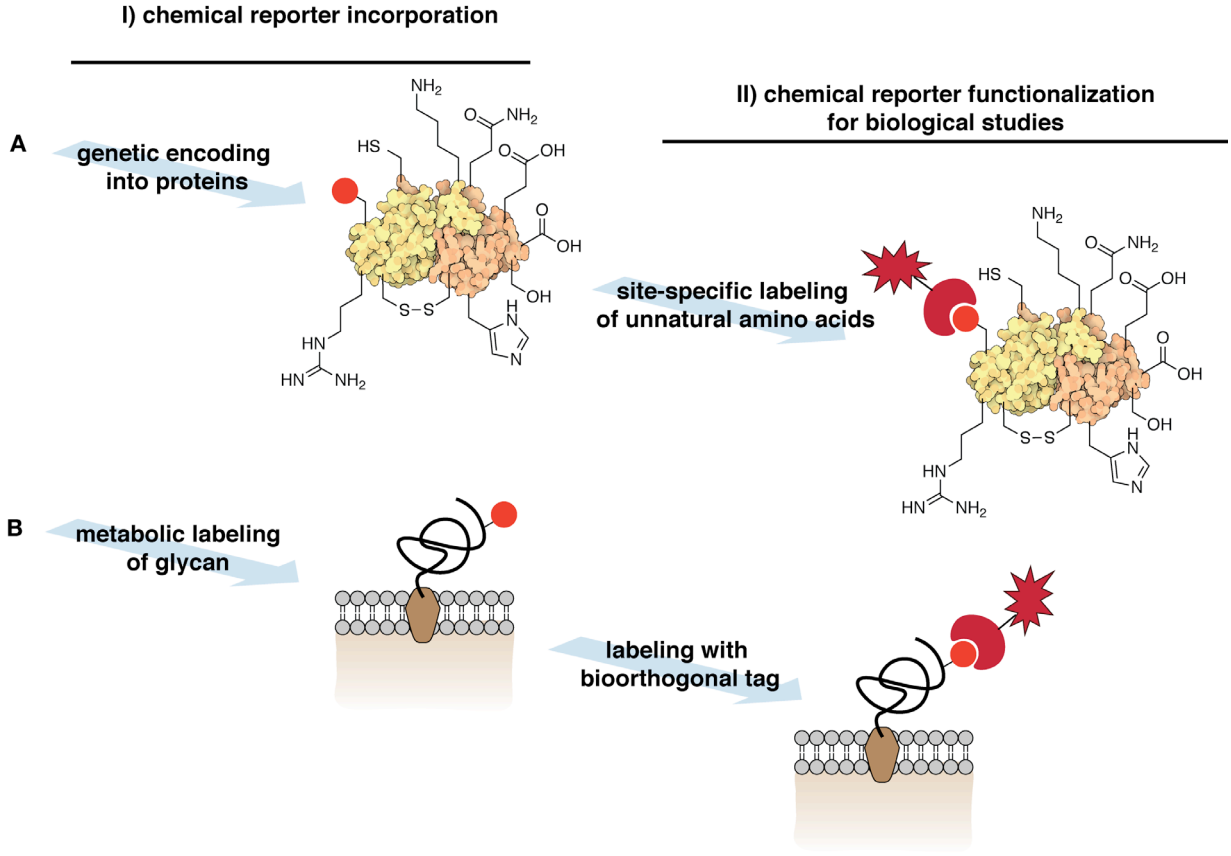

Figure 12: Bioorthogonal chemical reporter strategy A) Chemical reporter usage for protein functionalization B) Chemical reporter usage in cellular glycan structures.

Glycans with a functional handle can for example be metabolically incorporated into the glycocalyx of the cell (Figure 12B). Alternatively non-native amino acids with bioorthogonal functional groups can be incorporated into proteins of interest by genetic code expansion (Figure 12A). These so-called chemical reporters can then be functionalized site specifically with a bioorthogonal tag (Figure 12).[158] For the incorporation of bioorthogonal handles into proteins major advances have been made in the area of genetic code expansion techniques, throughout which unnatural amino acids can be incorporated into proteins genetically.[159,160] Functional groups that can be introduced into peptides and proteins and further reacted in a bioorthogonal way comprise azides, alkynes, strained alkynes, ketones, alkenes, strained alkenes, tetrazoles, anilines, 1,2-amino thiols, aryl halides and boronic acids.[161] One of the most versatile and popular functional group is the azide, because it can undergo numerous bioorthogonal reactions, is inert in aqueous environment and one of the smallest modifications possible.

4.3.2.1 Alkyne azide cycloadditions

The preparation of triazoles from azides and alkynes by a 1,3-dipolar cycloaddition is known since the 19th century[162] but was famously driven forward by Rolf Huisgen between the 1950s – 1970s using organic reactions at high temperatures[163]. The starting point of the immense attention this cycloaddition has gained in the last 15 years in life science applications, are two reports from 2002 from the Sharpless and Meldal labs.[164,165]

Here, it was shown that the cycloaddition reaction between azides and alkynes can be catalyzed by a copper (I) catalyst, which promotes the cycloaddition regiospecifically to the 1,4-disubstituted 1,2,3-triazole, at room temperatures in aqueous environment with increased reaction rates, compared to the thermal process used by Huisgen (Scheme 5A).[166] These properties are exactly what is needed for a truly bioorthogonal reaction and the reaction was therefore used in numerous applications in the life science field. To enhance the efficiency of the reaction, copper (I) stabilizing ligands were developed and advanced over the years. Mostly polytriazoles like TBTA[167], THPTA[168] or BTTAA[169] are being used as simple additives (Scheme 5B). Not only do these ligands stabilize the copper (I) by complexation, but also reduce its cytotoxic effect by coordinating to copper. Recently the *in cellulo* use of copper catalyzed alkyne azide cycloaddition (CuAAC) using the BTTAA ligand conjugated to a CPP has been reported.[170] But as copper is still avoided *in vivo* due to its cytotoxicity[171] new ligands are being developed in order to increase the copper activity and to be able to lower the copper content in the reaction. Betaine (**2**) is one ligand that can be

used with copper contents as low as 2.5 ppm, making it rather safe to use it also in *in vivo* settings.[172]

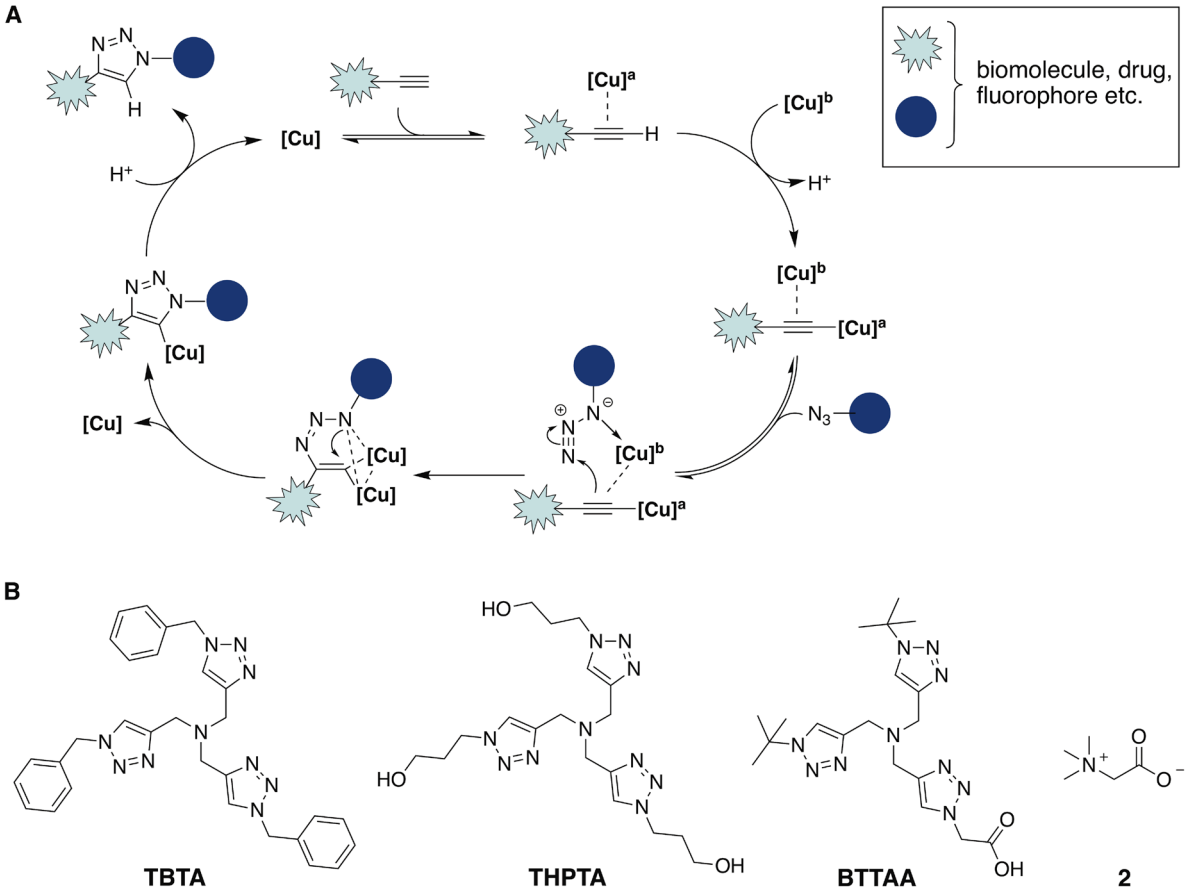

Scheme 5: A) Mechanism of the CuAAC like proposed by Worreell *et al.*[173] B) Ligands for the stabilization of copper(I) in the CuAAC.

Parallel to the advances of improving copper ligands, researchers still aimed to use no metal at all for bioconjugations. Affords were made to establish other means of activation to facilitate the cycloaddition and were found by the Bertozzi lab in old reports, which showed that highly strained cyclic alkynes undergo fast reactions with organic azides.[174] Inspired by these studies they synthesized a simple cyclooctyne (OCT, Figure 13), conjugated it to a biotin and could show rapid cycloaddition to an azide-bearing carbohydrate, which was metabolically incorporated into live cells without any catalyst needed.[175] It was simply enough to use the enthalpically favored release of ring-strain as catalytic driving force and therefore they termed this reaction strain promoted alkyne azide cycloaddition (SPAAC). Due to low water solubility and slower reaction kinetics compared to CuAAC, the first cyclooctynes were synthetically improved to exhibit faster kinetics and lower lipophilicity over the last years. Higher reaction rates were achieved by electronic activation of the triple bond through electron withdrawing fluorine adjacent to the alkyne (DIFO) (Figure 13).[176] Overall ring strain on the other hand was improved by fusing rigid aromatic rings to the core

octyne (DIBO or the more hydrophilic DIBAC) (Figure 13).[177,178] Due to the demanding synthesis of these improved cyclooctyne derivatives, a more feasible synthesis was also probed by fusing cyclopropane to the cyclooctyne (BCN), which also increased ring strain (Figure 13).[179] The downside of increasing the reactivity of the alkyne however is the loss of specificity towards azides and the increase of thiol-yne side reaction to a certain degree.[180]

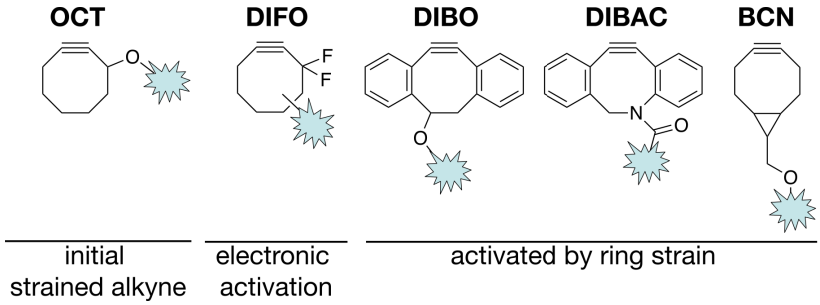

Figure 13: Different strained alkynes used for SPAAC.

4.3.2.2 Other cycloaddition reaction

In the search for more reactions that are compatible in a bioorthogonal chemical reporter strategy, strained alkynes were also reacted in a 1,3-dipolar cycloaddition with nitrones to yield N-alkylated isoxazolines (Scheme 6A).[181,182] This so called strain promoted alkyne-nitrone cycloaddition (SPANC) was significantly faster than the cycloaddition with azides. The reaction was used in the bioorthogonal labeling of proteins[181,183,184] and cellular surfaces[185]. Even though the reaction exhibits fast kinetics comparable to CuAAC, the incorporation of the nitrone reporter is not trivial. Nitrones are prone to hydrolysis and are in many cases incorporated by an *N*-terminal serine, which upon oxidation to an aldehyde can be converted to the nitrone. This oxidation step on protein level can be harmful to the protein structure and is furthermore limiting the conjugation to the *N*-terminal site.

Another 1,3-dipolar addition known is the reaction of diazo compounds with alkynes and alkenes (Scheme 6B).[163,186] The reaction was tuned and could give higher reaction rates compared to azides.[187,188] Because diazo compounds are more electron rich than azides, they also exhibit reactivity towards unstrained terminal alkenes and alkynes.[189–192] Stabilized diazo groups were further shown to be metabolically incorporated into mammalian cells.[193] One downside to the reaction is however the diazo group's tendency to undergo hydrolysis.

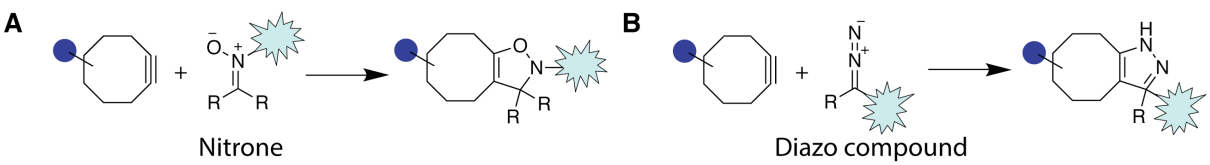

Scheme 6: Strain promoted labeling using A) nitrones (SPANC) B) diazo compounds.

Next to the 1,3-dipolar cycloadditions, Diels-Alder-Reactions achieved a lot of attention in the field of bioorthogonal reactions. It was observed that tetrazines react in an extremely fast fashion with strained alkenes and alkynes like transcyclooctene, norbonene or BCN in an inverse-electron demand Diels-Alder reaction (IEDDA) (Scheme 7A).[194,195] Its reaction rate is outcompeting all known bioorthogonal reactions with nitrogen gas as only byproduct.[124] The reaction kinetics for this bioorthogonal reaction were further fine-tuned by changing the electron deficiency of the substituents on the 1,2,4,5-tetrazine core motif or by modulating the ring strain and electronic effects of the dienophile (Scheme 7B/C).[196]

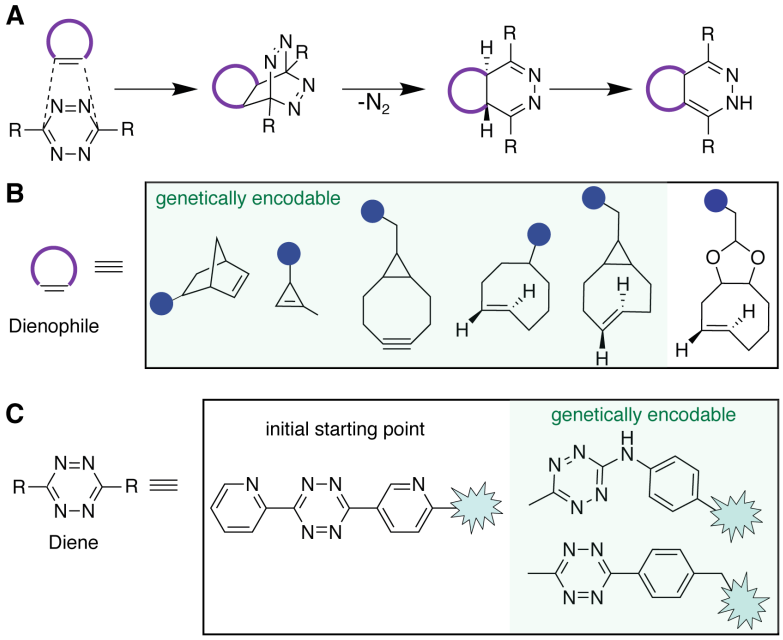

Scheme 7: A) Reaction mechanism of the IEDDA reaction Overview of B) dienophiles and C) dienes used in bioconjugations.

In early reports, the rather bulky functional chemical reporters were incorporated into proteins by other protein conjugation strategies, which resulted in a two step functionalization approach.[194,195] Due to its remarkable reaction kinetics many groups were interested in genetically encoding possibilities for strained alkenes and alkynes as well as tetrazines, which would elevate the reactions applicability immensely. Only four years after the first description of the IDDEA reaction in a bioorthogonal context, the genetic encoding of norbonenes[197,198], transcyclooctenes[197,198], cyclooctynes[198], bicyclononynes[197] and tetrazines[199] was accomplished, allowing convenient cell surface and intracellular labeling of proteins (Scheme 7B/C). Due to the fast kinetics and the high fluorogenicity of tetrazines IEDDA was also exploited for fluorogenic applications and is the go to reaction for bioorthogonal labeling *in vivo* nowadays.[200–203]

4.3.2.3 Staudinger type reactions

Another reaction in which azides are participating are Staudinger type reactions. In the classical Staudinger reaction reported by Hermann Staudinger in 1919 an azide is reacting with a phosphine to an iminophosphorane, which hydrolyses to phosphine oxide and amine in water (Scheme 8A).[204] In 2000 the Bertozzi lab discovered the utility of the Staudinger reaction for biomodification means, which they called Staudinger ligation (Scheme 8B).[205] They reported that one could label metabolically incorporated azido carbohydrates with a biotin-phosphine on cellular surfaces by using a version of the Staudinger reaction in which the phosphine and an electronic trap are tethered to the same phenyl group. The aza-ylide formed when azide and phosphine react can attack the internal electrophile and create an amide that is ensuring the covalent bond between carbohydrate and functional moiety. In mechanistic studies they could show that the rate-limiting step is the formation of the phospazide throughout the nucleophilic attack of phosphine on the azide. Hence electron donating groups on a phenylgroup that is directly attached to the phosphorous atom were shown to accelerate the rate of reaction.[206]

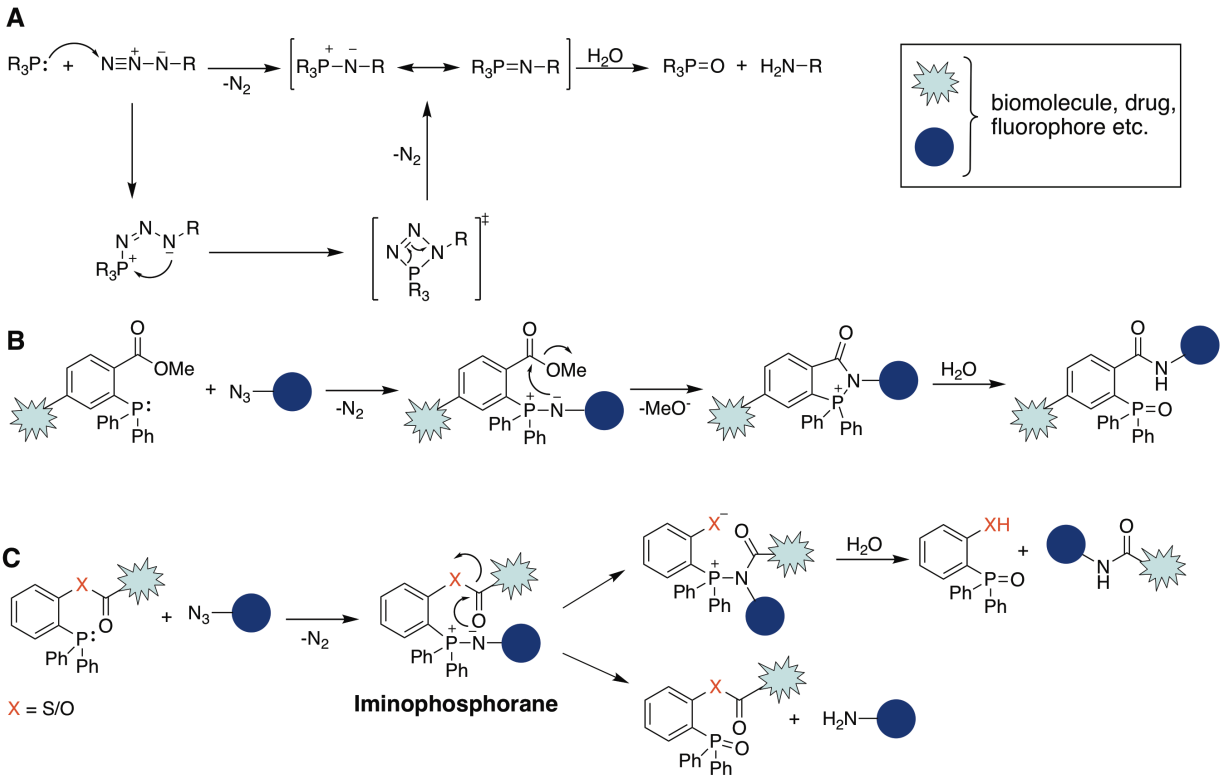

Scheme 8: A) Mechanism of the Staudinger Reduction. B) Mechanism of the Staudinger Ligation. C) Mechanism of the traceless Staudinger Ligation.

Also in 2000 the Bertozzi and the Raines lab further expanded this reaction to a traceless version. In this variant the phosphine oxide can be cleaved throughout the hydrolysis step,

which is generating a native amide bond (Scheme 8C).[207,208] The reaction was shown to be chemoselective and could be used on peptide level retaining stereoselectivity of the linked amino acids.[209–212] From here on many aspects of the Staudinger ligation were studied in detail. The electron density on the phosphorous atom was shown to play an important role in the reaction rate. It was demonstrated that an electron-donating group on the phospinothiol is accelerating the intermolecular reaction between azides and phosphines as observed for the non-traceless Staudinger ligation. The more electron-donating the substituent on phosphorous the more protonation of the nitrogen atom in the iminophosphorane stage and hence formation of amine byproduct is observed as well as unwanted oxidation of phosphorous (Scheme 8C). Here, they also stressed the high influence of the solvent on the electron density on phosphorous.[212,213] The Raines Lab also achieved the synthesis of a water soluble phosphine, that can undergo Staudinger ligation in an aqueous environment.[214,215] Furthermore the Hackenberger lab demonstrated the feasible use of borane protection of phosphines against oxidation and showed the deprotection mediated cyclization of peptides using the Staudinger Ligation under acidic conditions.[216,217] The Bertozzi lab could further generate fluorogenic phosphines, which are turned on upon reaction with an azide.[218,219] As described the traceless Staudinger Ligation has been used as bioorthogonal reaction but often the sensitivity of phosphorous towards oxidation and the iminophosphorane's tendency to hydrolyze to its amine, limits this reaction's use and scope.

A further development in Staudinger type reactions was reported in 2009 by the Hackenberger lab. They chemoselectively reacted an azido-functionalized biomolecule with phosphites yielding phosphoramidates (Scheme 9A).[220] The oxygen substituent on phosphorous in phosphites has a strong negative inductive effect that is making the phosphorous atom somewhat more resistant to oxidation. Furthermore changing the substituents on phosphorous is rather easy in phosphites and makes this reaction interesting for the synthesis of functional tags. Due to its versatility, this reaction could be used for the site-specific incorporation of phosphorylated amino acids,[220,221] PEGylations[222,223], lipidations[224], biotin tags[225] or glycans[226,227]. The ability of using this reaction to introduce site specifically photo-caged phospholysines and phosphocysteines into peptides and proteins is especially interesting, because this could not be done in such an elegant fashion before. Most notably is that the photo-caging group is protecting the highly instable post translational modification (PTM) from hydrolysis during the synthesis and storage and is hence opening a new way of generating and validating analytical methods for *e.g.* proteomics.

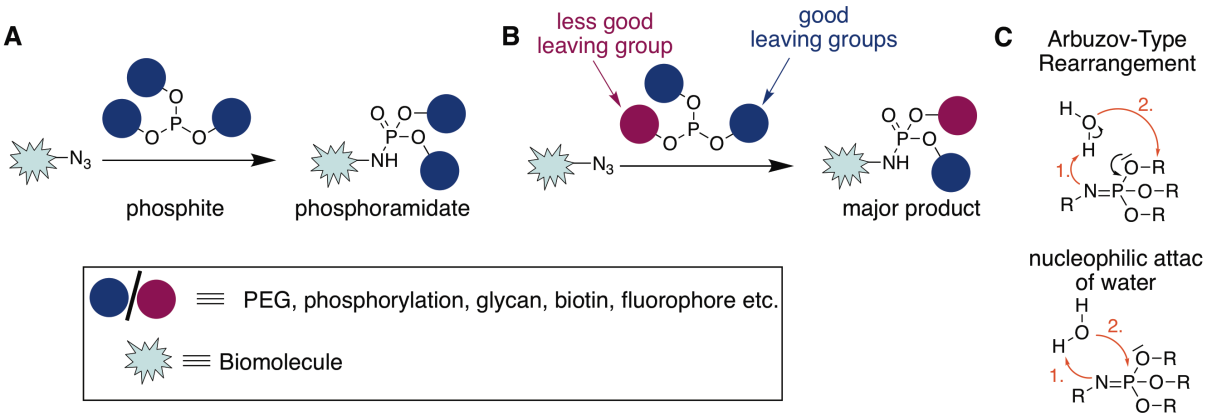

Scheme 9: A) Mechanism of the Staudinger Phosphite reaction. B) The unsymmetrical Staudinger Phosphite Reaction . C) Two different hydrolysis mechanisms.

A characteristic of the trifunctional phosphorous building block is the introduction of two equivalents of functional substituents into the biomolecule, which can be a big advantage *e.g.* for the PEGylation of a protein. If one only wants to incorporate one tag the Hackenberger Lab also showed the versatile usage of unsymmetrical phosphites (Scheme 9B).[224,225] Here they showed that by using good leaving groups like benzyl- and pyridyl-substituents they can control the hydrolysis in the final step, generating the wanted tagged biomolecule in high yields. The hydrolysis could occur here *via* two different pathways, either by an Arbuzov-Type rearrangement or *via* a nucleophilic attack by water at the phosphonimidate stage.[228,229] Another way of ensuring control over which of the three substituents on phosphorous is being kept in the molecule of interest throughout the hydrolysis step, was the development of the flexible Staudinger-phosphonite reaction. Phosphonites consist of one stable phosphorous – carbon bond, that can not be cleaved upon hydrolysis (Scheme 10A) and were first used on a protein for PEGylation purposes.[230]

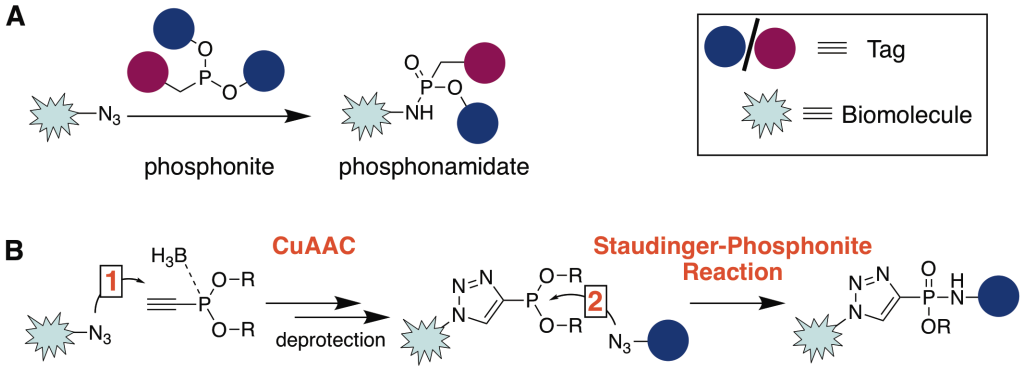

Scheme 10: A) Mechanism of the Staudinger Phosphonite reaction. B) Formal azide-azide conjugation using CuAAC in combination with the Staudinger Phosphonite Reaction.

This reaction was further developed into a formal azide-azide conjugation reaction. Here it was shown that it is possible to introduce an alkyne into the phosphonite, which can be utilized as bioorthogonal handle for the introduction of functional moieties by CuAAC (Scheme 10B).[231–233] The azido-group is undergoing CuAAC as well as Staudinger reactions, which seems to render this combination of reactions not chemoselective to each other, but the Hackenberger lab could show, that by protecting the phosphorous using borane they can totally prohibit the occurrence of the Staudinger phosphonite reaction pathway and only generate the product formed *via* CuAAC (Scheme 10B). Upon borane deprotection they could then achieve the selective reaction with a second azido-functionalized moiety in a Staudinger Phosphonite reaction to yield a phosphonamidate, which formally connects two azido building blocks.

5 Objectives

Peptides form a special class of molecules because they are highly complex in structure and chemical composition, yet easily synthetically accessible. Some functions of full-length proteins were shown to be reducible to an active structural motif. When reduced to this peptidic motif a biological active peptide can be gained. Those small peptidic protein mimics are of great potential when thinking of protein – protein inhibitors, protein – ligand inhibitors or even when using peptides as functional tags, as known for cell penetrating peptides. Hence peptides are getting a lot of attention in the field of peptide therapeutics. When working with biological active peptides in therapeutic or methodological applications one needs to plan strategically due to their complex chemical composition. Here conjugation, as well as modification approaches need to be addressed by chemoselective chemistry.

The aim of this work evolved around those two major topics. For once different biological active peptides were explored as part of an inhibitor, as inhibitor by itself or as functional tag for the cellular delivery of proteins. Furthermore novel chemoselective bioconjugation techniques were explored for the conjugation of biological active peptides to protein or polymer cargos. One bioconjugation technique was further developed for an intramolecular macrocyclization modulation of biological active peptides to stabilize and elevate their function. In detail the four different goals evolving around biological active peptides were:

1. Generation of a multivalent protein – ligand inhibitor for the influenza virus, comprised of a peptidic ligand multivalently displayed on a polymeric scaffold, to block the protein – ligand interaction.

2. Development of a bioconjugation method, designed to react a phosphonite linker chemoselectively with a peptidic tag, upon which a cysteine reactive center is formed that can be reliably conjugated to proteins to yield stable peptide – polymer conjugates.

3. The installation of a structure stabilizing linker into two different peptide motifs, by which these peptides gain a specific biologic function.

4. Conjugation of functional peptide tags to proteins *via* a chemoselective and bioreversible conjugation technique.

Project 1 – Multivalent Peptide-Nanoparticle Conjugates for Influenza-Virus Inhibition

Many cellular recognition processes are of multivalent nature. Underlying monovalent protein – ligand interactions are often weak and only a high number of ligands binding to the target are giving a precise and tight recognition. This also holds true for the first binding step in an influenza virus infection. Here, the influenza virus membrane protein Hemagglutinin (HA) is binding to sialic acids on the cellular surface.

Inspired by nature's example we envisioned the generation of an affine multivalent binder that is build of a peptidic ligand to HA and a polymeric nanoparticle. The HA binding peptide was derived from the CDR domain of a HA binding antibody and was supposed to be chemoselectively conjugated to the nanoparticle in a multivalent fashion. This functional nanoparticle is thought to block HA on the virus surface and hence make an effective binding to the cellular surface impossible. Differently sized nanoparticles decorated with this peptide were supposed to be screened *in vitro* as well as *in vivo.*

Project 2 – Staudinger Induced Thiol Addition as cysteine reactive conjugation

Popular bioconjugation reactions employ cysteine reactive probes, because the high nucleophilicity of cysteines makes chemoselective reactions possible. Furthermore, the low abundance of cysteines and their tendency to be masked in disulfides makes their usage attractive for controlled site-specific modifications. The most popular cysteine reactive conjugation for biological purposes to date is the maleimide reaction, which suffers from instabilities and especially thiol exchange reactions when circulating *in vivo*.

Here we wanted to apply the novel Staudinger induced thiol addition, developed in our lab, as new bioconjugation reaction for labeling proteins throughout a thiol addition of the protein to a modified peptidic tag. The linker molecule was envisioned to be an electron rich alkyne phosphonite that can undergo chemoselective Staudinger phosphonite reaction with an azide incorporated into the peptidic tag. Upon formation of the phosphonamidate the alkyne becomes electron poor, making it susceptible for a thiol addition by a protein. The stability of phosphonamidate as well as the thiol addition product was envisioned to be tested in detail and the applicability should be evaluated *in vitro*.

Project 3 – Intramolecular Staudinger Induced Thiol Addition as new peptide cyclization method

One of the major concern when dealing with biological active peptides that are derived from a certain part of a protein is loss of structural integrity, stability and hence loss of intended function. As already summed up in the introduction, there are numerous ways of installing a covalent linker inside the peptide structure, which is stabilizing its structural characteristic

found in the native protein. Especially for α-helical motifs, the so called “stapling” gained a lot of attention. Furthermore, macrocyclization techniques are more generally used to either render peptides more stable *in vivo* or in special cases to enhance function like shown previously for cCPPs.

In this project we wanted to introduce a novel highly flexible chemoselective macrocyclization method, which can be used for side chain stapling, as well as for macrocyclization reactions. This reaction was intended to be an intramolecular variant of the Staudinger induced thiol addition that has been used in project 2. The first application for this intramolecular reaction was the α-helical stabilization of a peptide sequence, which was derived from the protein structure of a protein involved in a PPI and should pose as inhibitor of exactly this interaction. Another application was thought to be the macrocyclization of a cell penetrating peptide. Upon macrocyclization the cell penetrating peptides ability to transduce a protein cargo into cells was tested.

Project 4 – Diazo-functionalized CPPs for bioreversible esterification of proteins

It has been reported that highly positively charged cell penetrating peptides derived from the RNA binding protein TAT exhibit a high affinity towards the RNA containing nucleolus inside the cell. Because this inherent attraction could pose disadvantages for some cargos that are supposed to be delivered into the cytosol, a bioreversible but covalent bioconjugation method should be explored in this project.

Here an esterification of a protein’s carboxyl groups *via* a diazo building block in an *O*-alkylation was aimed at. The ester linkage was then thought to be cleavable by endogenous esterases inside the cell, to deliver native protein into the cytosol followed by the traceless removal of the peptidic tag. The functionalization was envisioned to be tested by two different routes with either directly functionalizing the peptide with a diazo group at the *N*-terminus or by esterifying the protein with a chemical reporter that could subsequently be functionalized with a peptide. Finally the tagged protein should be evaluated *in vitro,* with high emphasis on the ester cleavage properties.

6 Results and Discussion

6.1 Multivalent Peptide-Nanoparticle Conjugates for Influenza-Virus Inhibition

6.1.1 Introduction to multivalent entry blockers for Influenza virus

The first step of infection with the influenza A Virus (IAV) is its binding to the host cell. The IAV binds to the cell surface *via* its trimeric spike protein hemagglutinin (HA), which recognizes sialic acids (SA) on the glycocalyx of cellular membranes.[234,235] Because the binding affinity of a single HA receptor binding site to a single SA is rather weak (~2 mM), a tight binding can only be achieved throughout multiple ligand-receptor binding events between virus (0.02-0.04 HA/nm) and the SA glycoconjugates on the glycocalyx (0.5-2 SA/nm).[236,237]

Because Multivalency is such a prominent work-principle, the idea of using this phenomenon to build synthetic entry blockers for the influenza virus became popular in the 1990s and was pioneered by Whitesides and coworkers.[236,238–240] The underlying idea was to create an entry blocker that consists of a large number of low affinity SA derived ligands tethered together on a large scaffold, which was envisioned to result in an high HA avidity. The scaffolds used to achieve this were ranging from polymers,[239,241,242] dendrimers,[243–246] liposomes,[238,247] proteins[248] to even gold nanoparticles[249].

Here, polyacrylamide-based inhibitors were one of the most successful scaffolds, giving the most affine binder when large numbers of SA were presented.[239] However those scaffolds had also a major disadvantage, which was their degradation products cytotoxicity.[239,250–253] Hence, using biocompatible polymers for example polyglycerol became desirable and was shown successfully by the Haag lab.[241]

Not only the scaffold was improved from the first reports but also the HA binding ligands. Here alternatives like peptides targeting HA were taken into account, due to their presumed higher affinity and selectivity.[35,254,255] Also peptides can be produced easily and changes to their structure and hence affinity towards a target can be optimized and screened more effectively compared to small molecules (see Chapter 4.2.2.).

In 2006 a peptide derived from the signal sequence of fibroblast growth factor 4 has been shown to inhibit infection by influenza virus.[255] Thereafter, a peptide was optimized for HA binding by selection from a phage-displayed random peptide library.[254] This work also showed a multivalent improvement of its binding properties by conjugation to either an amphiphilic *N*-stearoyl derivative, which formed self-assembled multivalent structures with

enhanced binding capabilities or by presenting up to six peptide copies on a carbosilane dendrimer.[254,256,257]

Memczak *et al*. recently reported peptide sequences directly obtained from an HA binding antibody. They could reduce the CDR binding part of the antibody to a 15 amino acid long wild type peptide sequence (PeB). This sequence they took as starting point for MD simulations and further microarray screens, in which they determined an even more affine double mutant peptide sequence (PeB^{GF}), which binds to HA monovalently in the micromolar range.[33]

6.1.2 Outline of the project

In this project, the aim was the design of a multivalent entry blocker for the influenza A virus (IAV), based on a biocompatible hyperbranched polyglycerol scaffold conjugated to multiple HA binding peptides. Both peptides PeB and PeB^{GF} reported previously by Memczal *et al*. were planned to be conjugated onto polyglycerol and should be compared to each other. Due to their monovalent more affine binding to HA than the natural ligand SA, we envisioned these ligands to have the potential to yield highly affine virus entry blocker, when multiply displayed as IAV binding nanoparticle. Here, also the multivalent difference between the monovalently weaker binding wild type sequence (PeB) and its improved sequence (PeB^{GF}) were of interest.

The conjugation of peptide to the polymer was planned *via* the chemoselective CuAAC, therefor the polymer was functionalized with multiple azido groups and the peptide with a single alkyne (Figure 14). Here, peptide – polymer conjugates with varying scaffold sizes and peptide ligand densities on the polymer were to be synthesized, characterized and the effect of size and ligand density was supposed to be analyzed in *in vitro* assays. Finally the best binders were planned to be tested in an *in vivo* setting.

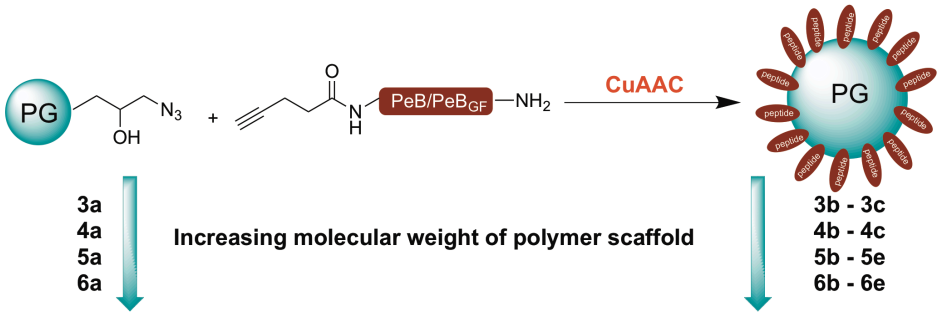

Figure 14: Schematic presentation of the peptide – polymer conjugate synthesis.

6.1.3 Responsibility assignment

Christian P. R. Hackenberger and Andreas Herrmann conceptualized the project. Daniel Lauster conducted all *in vitro* assays, namely the hemagglutination inhibiton assay, infection inhibition assay, and cellular fluorescence assay. He also conducted some of the *in vivo* experiments. The author synthesized the peptides, optimized their purification and conducted the conjugation reaction with the polymers, including purification and characterization by NMR and DLS. Markus Bardua and Ute Hoffmann conducted the *in vivo* experiments. Kai Ludwig analyzed the nanoparticle binding to virus by cryo-EM. Markus Hellmund synthesized the polymers for the conjugation reactions. Ute Hoffmann and Alf Hamann were responsible for the design of the *in vivo* study. Christoph Böttcher designed the cryo-EM experiments. Rainer Haag conceptualized the polymer synthesis.
This chapter was published under the title “Multivalent Peptide-Nanoparticle Conjugates for Influenza-Virus Inhibition” in *Angew. Chem. Int. Ed.* **2017**, *56*, 5931–5936.[258] The author, Daniel Lauster, Christian P.R. Hackenberger and Andreas Herrmann wrote the manuscript. Markus Bardua, Kai Ludwig, Markus Hellmund, Ute Hoffman, Alf Hamann, Christoph Böttcher and Rainer Haag proofread the manuscript.

6.1.4 Synthesis of peptide-polymer conjugates

We started our investigations into multivalent peptide – polymer conjugates by first synthesizing the peptidic ligands. The hydrophilic and biocompatible polyglycerol scaffolds functionalized with azido groups (Figure 15A) were obtained from the lab of Prof. Dr. Rainer Haag. In order to be able to conjugate the peptides to the azido-polymer *via* CuAAC, the HA binding peptides PeB and PeB^{GF} were synthesized with an alkyne handle *N*-terminally. The 15 amino acid long peptide sequences PeB (wild type) and PeB^{GF} (mutant) only differed by two site mutations (Figure 15B). It has been reported that these two mutations in PeB^{GF} increase the affinity of the wild type PeB towards HA.[33] However, these mutations also render PeB^{GF} more hydrophobic compared to PeB, which could be of relevance in *in vitro* and *in vivo* studies.
PeB and PeB^{GF} were synthesized *via* solid phase peptide synthesis and both were *N*-terminally caped with 4-pentynoic acid. After acidic cleavage of the peptide from rink-amide resin using a TFA/TIS/water mixture the crude peptides were purified by preparative HPLC and gained in moderate yields of 14%. It was observed that both peptides are badly soluble in acidic aqueous media, in which they behave gel-like. Therefore, purification of the

concentrated crude peptide had to be carried out under basic conditions (pH 9.0) in which both peptides were well soluble.

With both alkyne-functionalized peptides in hand the screening of the optimal polymeric scaffold was started. Here, we chose to investigate the antiviral potential of four different polymers with molecular weights ranging from 7.7 kDa to 340 kDa **3a – 6a**. Furthermore the ligand density on higher molecular weight compounds was analyzed, because it was emphasized previously in a study based on PAMAM as polymeric scaffold, that low ligand density and larger particle sizes can positively influence the inhibitory potential.[259] For the synthesis of peptide – polymer conjugates with lower ligand densities polymeric starting material with an azide degree of functionalization of 10% was chosen (**$5a_{10\%}$**/ **$6a_{10\%}$**) and for peptide – polymer conjugates with higher ligand densities a polymer with an azide degree of functionalization of 30% was chosen (**$5a_{30\%}$**/ **$6a_{30\%}$**). Meaning that either 10% or 30% of all polymeric alcohol end groups were transferred into an azide.

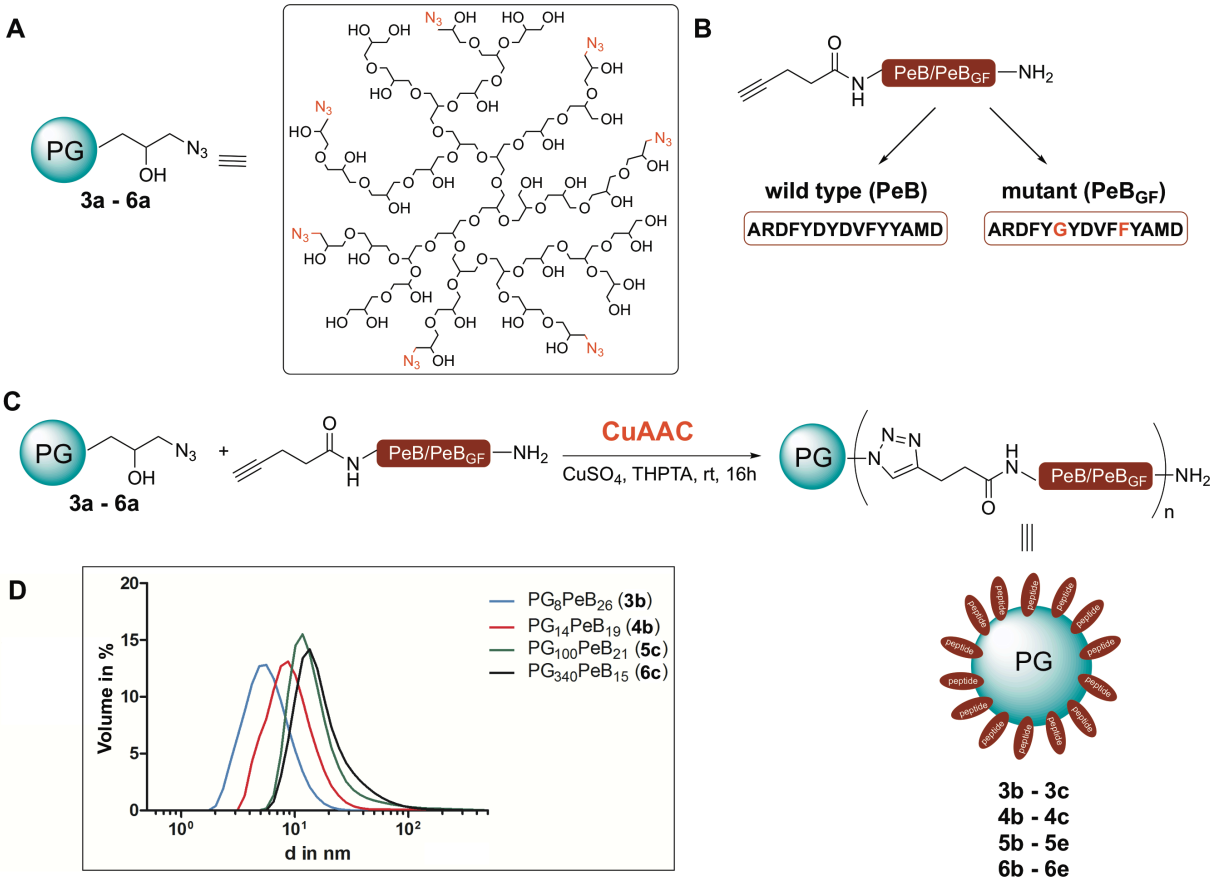

Figure 15: A) Representative structure of hyperbranched polyglycerol. B) Peptide sequence of the to be conjugated peptides PeB and PeB^{GF}. C). CuAAC conjugation between peptide and polymer (for polymer sizes see table 1). D) DLS data for screening of different molecular-weight dendritic PGs conjugated to PeB peptides.

The CuAAC between peptide and polymer was carried out in basic ammonium bicarbonate buffer (pH 9.0) at room temperature overnight (Figure 15C). Here, the basic medium was

again chosen to facilitate good solubility of the peptides. The reaction mixture was pre-purified by dialysis over several days against a mixture of 10 mM ammonium bicarbonate buffer (pH 9.0) with 10% acetonitrile, followed by size exclusion chromatography. Finally, the conjugation products were analyzed by NMR spectroscopy (see Chapter 8.2.3 Figure 8.3 and Chapter 10 Figure 10.1. to 10.11) and DLS (Figure 15D and Figure 8.4.) to obtain the degree of functionalization, number of ligands and the diameter of each conjugate (Table 1). Individual ligand densities for each compound could be determined from these parameters. One has to note that the ligand number for all nanoparticles is only an average number, which is based on the polymeric molecular weight distribution of the polyglycerol itself (see Chapter 8.2.2. Table 8.1).

Table 1: Overview over Polyglycerol – Peptide conjugates.

No.	Compound	M_p core [kDa][a]	DF[b] [%]	Lig.[c]	Diameter[d] [nm]	Density[e] [Lig./nm^2]
3a	dPG_8	7.7	0	0	2.4 ± 0.1	0.0
3b	dPG_8PeB_{26}	7.7	26	24	6.4 ± 0.7	1.3
3c	$dPG_8PeB^{GF}_{30}$	7.7	30	31	10.3 ± 0.6	1.7
4a	dPG_{14}	14.4	0	0	5.1 ± 0.5	0.0
4b	$dPG_{14}PeB_{19}$	14.4	19	37	11.3 ± 3.1	0.5
4c	$dPG_{14}PeB^{GF}_{19}$	14.4	19	36	11.3 ± 1.4	0.5
5a	dPG_{100}	100	0	0	8.0 ± 0.4	0.0
5b	$dPG_{100}PeB_8$	100	8	108	16.5 ± 2.7	0.5
5c	$dPG_{100}PeB_{21}$	100	21	284	20.2 ± 2.2	1.4
5d	$dPG_{100}PeB^{GF}_{10}$	100	10	135	22.4 ± 2.8	0.7
5e	$dPG_{100}PeB^{GF}_{29}$	100	29	392	15.1 ± 0.7	2.0
6a	dPG_{340}	340	0	0	11.7 ± 0.4	0.0
6b	$dPG_{340}PeB_9$	340	9	414	17.9 ± 0.9	1.0
6c	$dPG_{340}PeB_{15}$	340	15	690	24.8 ± 4.3	1.7
6d	$dPG_{340}PeB^{GF}_{10}$	340	10	460	27.6 ± 5.9	1.1
6e	$dPG_{340}PeB^{GF}_{16}$	340	16	736	29.8 ± 1.4	1.8

a) Molar mass at peak maximum (M_p) of polyglycerol. b) Degree of functionalization of all end groups determined by ^{1}H-NMR c) Average number of all ligands (Lig.) calculated from DF. d) Diameter determined from DLS measurements in 10 mM ammonium bicarbonate buffer (Values represent the means with the standard error of the mean (s.e.m.) of at least three measurements). e) Ligand density based on mean diameter of a sphere divided by the amount of ligands.

After characterization, all compounds were subjected to a hemagglutination inhibition assay (HAI) to assess their inhibitory potential. Therefore, the IAV Aichi H3N2 (X31) was pretreated with different concentrations of a peptide – polymer conjugate, followed by the incubation with a suspension of human erythrocytes. Influenza virus binding toward red blood cells could be observed by formation of a gel like clot, so called agglutination. Therefor, the lowest concentration of peptide – polymer nanoparticle, which was able to inhibit this visible agglutination, was defined as inhibition constant (K_i^{HAI}) and was determined in at least three replicates (Table 2) by Daniel Lauster in the Herrmann Lab.

Table 2: Results of HAI assay with human erythrocytes and infection inhibition assay of MDCK II cells. n.d. = not determined; - = no inhibition or binding.

No.	$K_i^{HAI}{}_{Lig}$ [µm][a]	$K_i^{HAI}{}_{NP}$ [nm][b]	$IC_{50\ Lig}$ [µm][c]	$IC_{50\ NP}$ [nm][d]
3a	-	-	-	-
3b	54 ± 15	2250 ± 629	-	-
3c	69 ± 9	2218 ± 295	-	-
4a	-	-	-	-
4b	2 ± 1	62 ± 14	-	-
4c	4 ± 1	99 ± 32	34.6 ± 0.1	960.6 ± 2.7
5a	n.d.	n.d.	-	-
5b	31 ± 0	289 ± 0	0.8 ± 0.1	7.5 ± 1.0
5c	75 ± 29	264 ± 102	4.4 ± 0.6	15.4 ± 0.6
5d	33 ± 8	247 ± 62	2.5 ± 0.1	18.5 ± 0.5
5e	42 ± 8	106 ± 21	17.3 ± 0.1	44.2 ± 0.2
6a	-	-	-	-
6b	4 ± 1	9 ± 2	0.3 ± 0.1	0.6 ± 0.3
6c	163 ± 22	236 ± 31	69.5 ± 0.0	100.7 ± 0.1
6d	12 ± 3	25 ± 6	0.2 ± 0.0	0.4 ± 0.1
6e	15 ± 6	20 ± 7	0.9 ± 0.0	1.2 ± 0.1

a) Value for HAI assay for ligand concentration with the s.e.m. ($n \geq 3$). b) Value for HAI assay for nanoparticle concentration with the s.e.m. ($n \geq 3$). c) IC_{50} values derived from a four parametric logistic fit shown with an asymmetric standard error (SE) of the logIC_{50}.

This assay showed, that increasing the molecular weight of the polymer backbone results in a drop of the K_i^{HAI} to low nanomolar values (Table 2, **6b**, **6d**, **6e**). Furthermore, it was observed that a higher degree of ligand functionalization was indeed not substantially increasing the inhibitory potential of the conjugate. The same trend was observed in

infection inhibition experiments, where cell viability of MDCK II cells was measured after incubation with a virus – inhibitor mixture. In this assay IC_{50} values in the sub nanomolar range were observed for the largest nanoparticles with low peptide densities (Table 2, **6b**, **6d**). From those values a multivalent enhancement factor of 129 for PeB and 136 for PeB^{GF} could be deduced (for calculation see Chapter 8.2.3). We appointed the drastic increase in effectiveness for larger constructs to the steric shielding character of the multivalent scaffolds, which can contribute additionally to the affinity of the peptidic ligand.[260]

In the HAI as well as the infection inhibition assay it was observed, that the difference in binding affinity between the monovalent mutant peptide PeB^{GF} and the wild type peptide PeB did not transfer toward the multivalent scenario. To investigate this further, a microscale thermophoresis (MST) experiment was set up to measure directly the binding of the best binders (**6b** and **6d**) toward fluorescently labeled X31 virus. Here, it was observed for the nanoparticles with a 340 kDa scaffold and a low ligand valency, that the mutant peptide nanoparticle $dPG_{340}PeB^{GF}{}_{10}$ **6d** is indeed binding IAV with 10 times higher affinity (KD_{app} of 3.1 µM peptide or 6.8 ± 1.1 nM multivalent nanoparticles) compared to the wild type peptide nanoparticle $dPG_{340}PeB_9$ **6b** (KD_{app} of 36.6 µM or 88.3 ± 13.6 nM of the multivalent nanoparticles) (Figure 16A). Therefore, we suspect that in the *in vitro* experiments pure affinity is not the sole factor in a successful inhibition.

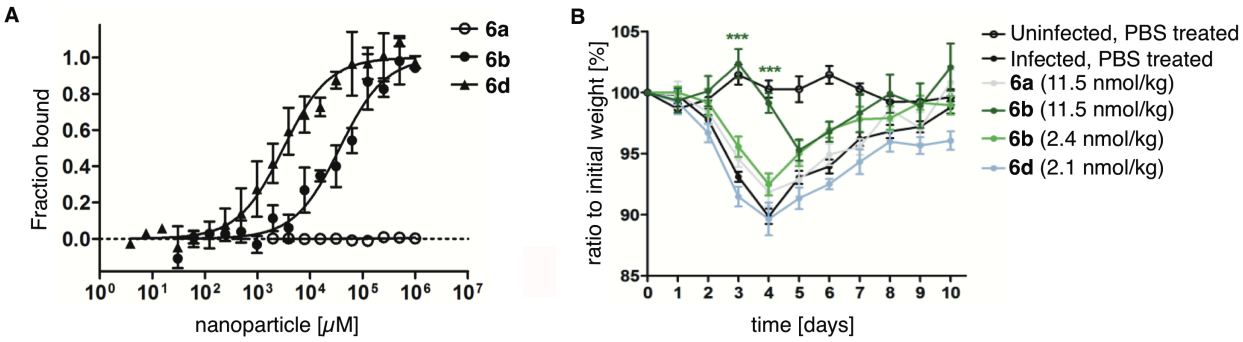

Figure 16: A) MST measurements with 340 kDa PGs against fluorescently labeled X31 virus. Error bars indicate the s.e.m. (n ≥ 3). B) *In vitro* infection test in BALB/c mice treated with pre-incubated X31 at indicated inhibitor amounts by an single intranasal dose. Inhibitor concentrations are referring to the nanoparticle concentration.

To further look into the binding between peptide – polymer conjugates and virus, cryo-EM microscopy was conducted by Dr. Kai Ludwig in the lab of Prof. Dr. Böttcher. It was observed that nanoparticles without any peptide attached did not interact with the virus. In contrast, incubating virus with **6d** clearly showed the virus surface being covered with nanoparticle (Figure 17).

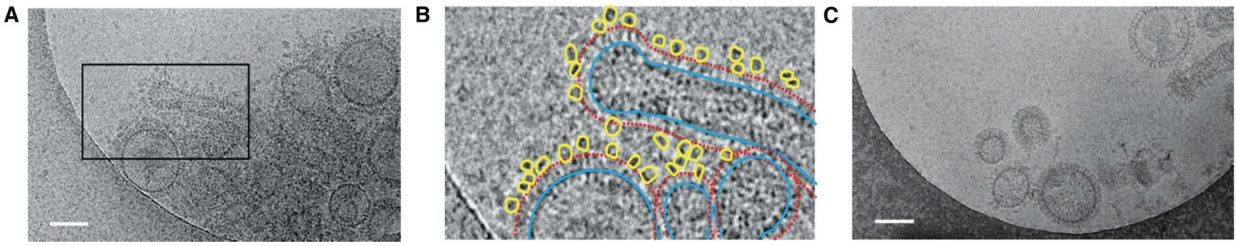

Figure 17: A) Cryo-EM image of **6d** incubated with Inluenza Virus X31. B) Detailed view of black frame in A. Bound nanoparticles **6d** are outlined in yellow, virons in blue and corona formed by HA in red. C) Incubation of X31 with negative control **6a.** All scale bars corresponds to 100 nm.

After these promising *in vitro* results, we aimed to test the peptide – polymer nanoparticles **6b** and **6d** in *in vivo* experiments. Here, sedated 8-weeks old BALB/c mice (body weight ~20 g) were infected upon intranasal administration with an inhibitor-virus mix and were monitored daily for 10 days on their body weight. The infection is manifested in the mouse model by a gradual loss of weight until day four and a slow recovery of weight until day 10 (Figure 16B; see positive control (Infected, PBS treated)).

While the control construct dPG_{340} **6a** did not protect from infection, mice treated with a single dose $dPG_{340}PeB_9$ **6b** (11.5 nmol/kg) maintained their body weight until day 4 (Figure 16B) but then started to loose weight on day 5. This could pinpoint toward peptide degradation and hence a second inhibitor dosing on day 4 would be necessary to continue protection from infection. However, such a procedure was not applicable in the give *in vivo* experiment.

A similar dosage with the $dPG_{340}PeB^{GF}_{10}$ **6d** was not feasible as we were facing solubility problems at higher concentrations. Lower inhibitor dosages with both inhibitors at ~2 nmol/kg concentrations did not significantly protect from infection. Nevertheless, mice treated with $dPG_{340}PeB_9$ **6b** protected the mice to a substantial higher extent as $dPG_{340}PeB^{GF}_{10}$ **6d** at similar inhibitor dosage. Because we observed lower solubility for PeB^{GF} , we cannot exclude unspecific binding of the coated nanoparticles to respiratory structures, interfering with virus inhibition. Already during handling of conjugates carrying PeB^{GF} and handling of the peptide alone, it was appreciable that for PeB^{GF} already slight changes to the pH resulted in some aggregation.

All in all, comparing $dPG_{340}PeB_9$ **6b** with multivalent siallyllactose (SL) presenting PAMAM dendrimes (50 µmol SL/kg)[259], **6b** was about ten times more efficient in protecting infection of mice (4.8 µmol PeB ligands/kg), revealing an advantage of more affine peptidic ligands over SA.

6.1.5 Conclusion and Outlook

In conclusion we could show the synthesis and application of a non-toxic influenza virus inhibitors based on a multivalent covalent peptide display on dendritic polymers. The highly potent influenza virus inhibitors effectiveness can be explained by the multivalent effect of numerous peptidic ligands binding towards the virus in co-occurrence with a steric shielding by the polymeric backbone. Although biocompatible dPGs decorated with PeB^{GF} showed higher affinity compared to those conjugated to PeB in MST experiments, we concluded that affinity is not the only factor determining effectiveness. Because we observed that the presumed lower affine dPG-PeB conjugates are superior to dPG-PeB^{GF} in some HAI assays, infection inhibition assays and *in vivo* experiments. We presume that the underlying rational behind this behavior is indeed the higher hydrophobicity and hence lower solubility of dPG-PeB^{GF}.

In this project we could show the feasibility of peptide ligands, which can be evolved and further modified to bind to different receptors, which in combination with nanoparticle engineering, opens further avenues to target other disease-relevant multivalent receptors than the one studied. Therefore, as an outlook this concept could be transferred to many different targets. Also one could think of using more defined scaffolds that can already guide the binding by structurally predefining the ligands.

6.2 Staudinger-induced thiol addition as cysteine reactive conjugation

6.2.1 Outline of the Project

In this project we aim to apply a novel chemoselective reaction toward the conjugation of biological active peptides to functional proteins. The focus was on the Staudinger-induced thiol addition, which was recently developed in our lab. The reaction is derived from the Staudinger-phosphonite reaction and its use in a formal azide – azide conjugation (see chapter 4.3.2.3.), in which an alkyne phosphonite **7** was employed in a CuAAC.[231] Now in the Staudinger-induced thiol addition however, this electron rich alkyne phosphonite **7** is first reacted chemoselectively with an azide in a Staudinger-phosphonite reaction, resulting in the formation of an electron poor alkyne phosphonamidate **8**, which is susceptible to the addition of a thiol-containing molecule to yield the addition product **9** in a second chemoselective reaction. This reaction cascade was first investigated on small molecule level in our lab and is used in this project to bioconjugate unprotected peptides to proteins.
More specifically, we aimed to use the Staudinger-phosphonite reaction for the modification of proteins with cyclic peptides ranging from the small model peptides like the integrin binder c(RGDfK)[261] to cyclic cell penetrating peptides (Figure 18). The chemoselective Staudinger-phosphonite reaction allows for the site-specific functionalization of an unprotected peptide *via* an azido moiety, which can be easily incorporated during SPPS. The consecutive thiol addition was planned for a model protein exhibiting only one addressable cysteine and equipped with an inherent function that can be used in *in vitro* assays. As model system we chose the eGFP mutant C70M S147C developed in our lab.[262]

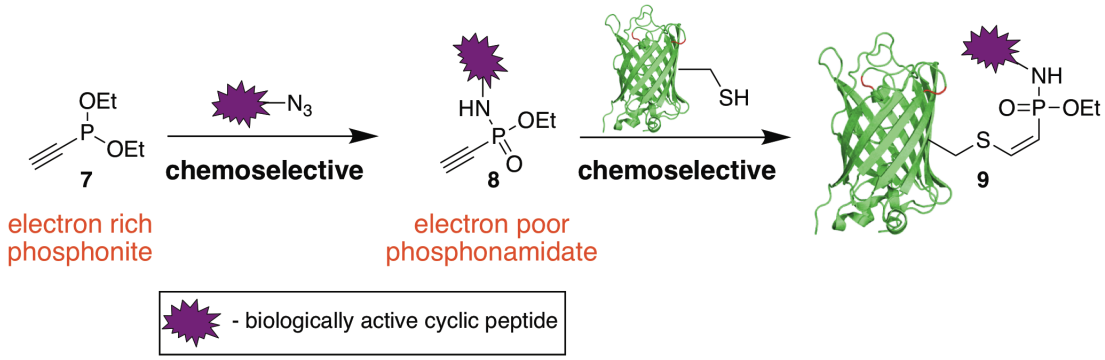

Figure 18: Concept of the Staudinger induced thiol addition for bioconjugation of peptides to proteins.

Here the inherent fluorescence of GFP could be used to further assess the biological behavior of the peptide – protein conjugates and to compare these to similar conjugates generated by different bioconjugation techniques. Furthermore, the stability of the activated electron-poor alkyne **8** as well as the thiol addition product **9** should be evaluated.

6.2.2 Responsibility Assignment

Christian P. R. Hackenberger conceptualized and designed the project. Tom Sauer developed the initial Staudinger phosphonite reaction and following thiol addition on small molecules. The author synthesized all peptides and conducted Staudinger phosphonite reactions on these peptides as well as thiol additions to glutathione and GFP. The author furthermore characterized of all compounds, measured their stability and used the conjugates in FACS experiments. In parallel to this work, the Staudinger induced thiol addition was studied in further detail by Marc-Andre Kasper on small molecule level and in the generation of ADCs, which provided mechanistic insights and further details concerning the stability and scope of this reaction. The author conducted the mutagenesis, expression and purification of hsGFP S3C. Kristin Kemnitz-Hassanin expressed and purified eGFP C70M S147C according to the protocol of Dominik Schumacher, developed in his PhD thesis.[262] Initial cellular uptake studies were carried out by Henry D. Herce in the group of Prof. Dr. Christina Cardoso and were then transferred to the author, who conducted all quantified assays shown in this thesis.

6.2.3 Establishment of Staudinger induced thiol addition with unprotected peptides and stability measurements in a model system

The Staudinger induced thiol addition for the conjugation of unprotected bioactive peptides to proteins was first established on the model peptide c(RGDfK). The peptide was synthesized on solid support according to a published protocol[263], differing only in the protecting group used on lysine. The Dde protected lysine residue was deprotected selectively after head-to-tail macrocyclization and the free ε-amine was reacted with 4-azidobenzoic acid to give the azido-c(RGDfK) **11** after cleavage from trityl resin. With this peptide in hand, we started our investigations into the Staudinger-phosphonite reaction on unprotected peptides. The reaction of phosphonite **7** with **11** showed clean conversion to the alkyne-c(RGDfK) **12** when carried out in dry DMSO under exclusion of air (Figure 19A). Product **12** could be isolated after preparative HPLC in good yields of 54%. The feasibility of the thiol addition to the electron-poor alkyne **12** was first tested with glutathione **13**. When reacting **12** and **13** in equimolar ratio in a mildly basic buffer, the thiol addition proceeded quantitatively in less than ten minutes according to LC-UV/MS (Figure 19B).

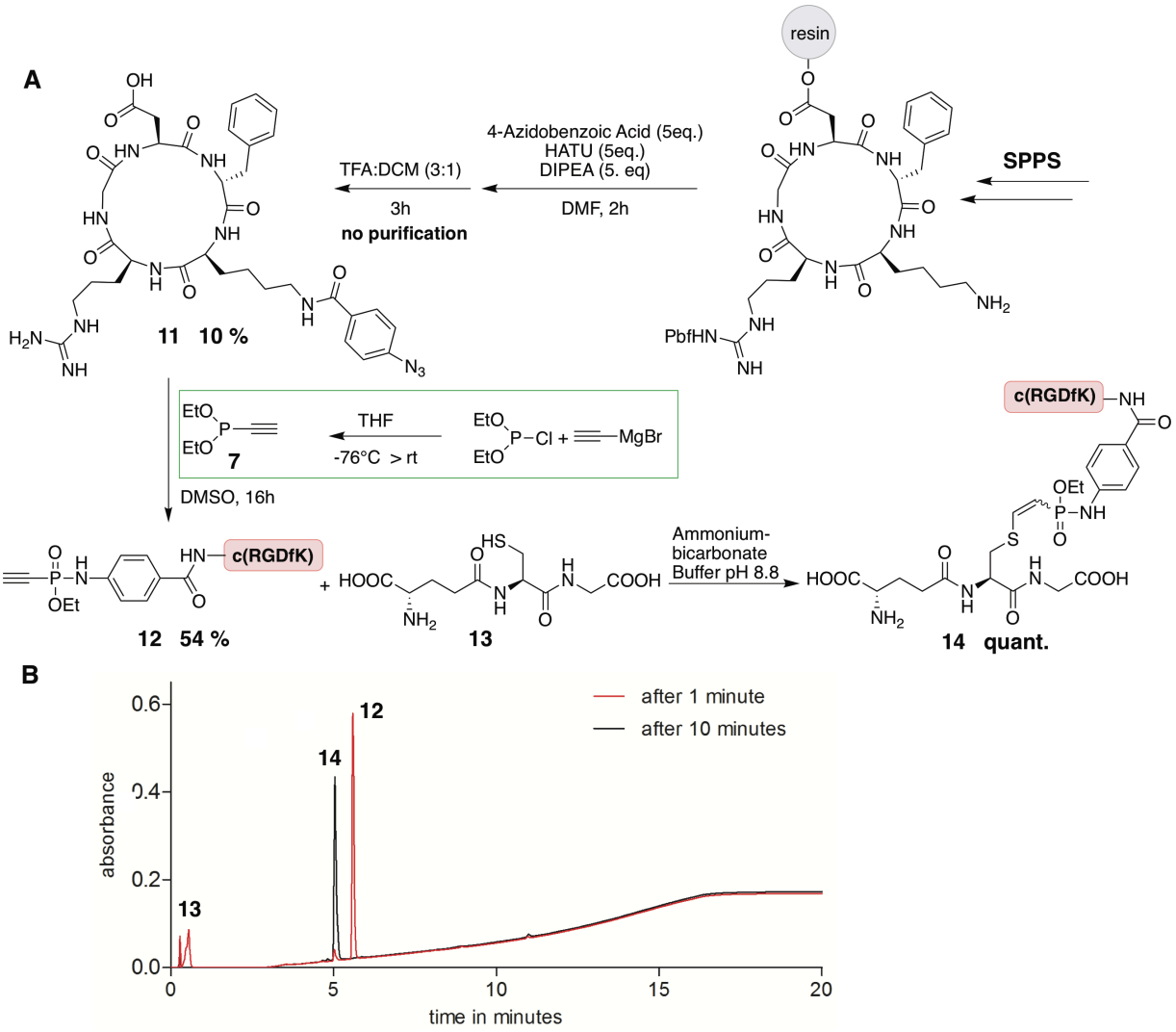

Figure 19: A) Peptide synthesis, Staudinger phosphonite reaction and thiol addition for a modelsystem. B) LC-UV spectra for the thiol addition of **13** to **12**.

The stability of the alkyne **12** as well as the thiol addition product **14** was investigated over a broad pH spectrum. The compounds were incubated in buffers ranging from pH 1 to pH 12 and peptide integrity was assessed *via* LC-UV/MS read out in presence of an internal standard. Here it could be shown that the electron poor alkyne **12** was completely stable at neutral pH and only about 10% of hydrolysis could be detected after 24 hours incubation at slightly basic and acid pH. High levels of hydrolysis were observed for pH 1.0 and pH 12.0 after 24 hours incubation. Interestingly, the thiol addition to the alkyne augmented the stability of **14** in comparison to **12**. **14** showed almost no decay over two days at pH 2.3 to pH 9.0. Furthermore, hydrolysis at pH 1.0 and pH 12.0 was slowed down significantly in comparison to **12** (Figure 20). Next, we tested if **14** was prone to thiol exchange in the presence of high amounts of external thiols, because thiol exchange reactions are the major drawback of the ubiquitously used maleimide reaction (see Chapter 4.3.1.1).

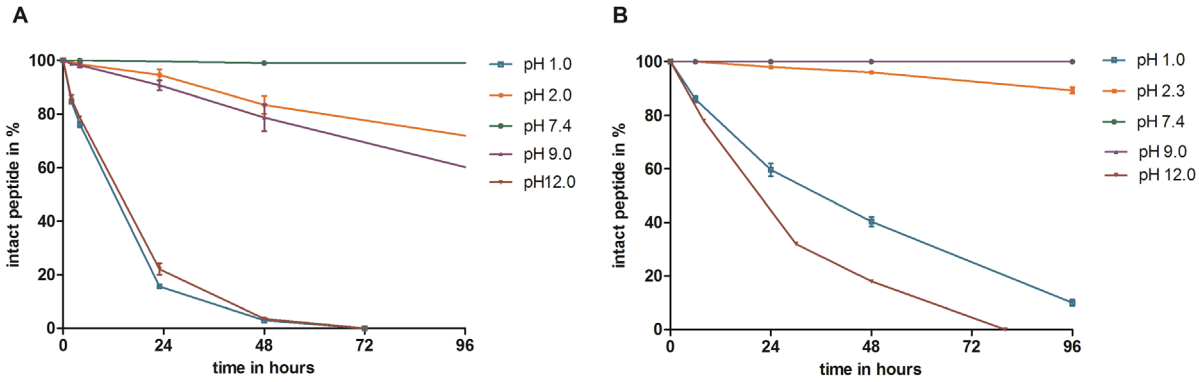

Figure 20: Stability studies of compounds A) **12** and B) **14** at different pH with read out by LC-UV.

Upon incubation with 100 eq. of MesNa at neutral pH **14** was completely stable over several days (Figure 21). When incubating with DTT at pH 7.4, a small additional peak was observed in the LC-UV after more than a day, which was correlated by LC-MS measurements to an addition of DTT to the alkene in compound **14** (Figure 21B)**.** Here, it is important to note that this addition to the alkene did not result in elimination of the covalently attached glutathione, which was verified by MS. The same thiol addition to the alkene was observed to a higher extend when incubating with 100 eq. of MesNa or DTT at pH 9.0, but no glutathione elimination could be detected despite the use of slightly elevated pH values either (Figure 21B). The observed thiol addition to **14** is a result of the still imminent electrophilicity of the alkene in the product. In conclusion it could be shown that treatment of **14** with high amounts of external thiols at physiological and slightly basic pH does not lead to the elimination of the conjugated cargo (Figure 21B). Furthermore, the alkyne starting material **12**, as well as the thiol addition product **14** were stable towards hydrolysis under physiological conditions. Compared to maleimides, which have been shown to undergo thiol exchange, these characteristics could be of great importance in the field of cysteine bioconjugation, especially when thinking about *in vivo* pharmaceutical applications. However, to verify the phosphonamidat stability *in vivo,* more stability studies have to be conducted e.g. in serum.

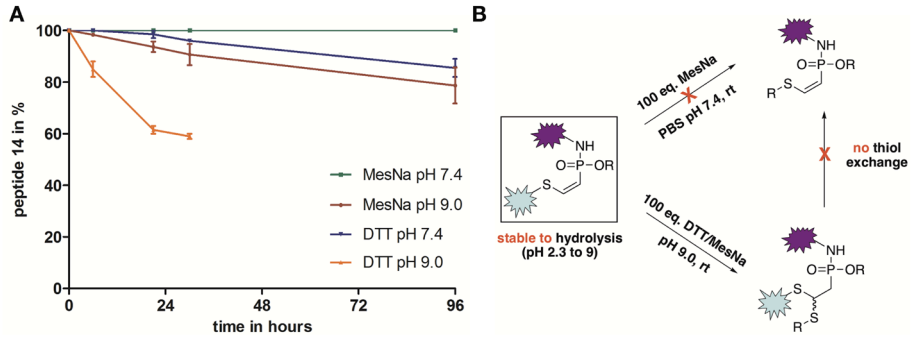

Figure 21: A) Product integrity upon incubation with high amounts of external thiols measured by LC-UV/MS over time. B) Overview over stability of peptide **14** and its reaction with external thiols at different pH values.

6.2.4 Thiol addition on protein level and *in vitro* application.

Encouraged by the feasible thiol addition reaction with glutathione and the stability of the conjugation product, we probed the thiol addition on protein level. Here, we chose a variant of eGFP (eGFP C70M S147C) as model protein with only one addressable cysteine that was previously developed in our group.[262] To our satisfaction, **12** reacted readily with the protein at quantitative yields without any side reactions or multiple additions to the protein, even when running the reaction at neutral pH in PBS (Figure 22A/B). After simple spin filtration to remove the excess peptide **12**, the pure cRGD-tagged eGFP **15** was isolated.

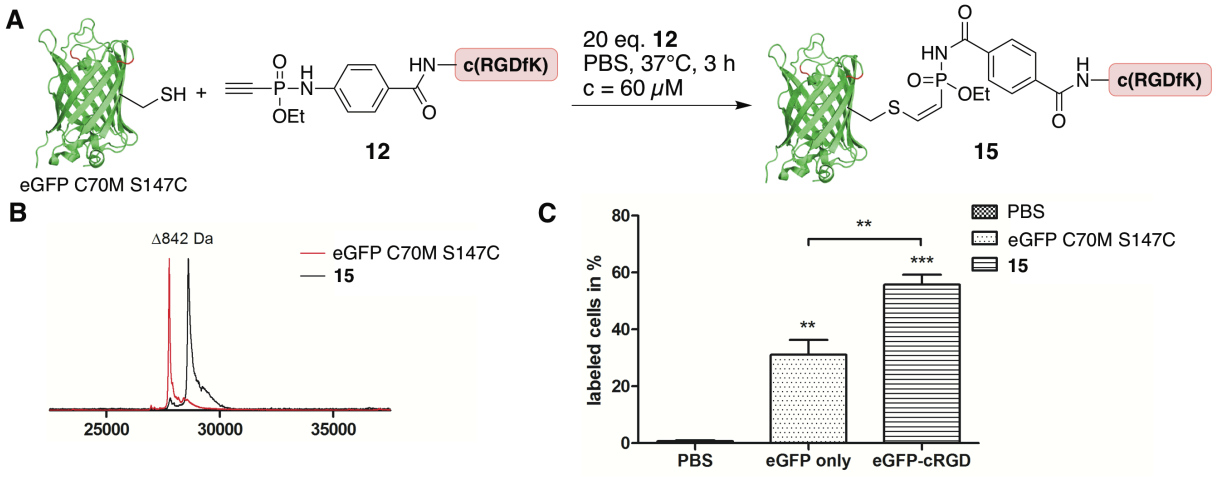

Figure 22: A) Synthesis of cRGD-tagged eGFP **15**. B) MALDI-TOF of thiol addition. C) Analysis of cellular labeling with 40μM protein in U87MG cells by FACS. Error bars correspond to the s.e.m. n=3. Data underwent statistical analysis using a one-way ANOVA followed by a Tukey's multiple comparison to the PBS treated control. ***=p<0.001.

To prove the *in vitro* applicability of the conjugate, a FACS assay with U87MG glioblastoma cells, which are known to overexpress integrins on their surface, was set up. Upon incubating cells with 40 μM of **15** for four hours, RGD-mediated binding could be analyzed by the inherent fluorescence of eGFP in flow cytometry measurements. Here, a significant increase of cellular fluorescence was observed upon incubating cells with **15** in comparison to a PBS control and a non-tagged eGFP (Figure 22C). Nevertheless, a large amount of fluorescence was observed when incubating the U87MG cells with non-tagged eGFP, suggesting a high unspecific binding of the protein to the cellular membrane, which could not be eliminated by thorough washing prior to the measurements. Furthermore, we observed cell detachment from the culture flask during treatment with **15**, probably due to binding of **15** to integrin and hence hindering the integrin to interact with the extracellular matrix. Due to these drawbacks of the assay set up and the desire to test the bioconjugation reaction with a more complex biologically active peptide, we planned an

analogous synthesis route for tagging eGFP with the cyclic cell penetrating peptides c(Tat) and c(R10).

6.2.5 Cell penetrating peptide – protein conjugates

It has been shown previously that the conjugation of c(Tat) or c(R10) peptides to cargos can drastically enhance their cellular uptake, even if this cargo is large in size, e.g. a protein.[121,122] Nischan *et al.* demonstrated the effective cytosolic uptake of GFP conjugated covalently to c(Tat) *via* CuAAC into HeLa cells. We wanted to follow up on this concept and use the novel Staudinger induced thiol addition as an alternative bioconjugation reaction to generate the c(Tat)-tagged GFP in a copper-free manner and without the need of introducing unnatural amino acids into the protein. Furthermore, it has been reported that the poly-arginine peptide c(R10) shows even higher transduction efficiency than c(Tat). This has been shown for nanobodies[122], which are half the size of GFP and should now also be assessed with GFP as cargo.

We synthesized the already published lactam cyclized CPPs with a PEG-linker and conjugated 4-benzoic acid to the *N*-terminus *via* SPPS on rink amide resin (Scheme 11A/B).

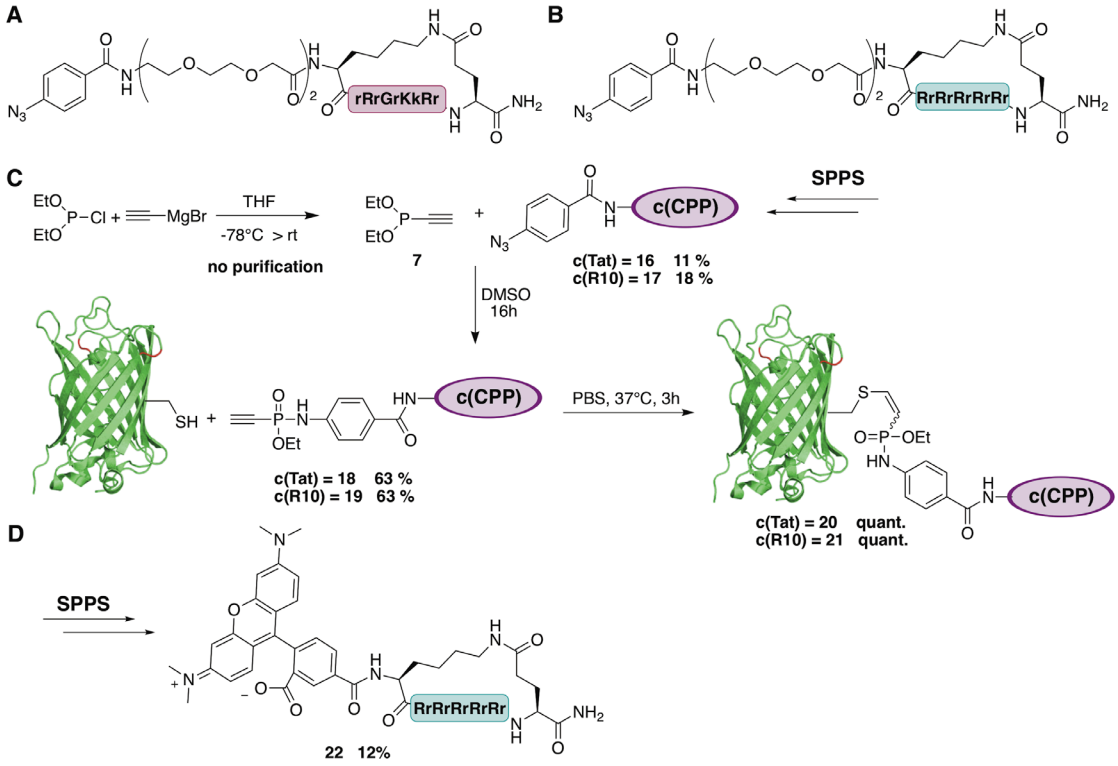

Scheme 11: A) Structure of **16**. B) Structure of **17**. C) Conjugation of c(CPP) to eGFP *via* Staudinger induced Thiol addition D) Structure of positive control **22** used in cellular uptake.

The azido-functionalized peptides **16/17** were gained after acidic cleavage and purification *via* preparative HPLC. The pure azido-peptides **16/17** underwent clean reaction with

phosphonite **7** in a Staudinger phosphonite reaction to **18/19**. After HPLC purification, the thiol addition of eGFP C70M S147C to **18/19** was carried out in PBS at 37°C. For a quantitative conversion either lower equivalents (6 eq.) of peptide were reacted over night at 37°C or slightly higher amounts of peptide (20 eq.) gave the product quantitatively after incubation for three hours at 37°C in PBS (Scheme 11C). The reaction conditions were varied depending on the availability of peptidic starting material. The purification from excess peptide could be easily achieved, either by spin filtration (mass weight cut-off membrane of 10 kDa) or by using desalting columns (mass weight cut off of 7 kDa). The quantitative conversion to the thiol addition product with even larger and more complex peptides shows the general utility of this bioconjugation reaction.

In vitro applicability was verified with cellular uptake studies in HeLa cells, with an analogous experimental setup to already published studies.[121,122] In short, HeLa cells were incubated with varying concentrations of **20, 21** or non-tagged eGFP in HEPES buffer for one hour at 37°C. After careful washing with DMEM medium including 10% FBS the cells were imaged using a confocal fluorescence microscope. For quantifying the cytosolic cellular uptake, the inherent attraction of c(Tat) and c(R10) to the negatively charged nucleolus was used. Every cell that exhibited nucleolar GFP fluorescence was counted as positive for c(CPP)-mediated cytosolic transduction. The uptake was compared to the incubation with non c(CPP) tagged eGFP, which showed no transduction into cells and no membrane localization (Figure 23A). As positive control, we incubated cells with TAMRA tagged c(R10) peptide **22**, which is known to be able to transduce effectively into HeLa cells (Scheme 9D, Figure 23B).[118] Upon covalent attachment of c(CPP)s to eGFP, protein transduction could be clearly observed at all tested concentrations. Using c(Tat)-conjugate **20** the percentage of cellular uptake increased slightly from 20 µM to 50 µM, but not at a significant rate (Figure 23 C). Incubation with c(R10)-conjugate **21** also showed a slight increase going from 20 µM to 30 µM, followed by a slight decrease when going up to 50 µM (Figure 23C). This behavior can be attributed to **21**'s tendency to aggregate. Aggregation was already observed after storing **21** for 48 hours at concentrations exceeding 50 µM at 4°C. Even though c(R10) seems to be slightly more effective in transducing GFP into cells at lower concentrations, this difference is not significant (Figure 23C). In comparison, Herce *et al.* reported a three-fold increase in the number of cells that take up their nanobody-CPP-conjugate for c(R10) compared to c(Tat).[122] An explanation for this uptake difference could be the significantly lower molecular weight of nanobodies in comparison to eGFP, which would be in accordance to previous reports, that the transduction ability of CPP's is highly dependent on the nature of the cargo.[101]

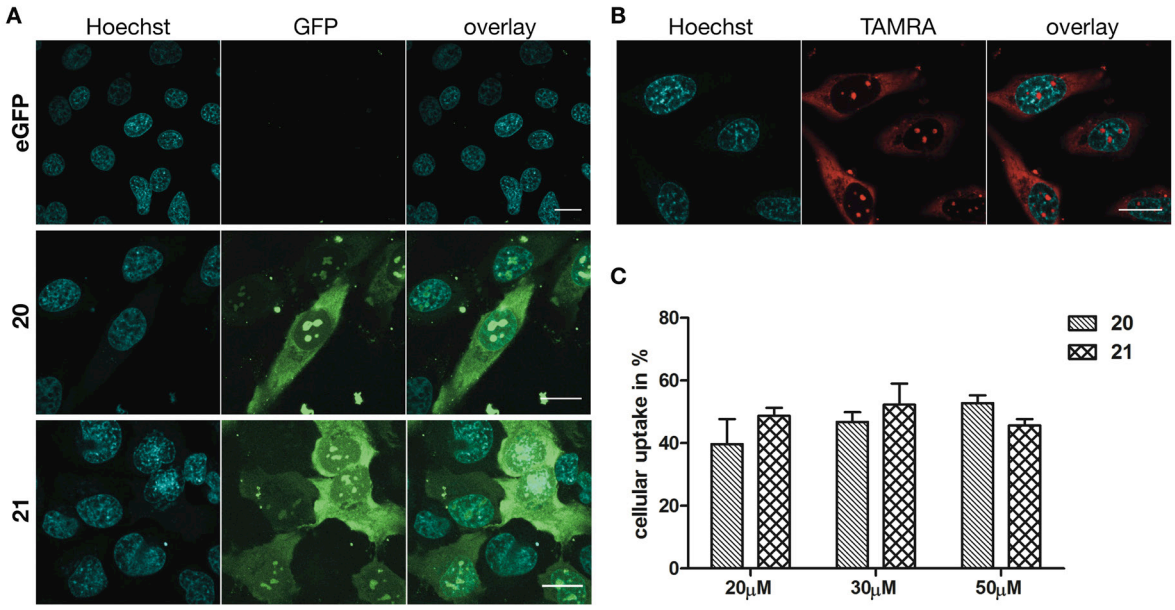

Figure 23: A) Confocal images of cellular uptake of c(CPP) tagged eGFP in HeLa cells at 30 µM. Scale bar = 20 µm B) Cellular uptake with 5 µM of positive control **22** (TAMRA labeled c(R10)). Scale bar = 20 µm. C) Quantification of cellular uptake with eGFP of biological replicates with n≥3.

In order to be able to directly compare the cellular uptake to the results of Nischan *et al.*, who also reported cellular uptake with a GFP-c(Tat) conjugates. We set out to study the Staudinger-induced thiol addition on the same hsGFP-variant they used. This hsGFP differs from eGFP in its protein structure by several point mutations (see Figure 8.10 in Chapter 8.2.3 for a detailed sequence comparison). Furthermore, Nischan *et al.* conjugated the c(Tat) peptide to the *N*-terminus throughout CuAAC. In our previous Staudinger-induced thiol additions with eGFP C70M S147C, the peptide was conjugated to C147 at the barrel in the middle of the protein structure. To find out if the differences in protein sequences and attachment point have an effect on cellular transduction, we mutated the hsGFP to contain a single addressable *N*-terminal cysteine for the conjugation with **18.** C71 was mutated to methionine and the *N*-terminal S3 to cysteine. Expression of the mutated hsGFP S3C C71M was tested in the *E. coli* strains T7, BL21 and Rosetta (Figure 24A) and was finally expressed in bigger scale in BL21 cells at 18°C overnight. The protein was purified by Ni-NTA column, followed by TEV cleavage and a second purification over a nickel column to remove the uncleaved protein and the His-tagged TEV protease. This resulted in the isolation of pure hsGFP S3C C71M, which was further verified by MALDI-TOF and SDS-page (Figure 24B). The *N*-terminal cysteine was found to be prone to form homodimers and therefore had to be reduced with TCEP prior to thiol addition to **18**. The addition reaction to form the c(Tat)-hsGFP **23** was again quantitative.

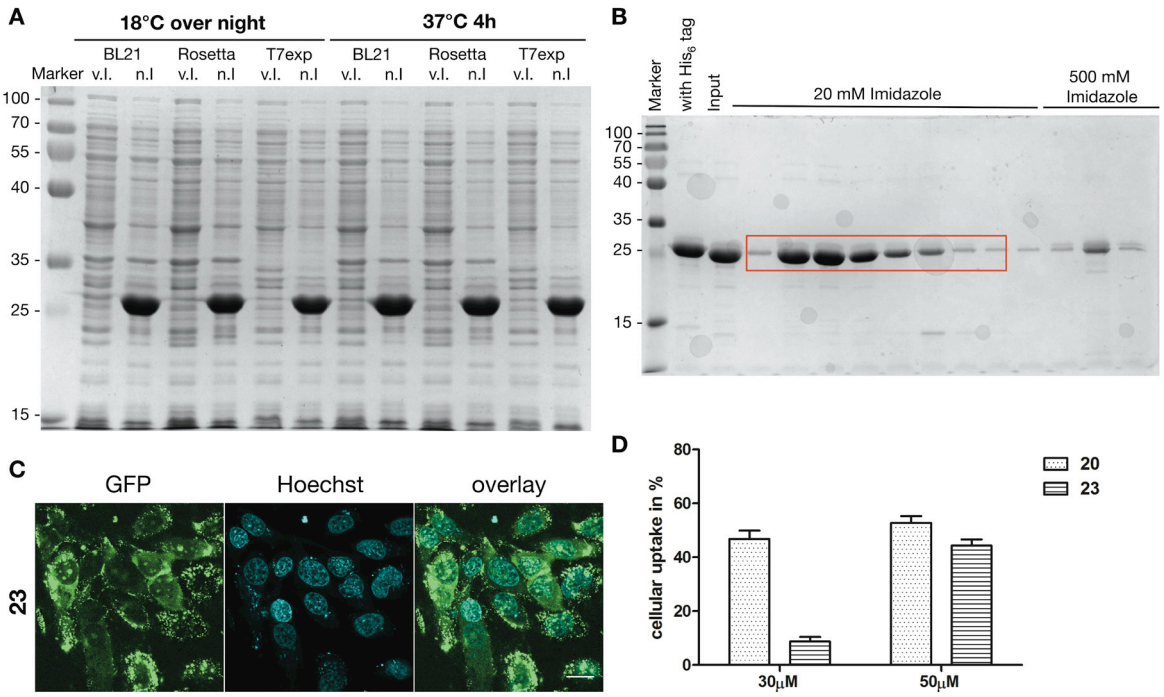

Figure 24: A) Testexpression of hsGFP S3C C71M in different cell strains. B) Purification of hsGFP S3C C71M after TEV cleavage. Pooled fractions are marked in red. C) Confocal images of cellular uptake of **22** in HeLa cells at 50 µM. Scale bar = 20 µm D) Quantification of cellular uptake with hsGFP for biological replicates with n≥3.

Interestingly, cellular uptake with **23** at 50 µM protein concentration did not differ much from the eGFP mutant **20** and the uptake efficiency was similar to the report from Nischan *et al.* (Figure 24C/D). However, hsGFP **23** displayed a higher interaction with the cellular membrane as observed by confocal fluorescence microscopy (Figure 24C), than the eGFP construct **20** (Figure 23A). This could pin-point towards a more difficult membrane crossing of the hsGFP variant. Lowering the concentration to 30 µM, showed a drastic decrease in cellular uptake for the *N*-terminal tagged hsGFP **23** compared to eGFP **20** (Figure 24D), again with high fluorescence at the cellular membrane but lower cytosolic distribution. From these cellular images we concluded that the membrane crossing is hindered for the hsGFP variant at lower concentrations. Because low concentrations were previously not tested by Nischan *et al.* and the uptake at higher concentrations is comparable to the literature known CuAAC conjugated c(Tat)-GFP we conclude that the Staudinger-induced thiol addition is generally suitable for *in vitro* applications.

To compare the reaction to other cysteine bioconjugation methods, we synthesized c(Tat) exhibiting a maleimide in **24** or iodoacetyl in **25** at the *N*-terminus. After purification, thiol addition to the eGFP C70M S147C was carried out with 6 eq. of **24** at 16°C for four hours and with 6 eq. **25** at room temperature for three hours (Scheme 12). Conversion to **26** and **27** was rapid and no unreacted eGFP was observed after four or three hours of reaction

time. It should be noted that traces of a side product, corresponding to a double c(Tat) addition were observed in the MALDI-TOF spectra during the reaction to **26** (Figure 25A).

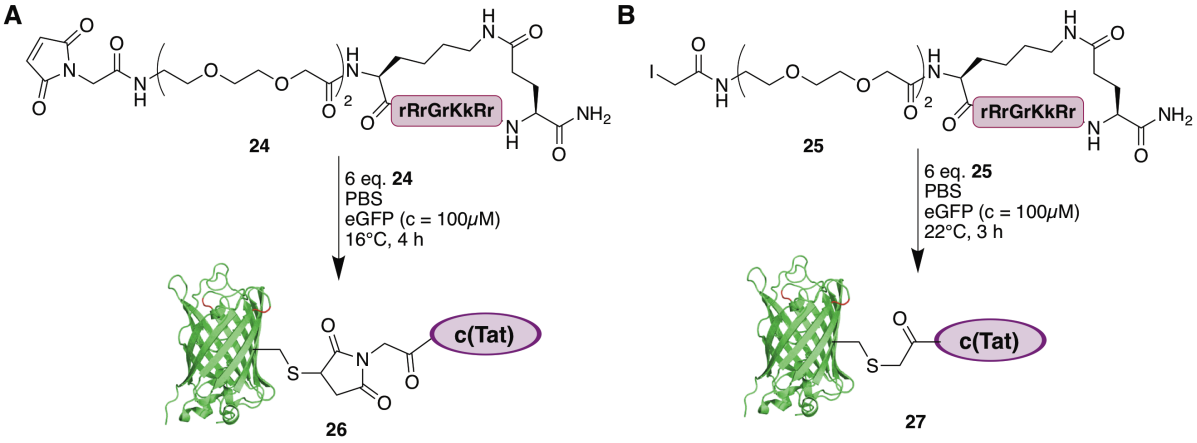

Scheme 12: Covalent conjugation of c(Tat) and eGFP *via N*-terminal A) maleimide or B) iodoacetyl functionality.

Upon cell treatment with the two c(Tat) tagged proteins **26** and **27,** we again observed high GFP fluorescence in the nucleoli of the cells (Figure 25C). This distinct fluorescence was used for quantification (Figure 25B). Here, a significant difference was observed for the uptake of **26** compared to **20**, with up to 20% more uptake at a concentration of 50 µM for **26.** A possible explanation could be the better cell penetrating properties of the partly double conjugated eGFP side product, which had formed during the reaction to **26. 27** however, showed a slight, but not significant increase in cellular uptake compared to **20**. As these differences were generated from only three biological replicates, an in depth analysis of the bioconjugation influence on the cellular uptake would have to be deducted with more replicates at diverse concentrations and on a more elaborated system.

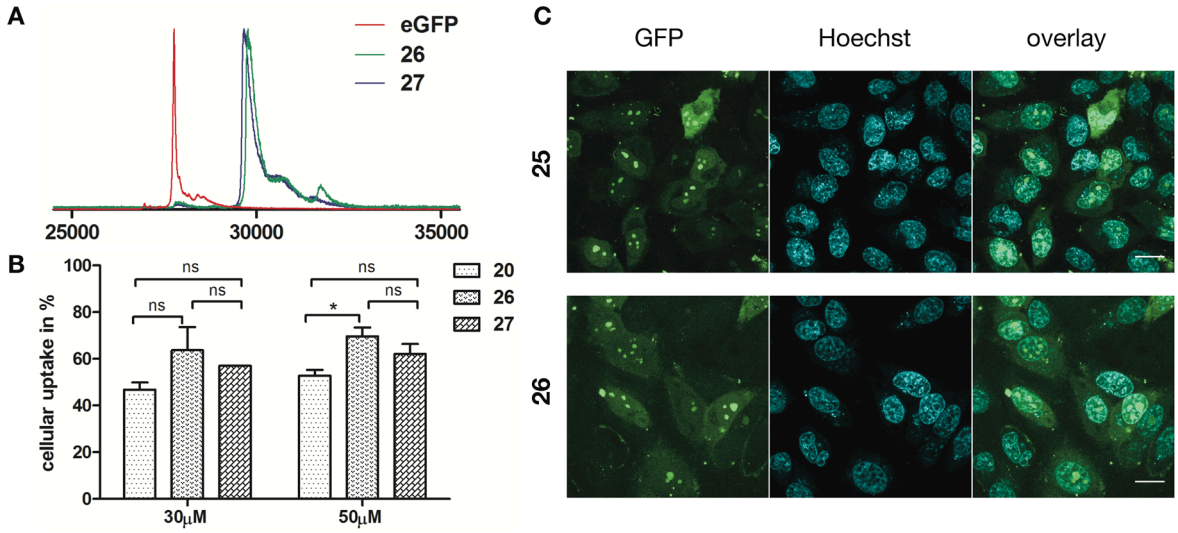

Figure 25: A) MALDI-TOF of bioconjugation to **26** and **27** B) Quantification of cellular uptake with eGFP. Error bars correspond to the s.e.m. n≥3. Data underwent statistical analysis using a one-way ANOVA followed by a Tukey's multiple comparison to the PBS treated control. *= p<0.05. C) Confocal images of cellular uptake of c(CPP) tagged eGFP in HeLa cells at 30 µM. Scale bar = 20 µm.

Nonetheless, in principle this comparison shows that all three cysteine reactive conjugation techniques can be used for the covalent labeling of eGFP with c(Tat). Furthermore, all three strategies delivered cell permeable eGFP constructs, which could localize in the cytosol and the nucleoli inside HeLa cells.

6.2.6 Conclusion and Outlook

In summary, we developed a new cysteine reactive bioconjugation technique for the covalent conjugation of unprotected peptides to proteins. We showed that the chemoselective Staudinger-phosphonite reaction of alkyne phosphonite **7** with an aromatic azide, which was incorporated into the peptide by SPPS, readily delivers the reactive alkyne peptide **8** in good isolated yields. Furthermore, we showed that the alkyne peptide **8** is stable at neutral to slightly acid or basic conditions for days. Thiol addition to the alkyne proceeded fast and quantitative for small molecule thiols as well as for larger, thiol-containing GFP constructs. Thiol addition product **14** was stable over days at pH between 2.3 and 9.0 and resistant towards thiol exchange reaction with external thiols, even at high thiol concentrations and at basic pH. We further could verified that the conjugation products were applicable in *in vitro* applications by using the Staudinger-induced thiol addition to conjugate c(CPP)s to thiol-containing GFP proteins and using the resulting conjugates in cellular transduction assays.
Currently, there are ongoing studies in the group to further explore the broad versatility of the Staudinger-induced thiol addition for bioconjugation purposes, especially for pharmaceutical applications.

6.3 Intramolecular Staudinger-induced thiol addition as a new peptide cyclization method

6.3.1 Introduction of the BCL9 – β-Catenin interaction as therapeutic target

The Wnt signaling cascade is a highly conserved signal transduction pathway that influences embryonic development and homeostasis, cell regeneration and renewal in adult organisms. During the development stages, the pathway is strictly regulated and any mutation or deregulation can trigger diseases. A deregulated Wnt signaling pathway is often reported for different cancer types.[264–266] There are mainly two different types of Wnt signaling cascades: a canonical and noncanonical pathway. Here, we focus on the canonical pathway that can lead to gene transcription and is mostly influenced by the stability of the protein β-Catenin.

β-Catenin exhibits two major functionalities. It can be involved in signaling and also in structural processes. Structurally, it consists of a central region that is build up from 12 rigid Armadillo repeats (R1-12) flanked by specific *N*- and C-terminal regions that are, in contrast, somewhat flexible. In the absence of Wnt ligands β-Catenin is found in the cytoplasm. Here, it gets regulated by recruitment into a destruction complex consisting of adenomatous polyposis coli (APC), axin and glycogen synthase kinase 3β (GSK3β), where it is phosphorylated and targeted for degradation. Low β-Catenin levels and repression of Wnt-specific target genes characterize the non-activated state.

If the Wnt signaling pathway gets activated by binding of Wnt proteins to the cell receptor frizzled and the Low-density lipoprotein receptors (LRP5/LRP6), the destruction complex that regulates β-Catenin is inhibited, leading to a high cytosolic β-Catenin concentration. Upon cytosolic enrichment, β-Catenin can translocate into the nucleus, where it forms a transcriptionally active complex with LEF, TCF and co-activators such as B-cell lymphoma 9 (BCL9) or Pygopus. Upon formation of this transcription complex cell proliferation, migration and survival genes are expressed, which drive oncogenesis.[266,267] Many different components in this pathway can act as oncogenes or tumor suppressors. One of the oncogenes was found to be the protein BCL9 that is involved in formation of the transcription complex.[268] It was reported that BCL9 enhances β-Catenin-mediated transcriptional activity and BCL9 knockdown increases the survival rate of xenograft mouse models. Most significantly oncogenic Wnt target expression could be downregulated by shRNA.[268] Further it was shown that the PPI between BCL9 and β-Catenin could be disrupted by a short peptide that is derived from the structure of BCL9 itself and is

stabilized in its α-helical structure by peptide stapling (see chapter 4.2.3). By disrupting the PPI with the stabilized peptide oncogenic Wnt transcription was selectively suppressed.[269]

6.3.2 Outline of the Project

In this project we aim to engineer an intramolecular variant of the Staudinger-induced thiol addition for the cyclization of peptides, in particular to stabilize peptidic structures by covalent linkage of two side chains (see chapter 4.2.3). We envisioned incorporating an azide and a thiol into a peptide sequence by SPPS, which can then be bridged with an unsaturated electron-rich phosphonite. We propose that the phosphonite first reacts chemoselectively with the azido moiety of the peptide, upon which an electron poor unsaturated phosphonamidate is formed, which is susceptible toward thiol addition as shown before (see chapter 6.2). Because the thiol moiety is present intramolecularly in the peptide, the addition to the unsaturated phosphonite yields a macrocyclized peptide. The order in which the reaction cascade is taking place is controlled, because the thiol reactivity is only induced upon Staudinger-phosphonite reaction and the thiol addition can only occur on the electron-poor unsaturated phosphonamidate. The interesting aspect in comparison to other macrocyclization strategies is that the Staudinger-induced thiol addition is a chemoselective way to introduce an electrophilic center into a peptide. Furthermore the third substituent on phosphorous that is not directly involved in the bridging of azide and cysteine can be further functionalized to fine-tune the peptide's properties.

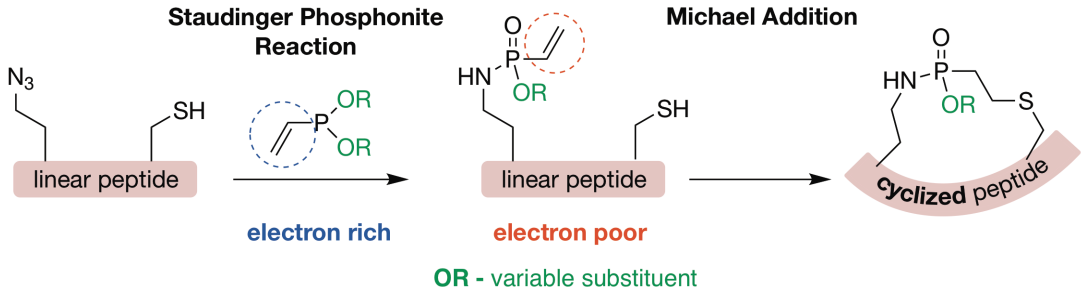

Figure 26: Schematic project outline of intramolecular peptide stapling using the Staudinger-induced thiol addition.

We envisioned the application of this macrocyclization reaction on two different peptide substrates. One is the BCL9 derived peptide, which has been previously shown to be structurally stabilized in its α-helix by stapling and can effectively inhibit the PPI between the BCL9-protein and β-Catenin when present in its cyclized form (Figure 26).[269] The other peptide is the literature known cell-penetrating peptide cR10, which has been discussed in this thesis before (see chapter 6.2).[118,122] The macrocyclization of the poly-arginine peptide enhances cellular uptake and provides cytosolic delivery of protein cargos.[118,121,122]

In addition to establishing a new synthetic route to macrocyclized peptides *via* the Staudinger-induced thiol addition, we aim for the validation of the intact biological activity after macrocyclization and seek to compare our technique with reported strategies. In case of the stapled BCL9 peptide, *in vitro* activity can be demonstrated by its disruption ability of the BCL9/β-Catenin complex. For the cell penetrating peptide (cR10), the cytosolic cellular delivery properties of the CPP-conjugated eGFP are compared to the lactam-cyclized cR10 (see chapter 6.2).

6.3.3 Responsibility Assignment

Christian P. R. Hackenberger conceptualized and designed the project. The author synthesized all peptides, conducted the cyclization reactions, characterizations and cellular uptake studies. The cyclization reactions with alkene-phosphonites were based on previous experiments by Marc-Andre Kasper, who developed the Staudinger induced thiol addition with alkene phosphonites for intermolecular reaction with small molecules and ADCs in the Hackenberger lab. The homogenous time resolved fluorescence (HTRF) setup was discussed with Dr. Jens Peter von Kries and the assay was conducted by Andreas Oder in the Screening Unit of the FMP. Dr. Peter Schmieder, Brigitte Schlegel and Niels Trieloff carried out cyclization determinations *via* NMR.

6.3.4 Peptide stapling *via* Staudinger-induced thiol addition

In a report from 2012, a BCL9 derived peptide sequence cyclized by ring closing methathesis **28**, was shown to effectively disrupt the BCL9 and β-Catenin PPI.[269] Due to its remarkable *in vitro* behavior it was chosen to be the model system for the establishment of the intramolecular macrocyclization of two amino acid side chains using the Staudinger-induced thiol addition. To probe the intramolecular stapling by the Staudinger induced thiol addition, the BCL9-derived peptide sequence was synthesized with azidohomoalanine and cysteine **30** replacing the olefinic amino acids used for RCM in the reported peptide **28**. By choosing those two amino acids as replacements the final linker after Staudinger phosphonite reaction with alkyne phosphonite **7** would have the length of eight atoms in **29**. This is the same length as found for the literature known RCM stapled peptide with the double bond only slightly shifted in the linker structure (Scheme 13).

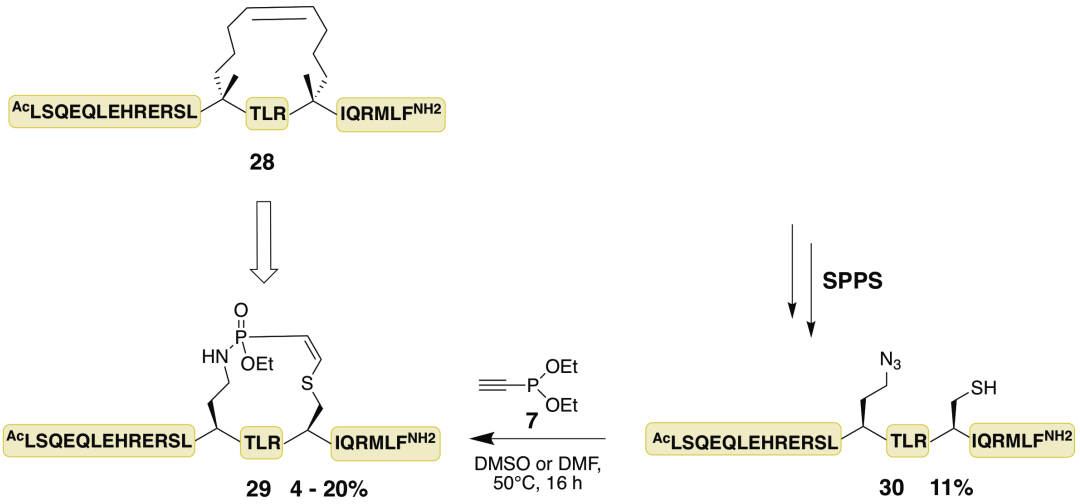

Scheme 13: Synthesis scheme of the macrocyclization of BCL9-derived peptide by the Staudinger induced thiol addition reaction.

After the successful SPPS and purification of peptide **30**, the initial intramolecular Staudinger-phoshphonite reaction was performed by synthesizing alkyne-phosphonite **7** in a Grignard reaction from its chloride and adding it to the peptide solubilized in dry DMSO as crude at 50°C. It was observed that the reaction did not proceed cleanly and the major product was a side product with a mass difference of 28 Da to the desired product **29**. We hypothesized an intramolecular alkylation reaction of the amine with the ethyl substituent could have resulted in the side product formation. The Hackenberger group has previously reported alkylation of the *N*-substituent during a Staudinger-phosphite reaction at elevated temperatures.[270] Repetitions of the reaction delivered different amounts of the desired

product **29** ranging from moderate to low yields, which illustrates the low reproducibility and reliability of the Staudinger-induced thiol addition with alkyne-phosphonamidates.

Nonetheless, these initial tests provided some useful insights into some aspects of the reaction. In particular, the solvent was found to have a major influence on the *in situ* cyclization to the desired product. When the reaction was carried out in dry DMSO, no free sulfhydryl groups could be identified by Ellman's test (Figure 27A). If the reaction was carried out in dry DMF instead, the Ellman's test showed 94% free sulfhydryl groups in the sample (Figure 27B). Upon basic incubation of this sample at pH 9.0 only disulfide dimers were detected by LC-UV/MS and no thiol addition could be observed for the reaction carried out in DMF. Following these discoveries, all reactions were performed in dry DMSO to facilitate *in situ* cyclization.

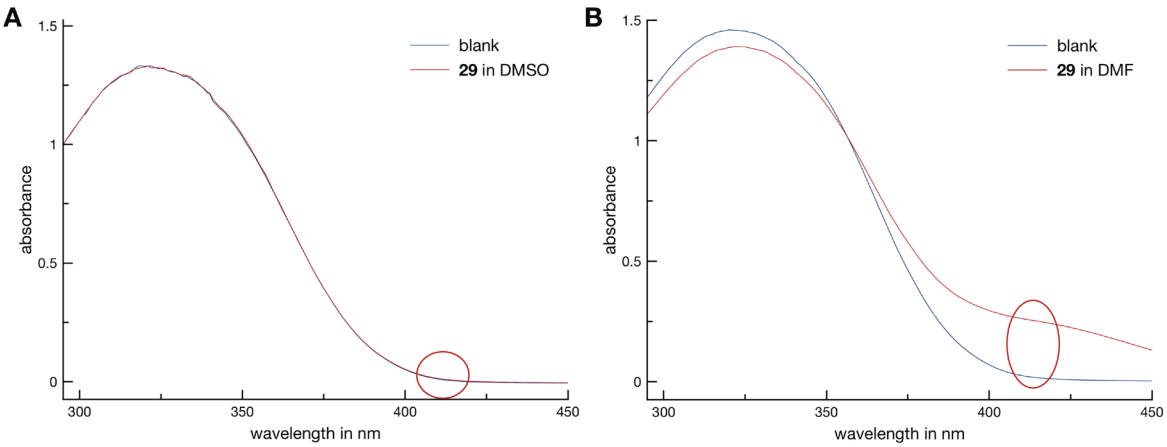

Figure 27: UV traces of ellman's test with **29** for A) the reaction carried out in dry DMSO and B) the reaction carried out in dry DMF. From the difference of absorbance at 412 nm for the sample vs. a blank, the concentration of free sulfhydryl groups was determined.

All reactions performed to yield **29** (Scheme 13) were either purified by preparative HPLC with acidic or basic eluents. Purification with eluents containing 0.1% TFA resulted in a better peak separation compared to the purification in 10 mM ammonium acetate buffer at pH 9.0, but also promoted methionine oxidation in reactions using DMSO as solvent. To prevent methionine oxidation a slightly different peptide was used in the following experiments, where methionine was substituted by norleucine (**30a/b**) (Figure 28).

Due to the unreliable reaction rates and poor yields with phosphonite **7**, the alkene-phosphonite **31** was tested in the intramolecular reaction. The synthesis and Staudinger induced thiol addition of **31** has previously been investigated in intermolecular reactions by Marc-André Kasper in the Hackenberger lab on small molecules and for the generation of ADCs. Furthermore, he compared reaction speed of alkene- and alkyne-phosphonites, which showed a faster conversion in the Staudinger-Phosphonite reaction but a slower thiol

addition with the alkene-phosphonite compared to the alkynes. Hence this established alkene-derivative could be transferred to the intramolecular approach and observations could be embedded with already known small molecule observations. Here, the alkene-phosphonite **31** synthesis (Figure 28A) was carried out analogously to the alkyne-phosphonite **7** (Scheme 11C). The temperature for the Staudinger-phosphonite reaction with **31** could be loweredfrom 50°C to room temperature due to faster conversion with **31** towards **32a/32b** compared to the reaction with alkyne-phosphonite **7**. The azide conversion to the phosphonamidate product was fast and no major side products were observed (Figure 28B). Thiol addition to the alkene occurred *in situ,* which was confirmed by NMR (see Figure 10.4 and 10.5 in the Appendix) and Ellman's test.

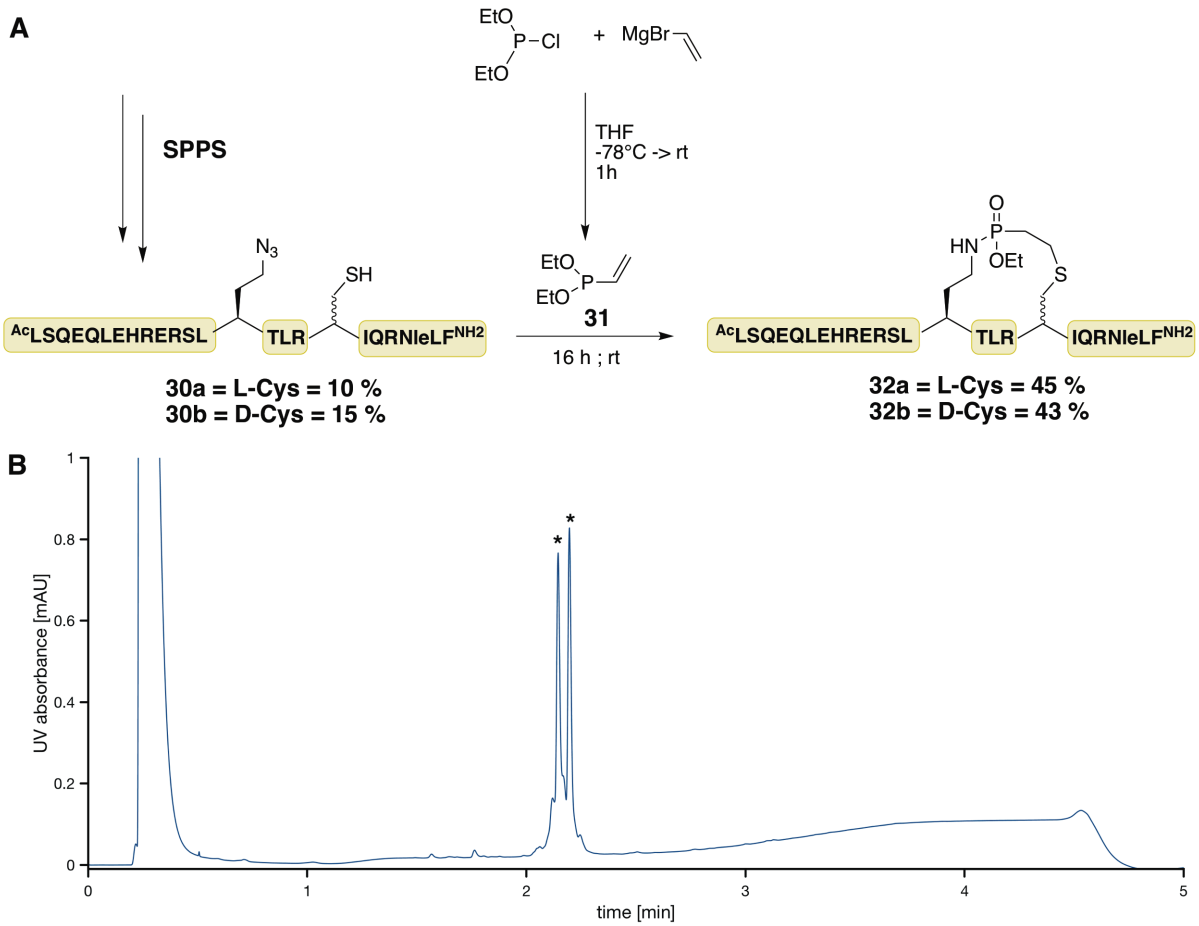

Figure 28: A) Synthesis route for stapling of BCL9 peptides using the Staudinger-Phosphonite induced Thiol addition. B) Analytical UPLC-UV trace of crude reaction mixture of **32b**. Product is indicated by asterisk and appears as double peak due to formed stereoisomers with phosphorous as stereocenter.

From the detailed small molecule studies of the intermolecular Staudinger induced thiol addition with alkene-phosphonites carried out by Marc-André Kasper, we expected the thiol addition to the alkene to be much slower at room temperature than actually observed during our reactions forming **32a/b**. Since the cyclization product was gained quantitatively directly

after the Staudinger-phosphonite reaction, we wanted to elucidate the factors that contribute to the unexpectedly fast thiol addition.

First, a proximity-based effect was investigated. The cysteine of **30a** was alkylated to give **33**, which was reacted with **31** in presence of glutathione (Figure 29A reaction I). Conversion to the glutathione addition product **34** was observed after over night incubation *via* LC-UV/MS (Figure 29B) comparable to the reaction with **30a**, which indicates that a proximity based addition reaction is not responsible for unexpectedly fast and quantitative addition to the alkene. Another difference to the intermolecular thiol addition was the thiol addition reaction being carried out in pure DMSO. Hence the alkene-phosphonamidate peptide **35** was synthesized (Figure 29A, reaction II) and after hydrolysis the reaction mixture was lyophilized and re-dissolved in dry DMSO. After incubating **35** for 24 hours with equimolar amounts of glutathione, no thiol addition could be observed *via* LC-UV/MS (Figure 29C).

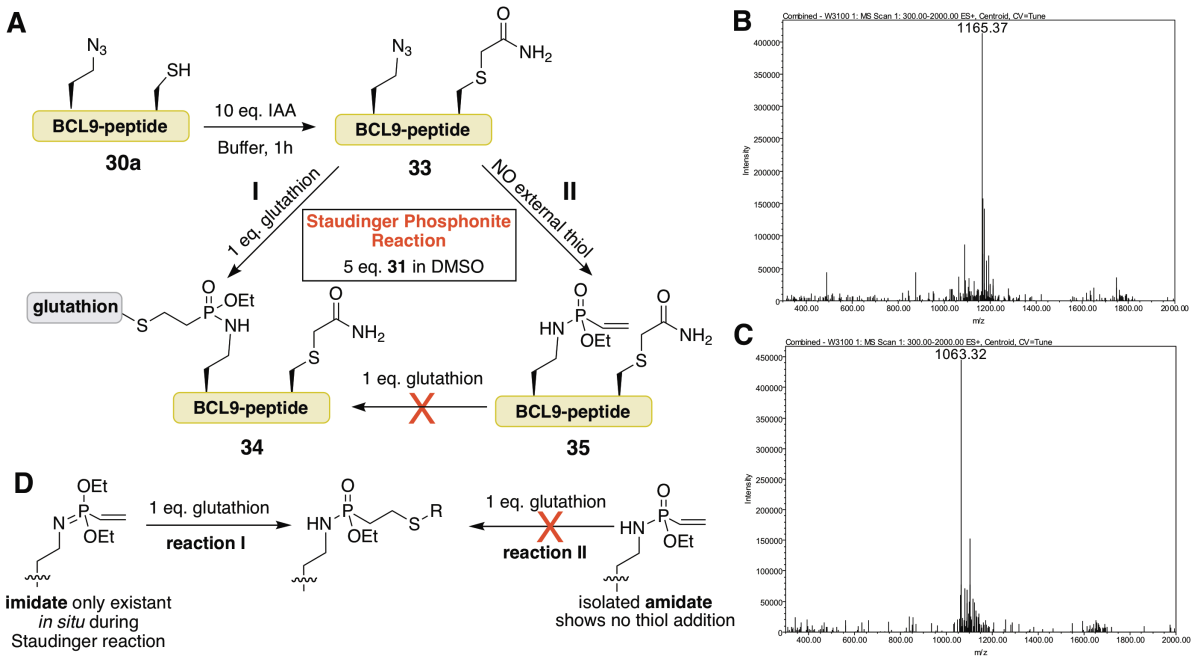

Figure 29: A) Synthetic plan for the evaluation of *in situ* thiol addition B) LRMS for crude reaction I. Expected $[M+3H]^{3+}$ for **34:** 1164.5976 m/z. C) LRMS for crude reaction of II after glutathione incubation. Expected $[M+3H]^{3+}$ for **35:** 1062.2363 m/z D) Comparison of thiol addition in reaction I, with the alkene imidate present and in reaction II with only the alkene amidate available for thiol addition.

This experiment led to conclude that the thiol addition is likely to occur at the imidate stage during the Staudinger-phosphonite reaction (see Scheme 8 in Chapter 4.3.2.3), because the co-occurrence of the imidate and the thiol is the only difference between reaction I and reaction II (Figure 29D).

Next, we studied the stability of the newly generated phosphonamidate linkage in **32a/b** over a broad range of pH values. Incubation of **32a** at pH values from 7.5 to 11.5 showed no

significant degradation of the peptide after four days (Figure 30A). However, at acidic pH a second peak appeared in the LC-UV/MS trace over time (Figure 30B), with a mass difference of about +18 Da, which could correspond to a water addition after P-N bond hydrolysis (Figure 30C).

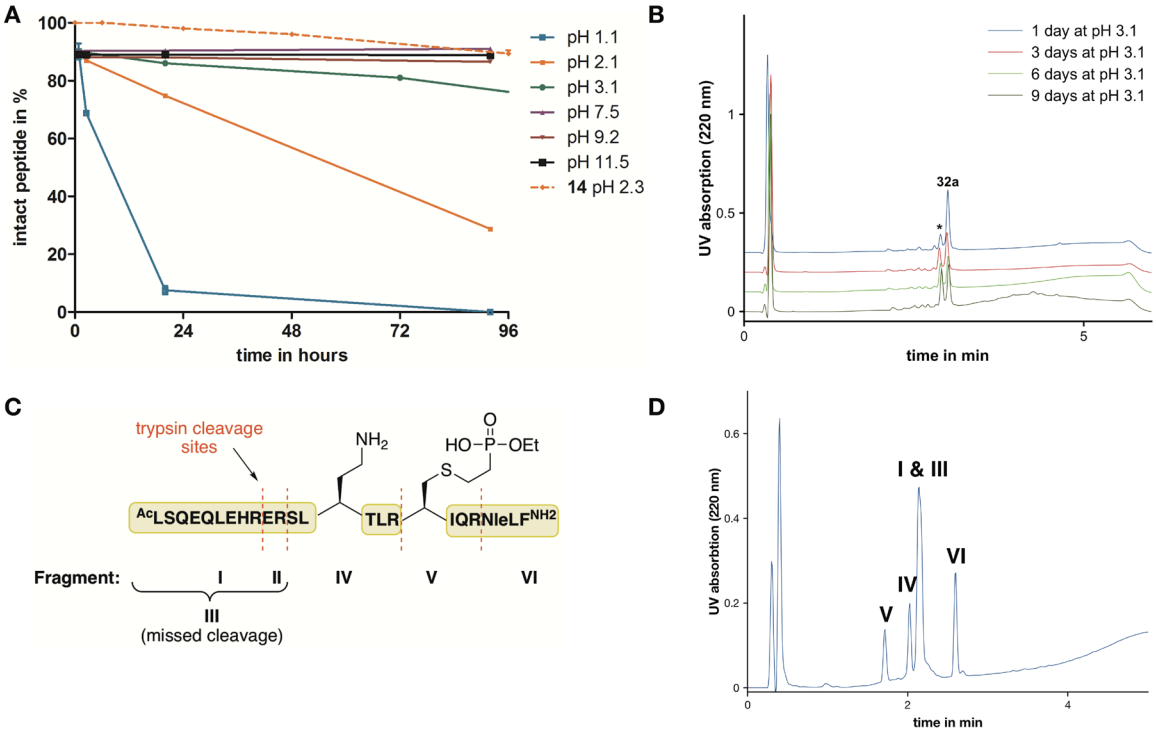

Figure 30: A) Stability studies of **32a** at different pHs and comparison to **14**. B) LC-UV of **32a** incubation at pH 3.1 over several days. P-N bond cleavage observed with peak *. C) Overview of expected structures after P-N bond hydrolysis and tryptic digest cleavage sites. D) Tryptic digest of **32a** incubated at pH 1.1 for 48 hours.

To provide further evidence for this, **34a** was incubated at pH 1.1 for 24 hours, lyophilized, re-dissolved in 100 mM ammonium bicarbonate buffer pH 8.0 and digested with trypsin. In the analysis of the tryptic digest *via* LC-UV/MS, all proposed fragments where observed, showing that the P-N bond cleavage is indeed the degradation product found at acidic pH (Figure 30D). The overall stability at acidic pH was significantly lower compared to the previously investigated phosphonamidate linkage with an aromatic substituent at the nitrogen atom in molecule **14** (see Chapter 6.2). The rationale behind the lower stability lies in the higher basicity of the aliphatic amine in comparison to the aromatic amine, which renders it more susceptible to protonation in acidic media and therefore higher degrees of P-N hydrolysis.

In an attempt to further derivatize this macrocyclization method, the third substituent on the phosphorous atom was considered as point of derivatization, as it is not directly involved in the formation of the linkage. Different substituents can be envisioned at this position,

including hydrophobic or hydrophilic moieties to influence peptidic properties or chemoselective handles. Because it is literature known that the cellular uptake of stapled peptides is heavily influenced by the overall hydrophobicity of the peptide (see chapter 4.2.3.), a more hydrophobic staple linker was synthesized. For this purpose, the synthesis route of the phosphonite was changed, starting from bis(diisopropylamino) chlorophosphine **36** (Scheme 14). Here, the first step is a Grignard reaction with the vinyl phosphine followed by an exchange of the diisopropylamine substituents with benzyl groups to yield vinylphosphonite **37**. The Staudinger-phosphonite reaction with **37** was carried out at slightly elevated temperatures than employed with phosphonite **31**, because a reduced rate of reaction was observed. The reaction progress was monitored by MALDI-TOF and gave slightly lower yields compared to the reaction employing **31** after HPLC purification.

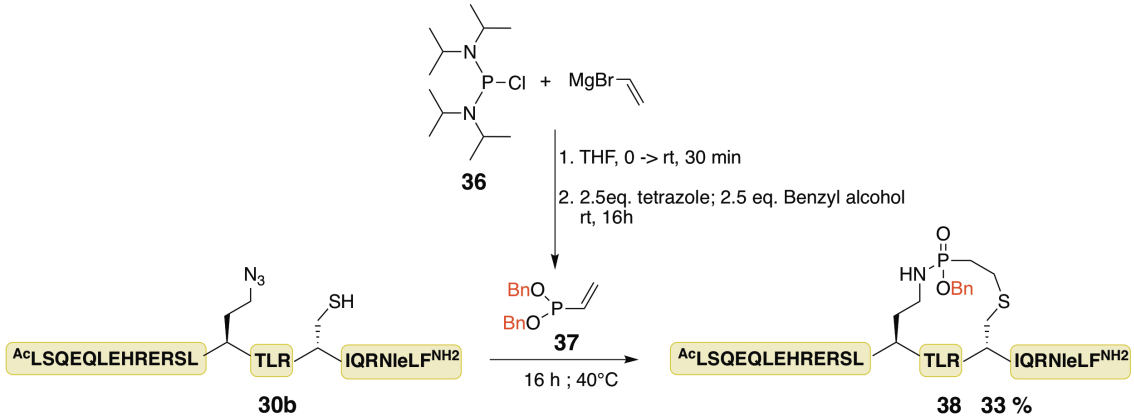

Scheme 14: Synthesis route for stapling of BCL9 peptides using a benzyl substituted linker.

Unlike before, only the D-cysteine peptide **30b** was macrocyclized with **37,** because the ethyl substituted cyclized D-cysteine peptide **32b** showed superior activity compared to L-cysteine variant **32a** in first *in vitro* test (see Chapter 6.3.6). Finally, the secondary structure of all cyclized peptides was analyzed by CD spectrometry. Induction of α-helicity in **32a, 32b** and **38** was compared to the non-cyclized peptide **30b** and the literature-known stapled version of the BCL9 peptide with methionine substituted to norleucine **39**, which was synthesized as a reference *via* SPPS (Figure 31B). After the Staudinger induced thiol addition, the helicity increased from 20% for the linear peptide **30b** to about 50% for peptides **32a, 32b** and **38** (Figure 31A). Here, the substituent on the phosphorous atom did not influence the secondary structure of the peptide. Even though the helicity increase is not as strongly pronounced compared to the literature known RCM stapled BCL9 **39**, nevertheless it is significant. It is known that helicity is not the only factor determining the effectiveness of a stapled peptide for PPI disruption, but rather the interplay between the cellular uptake and the structural stabilization. Hence, we set out to test the peptides' ability

to disrupt the interaction between the BCL9 protein and β-Catenin PPI in an homogenous time resolved fluorescence (HTRF) assay and to evaluate their ability to enter cells.

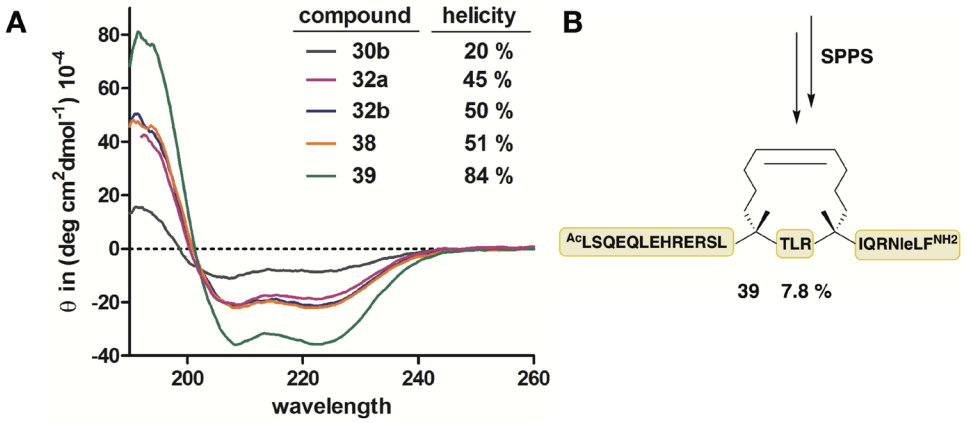

Figure 31: A) CD spectra for BCL9 peptides stapled by Staudinger-induced thiol addition or RCM compared to the linear peptide. B) Structure of positive control **39**.

6.3.5 Protein expression for HTRF assay

In an HTRF assay, a FRET system is created between two fluorescently labeled antibodies recognizing a tag on each of the interacting proteins. If the proteins interact a FRET signal is generated. If the interaction is disturbed this signal will vanish. In order to perform HTRF assays the interacting proteins will therefore have to be expressed with different tags for the antibody recognition. β-Catenin was envisioned as GST-tagged protein and BCL9 as His-tagged protein. The cDNA for GST-tagged β-Catenin was purchased and the protein expression was carried out in BL21 cells at 18°C for 18 hours. After expression, harvesting and lysis of the cells the pure protein was obtained after a straightforward purification over a GST-column (Figure 32).

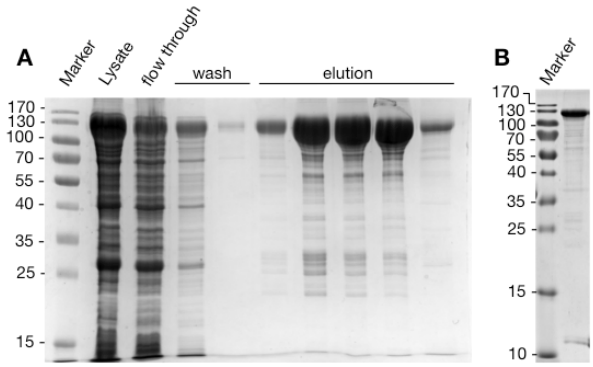

Figure 32: A) Purification of GST- β-Catenin. B) Pooled elution fractions rebuffered to PBS.

For the His_6-tagged BCL9 protein, the interacting protein domain of BCL9 [243 – 469] was ligated into a pET-28a vector exhibiting a *N*-terminal thrombin cleavage site and a *C*-

terminal His_6-tag. First attempts using NheI and XhoI restriction sites failed in the ligation. After switching restriction sites to BamHI and HindIII, the ligation and transformation delivered positive colonies with the expected DNA sequence. Expression was tested in two different cell strains at 18°C and 37°C. In these test expressions, an overexpressed protein was observed in an SDS gel at the migration height of 35 kDa (Figure 33A). As the expected protein has a mass of 27162 Da, the test expression from BL21 cells at 18°C was purified over Ni-NTA beads and the pooled elution fractions were analyzed by MALDI-TOF. A single peak with the expected mass was observed, confirming the successful cloning and expression of the desired protein. On these grounds, a big scale expression of BCL9-His_6 was conducted in BL21 cells at 18°C for 18 hours. After harvesting, cell lysate was purified *via* Ni-NTA beads (Figure 33B) and polished in a size exclusion chromatography (SEC) step to yield the pure His_6-tagged BCL9 protein (Figure 33C). The pooled fractions were analyzed with MALDI-TOF, which confirmed the isolation of pure protein (Figure 33D). With these proteins in hand we performed the *in vitro* assays to determine the inhibitory activity of our macrocyclized peptides on the PPI between BCL9 and β-Catenin.

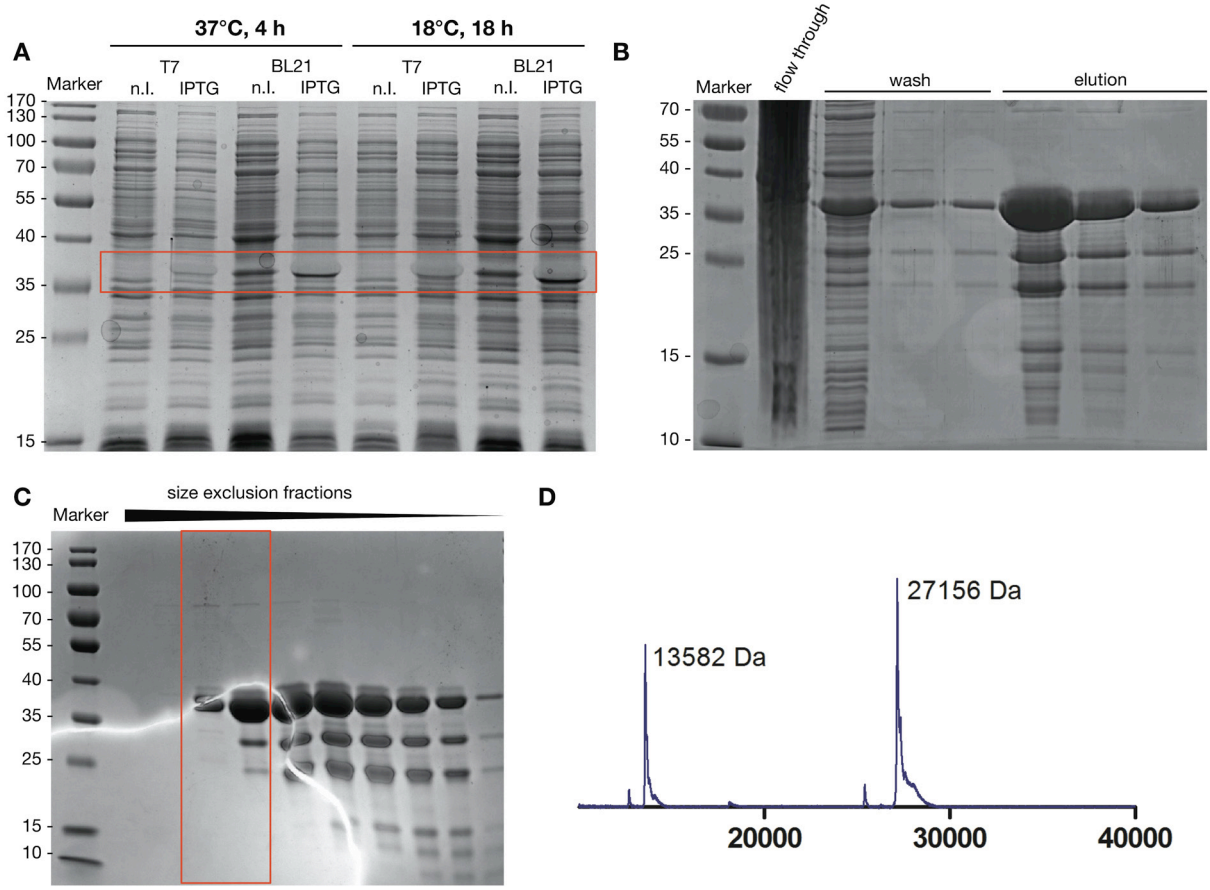

Figure 33: A) Test expressions of BCL9-His_6 in different cell strains and under different conditions. B) Purification of BCL9-His_6 *via* Ni-NTA beads. C) Further purification *via* SEC. D) MALDI-TOF spectra of pooled fractions.

6.3.6 Functionality assays with cyclized peptides

The HTRF assay was first conducted on the ethyl-substituted peptides **32a** and **32b** and was then compared to literature values. An inhibition of the protein-protein interaction was observed at nanomolar IC_{50} values for both peptides. The D-cysteine peptide **32b** however, could be identified as the most potent inhibitor with an IC_{50} of 144 nM, which is comparable with the IC_{50} value determined by GST-pulldown assays and reported in literature for the RCM stapled peptide[269]. Encouraged by these results we also tested a more hydrophobic phosphonite in the Staudinger induced thiol addition with the D-cysteine peptide **30b** (see chapter 6.3.4). For this benzyl substituted cyclized peptide **38** an almost identical IC_{50} value was observed in the HTRF assay, which illustrates that a more bulky substituent does not influence the disruption ability of this peptide inhibitor. As negative control a scrambled version of the BCL9-peptide (QSEQLERLEHRLQAhaRTLCNleSILRF - **40**) was used in the assay, which showed no inhibitory activity at all (Figure 34). The literature-known RCM stapled peptide **39** served as positive control. Surprisingly, **39** inhibited the protein-protein interaction between BCL9 and β-Catenin with a much higher IC_{50} value compared to **32b** and **38** and was not in accordance with the reported IC_{50} value by Takada *et al.*. Because two different assays were used to determine the IC_{50} values, which limit their comparability, we decided to investigate the binding affinity of the peptides to β-Catenin by ITC to gain more insight into the binding behavior of the cyclized peptides. Unfortunately, the peptides were not soluble at the concentrations needed for well-resolved signals in the ITC set-up. Especially peptide **39** was observed to be hardly soluble at concentrations exceeding 40 µM. Furthermore precipitation was observed during the titration of **39** to β-Catenin pointing also towards insolubility of the peptide – protein complex. This insolubility, which was much more pronounced for **39** compared to **32b** or **38**, could also be the reason for the surprisingly high IC_{50} value determined in the HTRF-assay.

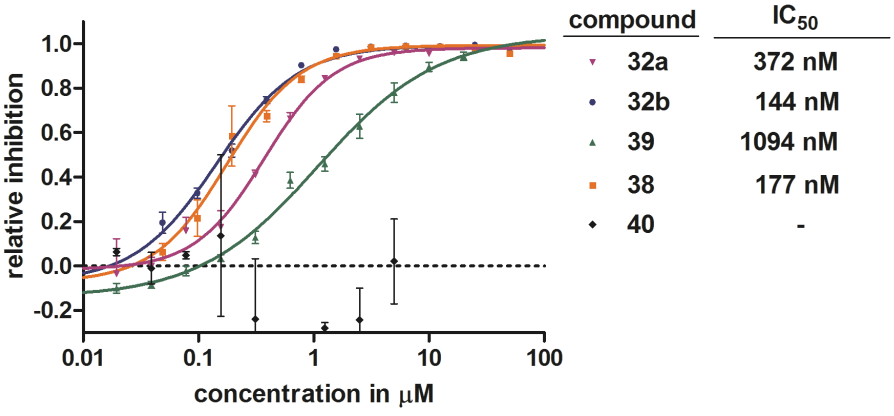

Figure 34: Inhibition of BCL9 – β-Catenin in HTRF assay.

In order to reach its intracellular target, the stapled peptides need to translocate into cells. The cellular uptake of cyclized peptides was to be analyzed by confocal fluorescence microscopy with HeLa cells, for which fluorescently labeled peptides were synthesized by attachment of fluorescein to the *N*-terminus of the peptide (Figure 35A/B). Cells were incubated with 10 µM peptide in serum free DMEM for two hours and imaged afterwards. The peptide fed to the cells consisted of only 10% fluorescein-labeled peptide to ensure that self-quenching is not hampering the fluorescence read out during microscopy. At first, only bright dots were visible for **38** and **39**, suggesting the peptides were trapped in endosomes. Upon imaging for longer than 20 seconds using an argon laser at 488 nm, bright fluorescence was observed over the whole cell for both peptides. This phenomenon could be explained by an endosomal disruption induced by laser irradiation during the imaging process. When comparing the fluorescence intensity inside cells, it was apparent that peptide **32b** did not show any uptake. Compared to that, a significant amount of the benzyl substituted linker peptide **38** had been taken up by the cell, comparable to the RCM stapled peptide **39** (Figure 35C). However, it should be noted that all the peptides were first trapped in endosomes, which makes a quantitative comparison difficult. Nonetheless, this shows that a more hydrophobic linker does have a significant influence on the cellular uptake, which has also been observed by the Futaki lab recently.[271] Using the *O*-substituent for influencing hydrophobicity of the linking molecule seems to be feasible and indeed has dramatic effects on the cellular uptake.

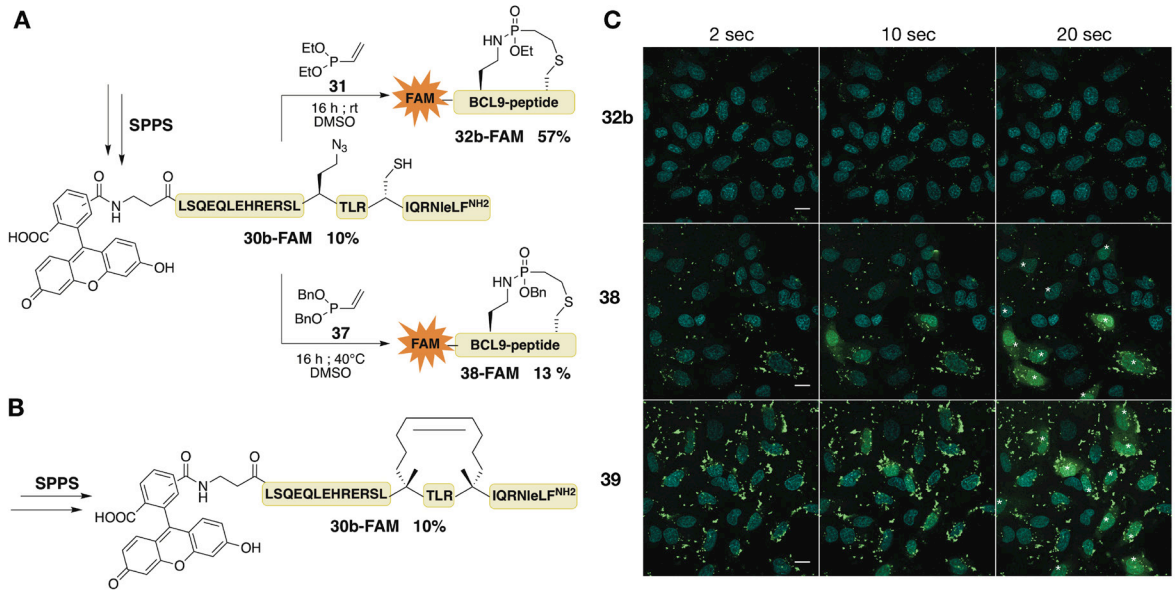

Figure 35: A) Synthesis of FAM-labeled BCL9 peptides cyclized *via* Staudinger induced thiol addition. B) Synthesis of FAM-labeled BCL9 peptide, which is stapled *via* RCM. C) Cellular uptake of 10 µM peptide (10% FAM-labeled peptide) for 3 h at 37°C 5%CO_2 in HeLa cells. Pictures show the overlay of FITC fluorescence and Hoechst stain after 2/10/20 seconds of imaging with an argon laser (405/488 nm). Scale bar = 20µm.

6.3.7 Intramolecular cyclization of R10 peptide.

As second substrate for the intramolecular Staudinger induced thiol addition, the cyclic cell penetrating poly-arginine peptide c(R10) was chosen (see chapter 6.2). The linear R10 peptide **41** with a C-terminal cysteine and an azidohomoalanine *N*-terminally of the polyarginine segment was synthesized by Fmoc-based automated SPPS. After purification of peptide **41** *via* preparative HPLC, the azidohomoalanine was reacted with the crude alkene phosphonite **31** analogously as done for the BCL9 peptide **30** (see chapter 6.3.4). After over-night reaction and purification, the successful cyclization to **42** was confirmed by a negative Ellman's test and *via* NMR. To assess the cell-penetrating properties of the c(R10), we tested the bioconjugation to eGFP C70M S147C and compared it to GFP conjugate **21** in its cellular transduction behavior (see Chapter 6.2). For this purpose, the free *N*-terminus was functionalized with an alkyne phosphonamidate-NHS building block (**43**), which was synthesized by Marc-André Kasper in the Hackenberger group (Figure 36A).

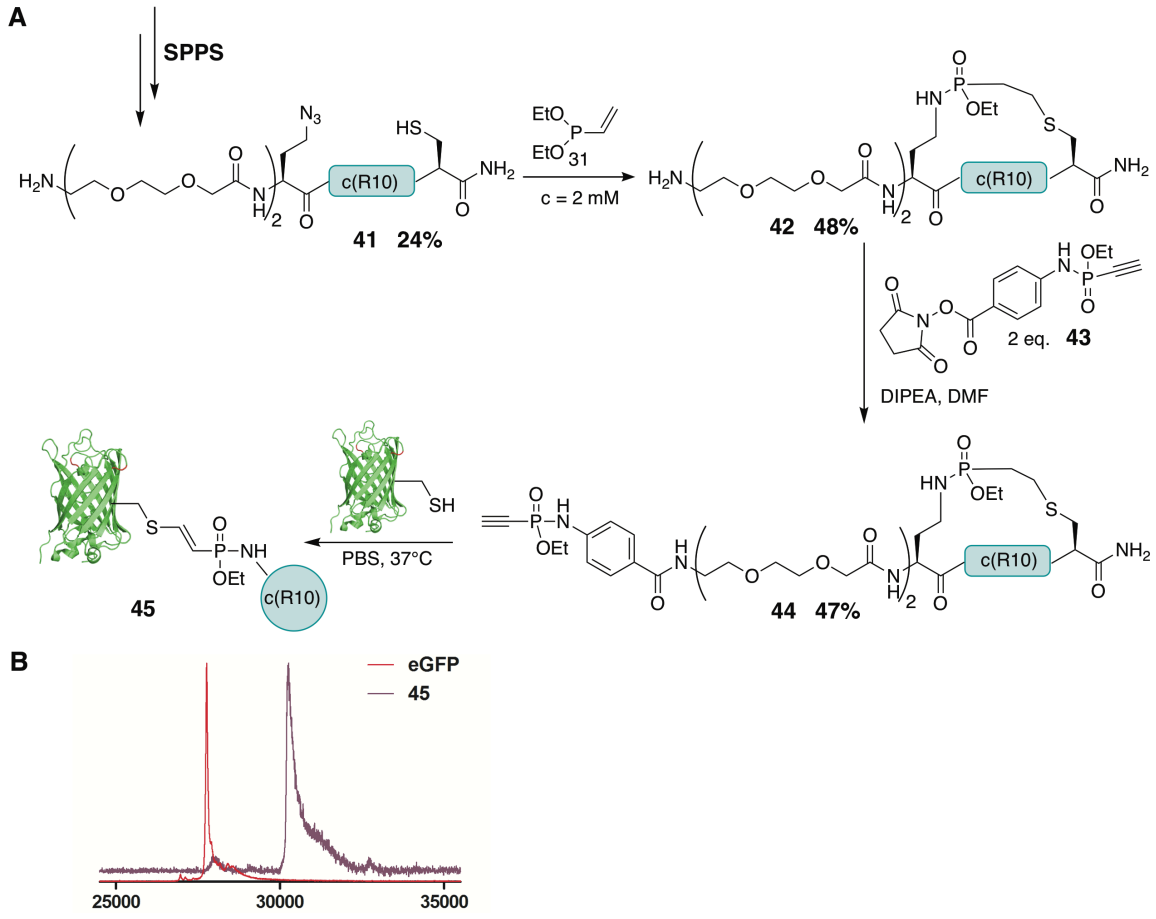

Figure 36: A) Synthesis route for Staudinger induced thiol addition cyclized R10 functionalization of eGFP C70M S147C B) MALDI-TOF of thiol addition eGFP to **44**.

After amide bond formation and purification, peptide **44** only differed to peptide **19** in the linker used for cyclization. The conjugation towards eGFP C70M S147C was carried out under the same reaction conditions as for the lactam cyclized CPPs (see chapter 6.2.), yielding **45** in a quantitative fashion according to the MALDI spectra (Figure 36B). The biological behavior of peptide – protein conjugate **45** was now directly comparable to **21** in cellular uptake studies. The c(R10)-eGFPs were incubated for one hour with HeLa cells at 37°C in HEPES buffer, afterwards washed with DMEM including 10% FBS and then imaged. For quantification purposes the nucleus was stained with Hoechst. In three biological replicates no significant differences were observed for the intramolecular Staudinger induced thiol addition cyclized cR10-eGFP conjugates compared to the lactam cyclized peptide-protein conjugates (Figure 37A). Both conjugates showed mainly diffuse cytosolic and nucleolar localization of GFP fluorescence, which accounts for the cytosolic availability of the protein (Figure 37B).

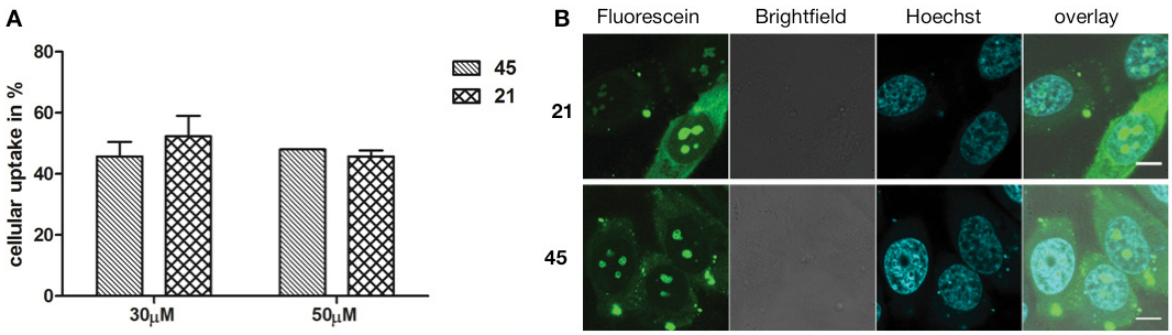

Figure 37: Cellular uptake of CPP-eGFP conjugates A) Quantification of cellular uptake of three replicates B) Confocal images scale bar = 10 µm.

6.3.8 Conclusion and Outlook

In summary, we applied the Staudinger induced thiol addition as an intramolecular macrocyclization tool on two different peptidic targets. The cyclized BCL9 derived peptides showed an increased α-helicity upon macrocyclization and were capable of disrupting the protein – protein interaction between the BCL9-protein and β-catenin at nanomolar concentrations in an HTRF assay. We furthermore demonstrated that the interchangeable substituent on the phosphorous could be used to influence the peptides hydrophobicity, which facilitated cellular uptake. In a second example, the Staudinger induced thiol addition was used for the macrocyclization of a polyarginine peptide, in which the reacting amino acid side chains were separated by a longer peptide sequence than in the BCL9 peptide. In this case the macrocyclization was also successful and delivered bioactive peptides, whose transduction behavior were compared with the lactam-cyclized peptides investigated in chapter 6.2. It was shown that the macrocyclization of the cell penetrating peptide *via* Staudinger induced thiol addition facilitates transduction of a covalently conjugated eGFP into HeLa cells to the same extend as lactamization does. The use of easily incorporable functional groups for the cyclization reaction *via* SPPS as well as the ability to adjust the 3rd substituent on phosphorous of the phosphonite clearly demonstrates the great feasibility of this cyclization strategy.

Future projects will focus on evaluating the influence of different P(III) substituents on the structure and biological behavior of cell-penetrating peptides. Furthermore one could envision the usage of this substituent as anchoring point for the introduction of other functional tags. It is also possible that this reaction could be used for generating highly efficient cyclic cell-penetrating peptides in an expressed protein system of interest without the need of external peptide synthesis and bioconjugation. Here, we envision the expression of a linear CPP-tagged protein, including a spacer, azidohomoalanine, the CPP sequence and a cysteine (Figure 38). After expression and purification, the azidohomoalanine could be reacted chemoselectively with an alkene-phosphonite and thiol addition to the proximal cysteine would generate the c(CPP) tag without the need of peptide synthesis and bioconjugation.

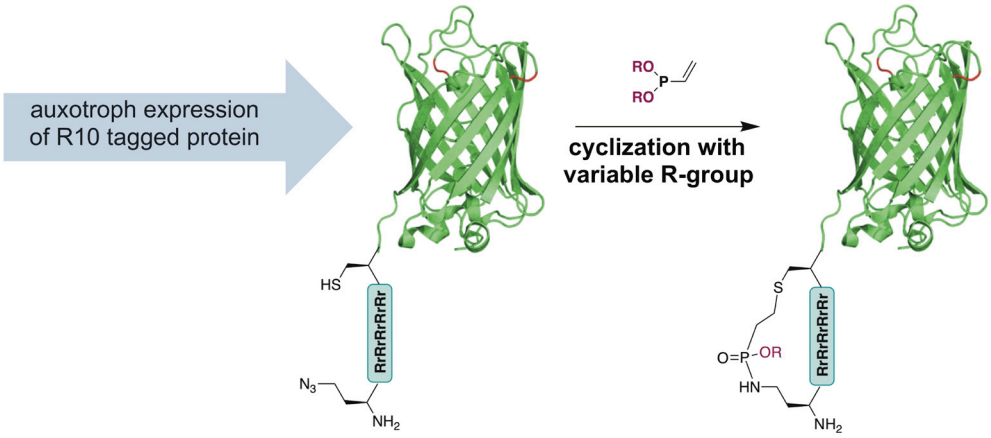

Figure 38: Concept for the expression of a CPP-tagged protein and its intramolecular cyclization.

6.4 Diazo-functionalized CPPs for bioreversible esterification of proteins

6.4.1 Outline of the Project

In this project we wanted to apply the literature-known bioreversible esterification of proteins with diazo compounds[152,155] as alternative bioconjugation strategy for the generation of cyclic CPP – protein conjugates. To conjugate peptides to proteins, esterification *via* two different routes was envisioned. One route was the *N*-terminal functionalization of the c(R10) peptide **47** with the NHS – diazo building block **46**, followed by straightforward esterification of eGFP with this diazo-c(CPP) **48** (Figure 39A). The second route was the esterification of eGFP with the diazo-compound **50** bearing an alkyne handle, followed by post-esterification modification with an azide-functionalized c(CPP) **52** *via* CuAAC (Figure 39B).

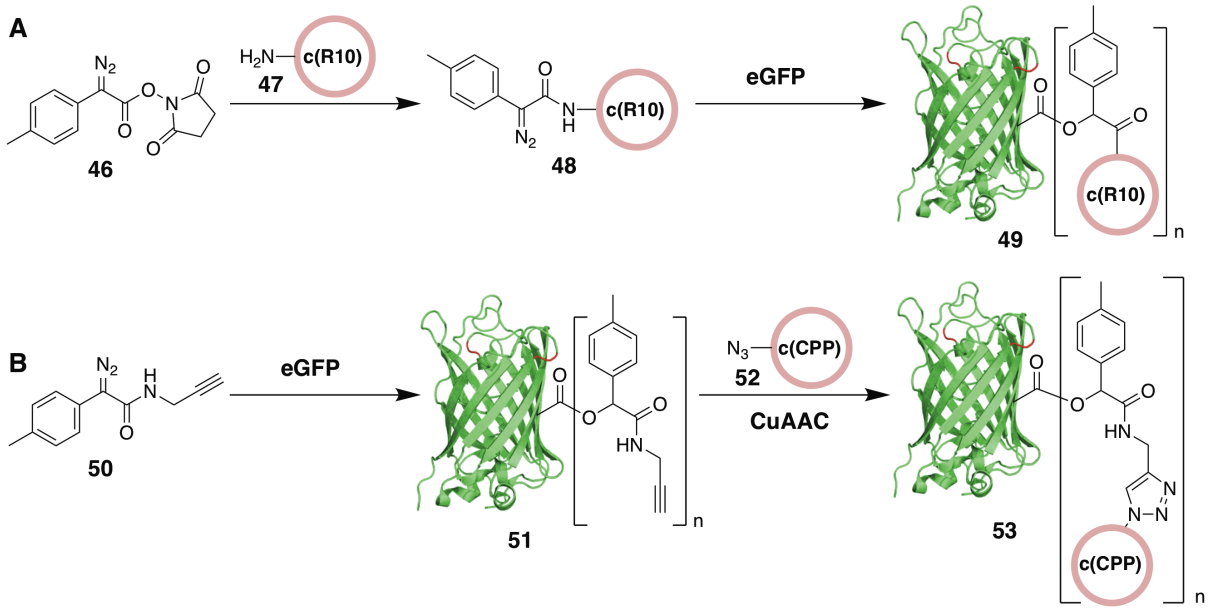

Figure 39: Bioreversible cCPP conjugation to eGFP by esterification with diazo compounds. A) Route *via* diazo-peptide. B) Route *via* post-esterification functionalization.

After esterification, the cellular uptake of the c(CPP)-protein conjugate should be monitored by fluorescence microscopy by exploiting the inherent fluorescence of GFP. Furthermore, the bioreversibility of the ester formed in the conjugation was to be analyzed *in vitro*. The c(CPP) – eGFP constructs, which were already described in this thesis (Chapter 6.2 and 6.3), served as the perfect model system for this purpose, thanks to the c(CPP)'s attraction towards the nucleolus of the cell. It has been shown previously that this attraction is strong enough to transport covalently bound cargos like eGFPs towards the nucleolus. We hypothesized that upon cellular transduction the ester-linked c(CPP) – eGFP conjugate gets

cleaved by esterases inside the cell. As the eGFP without the c(CPP) does not exhibit any nucleolar attraction it would remain freely inside the cytosol, without nucleolar localization, making the cleavage well observable by microscopy. With this setup, the esterification of c(CPP)s to eGFP was established with two different diazo building blocks and finally the conjugates were envisioned to be tested in their cellular uptake behavior using fluorescence microscopy.

6.4.2 Responsibility Assignment

The project was designed and planned by Prof. Dr. Christian P.R. Hackenberger and Prof. Dr. Ronald T. Raines. Dr. Kalie Mix synthesized the diazo compounds **46/50** as part of her PhD thesis. The author synthesized the peptides, performed the peptide functionalizations with the provided diazo compounds and conducted esterification reactions on protein level. Kristin Kemnitz-Hassanin expressed and purified the eGFP C70M S147C according to the protocol Dominik Schumacher developed in his PhD thesis.[262] Initial cellular uptake studies were carried out by Henry D. Herce in the group of Prof. Dr. Christina Cardoso and were continued by the author.

6.4.3 Results and Discussion

6.4.3.1 Esterification *via* diazo functionalized peptide (Route A)

We started our investigations with the synthesis of the diazo-functionalized peptide **48.** To do so, the cyclic R10 peptide **47** was first synthesized by SPPS. After cleavage of the peptide from solid support and its purification, the free *N*-terminus was reacted with the NHS-diazo building block **46** to form a stable amide bond (Figure 40A). The reaction was complete after four hours and the functionalized peptide could be precipitated from the reaction mixture in cold diethylether to provide **48** in purity >90% (Figure 40B). Due to the high lability of the diazo group, purification *via* HPLC was avoided. As the amide bond-forming step was conducted on a deprotected peptide, the reaction was limited to peptides with only one free amine and was therefore compatible with the structure of c(R10), but not c(Tat) (see Chapter 6.2). Functionalization of the protected peptide attached to solid support was not possible due to the inherent lability of the diazo compound towards acids that would be needed for deprotection and cleavage. With **48** in hand, we set out to test the esterification on protein level using eGFP C70M S147C as model substrate (Figure 41A).

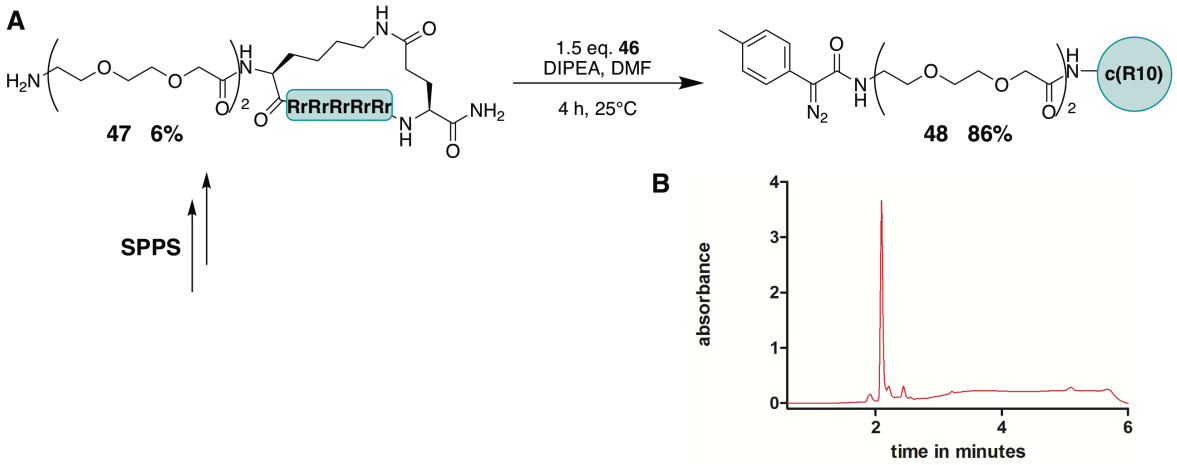

Figure 40: A) Synthesis of diazo-functionalized cR10 and B) LC-UV spectra of **48**.

The esterification reaction was carried out in different buffers with or without additional co-solvent and at pH ranging from 5.8 to 7.4 for 4 to 16 hours. All reactions were carried out at 37°C with varying equivalents of peptide **48** (Table 3). Our first observation was that the reaction did not proceed in PBS at pH 7.4 (Entry 1) and it is indeed known that the targeted carboxylic acid needs to be deprotonated in order to react in an esterification. We lowered the pH to 5.8, which is roughly the pH that was used in previous protein esterifications with diazo compounds.[155] We observed that eGFP precipitates at this pH, even when using a

buffer with high NaCl content (Entry 3-4). At pH 6.5, the eGFP also precipitated when using a buffer without additional NaCl (Entry 2). However, by adding 100 mM NaCl to the buffer, the protein remained solubilized and the reaction proceeded to a satisfying result of up to two peptides bound to eGFP (Entry 6). As it has been reported before that a buffer-acetonitrile mixture provides the best conjugation results[152,155], the reaction was also probed with an additional 20% of acetonitrile, which also led to protein precipitation (Entry 5). Finally, 10 mM BisTris buffer with 100 mM NaCl at pH 6.5 was chosen as optimal reaction buffer, since the eGFP used showed the highest stability in these conditions. To further optimize the reaction, it was conducted with different equivalents of **48**, different reaction times and purification methods. First of all, we discovered that prolonging the reaction time from 4 to 16 hours did not yield significantly more conjugation product (Entry 8/9). When comparing different amounts of **48** added to the reaction, it was observed that 10 equivalents yielded a mixture between 0 – 1 modifications, whereas at 50 equivalents yielded 1 – 3 modifications. Another interesting observation was the influence of the purification method on the result. When Zeba spin desalting columns (MWCO 7 kDa) were used, we could not observe high amounts of eGFP with multiple copies of peptide attached, probably due to a tendency of the multiply cR10-tagged GFP to unspecifically bind to the column material (Figure 41B, Entry 9).

Table 3: Screening of different conditions for esterification of eGFP. * = including 100 mM NaCl.

entry	buffer	time	eq. of **48**	pH	purification	result from MALDI
1	PBS	4 h	50	7.4	ZebaSpin	no reaction
2	10 mM BisTris	4 h	50	6.5	-	precipitation
3	10 mM BisTris*	16 h	10	5.8	-	precipitation
4	10 mM BisTris*	16 h	30	5.8	-	precipitation
5	10 mM BisTris* + 20% MeCN	4 h	50	6.5	ZebaSpin	precipitation after two hours
6	10 mM BisTris*	4 h	50	6.5	ZebaSpin	0 – 2 modifications
7	10 mM BisTris*	16 h	50	6.5	dialysis	1 – 3 modifications
8	10 mM BisTris*	4 h	30	6.5	ZebaSpin	0 – 2 modifications
9	10 mM BisTris*	16 h	30	6.5	ZebaSpin	0 – 2 modifications
10	10 mM BisTris*	16 h	30	6.5	dialysis	1 – 3 modifications
11	10 mM BisTris*	16 h	10	6.5	ZebaSpin	0 – 1 modifications

In contrast when using dialysis for purification, we observed a distribution of up to three modifications (Entry 7 and 10). Taken together all these observations, we synthesized different eGFP constructs with either predominantly double (conditions for Entry 10) or single c(R10) conjugations (conditions Entry 8), to test whether multiple peptide copies have an effect on the cellular uptake rate and if the ester is cleaved inside the cell to release the model cargo eGFP from the peptide.

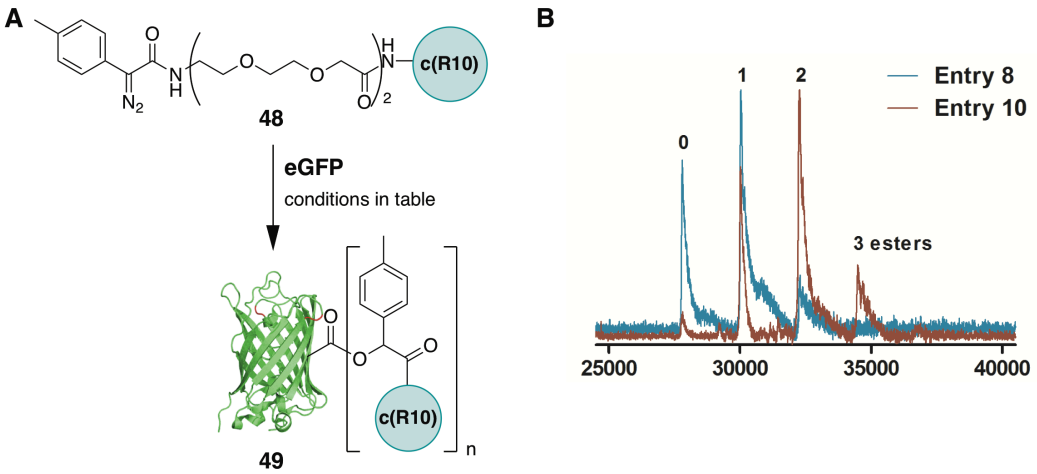

Figure 41: A) Esterification of eGFP with **48**. B) MALDI-TOF analysis for entry 8 and 10 of table 3.

6.4.3.2 Post-esterification peptide functionalization *via* CuAAC (Route B)

Since the direct site-specific peptide functionalization with the diazo compound **46** is limited to peptides with only one free amine in their sequence, we also explored the more flexible possibility of esterifying a protein with diazo compound **50** first, before further functionalizing the conjugated reactive handle *via* CuAAC (Figure 39B). The peptides employed for the conjugation were azido-functionalized cyclic Tat **52a** (Scheme 15A) and azido-functionalized Cy3-tagged cR10 **52b**.

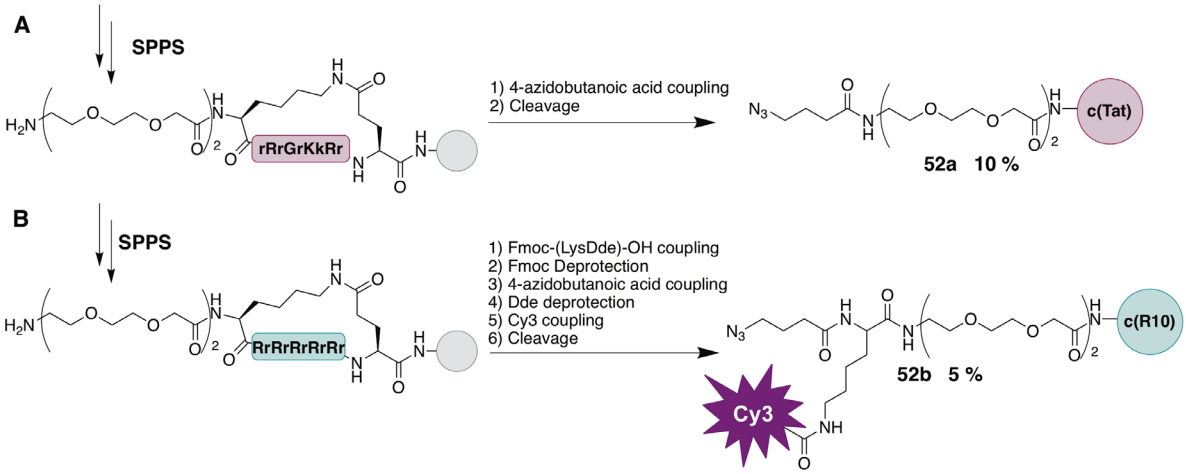

Scheme 15: A) Synthesis of **52a**. B) Synthesis of **52b**.

The first step of the protein conjugation was the esterification with diazo compound **50**. The reaction was carried out in a BisTris buffer at pH 5.8 with 1% DMF. The amount of carboxylic acid side chains esterified with the alkyne, could be influenced by adjusting the reaction time and the number of diazo equivalents (Table 4). The CuAAC with peptide **52a** was carried out with an alkyne-functionalized eGFP **51** with up to five modifications, synthesized using the conditions described in entry 4 (Table 4), because our initial goal was to conjugate multiple peptide copies to eGFP (Table 4; Figure 42B, Entry 4).

Table 4: Screening of different conditions for esterification of eGFP.

entry	eq. of **50**	time	results according to MALDI
1	20	2 h	0 – 1 modifications
2	20	4 h	0 – 2 modifications
3	20	16 h	mainly 3 modifications
4	30	16 h	2 – 5 modifications

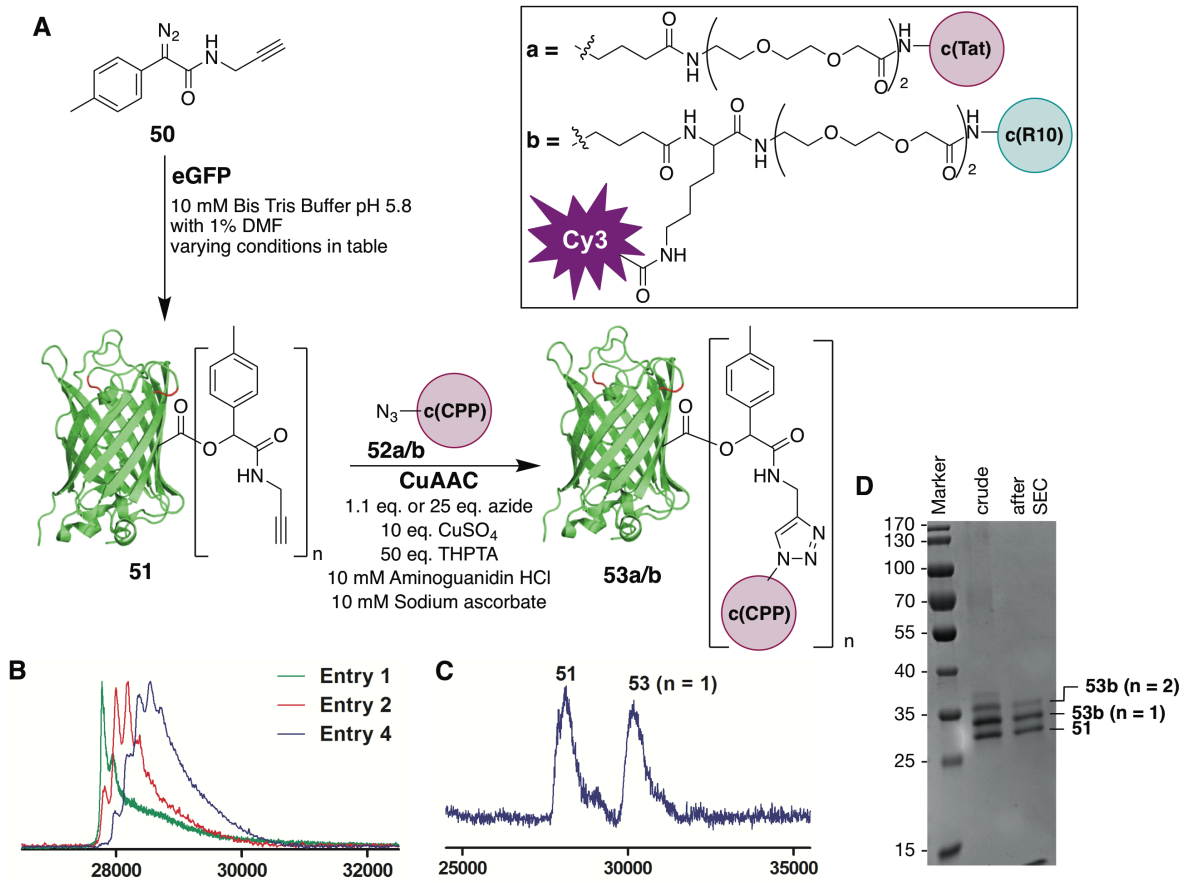

Figure 42: A) Synthsis of alkyne tagged eGFP and further functionalization with c(CPP)s. B) MALDI-TOF spectra of sterification screen with **50**. C) MALDI-TOF of **53a**. D) SDS-page of **53b**.

In the subsequent CuAAC reaction we reacted **51** with 25 equivalents of **52a**. After overnight reaction, **51** had only reacted partially to the single modified peptide – protein conjugate **53**. Due to the already heterogeneous mixture of the starting material **51,** the analysis of product **53** *via* MALDI-TOF showed broad peaks, most likely due to the high complexity of the final product **51** (Figure 42C). To reduce this complexity, especially when synthesizing the FRET-system, we focused on synthesizing lowly functionalized version of protein **51**. We aimed at a maximum functionalization of two alkynes per protein by using 20 equivalents diazo compound **50** for four hours during the esterification reaction (Figure 42B, Entry 2). The CuAAC with **52b** was then carried out with 1.1 equivalents of azido peptide **52b** and was analyzed by SDS-Page (Figure 42D). Purification was carried out *via* different methods, namely dialysis, spin filtration and purification *via* desalting columns, in order to compare their performance. Due to the high hydrophobicity of the Cy3-label, multiply tagged eGFPs were prone to stick to both dialysis tubing and spin filters. The best recovery was achieved by using desalting columns (MWCO 7 kDa), which yielded **53b** in a mixture of mainly 0 – 1 peptides attached (Figure 42D).

6.4.3.3 In vitro application of ester linked cCPP-eGFP

Cellular uptake studies were carried out with HeLa cells in HEPES Buffer with **49** modified with mainly one cR10 (Figure 43A, Table 3: Entry 6). The cells were incubated with 10 µM of **49.** In the confocal images, a high cellular uptake into the cytosol as well as the nucleolus was observed, hinting towards an insufficient or slow cleavage of the ester bond by esterases inside the cell. Furthermore, we observed a very high toxicity in the cells that has not been observed for the cCPP-eGFP conjugates discussed previously in this thesis. After one hour of incubation, most of the cells that showed high fluorescence were still attached to the Ibidi-slide, but were rounding up. Therefore they were found in a different plane in confocal microscopy compared to the ones with lower fluorescence. Also they showed a completely different Hoechst staining pattern compared to the cells with little or no uptake (Figure 43B).

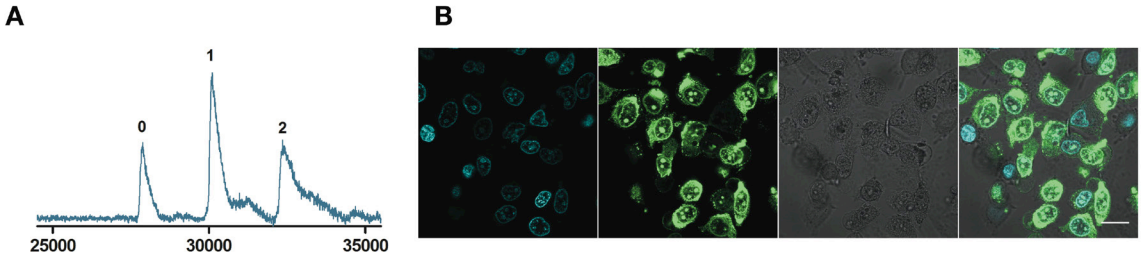

Figure 43: A) MALDI-TOF of **49** used on HeLa cells. B) Confocal images of HeLa cells after incubation with **49.** Scale bar = 20µm.

Multiple factors could be the cause for the observed toxicity. On one hand, the amount of doubly modified protein used in the cellular experiments could lead to a much higher toxicity than previously observed for the singly modified c(CPP) – eGFP constructs (Chapter 6.2 and 6.3). But also when using fewer equivalents in the esterification, resulting in lower amounts of doubly esterified **49,** cytotoxicity in the cellular uptake study was not reduced. Another factor could be the ester linkage itself, because this constitutes the biggest difference to **20**. Due to this toxicity effect, we did not further test compounds *in vitro* and studies to explain toxicity have not yet been conducted.

6.4.4 Conclusion and Outlook

In summary, we showed that the esterification with diazo-compounds could be carried out with functional peptides on protein level using two different diazo building blocks. Furthermore, we found that the amount of peptidic copies covalently attached to the protein can be influenced by the amount of diazo-compound added and by the length of reaction time. Unfortunately the *in vitro* application of final peptide – protein conjugates revealed high toxicity of **49** due to an unclear cause.

This toxicity needs to be further evaluated and pin pointed toward either the conjugation method, the multiple attachments of cyclic cell penetrating peptides or a different not yet considered source, by testing a more defined system *in vitro.*

7 Summary

Throughout this work the high versatility of peptides could be used to address diverse targets. Peptides could be applied as protein – protein and protein – ligand inhibitors as well as cellular transduction tags. A special focus was further laid on their bioconjugation to protein or polymer scaffolds to either foster their potency or simply transfer their properties to a cargo of choice. For these purposes, this work resulted in a bioconjugation method that cannot only conjugate a chemically modified peptide to a protein cargo, but which can further induce intramolecularly a function within the peptide itself by constraining its conformation, which underlies that function.

Project 1: Multivalent Peptide-Nanoparticle Conjugates for Influenza-Virus Inhibition.

In nature many tight binding events are built up by multiple low affinity interactions happening in close proximity on the same target. This concept is termed multivalency and was used in this project for the creation of a virus blocking peptide-polymer-nanoparticle. Here presentation of multiple peptidic HA binding ligands on a nanoparticle, which consists of polyglycerol was the underlying rational (Figure 44).

In this thesis it was shown *in vitro* as well as *in vivo* that using this concept leads to the development of a potent inhibitor for the infection of cells with the influenza virus. The hemagglutinin binding peptide sequences **PeB** and **PeB^{GF}** have previously been generated from the CDR-domain of the HA binding antibody, with higher monovalent binding affinities towards HA than its natural ligand sialic acid and was thought to be even more potent in a multivalent setting.[33] The polymer scaffold offered the opportunity to vary the size as well as the density of presented peptidic ligands, which were compared in initial *in vitro* assays. The ligand was conjugated onto differently sized polymers **(3a – 6a)** that were functionalized with azido groups at varying densities throughout CuAAC.

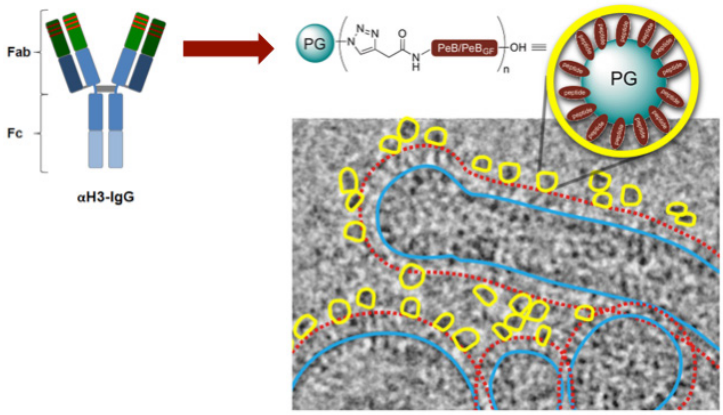

Figure 44: Schematic outline of the generation of entry blockers for the influenza – virus.

Comparing the different conjugates, we found that the biggest nanoparticles with a ligand density of about 1.0 ligand/nm^2 (**6b** and **6d**) gave indeed the best results in hemagglutination inhibition assays as well as infection inhibition assays. We further carried out *in vivo* tests in mice, which also verified the applicability of multivalent peptide-polymer-nanoparticles for the inhibition of influenza virus infection.

Project 2: Staudinger-induced thiol addition as cysteine reactive conjugation.

In this project we applied the Staudinger induced thiol addition for the additive free conjugation of biological active peptides to proteins. First this reaction was tested on the small cyclic RGDfK peptide[272]. Here the Staudinger phosphonite reaction was carried out between the 4-azido-benzoic acid, incorporated into the peptide by SPPS, with the electron rich alkyne phosphonite **7** to yield an electron poor phosphonamidate **12**. Thiol addition to **12** was first tested with glutathione and the conjugation products **14** stability was analyzed. Here, it was found that the conjugation product exhibits a high stability between pH 2.3 and pH 9 and does not show any signs of thiol exchange, when being incubated with high excess of external thiols. This poses an advantage to the often-used maleimide bioconjugation.

The bioconjugation toward proteins was addressed. A quantitative conjugation of alkyne peptide **12** to eGFP was achieved. Due to this demonstration of feasible bioconjugation between peptides and proteins, the application was expanded to more challenging peptide substrates cTat **16** and cR10 **17**. In all cases the activated electron poor alkyne peptides (**18/19**) were yielded after Staudinger-phosphonite reaction with **7**, and could be further conjugated quantitatively to eGFP (**20/21**). *In vitro* applicability of these cCPP-eGFP conjugates was verified by cellular transduction, which was compared to literature[121] and literature known cysteine bioconjugation reactions, namely maleimides and iodocarbonyl linkers. Here it could be shown that the phosphonamidate thiol adduct linked cCPP-eGFPs are indeed capable to transduce into cells. Further the transduction behavior is comparable to cCPP-eGFP conjugates obtained by other cysteine reactive bioconjugation methods and also to previous reports using CuAAC[121] for bioconjugation, making the Staudinger induced thiol addition an attractive strategy for chemoselective incorporation of a cysteine reactive handle into peptides and its further use in bioconjugations.

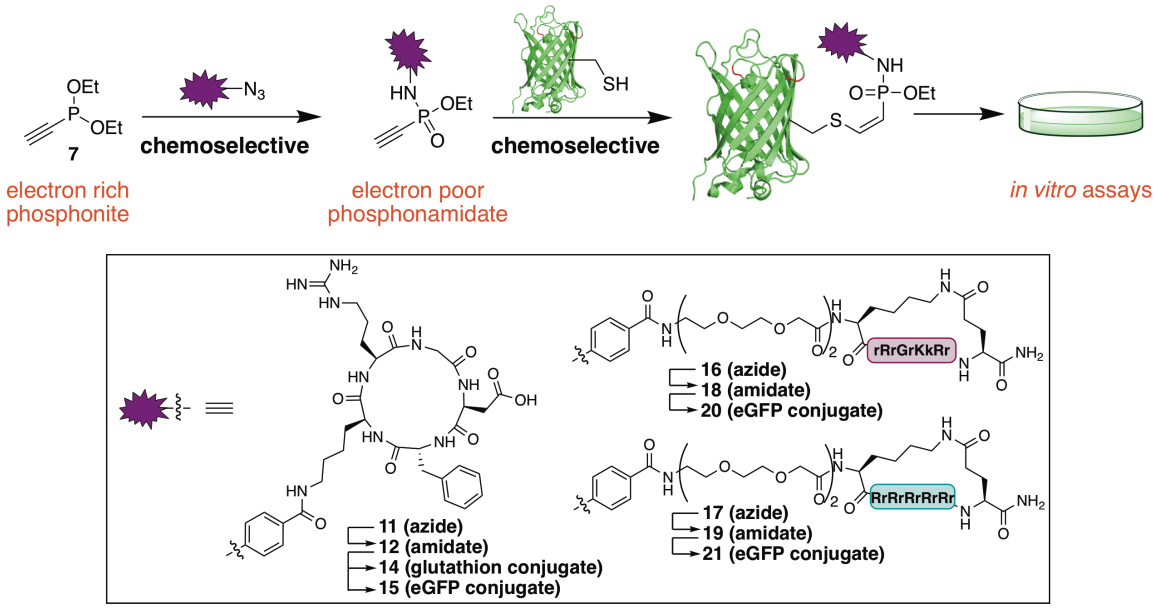

Figure 45: Schematic outline of the Staudinger induced thiol addition for bioconjugation of functional peptides with proteins, with an overview of substrate used in the reaction.

Project 3: Intramolecular Staudinger-induced thiol addition as new peptide cyclization method.

Intrigued by the feasible intermolecular bioconjugation *via* the Staudinger induced thiol addition shown in project 2, we set out to also investigate the reaction in an intramolecular fashion, as novel peptide macrocyclization strategy. Two different peptide substrates were synthesized with an azidohomoalanine as well as a cysteine at strategic points in their structure to demonstrate macrocyclization using a phosphonite linker. A literature known peptide derived from the BCL9 protein was envisioned to be stabilized in its α-helical structure by covalently linking two amino acid side chains in i, i+3 position representing one helical turn (Figure 46A). In addition, the R10 peptide discussed previously in project 2, was anticipated to be macrocyclized in order to promote its cellular transduction efficiency, which it only exhibits upon cyclization as described previously in literature (Figure 46B).[118,121] The intramolecular Staudinger-induced thiol addition on BCL9-peptide **30** was carried out using alkene-phosphonites **31** and **36,** which reacted successfully with the *via* SPPS incorporated azidohomoalanine, upon which the thiol addition of cysteine to alkene was observed *in situ*. Upon covalent linkage an increase in peptidic helicity was observed *via* CD-spectrometry, indicating the stabilization of the helical structural motif. It is known that upon macrocyclizing this peptide sequence *via* RCM, it is capable to disrupt the BCL9 – β-catenin interaction. This behavior was also evaluated for the Staudinger cyclized peptides and an almost identical IC_{50} value could be determined for the Staudinger linked peptide compared to the literature values for the RCM-linked peptide. Furthermore, the reaction with an alkene-phosphonite **36** with a more hydrophobic *O*-substituent could be carried out

successfully. The more hydrophobic linker did not interfere with the stabilization of helical conformation or the peptides ability to disrupt interaction of BCL9 and β-Catenin (Figure 46A). In cellular uptake assays a higher endosomal uptake could be observed for the more hydrophobic peptide, which showed comparable uptake behavior than the RCM stapled literature known peptidic inhibitor.

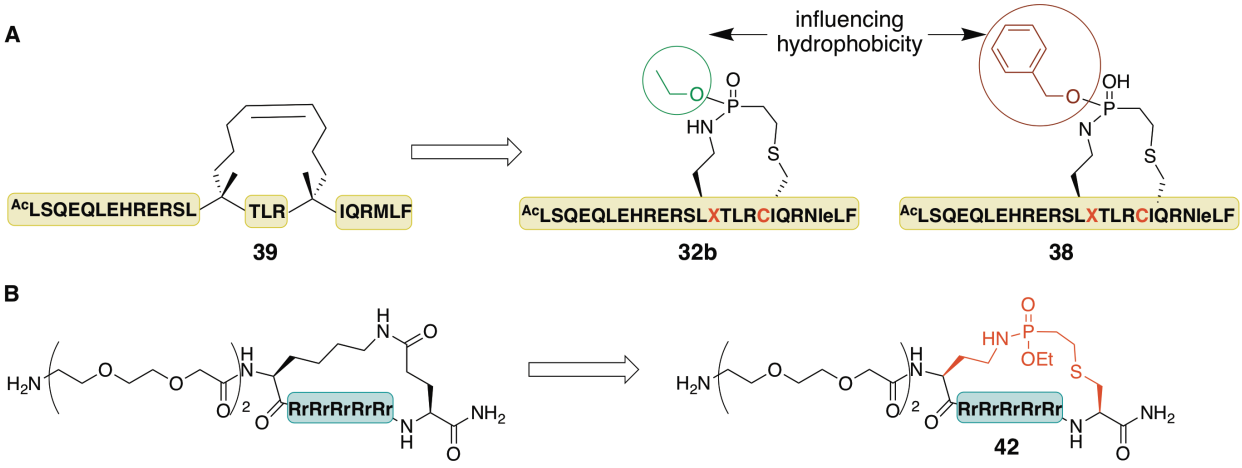

Figure 46: Schematic outline of the literature known peptides and its macrocyclized variants obtained by intramolecular Staudinger induced thiol addition for A) the BCL9-peptide and B) the c(R10) peptide.

Furthermore, the intramolecular Staudinger induced thiol addition was used in the cyclization of the R10 peptide, which was cyclized by lactamization in project 2. Here cysteine was incorporated at the *C*-terminus and azidohomoalanine *N*-terminally from the arginine sequence by SPPS. Both functionalities were covalently linked by alkenephosphonite **31**. After cyclization and conjugation to GFP, the cellular transduction properties were directly comparable to the lactam-linked peptide – protein conjugate **21**. Here the applicability of this linker *in vitro* was confirmed as well as its transduction properties, which were similar compared to the ones of lactam-cyclized peptides. Also for the cR10 peptide the derivatization of the *O*-substituent in the phosphonamidate linker could be of great interest in future projects. Here a methodological correlation between peptidic properties and cellular transduction ability could be established in a feasible manner.

Project 4: Diazo-functionalized CPPs for bioreversible esterification of proteins

The aim of this project was the generation of intracellularly cleavable cCPP-eGFP conjugates by esterification of carboxylic acids on GFP with cCPPs throughout diazo compounds. The reaction itself was developed in the Raines lab[152,155], who also provided the diazo building blocks used in this project. Here two different routes of bioconjugation were explored. One route was the *N*-terminal functionalization of the to be conjugated peptide

with an NHS-diazo building block **46**, followed by the direct esterification with the protein (Figure 47, Route A). The cyclic R10 peptide was successfully functionalized with **46** and esterification was tested on eGFP. Here it was shown that the amount of conjugated peptide could be controlled, by varying peptide equivalents.

In parallel a second approach for the diazo mediated conjugation was tested. Here the protein was first esterified with diazo-alkyne building block **50**, followed by a CuAAC with an azido-functionalized peptide-tag. Due to the fact that two non-quantitative reactions are carried out on protein level, this route was producing diverse conjugation product mixtures (Figure 47, route B). Nonetheless, this reaction sequence allowed the conjugation of more complex peptides, which cannot be functionalized with diazo compound **46**, Conditions were found to control the amount of alkyne handles attached in the esterification step and the CuAAC with azido-peptides cTat **52a** and Cy3-cR10 **52b** to alkyne tagged GFP was successfully carried out.

Finally cR10-eGFP conjugates, gained throughout route A with mainly one cR10 peptide attached to GFP were tested for their transduction capability in HeLa cells. Unfortunately the treatment of cells showed high toxicity, which could not be explained in the presented set up and should be elucidated further in the future.

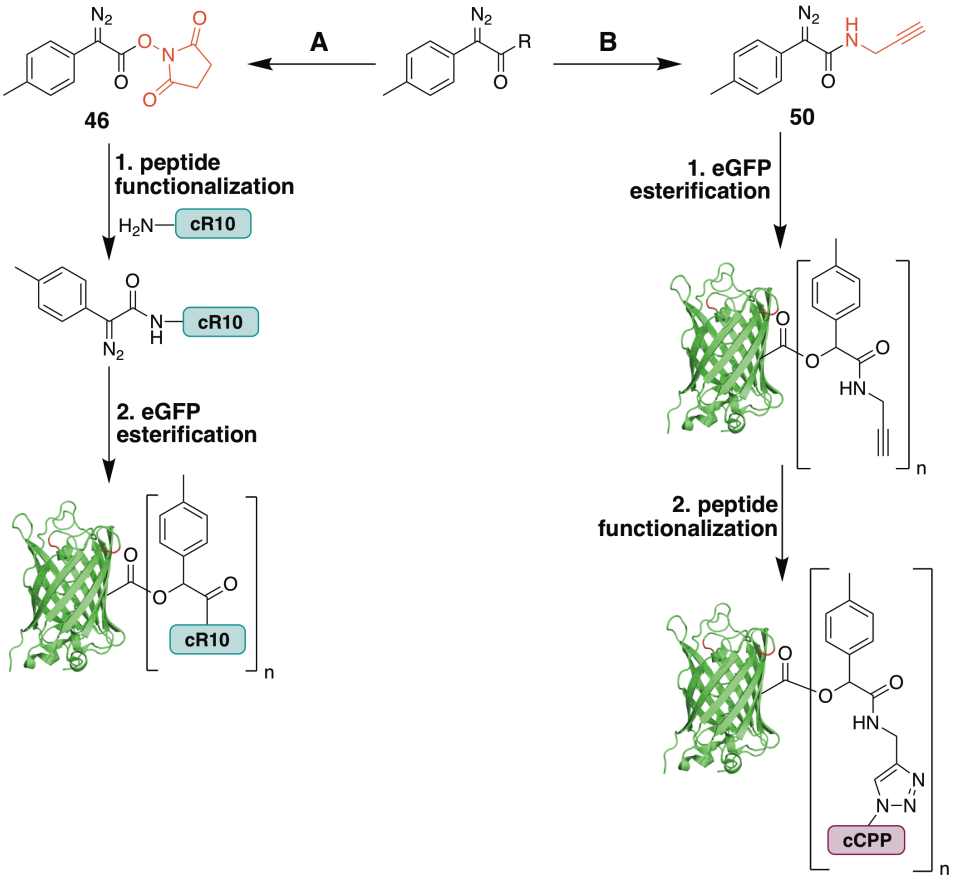

Figure 47: Schematic outline of bioreversible conjugation of CPPs to eGFP using diazo compounds.

8 Experimental Part

8.1 Materials and Methods

Reagents and solvents, unless stated otherwise, were commercially available and used without further purification. Amino acids and resins for SPPS were purchased from Novabiochem (Merck) or Iris Biotech GmbH.

Compound 43 was synthesized and characterized by Marc-Andre Kasper throughout his PhD Thesis in the lab of Prof. Dr. Christian Hackenberger.

Compounds 46 and **50** were synthesized and characterized by Dr. Kalie Mix throughout her PhD-Thesis in the lab of Prof. Dr. Ronald Raines.

Dendritic Polyglycerols were synthesized and characterized by Markus Hellmund during his PhD Thesis in the lab of Prof. Dr. Rainer Haag.

NMR ^{31}P-NMR spectra were recorded on a Bruker AV300. The chemical shifts are reported in ppm relative to the residual solvent peak. ^{1}H-NMR spectra were recorded on a Bruker 300 UltraShield in [D6] DMSO. The chemical shifts are reported in ppm relatively to the residual solvent peak

SPPS was carried out manually or on a Tribute-UV peptide synthesizer (Protein technologies, USA) *via* standard Fmoc-based protocols.

Preparative HPLC of peptides was carried out on a Gilson PLC 2020 personal Purification System (Gilson Inc., Middleton, WI, USA) including either a Nucleodur column (VP250/32 C18 HTec 5µm) or a Nucleodur column (VP250/21 C18 HTec 5µm) by Macherey-Nagel with a flow rate of either 30ml/min or 16ml/min.

Analytical UPLC-UV/MS was measured at 220 nm on an Aquity UPLC H-Class with a quaternary solvent manager, a waters autosampler and an Aquity UPLC-BEH C18 1.7µm, 2.1 x 50 mm RP column with a flow rate of 0.6 ml/min connected to a waters UV detector and a QDa^{TM}detector.

The following gradients were used with solvents A = H_2O + 0.1%TFA; B = MeCN + 0.1%TFA:

Method A (5 min): 0 – 0.5 min (with 5%B in A); from 0.5 – 3 min (5% B to 95% B in A); 3 – 3.9 min (with 95% B in A); 3.91 – 5 min (with 5% B in A).

Method B (15 min): 0 – 1.5 min (with 5%B in A); from 1.5 – 13 min (5% B to 95% B in A); 13 – 13.9 min (with 95% B in A); 13.91 – 15 min (with 5% B in A).

Method C (50 min): 0 – 2.5 min (with 5%B in A); from 2.5 – 40 min (5% B to 95% B in A); 40 – 45 min (with 95% B in A); 45 – 50 min (with 5% B in A).

Analytical HPLC-UV/MS was measured at 220 nm on a Waters system consisting of a 600S controller, a 616 pump, a 717 plus autosampler and a 2489 UV/Visible detector and a

3100 mass detector, with a C18-column (Eclipse, Agilent Technologies, US, 100 Å, 5 µm, 4.6 mm x 250 mm).

ESI-MS was measured on an Aquity UPLC H-Class coupled to a Xevo G2-XS Q-Tof.

MALDI-TOF was measured on a Bruker LT microflex using a 2,5-DHAP matrix. Proteins were precipitated in cold acetone and resolved in 10 mM Ammoniumbicarbonate buffer at pH 7.4. Protein sample (0.8 µl) was mixed with 2% TFA in water (0.8 µl) and matrix (0.8 µl). After addition of matrix the solution (0.8 µl) was transferred a MSP 96 target (polished steel BC).

Protein concentrations were determined by absorption spectroscopy measurements at 280 nm using the extinction coefficient and molecular weight of the protein with a NanoDrop ND-1000. In addition or as alternative method concentrations were determined by BCA assay (Thermo Fisher Scientific, USA) according to the manufacturers protocol.

Protein purification was accomplished either with an ÄKTA purifier FPLC or a BioRad NGC system.

CD-spectroscopy was measured on a Jasco J-720 spectropolarimeter at 20°C and parameters set to: measured wavelength range 190 – 260 nm; data pitch of 0.1 nm; continuous scanning mode; 100 nm/min scanning speed; 1sec. response; 1.0 nm band width; 0.1 cm cell length; 5 accumulations.

FACS measurements were carried on dual laser BD FACSCalibur.

Dialysis was performed with regenerated cellulose tubing, MWCO 12000 – 14000 Da purchased from Spectrum labs against buffer/MeCN for several days with frequent changing of the solvent.

8.2 Multivalent Peptide-Polymer Conjugates for Influenza-Virus Inhibition

8.2.1 Peptide Synthesis

Both peptides were synthesized on a Rink-Amide-Resin with a loading of 0.74 mmol g^{-1}. Single coupling was applied for all standard amino acids (5 eq., 1 h each) on a PTI peptide synthesizer. After the peptide sequence was assembled on resin the peptide was capped with 4-pentynoic acid *N*-terminally by treating the resin with 4-Pentynoic acid (5eq), HOBt (5 eq), HBTU (5 eq.) and DIPEA (5 eq.) in DMF. After two hours of coupling, the resin was washed with DMF and DCM. Cleavage from the resin was performed using TFA/TIS/water (95/2.5/2.5) for 2 h. Precipitation was carried out in cold and dry ether. The precipitate was dissolved in a 1:1 mixture of acetonitrile and water and further lyophilized. The dry crude product was then solved in 10 mM ammonium acetate buffer at pH 9.0 and purification was accomplished *via* basic (10 mM ammonium acetate buffer pH 9.0/MeCN) semi-preparative HPLC (0-5 min 95/5, Buffer/MeCN; 5-70 min 10/90, Buffer/MeCN).

PeB-alkyne:

The final product PeB-alkyne was obtained in a yield of 13.6 % (53 mg, 27.1 µmol) and characterized by analytical HPLC-MS (m/z: obs. 1016.9 $[M+2]^{2+}$, calc. 1016.9254) (Method C; rt.: 19.2 min).

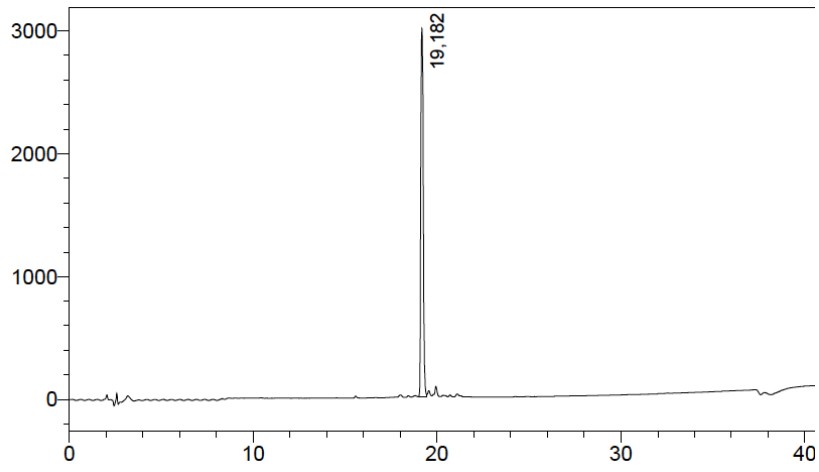

Figure 8.1: LC-UV chromatogram of **PeB-alkyne**.

PeB^{GF}-alkyne

The final product PeB^{GF}-alkyne was obtained in a yield of 13.6 % (53 mg, 27.1 µmol) and characterized by analytical HPLC-MS (m/z: obs. 979.9 $[M+2]^{2+}$, calc. 979.9252) (Method C; rt.: 20.1 min)

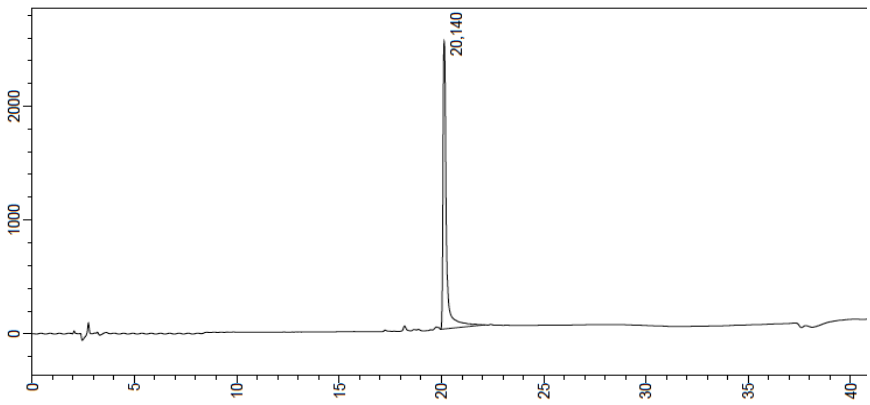

Figure 8.2: LC-UV chromatogram of **PeB^{GF}-alkyne**.

8.2.2 Polymer synthesis

The polyglycerol sysnthesis was carried out by Markus Hellmund in the group of Prof. Dr. Rainer Haag. The synthesis of the hyperbranched polyglycerols was performed according to the published procedure.[273,274]
Yield: 67%, molecular weight distribution and PDI (see Table 8.1).[258]

The surface modifications on all polyglycerol cores was performed by Markus Hellmund according to the published procedure[273] and all experimental details are published[258].

Table 8.1. Overview of high molecular weight polymers with number average molar mass (M), mass average molar mass (M), molar mass at peak maximum (M), poly dispersity index (PDI) and degree of branching (DB).

Sample	$PG_{100\ kDa}$	$PG_{340\ kDa}$
M_n	66 kDa	117 kDa
M_w	117 kDa	420 kDa
M_p	96 kDa	340 kDa
PDI	1.8	2.0
DB	56%	59%
Azide conversion	10% / 30%	10% / 30%

8.2.3 Peptide – Polymer conjugation

The alkyne-functionalized peptide (15.9 µmol, 1.5 eq.) was solubilized in 10 mM ammonium bicarbonate buffer and polyglycerol azide (10.6 µmol, 1 eq.) was added. CuSO4 in water (20 mM, 177 µl, 20 mol%) and THPTA (100 mM, 177 µl, 100 mol%) in water were premixed and added to the reaction mixture. The reducing agent sodium ascorbate (1 eq.) was added in two portions at the beginning of the reaction and after 5 h. After the last addition of

sodium ascorbate the reaction was stirred overnight. The reaction was quenched by adding ethylenediaminetetraacetic acid and further dialyzed for five days against a mixture of 10 mM ammonium bicarbonate buffer containing 10% acetonitrile. The product was lyophilized to yield the crude product. Finally, it was further purified by gel filtration over Sephadex 50 fine and fractions with no free peptide visible in MALDI combined. Loading was determined by ^{1}H-NMR integration of aromatic tyrosine signals to polymer backbone signals (see below).

The enhancement factor (β) was calculated as followed using the reported IC_{50} values for monovalent PeB and PeB^{GF}.[33]

$$\beta = \frac{IC_{50_{monovalent}}}{IC_{50_{mulitvalent}}} \; ; IC_{50_{multivalent}} = IC_{50_{nanoparticle}} \times number\ of\ ligands$$

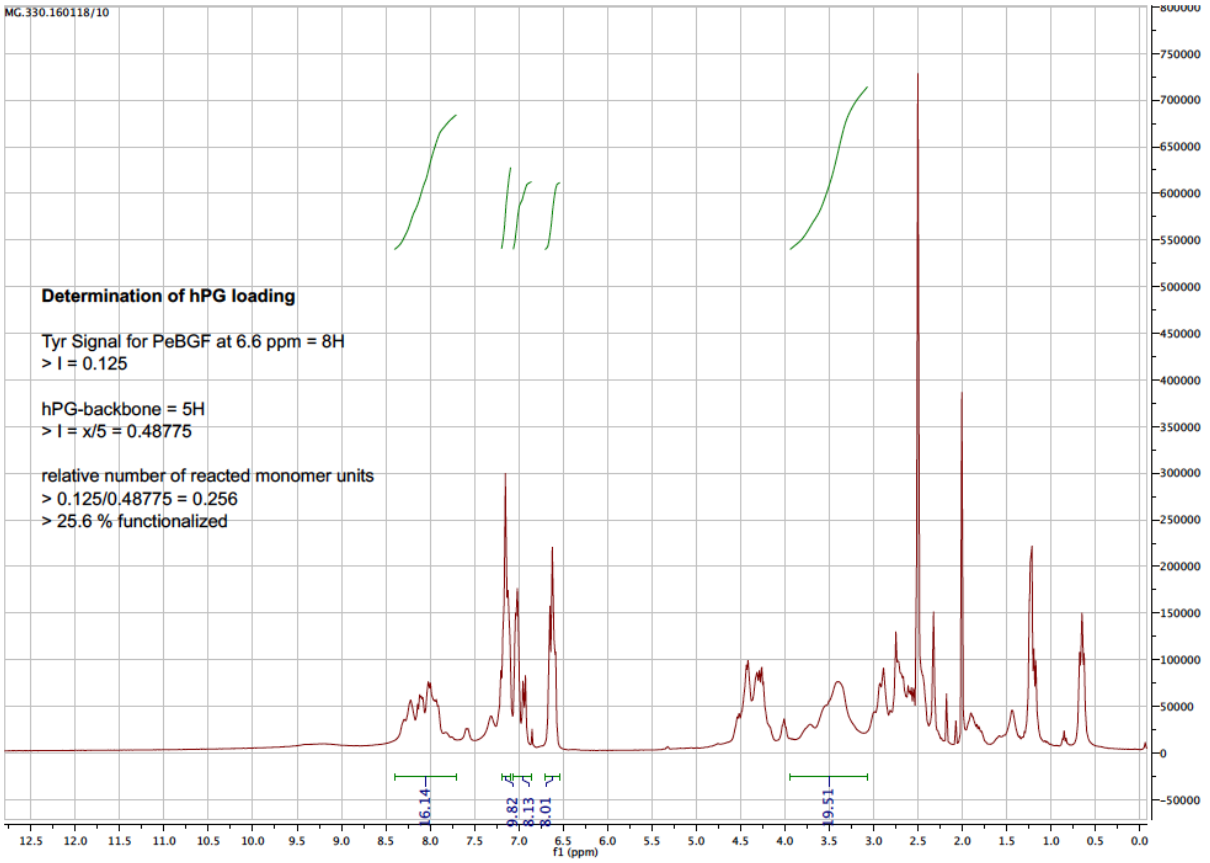

Figure 8.3. Determination of dPG loading by ^{1}H-NMR.

8.2.4 Dynamic Light Scattering

The dynamic light scattering (DLS) measurements were performed using Malvern Zetasizer Nano ZS (Malvern Instruments GmbH, Herrenberg, Germany). All samples were measured at a constant scattering angle of 173°, 25°C, and freshly solubilized before measurement in 10 mM ammonium bicarbonate. All measurements were repeated at least three times.

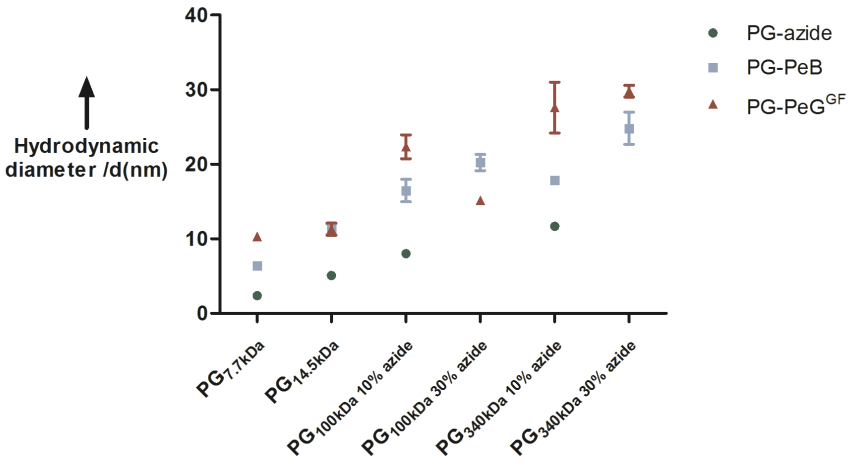

Figure 8.4. Overview of DLS Data with with its s.e.m. (n≥ 3)

8.2.5 *In vivo* and *in vitro* studies

Daniel Lauster conducted the hemagglutination inhibiton assays, the infection inhibiton assays and MST measurements according to the details given in the published manuscript.[258] Mouse experiments performed by Markus Bardua and Ute Hoffmann are also described in the manuscript. [258]

8.3 Staudinger-induced thiol addition as cysteine reactive conjugation

8.3.1 Peptide synthesis

Cyclic-(RGDfK)-azide (11)

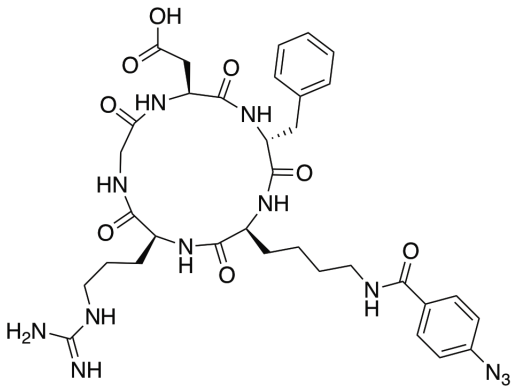

The cyclic-RGDfK-azido peptide (**11**) was synthesized manually on a NovaSynTGT alcohol resin with a loading of 0.26 mmol/g. First the resin was activated by stirring 480.7 mg resin in 2.5 ml toluene and 480 µl acetylchloride at 60°C for three hours. Double coupling of Fmoc-Asp(OAll)-OH (123.56 mg, 0.3125 mmol, 2.5 eq) was performed in CH_2Cl_2 using DIPEA (212.6 µl, 1.25 mmol, 10 eq.) as activating base, each for one hour. Further amino acid couplings were performed by mixing amino acid (0.25 mmol, 2 eq.), HATU (0.25 mmol, 2 eq.) and DIPEA (0.5 mmol, 4 eq.) in DMF and coupling once for 30 minutes and once for one hour. Fmoc deprotection was accomplished with 20 % piperidine in DMF. After the final amino acid coupling the alloc deprotection was achieved by treating the resin with $Pd(P(Ph_3)_4)$ (433 mg, 0.375 mmol, 3 eq.) in a chloroform/acetic acid/NMM (37:2:1;v:v:v) mixture for two hours in an argon atmosphere, followed by Fmoc deprotection and cyclization with HATU (0.25 mmol, 2 eq.) and DIPEA (0.5 mmol, 4 eq.) in DMF for 16 hours. To install the aromatic azide on the lysine residue Fmoc-Lys(dde)-OH was used in the solid phase synthesis and was orthogonally deprotected on resin using 5 ml of a 2% hydrazine in DMF solution three times for three minutes, followed by coupling of 4–azidobenzoic acid (81.65 mg, 0.5 mmol, 4 eq.) with HATU (190 mg, 0.5 mmol, 4 eq.) and DIPEA (1 mmol, 8 eq.) in DMF for two hours. Cleavage from the resin was performed with TFA/CH_2Cl_2 (75:25;v:v) for 2.5 hours. Precipitation was carried out in cold and dry ether. The crude was analyzed by UPLC-MS and either used as crude in the following Staudinger reaction or purified by preparative reverse phase C18 HPLC (0-5 min 95/5, water (0.1%TFA)/MeCN (0.1%TFA); 5-60 min 10/90, water (0.1%TFA)/MeCN (0.1%TFA)). The product **11** was gained as white powder (9.4 mg, 12.8 µmol, 10.2 % yield) and was analyzed by analytical UPLC (Method A; rt.: 1.72 min).

LRMS: m/z: 749.66 $[M+H]^+$ (calc. m/z: 749.3485).

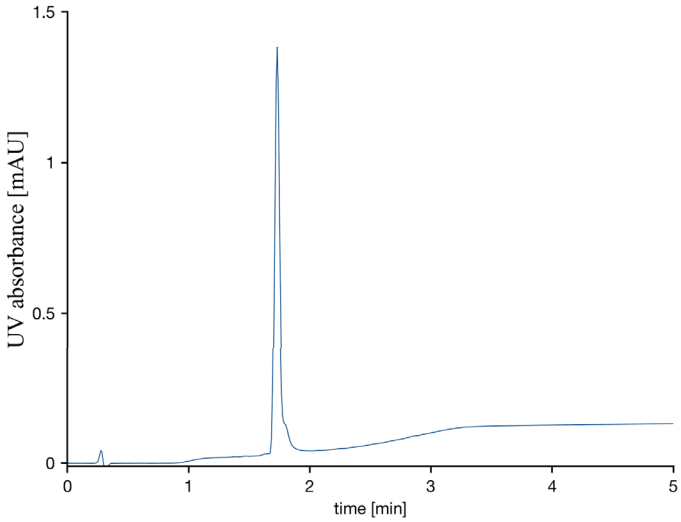

Figure 8.5: UPLC-UV chromatogram of **11**.

Cyclic-(Tat)-azide (16)

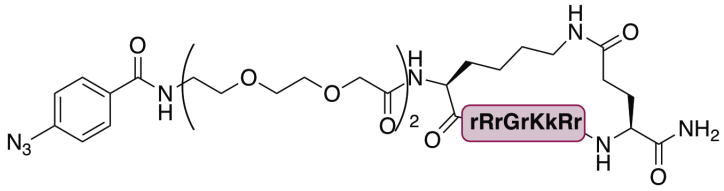

The cyclic-(Tat)-azido peptide (**16**) was synthesized in a 0.1 mmol scale on a Rink Amide Resin with a loading of 0.78 mmol/g. The synthesis was carried out on a PTI synthesizer with single couplings of each amino acid (10 eq. amino acid for 40 min) in DMF. After the final PEG building block coupling the peptide, still Fmoc protected, was treated with $Pd(PPh_3)_4$ (24 mg, 20 µmol, 20 mol%) and phenylsilane (308 µl, 2.5 mmol, 2.5 eq.) in 4 ml dry CH_2Cl_2 for one hour in order to cleave the alloc and allyl protecting groups in one step. After confirmation of full deprotection by test cleavage, cyclization with 2 eq. HATU 4 eq. DIPEA was carried for four hours in DMF.

The peptide was then Fmoc-deprotected using 20% piperidine in DMF and the 4-azidobenzoic acid (81.6 mg, 0.5 mmol, 5 eq.) was coupled to the *N*-terminus with HATU (190.1 mg, 0.5 mmol, 5 eq.) and DIPEA (170 µl, 1.0 mmol, 10 eq.) for one hour. Finally, the peptide was cleaved from the resin by treatment with 4 ml of a TFA:TIS:H_2O (95:2.5:2.5) mixture for three hours and precipitated in cold diethylether. The crude peptide was purified by preparative reverse phase C18 HPLC (0-5 min 95/5, water (0.1%TFA)/MeCN (0.1%TFA); 5-60 min 10/90, water (0.1%TFA)/MeCN (0.1%TFA)). The product **16** was gained as white powder (30.0 mg as TFA-salt, 11.4 µmol, 11.4% yield) and was analyzed by analytical UPLC (Method A; rt: 2.18 min).

LRMS: m/z: 648.49 $[M+3H]^{3+}$ (calc. m/z: 648.0569).

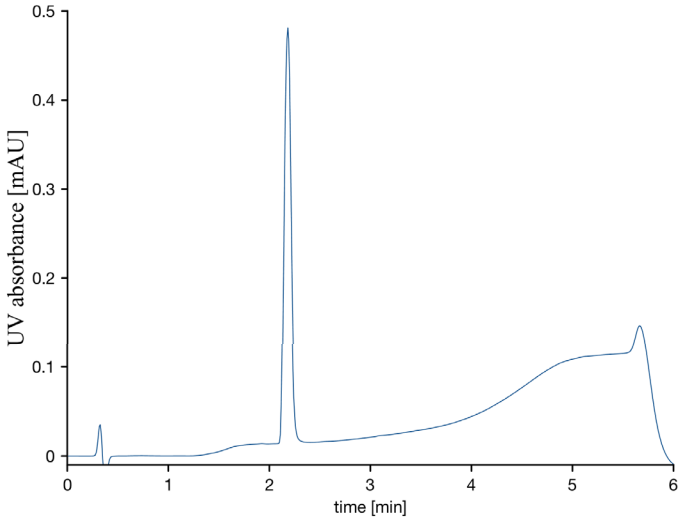

Figure 8.6: UPLC-UV chromatogram of **16**.

Cyclic-(R10)-azide (17)

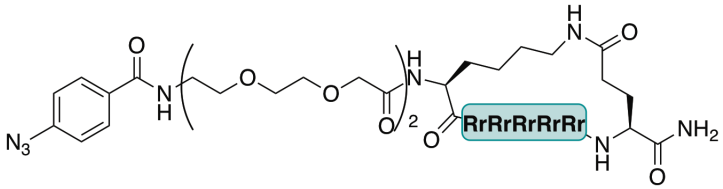

The cyclic-(R10)-azido peptide (**17**) was synthesized in a 0.1 mmol scale on a Rink Amide Resin with a loading of 0.78mmol/g. The synthesis was carried out on a PTI synthesizer with double couplings of each amino acid (5 eq. amino acid for 40 min) in DMF. After the final PEG building block coupling the peptide, still Fmoc protected, was treated with $Pd(PPh_3)_4$ (24 mg, 20 µmol, 20 mol%) and phenylsilane (308 µl, 2.5 mmol, 2.5 eq.) in 4 ml dry CH_2Cl_2 for one hour in order to cleave the alloc and allyl protecting groups in one step. After confirmation of full deprotection by test cleavage, cyclization with 2 eq. HATU 4 eq. DIPEA was carried out over night in DMF. The peptide was then Fmoc-deprotected using 20% piperidine in DMF and the 4-azidobenzoic acid (81.6 mg, 0.5 mmol, 5 eq.) was coupled to the *N*-terminus with HATU (190.1 mg, 0.5 mmol, 5 eq.) and DIPEA (170 µl, 1.0 mmol, 10 eq.) for one hour. Finally the peptide was cleaved from the resin by treatment with 4 ml of a TFA:TIS:H_2O (95:2.5:2.5) mixture for three hours and precipitated in cold diethylether. The crude peptide was purified by preparative reverse phase C18 HPLC (0-5 min 95/5, water (0.1%TFA)/MeCN (0.1%TFA); 5-60 min 10/90, water (0.1%TFA)/MeCN (0.1%TFA)) and gained as white powder (62 mg as TFA-salt, 18.3 µmol 18.3% yield) and was analyzed by analytical UPLC (method A, rt.: 1.93 min).

LRMS: m/z: 752.35 $[M+3H]^{3+}$ (calc. m/z: 751.7879).

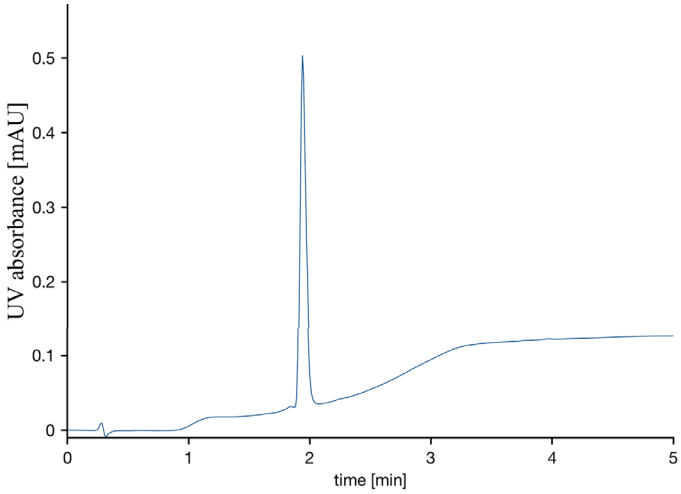

Figure 8.7: UPLC-UV chromatogram of **17**.

Cyclic-(Tat)-maleimide (24)

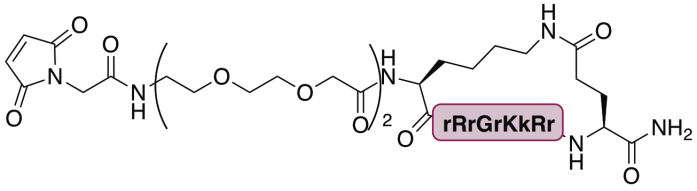

The cyclic-(Tat)-maleimide peptide (**23**) was synthesized in a 0.05 mmol scale on a Rink Amide Resin with a loading of 0.78 mmol/g. The synthesis was carried out on a PTI synthesizer with single couplings of each amino acid (10 eq. amino acid for 40 min) in DMF. After the final PEG building block coupling the peptide, still Fmoc protected, was treated with $Pd(PPh_3)_4$ (12 mg, 10 µmol, 20 mol%) and phenylsilane (154 µl, 1.25 mmol, 2.5 eq.) in 2 ml dry CH_2Cl_2 for one hour in order to cleave the alloc and allyl protecting groups in one step. After confirmation of full deprotection by test cleavage, cyclization with 2 eq. HATU 4 eq. DIPEA was carried for four hours in DMF.

The peptide was then Fmoc-deprotected using 20% piperidine in DMF and then 2-maleimido acetic acid (15.5 mg, 0.1 mmol, 2 eq.) was coupled to the *N*-terminus with HATU (38.0 mg, 0.1 mmol, 2 eq.) and DIPEA (34 µl, 0.2 mmol, 4 eq.) for four hours. Finally the peptide was cleaved from the resin by treatment with 4 ml of a TFA:TIS:H_2O (95:2.5:2.5) mixture for three hours and precipitated in cold diethylether. The crude peptide was purified by preparative reverse phase C18 HPLC. The product **23** was gained as white powder (6 mg as TFA-salt, 2.3 µmol, 4.6 % yield) and analyzed by UPLC (method B; rt.: 3.13 min).

HRMS: m/z: 645.3615 $[M+3H]^{3+}$ (calc. m/z: 645.3848).

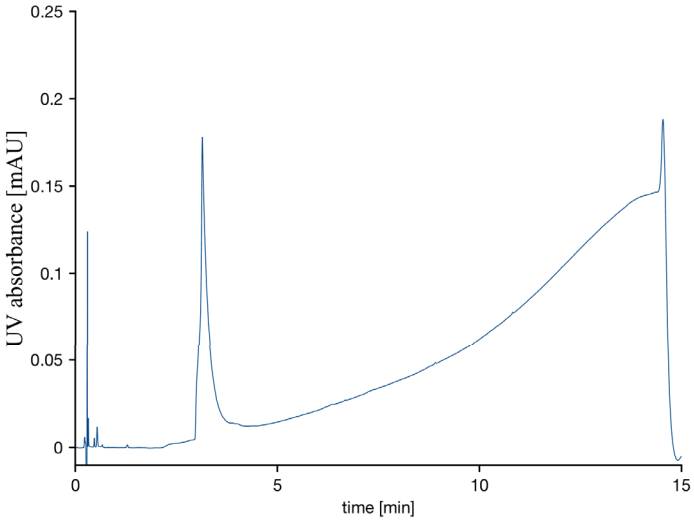

Figure 8.8: UPLC-UV chromatogram of **24**.

Cyclic-(Tat)-Iodoacetate (25)

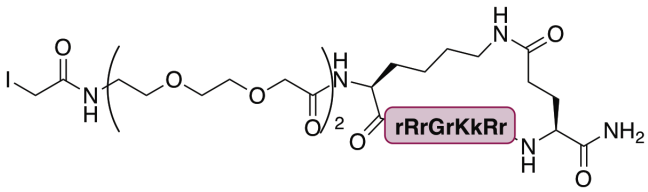

The cyclic-(Tat)-iodoacetate (**24**) peptide was synthesized in a 0.05 mmol scale on a Rink Amide Resin with a loading of 0.78 mmol/g. The synthesis was carried out on a PTI synthesizer with single couplings of each amino acid (10 eq. amino acid for 40 min) in DMF. After the final PEG building block coupling the peptide, still Fmoc protected, was treated with $Pd(PPh_3)_4$ (12 mg, 10 µmol, 20 mol%) and phenylsilane (154 µl, 1.25 mmol, 2.5 eq.) in 2 ml dry CH_2Cl_2 for one hour in order to cleave the alloc and allyl protecting groups in one step. After confirmation of full deprotection by test cleavage, cyclization with 2 eq. HATU 4 eq. DIPEA was carried for four hours in DMF.

The peptide was then Fmoc-deprotected using 20% piperidine in DMF and then *N*-hydroxysuccinimidyl Iodoacetate (28.3 mg, 0.1 mmol, 2 eq.) was coupled to the *N*-terminus with DIPEA (25 µl, 0.25 mmol, 3 eq.) for four hours. Finally the peptide was cleaved from the resin by treatment with 4 ml of a TFA:TIS:H_2O (95:2.5:2.5) mixture for three hours and precipitated in cold diethylether. The crude peptide was purified by preparative reverse phase C18 HPLC (0-5 min 95/5, water (0.1%TFA)/MeCN (0.1%TFA); 5-60 min 10/90, water (0.1%TFA)/MeCN (0.1%TFA)). The product **24** was gained as white powder (8 mg as TFA-salt, 3.0 µmol, 6.0 % yield) and analyzed by UPLC (method B; rt: 3.17 min).

HRMS: m/z: $[M+3H]^{3+}$ 655.6872 (calc. m/z: 655.6834).

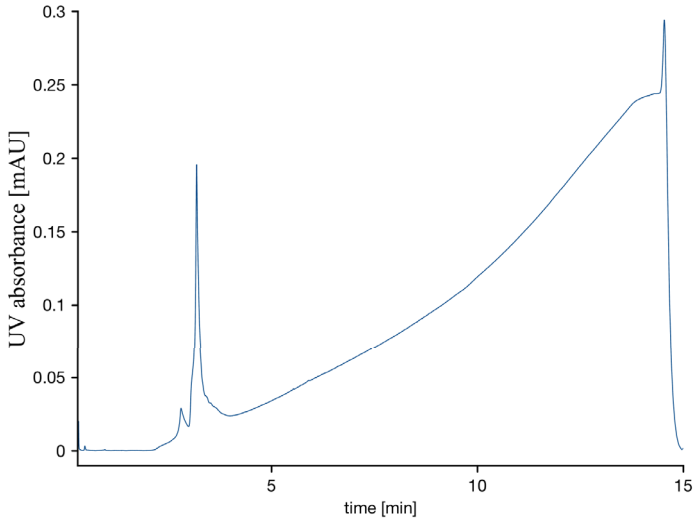

Figure 8.9: UPLC-UV chromatogram of **25**.

TAMRA-c(R10) (22)

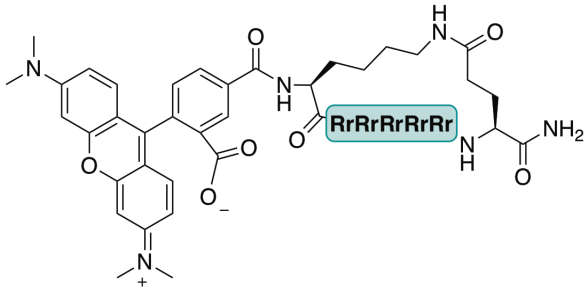

The TAMRA labeled cyclic-(R10) (**22**) peptide was synthesized in a 0.05 mmol scale on a Rink Amide Resin with a loading of 0.78 mmol/g. The synthesis was carried out on a PTI synthesizer with double couplings of each amino acid (5 eq. amino acid for 40 min) in DMF. After the final PEG building block coupling the peptide, still Fmoc protected, was treated with $Pd(PPh_3)_4$ (24 mg, 20 µmol, 20 mol%) and phenylsilane (308 µl, 2.5 mmol, 2.5 eq.) in 4 ml dry CH_2Cl_2 for one hour in order to cleave the alloc and allyl protecting groups in one step. After confirmation of full deprotection by test cleavage, cyclization with 2 eq. HATU 4 eq. DIPEA was carried out over night in DMF. The peptide was then Fmoc-deprotected using 20% piperidine in DMF, followed by coupling of 5-carboxytetramethylrhodamine (32.3 mg, 0.075 mmol, 1.5 eq.) was coupled to the *N*-terminus with HATU (28.5 mg, 0.075 mmol, 1.5 eq.) and DIPEA (25.5 µl, 0.15 mmol, 3 eq.) over night. Finally the peptide was cleaved from the resin by treatment with 2 ml of a TFA:TIS:H_2O (95:2.5:2.5) mixture for three hours and precipitated in cold diethylether. The crude peptide was purified by preparative reverse phase C18 HPLC, gained as pink powder (22.2 mg as TFA-salt, 6.1 µmol 12.2% yield) and analyzed by UPLC (method B; rt.: 3.90 min).

HRMS: m/z: $[M+3H]^{3+}$ 744.0772 (calc. m/z: 744.4460).

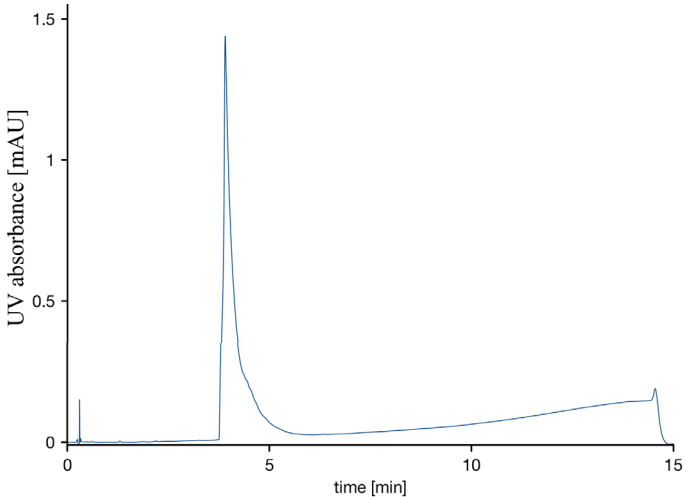

Figure 8.10: UPLC-UV chromatogram of **22**.

8.3.2 Staudinger phosphonite reaction

Bisethoxyalkyne-phosphonite synthesis (7)

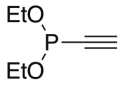

Ethynyl magnesium bromide in THF (0.5 M, 2 ml, 1 mmol, 1 eq.) was cooled to - 78°C in a flame dried schlenk flask and diethylchlorophosphite (0.143 ml, 1 mmol, 1 eq.) was added. The solution was stirred for 10 minutes at - 78°C and let warm to room temperature and stirred for another 90 minutes. The full consumption of starting material was confirmed by ^{31}P-NMR and used as crude in the following Staudinger reaction with azido peptides. Due to the inherent lability of bisethoxyalkyne-phosphonite toward water and air the compound was not isolated. The correct product formation *via* this reaction route however was previously confirmed, by additionally protecting the P(III)-compound with borane, which makes it possible to isolate and characterize the compound as reported by Robert Vallée.[231]

General procedure P1 for the generation of alkyne – phosphonamidates (8)

Purified azido-peptide was dissolved in DMSO at a 6 mM concentration and dried in a flame-dried flask for one hour prior to adding 4 eq. of bisethoxyalkyne-phosphonite (volume according to percentage of product determined by NMR). After the reaction mixture was stirred over night at room temperature, water was added and the reaction mixture directly lyophilized. The crude product was purified by semi-preparative HPLC.

Cyclic-(RGDfK)-phosphonamidate-alkyne (12)

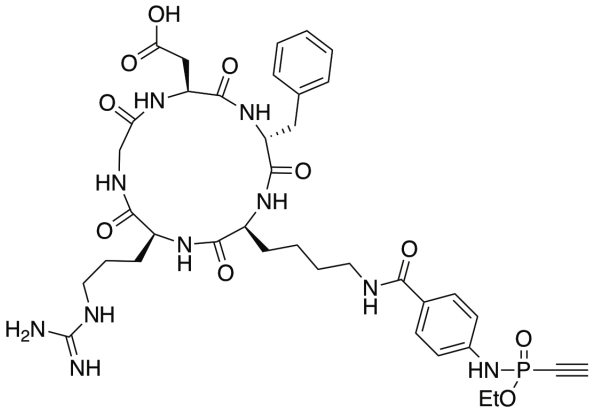

With peptide **11** (6.9 mg, 9.14 µmol, 1 eq.) the Staudinger-phosphonite synthesis was carried out according to the general procedure **P1**. The crude product was purified by semi-preparative HPLC (0-5min 95/5, water (0.1%TFA)/MeCN (0.1%TFA); 5-60min 10/90, water (0.1%TFA)/MeCN (0.1%TFA)), gave the product **12** as a white powder (4.1 mg, 4.89 µmol, 53.5 % yield) and analyzed by UPLC (method A; rt.: 1.55 min).

LRMS: m/z: 839.72 $[M+H]^+$ (calc. 839.3606 m/z).

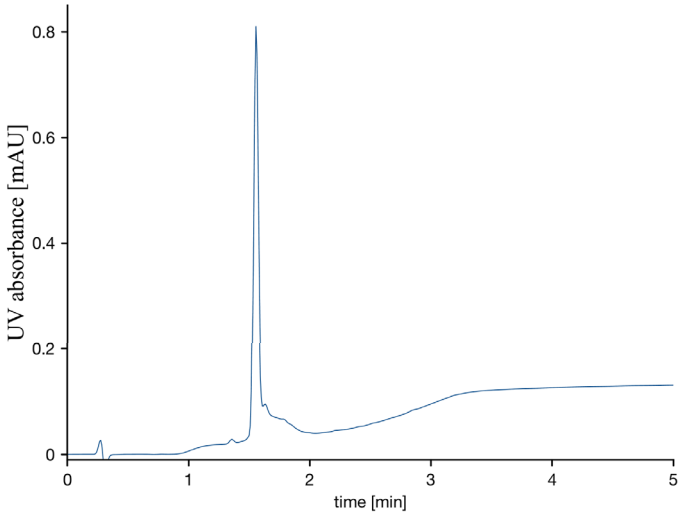

Figure 8.11: UPLC-UV chromatogram of **12**.

Cyclic-(Tat)-phosphonamidate-alkyne (18)

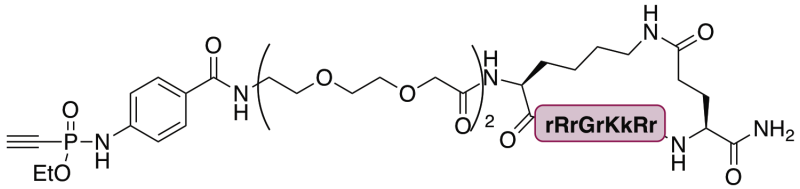

Cyclic-(Tat)-azide **16** (20 mg (as TFA-salt), 7.6 µmol, 1 eq.) and bisethoxyalkyne-phosphonite **7** were reacted in a Staudinger-phosphonite-reaction according to the general procedure **P1**. The product **18** was gained after semi-preparative HPLC (0-5min 95/5, water

(0.1%TFA)/MeCN (0.1%TFA); 5-60min 10/90, water (0.1%TFA)/MeCN (0.1%TFA)) as white powder (13 mg, 4.8 µmol, 62.9% yield) and analyzed by UPLC (method B; rt.: 3.50 min). HRMS: m/z: 678.0569 $[M+3H]^{3+}$ (calc. m/z: 678.0610).

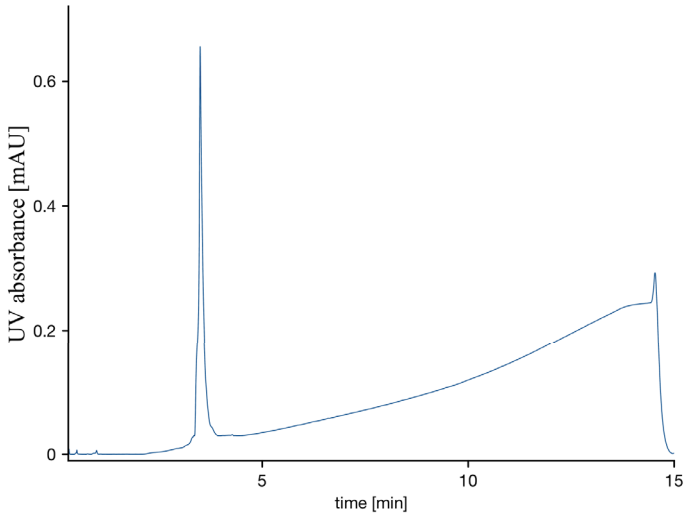

Figure 8.12: UPLC-UV chromatogram of **18**.

Cyclic-(R10)-phosphonamidate-alkyne (19)

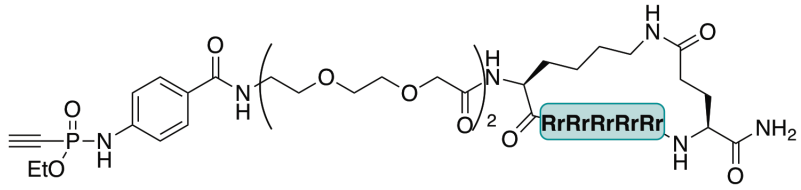

Cyclic-(R10)-azide **17** (35 mg (as TFA-salt), 10.3 µmol, 1 eq.) and bisethoxyalkyne-phosphonite **7** were reacted in a Staudinger-phosphonite reaction according to the general procedure **P1.** The product **19** was gained after semi-preparative HPLC (0-5min 95/5, water (0.1%TFA)/MeCN (0.1%TFA); 5-60min 10/90, water (0.1%TFA)/MeCN (0.1%TFA)) as white powder (13 mg, 4.79 µmol, 62.9% yield) and analyzed by UPLC (method B; rt.: 3.70 min). HRMS: m/z: 781.7965 $[M+3H]^{3+}$ (calc. m/z: 781.7920).

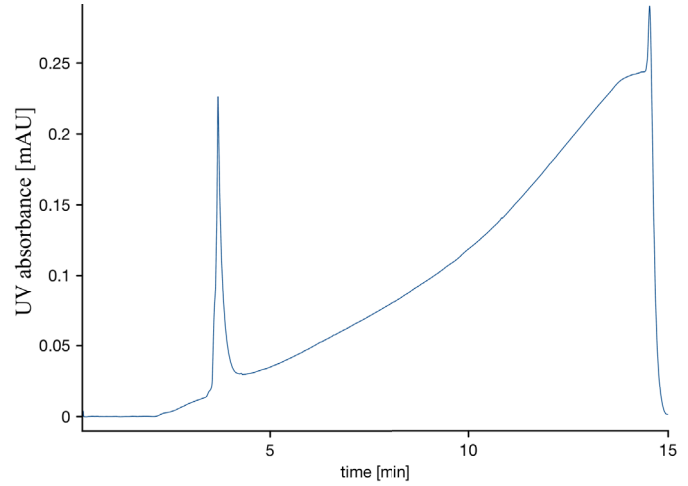

Figure 8.13: UPLC-UV chromatogram of **19**.

8.3.3 Cloning and expression of GFP mutants

eGFP C70M S147C was expressed according to published protocol[262] by Kristin Kemnitz-Hassanin.

Mutagenesis PCR

For mutation of eGFP C70M to eGFP S6C C70M, the cDNA of eGFP C70M was kindly provided in a pET28a vector and reported on previously by Dr. Dominik Schumacher[262]. The mutations were carried out by mutagenesis PCR using complementary primer pairs (for conditions see table 8.2 and 8.3).

eGFP S6C: GCAGCCATATGGGATGCATTCAGATGG and CCATCTGAATGCATCCC ATATGGCTGC

For mutation of hsGFP to hsGFP C71M and hsGFP S3C C71M, the group of Prof. Dr. Budisa kindly provided the cDNA of hsGFP in a pET30b vector. The mutations were carried out by mutagenesis PCR using complementary primer pairs (for conditions see Table 8.1 and 8.2).

hsGFP C71M: GTTATGGTGTGCAGATGTTTGCACGTTATCCG and CGGATAACGT GCAAACATCTGCACACCATAAC
hsGFP S3C: GGAGATATACATATGCAGTGCAAAGGCGAAG and CTTCGCCTTTGC ACTGCATATGTATATCTCC

Table 8.2: Reaction mix of mutagenesis PCR.

ddH_2O	18.5 µl
Pfu buffer (10x) (Thermo scientific, USA)	2.5 µl
template DNA (1 ng/µl)	2 µl
primer mix (10 µM each)	1 µl
dNTP mix (10 mM each) (Thermo scientific, USA)	0.5 µl
Pfu polymerase (Thermo scientific, USA)	0.5 µl

Table 8.3: Cycle steps in mutagenesis PCR.

		eGFP		hsGFP	
step	**cycles**	**temp.[°C]**	**time**	**temp.[°C]**	**time**
initial denaturation	1	95	30''	95	3'
denaturation	22	95	30''	95	30''
annealing		65	1'	58	1'
extension		72	3'	72	3'
final extension	1	72	10'	72	10'
hold		4	∞	4	∞

DPNI digest

Digestion of mutated DNA was carried out using DPNI according to Table 8.4 for 4h at 37°C.

Table 8.4: Reaction mixture of DPNI digest.

PCR product (not purified)	20 µl
FastDigest™ Buffer (10x)	4 µl
DpnI (10 U/µl) (Thermo scientific, USA)	2 µl
ddH_2O	34 µl

Purification of the digestion mixture was carried out using a GeneJET™ Gel extraction kit. The digestion mixture was mixed 1:1 with binding buffer and then purified according to the manufacturer's protocol. Final elution was done in 30µl of ddH_2O.

Transformation of competent *E. coli* cells

Cells were transformed by heat shock procedure. Hereby 50 µl cells were thawed on ice and 1 µl of purified DNA was added and incubated on ice for 30 minutes. The cells were heat shocked at 42°C for 45 seconds followed by the addition of 300 µl prewarmed SOC medium. The mixture was then incubated for one hour at 37°C. Everything was plated on LB agar plates supplemented with the respective antibiotic and incubated at 37°C over night.

DNA isolation

Clones were picked and grown in 5 ml of LB medium in presence of the respective antibiotic over night at 37°C, 180 rpm. Plasmid-DNA was isolated with a GeneJET Plasmid Miniprep Kit (Thermo scientific, USA) according to the manufacturer's protocol, with the

alteration of eluting the DNA in 20 µl ddH_2O instead of the included elution buffer. The DNA was stored at - 20°C and its concentration was determined by absorption spectrum measurement at 260 nm by NanoDrop. Correct DNA sequence was verified by sequencing.

Protein expression

Protein expression was done in *E. coli* BL21 (DE3) using LB medium containing 100 µg/ml Kanamycin. Cells were grown at 37°C, 180 rpm until they reached an OD_{600} of approximately 0.7 and then expression induced by adding 0.5 mM IPTG and further incubated at 18°C over night. Cells were harvested by centrifugation at 4000 g for 15 minutes at 4°C followed by cell lysis, which was carried out in Dulbecco's PBS with a sonicator at 30% for six minutes. Finally debris was centrifugation at 27000 g for 20 minutes. The His_6-tagged-GFP mutant was purified *via* a 5 ml HisTrap™ FF column on a BioRad NGC system and a. Elution was performed in PBS with 500mM Imidazole. The fractions containing the wanted protein were combined and dialysis (Slide-A-lyzer, MWCO 10kDa) against Tris Buffer (TrisHCl 50 mM, 0.5 M NaCl, pH 8.0).

For hsGFP-mutants TEV protease was added to the protein and incubated at 20°C over night followed by another purification *via* HisTrap FF column. The product fractions were combined, concentrated and rebuffered to PBS with a Vivaspin 20 filter unit (MWCO 10 kDa) then shock frozen and stored at - 80°C.
For eGFP-mutants 1 µl thrombine (1 U/ml) was added to the protein and incubated at 16°C over night and purified by size exclusion chromatography using a Superdex 75 10/300 GL column. The product fractions were combined and concentrated with a Vivaspin 20 filter unit (MWCO 10 kDa) then shock frozen and stored at - 80°C.

Final GFP sequences

eGFP C70M S147C

GSIQMVSKGE ELFTGVVPIL VELDGDVNGH KFSVSGEGEG DATYGKLTLK FI**C**TTGKLPV
PWPTLVTTLT YGVQ**M**FSRYP DHMKQHDFFK SAMPEGYVQE RTIFFKDDGN YKTRAEVKFE
GDTLVNRIEL KGIDFKEDGN ILGHKLEYNY N**C**HNVYIMAD KQKNGIKVNF KIRHNIEDGS
VQLADHYQQN TPIGDGPVLL PDNHYLSTQS ALSKDPNEKR DHMVLLEFVT AAGITLGMDE
LYK

hsGFP S3C C71M

MQ**C**KGEELFT GVVPILVELD GDVNGHKFSV RGEGEGDATN GKLTLKFI**C**T TGKLPVPWPT
LVTTLGYGVQ **M**FARYPDHIK RHDFFKSALP EGYVQERTIS FKDDGTYKTR AEVKFEGDTL
VNRIELKGID FKEDGNILGH KLEYNFNSHK VYITADKQKN GIKANFKIRH NVEDGSVQLA
DHYQQNTPIG DGPVLLPDNH YLSTQSVLLK DPNEKRDHAV LLEFVTAAGI THGKDELYKE
NLYFQ

Comparison of both sequences

Figure 8.14: Comparison between hsGFP and eGFP sequences and cysteine mutation.

8.3.4 Hydrothiolation of electron-deficient phosphonamidate alkyne

Modelreaction with Glutathion to 14

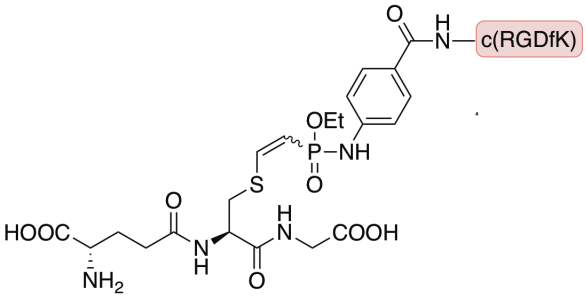

Glutathione (**13**) (1 mg, 3.25 µmol, 1 eq.) and **12** (1.24 mg, 3.25 µmol, 1 eq.) were mixed in 135 µl 10 mM ammoniumbicarbonate buffer pH 9.2 and 15 µl acetonitrile (c = 21.6 mM). After 10 minutes of shaking at room temperature quantitative conversion to the addition product **14** was observed by LC-UV/MS.

The final product was analyzed by LC-UV: (0-1min 95/5, water (0.1%TFA)/MeCN (0.1%TFA); 1-16.5 min 5/95, water (0.1%TFA)/MeCN (0.1%TFA) on RP-C18 column) rt.: 5.04 min.

HRMS: m/z: 1146.4451 $[M+H]^+$ (calc. m/z: 1146.4444).

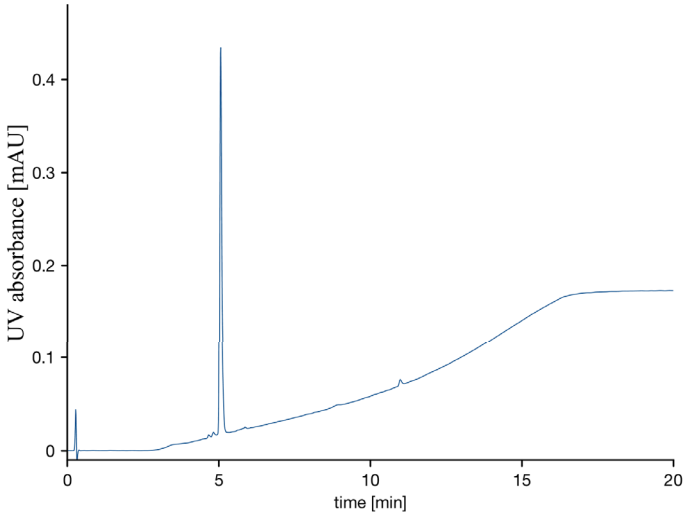

Figure 8.15: UPLC-UV chromatogram of **14**.

Stability Studies of 12

Peptide **12** was dissolved at a concentration of 0.3 mM in different solvents (0.1 M HCl at pH 1; water containing 0.1%TFA with a pH of 2; PBS buffer at pH 7.4; ammonium acetate buffer at pH 9.0; 0.05 M NaOH at pH 12). As internal standard 0.3 mM tryptophan was added. The stability of the starting material was monitored over time *via* LC-UV.

Stability Studies of 14

Conjugate **14** was dissolved at a concentration of 2 mM in different solvents (0.1 M HCl at pH 1; water containing 0.1%TFA with a pH of 2.3; PBS buffer at pH 7.4; ammonium acetate buffer at pH 9.0; 0.05 M NaOH at pH 12). As internal standard 0.5 mM inosine was added. The stability of **14** was monitored over time *via* LC-UV.

For the stability studies in presence of a competing thiol, **14** was solved in either PBS or 1M Tris HCl pH 9.0 at a concentration of 2 mM and 10 eq. DTT or MesNa were added. The mixture was monitored over several days.

General procedure P2 for thiol addition reaction with eGFP C70M S147C

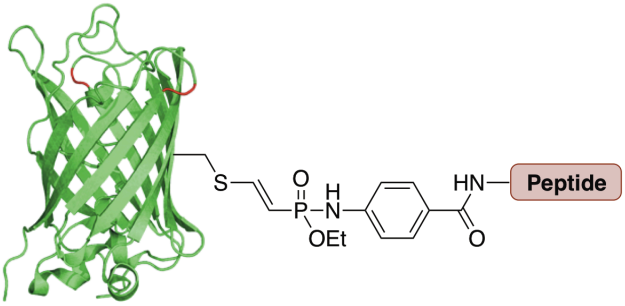

To eGFP C70M S147C buffered in PBS phosphonamidate-alkyne-peptides (20 eq.) were added to give the final concentration of 100 µM. The reaction mixture was shaken at 37°C and 800 rpm for three hours. The excess peptide was removed by spinfiltration using Amicon Spin filters with a 10 kDa MWCO. The sample was filtered five times at 14000 rpm for 5 minutes.

Cyclic-(RGDfK)-eGFP (15)

Peptide **12** (0.84 mg, 1.13 µmol, 20 eq.) was reacted with eGFP C70M S147C (56.3 nmol) according to general procedure **P2**. After removal of excess peptide **12** by spin filtration the sample was analyzed by MALDI-TOF after acetone precipitation and re-solvation in 10 mM ammonium bicarbonate buffer. Here the quantitative conversion to the product **15** was observed.

MALDI TOF: expected (in Da): 28602.4 ($M+H^+$); found (in Da): 28606.5 ($M+H^+$).

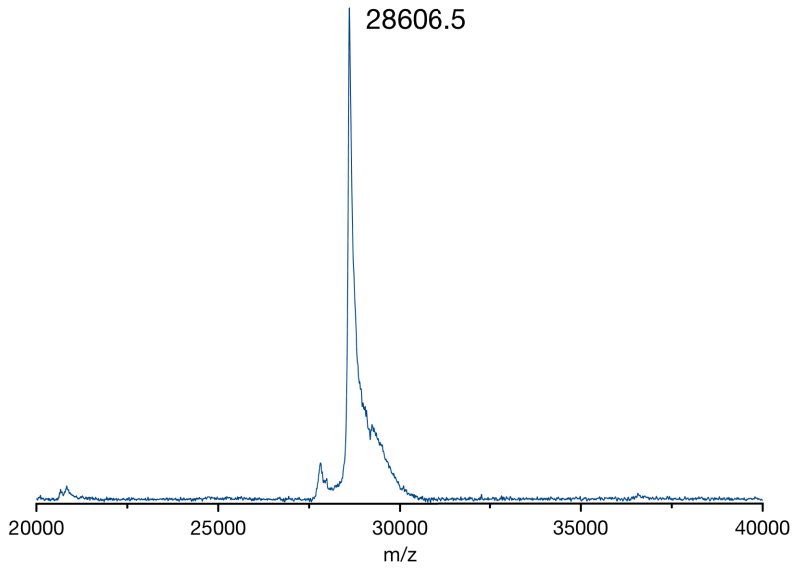

Figure 8.16: MALDI-TOF spectrum of **15**.

Cyclic-(Tat)-eGFP (20)

Peptide **18** (3.06 mg as TFA-salt, 1.13 µmol, 20 eq.) was reacted with eGFP C70M S147C (56.3 nmol) according to general procedure **P2**. After removal of excess peptide **18** by spin filtration the sample was analyzed by MALDI-TOF after acetone precipitation and re-solvation in 10 mM ammonium bicarbonate buffer. Here the quantitative conversion to the product **20** was observed.

MALDI TOF: expected (in Da): 29795.2 ($M+H^+$); found (in Da): 29851.4 ($M+H^+$)

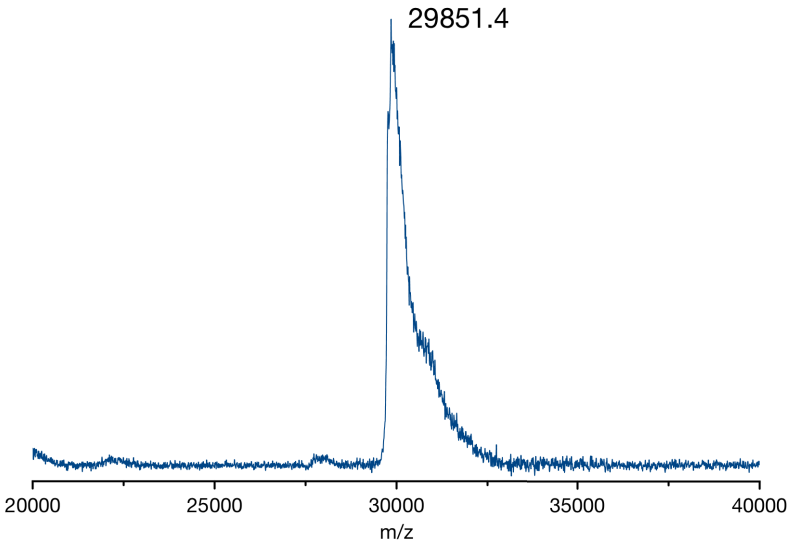

Figure 8.17: MALDI-TOF spectrum of **20**.

Cyclic-(R10)-eGFP (21)

Peptide **19** (3.94 mg as TFA-salt, 1.13 µmol, 20 eq.) was reacted with eGFP C70M S147C (56.3 nmol) according to general procedure **P2**. After removal of excess peptide **19** by spin filtration the sample was analyzed by MALDI-TOF after acetone precipitation and re-solvation in 10 mM ammonium bicarbonate buffer. Here the quantitative conversion to the product **21** was observed.

MALDI TOF: expected (in Da): 30106.4 ($M+H^+$); found (in Da): 30128.0 ($M+Na^+$).

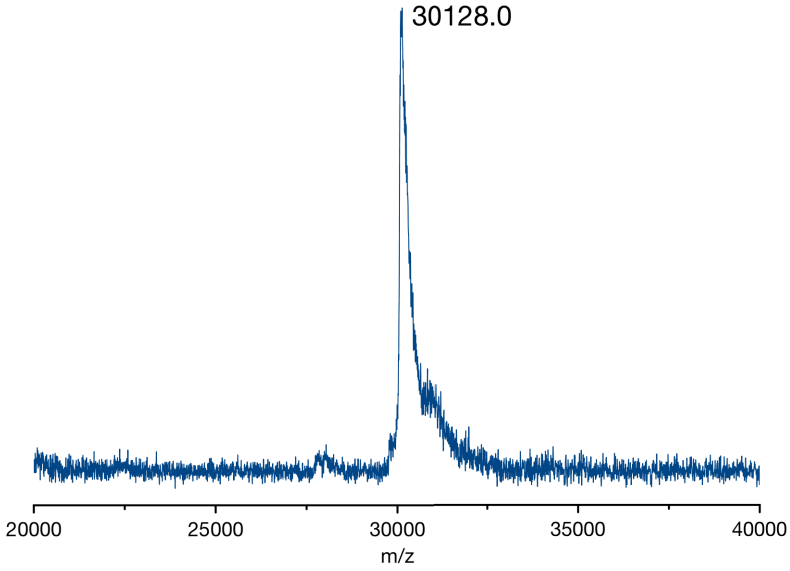

Figure 8.18: MALDI-TOF spectrum of **21**.

General procedure P3 for thiol addition at N-terminal cysteines

N-terminal cysteine GFP (hsGFP S3C C71M or eGFP S6C C70M) buffered in PBS was reduced with TCEP for 30 minutes at 37°C prior to the conjugation reaction. After removal of TCEP *via* ZebaSpin filtration, the protein (100 µM) was incubated with cell penetrating peptide (20 eq.) for three hours at 37°C. Removal of excess peptide was achieved by spinfiltration using Amicon Spin filters with a 10 kDa MWCO. The sample was filtered five times at 14000 rpm for 5 minutes.

Cyclic-(Tat)-hsGFP S3C C71M (23)

Peptide **18** (1.02 mg as TFA-salt, 0.38 µmol, 20 eq.) was reacted with hsGFP S3C C71M according to general protocol **P3**. After removal of excess peptide **18** by ZebaSpin filtration the sample was analyzed by MALDI-TOF after acetone precipitation and re-solvation in

10 mM ammonium bicarbonate buffer. Here the quantitative conversion to the product **22** was observed.

MALDI TOF: expected (in Da): 29698.5 ($M+H^+$); found (in Da) 29698.4 ($M+H^+$)

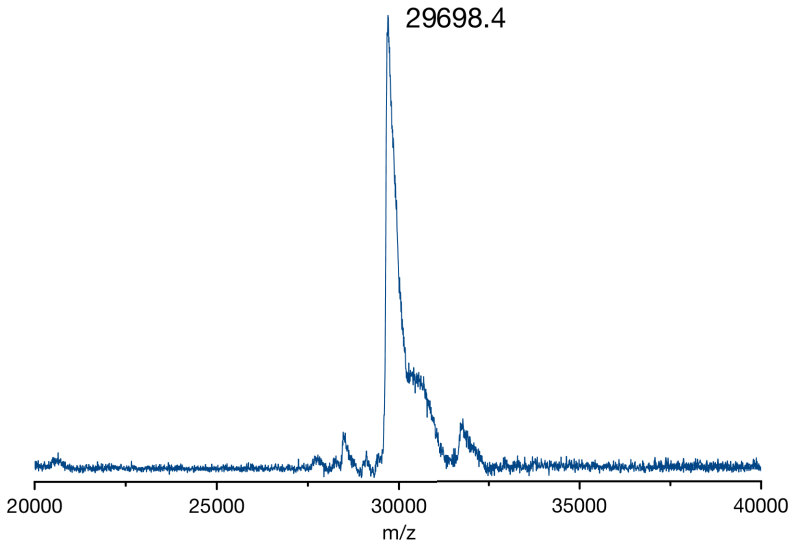

Figure 8.19: MALDI-TOF spectrum of **23**.

Cyclic-(Tat)-eGFP S6C C70M

Cyclic-(Tat)-phosphonamidate-alkyne (1.0 mg as TFA-salt, 0.36 µmol, 6 eq.) was reacted with prior reduced eGFP S6C C70M (57.9 nmol, 1eq) (reduction according to procedure **P3**) in PBS for 16 hours at 37°C, 180 rpm. After purification and rebuffering to HEPES by ZebaSpin filtration (7 kDa MWCO) the sample was analyzed by MALDI-TOF after acetone precipitation and re-solvation in 10 mM ammonium bicarbonate buffer.

MALDI TOF: expected (in Da): 29794.2 ($M+H^+$); found 29904.6 (in Da): ($M+H^+$)

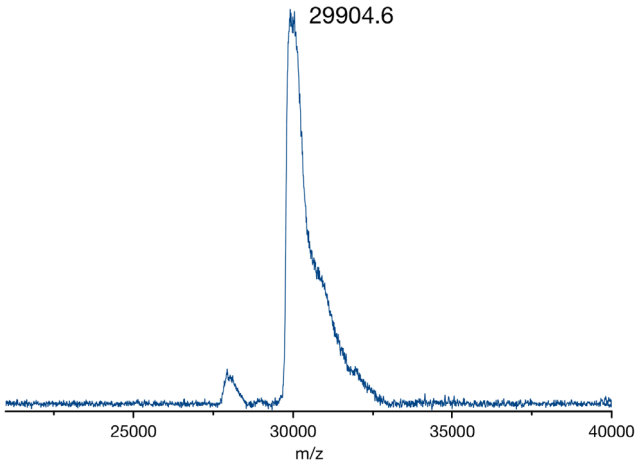

Figure 8.20: MALDI-TOF spectrum of cyclic-(Tat)-eGFP S6C C70M.

Cyclic-(Tat)-maleimide-eGFP (26)

Peptide **23** (0.3 mg as TFA-salt, 0.11 µmol, 5.5 eq.) was reacted with eGFP C70M S147C (20.36 nmol, 1eq.) buffered in PBS at a concentration of 50 µM at 16°C. After four hours shaking with 800 rpm the excess peptide was removed by ZebaSpin filtration and rebuffering to HEPES buffer pH 7.5. The sample was analyzed by MALDI-TOF after acetone precipitation and re-solvation in 10 mM ammonium bicarbonate buffer. Quantitative conversion to the product **25** was observed.

MALDI TOF: expected (in Da): 29697.1 ($M+H^+$); found (in Da): 29768.2 ($M+K^++Na^+$)

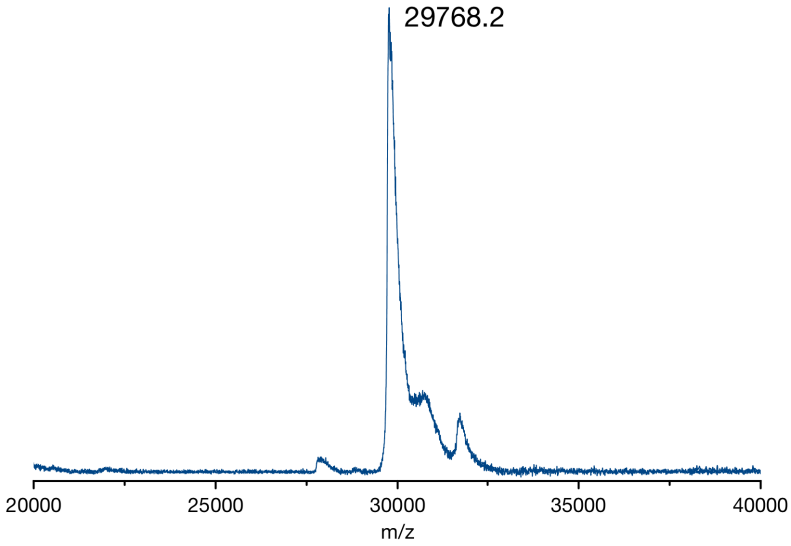

Figure 8.21: MALDI-TOF spectrum of **26**.

Cyclic-(Tat)-iodoacetate-eGFP (27)

Peptide **24** (0.3 mg as TFA-salt, 0.11 µmol, 5.5 eq.) was reacted with eGFP C70M S147C (20.36 nmol, 1eq.) buffered in PBS at a concentration of 50 µM at room temperature. After three hours shaking with 800 rpm the excess peptide was removed by ZebaSpin filtration and rebuffering to HEPES buffer pH 7.5. The sample was analyzed by MALDI-TOF after acetone precipitation and re-solvation in 10 mM ammonium bicarbonate buffer. Here the quantitative conversion to the product **26** was observed.

MALDI TOF: expected (in Da): 29727.0 (M+); found (in Da): 29706.5 (M+)

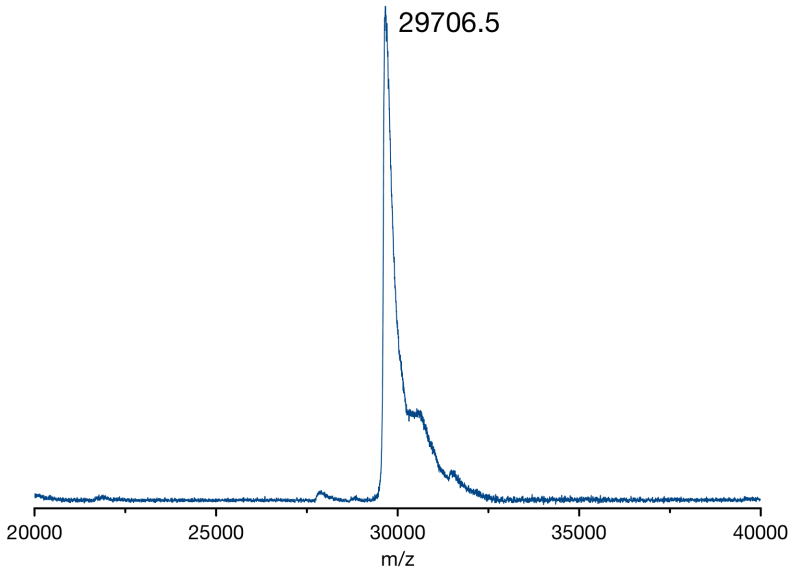

Figure 8.22: MALDI-TOF spectrum of **27**.

8.3.5 FACS measurements

U87MG cells were cultured in Dulbecco's MEM medium supplemented with 10% FBS and 1% Penicillin Streptomycin. 70 000 cells were seeded in an uncoated glass bottom 8-well µ-slide (Ibidi) 24 hours prior to treatment. Finally cells were incubated with 40 µM cRGD-eGFP conjugate in serum free medium at 37°C in a 5% CO_2 atmosphere. After four hours cells were washed with PBS and treated with acutase to detach cells from the dish. Detached cells were transferred into a tube washed with PBS (including 0.5% BSA) three times and centrifuged each time at 1200 rpm for 5 minutes. After the final wash the cell pellet was solved in 400 µl PBS and measured.

8.3.6 Cellular uptake experiments

All cell uptake experiments were carried out according to literature[122], with HeLa (ATCC CCL-2) cells cultured in Dulbecco's MEM medium supplemented with 10% FBS and 1% Penicillin Streptomycin. 70 000 cells were seeded in an uncoated glass bottom 8-well µ-slide (Ibidi) 24 hours prior to treatment. The cellular uptake was carried out by gently washing cells three times with HEPES buffer pH 7.5 (5 mM HEPES, 140 mM NaCl, 2.5 mM KCl, 5 mM glycine). The peptide-protein conjugate buffered in the same HEPES buffer was added to the cells in 200 µl at respective concentration and incubated for at 37°C in a 5% CO_2 atmosphere. After one hour cells were gently washed with 25 mM HEPES in Dulbecco's MEM supplemented with 10% FKS and cells were rested for 30 minutes at

37°C. The cell nucleus was stained with Hoechst 33342 and cells imaged with a Zeiss 710 confocal microscope.

The percentage of cells that took up the GFP conjugate was determined by counting all cells showing nucleolar GFP relative to the total number of cells (all Hoechst stained nuclei). Each uptake experiment was repeated at least three times.

8.4 Intramolecular Staudinger induced thiol addition as new peptide cyclization method

8.4.1 Peptide synthesis

General procedure P4 for peptide synthesis of all BCL9-peptides

The BCL9 peptide was synthesized in a 0.1 mmol scale on a Rink Amide Resin with a loading of 0.78mmol/g. The synthesis was carried out on a PTI synthesizer with a single coupling of each standard amino acid (5 eq. amino acid for 40 min). Fmoc-Azidohomoalanin (2 eq.) was coupled with HATU (2 eq.) for four hours. Fmoc deprotection was accomplished by treating the peptide with 20% piperidine in DMF for 3 minutes two to three times according to UV read out. *N*-terminal acetylation was done by incubation with a mixture of lutidine:acetic acid:DMF (6%:5%:89%;v;v;v) for 10 minutes. Final cleavage from solid support was carried out by incubating the resin with 4 ml of a TFA:TIS:H_2O (95:2.5:2.5) mixture for two hours and precipitated in cold diethylether.

BCL9-Nle-wt peptide synthesis

^{Ac}LSQEQLEHRERSLQTLRDIQRNleLF^{NH2}

The peptide was synthesized according to general procedure **P4**. The crude peptide was purified by preparative reverse phase C18 HPLC (0-5 min 95/5, water (0.1%TFA)/MeCN (0.1%TFA); 5-60 min 10/90, water (0.1%TFA)/MeCN (0.1%TFA)). The product was gained as white powder (95.2 mg as TFA-salt, 13.2 µmol, 26.4 % yield) and analyzed by UPLC (method B; rt.: 6.10 min).

HRMS: m/z: 1017.2160 $[M+3H]^{3+}$ (calc. 1017.2273 m/z).

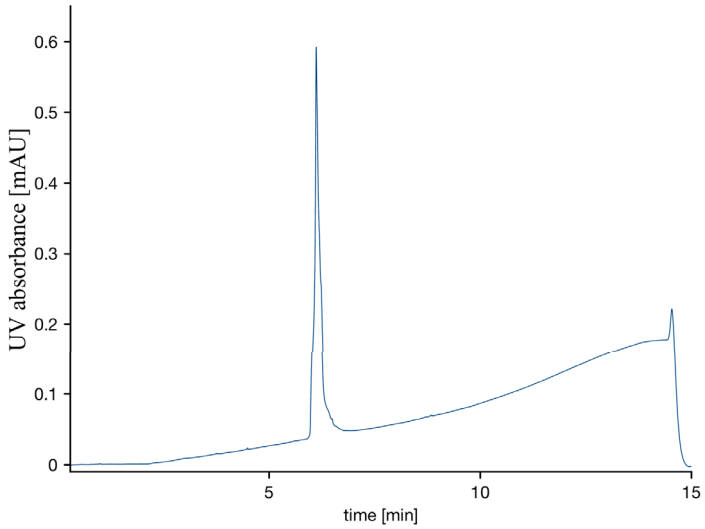

Figure 8.23: UPLC-UV chromatogram of BCL-Nle-wt.

BCL9-Nle-Aha-LCys peptide synthesis (30a)

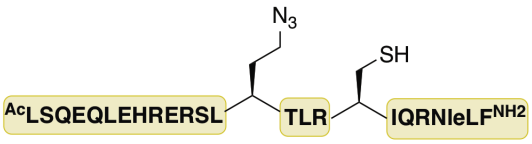

The peptide was synthesized according to general procedure **P4**. The crude peptide was purified by preparative reverse phase C18 HPLC (0-5 min 95/5, water (0.1%TFA)/MeCN (0.1%TFA); 5-60 min 10/90, water (0.1%TFA)/MeCN (0.1%TFA)). The product **45** was gained as white powder (35 mg as TFA-salt, 9.7 µmol, 9.7 % yield) and analyzed by UPLC (method B; rt.: 6.95 min).

HRMS: m/z: 1012.5317 $[M+3H]^{3+}$ (calc. 1012.5532 m/z).

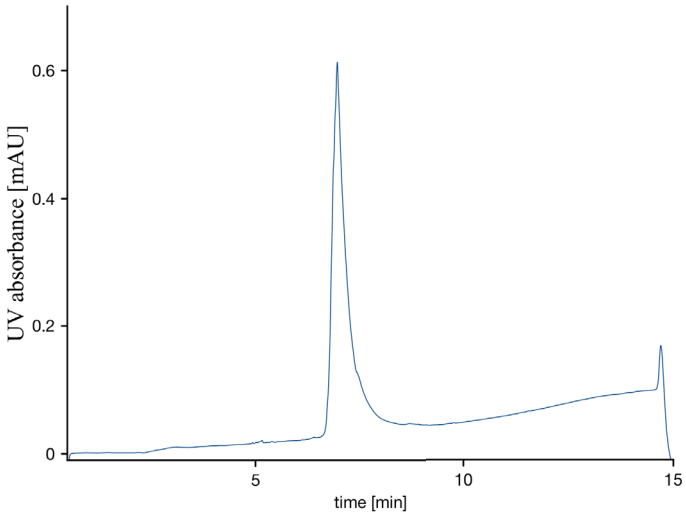

Figure 8.24: UPLC-UV chromatogram of **30a**.

Alkylated-BCL9-Nle-Aha-LCys peptide synthesis (33)

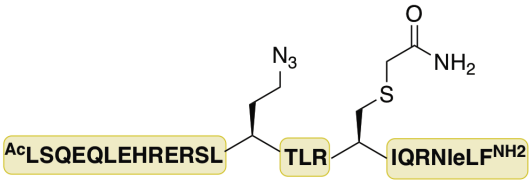

Peptide **30a** (43.2 mg, 12.0 µmol) was incubated with iodoacetamide (22.2 mg, 120 µmol, 10eq.) in a mixture of ammoniumbicarbonate buffer and acetonitrile (6:2) with a final pH of 8.5. After one hour the mixture was purified by preparative HPLC 0-5 min 95/5, water (0.1%TFA)/MeCN (0.1%TFA); 5-60 min 10/90, water (0.1%TFA)/MeCN (0.1%TFA)). The product was gained as white powder (25 mg as TFA-salt, 6.8 µmol, 57 % yield) and analyzed by UPLC (method A; rt.: 2.34 min).

HRMS: m/z: 1031.5342 $[M+3H]^{3+}$ (calc. 1031.5604 m/z).

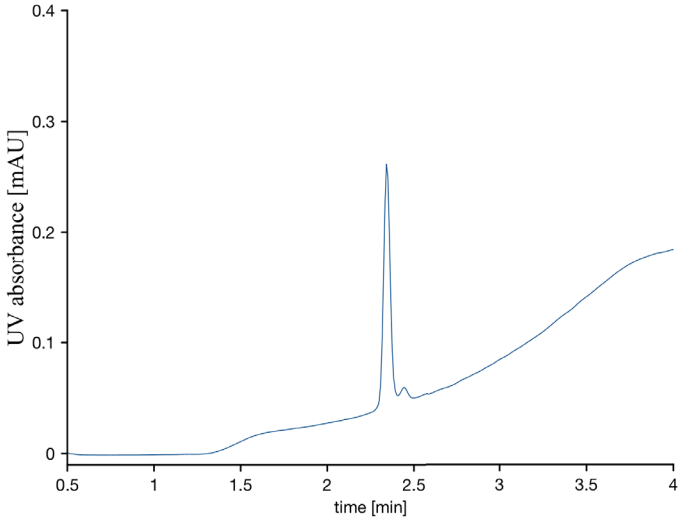

Figure 8.25: UPLC-UV chromatogram of **33**.

BCL9-Nle-Aha-DCys peptide synthesis (30b)

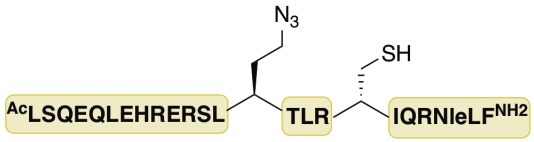

The Peptide was synthesized according to general procedure **P4**. The crude peptide was purified by preparative reverse phase C18 HPLC (0-5 min 95/5, water (0.1%TFA)/MeCN (0.1%TFA); 5-60 min 10/90, water (0.1%TFA)/MeCN (0.1%TFA)). The product was gained as white powder (50.5 mg as TFA-salt, 14.0 µmol, 14 % yield) and analyzed by UPLC (method B; rt.: 6.20 min).

HRMS: m/z: 1012.5383 $[M+3H]^{3+}$ (calc. 1012.5532 m/z).

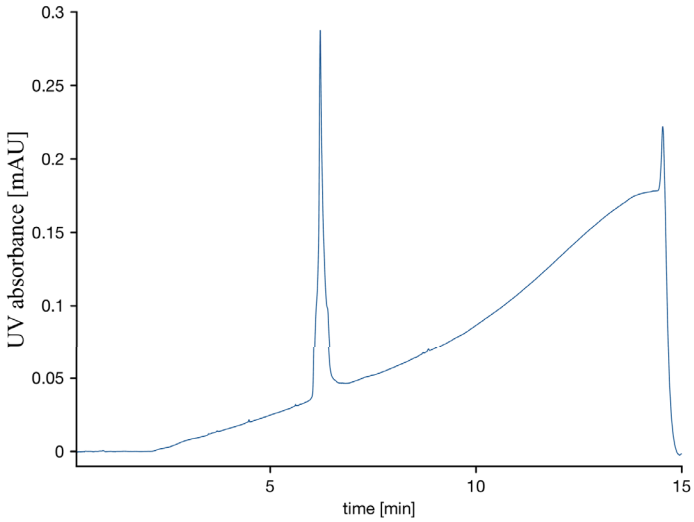

Figure 8.26: UPLC-UV chromatogram of **30b**.

Scrambled-BCL9-Nle-Aha-DCys peptide synthesis

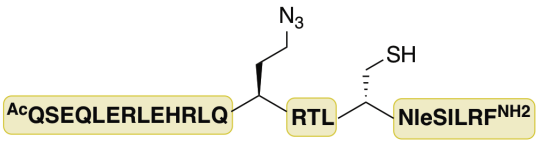

The Peptide was synthesized according to general procedure **P4**.The crude peptide was purified by preparative reverse phase C18 HPLC (0-5 min 95/5, water (0.1%TFA)/MeCN (0.1%TFA); 5-60 min 10/90, water (0.1%TFA)/MeCN (0.1%TFA)). The product was gained as white powder (13 mg as TFA-salt, 3.6 µmol, 3.6 % yield) and analyzed by UPLC (method B; rt.: 6.05 min).

HRMS: m/z: 1012.5481 $[M+3H]^{3+}$ (calc. 1012.5532 m/z).

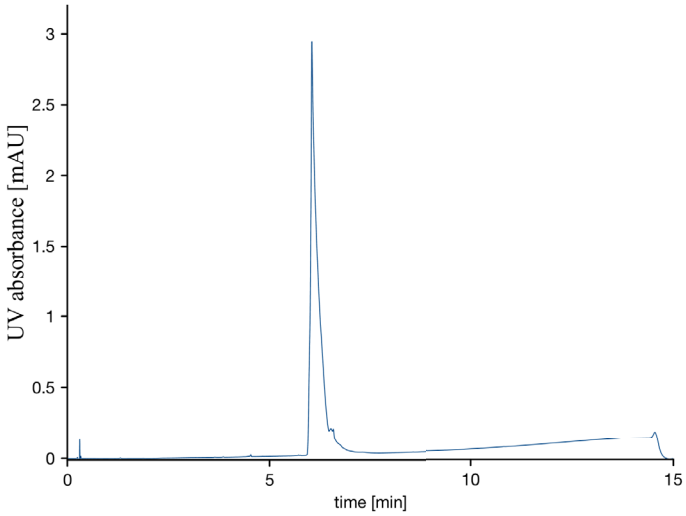

Figure 8.27: UPLC-UV chromatogram of **scrambled-BCL9-Nle-Aha-DCys**.

RCM-BCL9-Nle peptide synthesis (39)

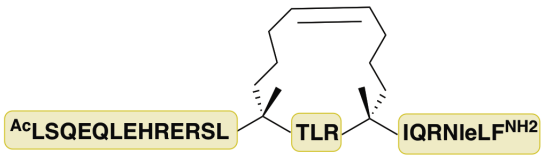

The RCM-BCL9 peptide was synthesized in a 0.05 mmol scale on a Rink Amide Resin with a loading of 0.78 mmol/g. Until the first olefinic amino acid the synthesis was carried out on a PTI synthesizer with single couplings (5 eq. amino acid for 40 minutes). Olefinic amino acids (2 eq.) were coupled manually with HATU (2eq.) and DIPEA (4 eq.) for two hours and full conversion was checked by trial cleavage. The three amino acids in between the olefinic ones were coupled manually (5 eg. for 40 minutes) all amino acids following the olefinic ones were coupled in double coupling steps with five equivalents for 40 minutes. After the second olefinic amino acids the synthesis was resumed by automated SPPS on the PTI synthesizer. The *N*-terminus was acetylated by treatment with a lutidine:acetic

anhydride:DMF (5:6:89;v:v:v) for 10 minutes. To generate the hydrocarbon staple the resin was incubated with a 10 mM solution of bis(tricyclohexylphosphine)-benzylidene ruthenium (IV) (1st generation Grubb's catalyst) in 1,2-dichloroethane for one hour twice.

The final cleavage from resin was achieved by incubation with a mixture of TFA:TIS:H_2O (95:2.5:2.5;v:v:v) for two hours followed by precipitation in cold diethylether. The crude peptide was purified by preparative reverse phase C18 HPLC, the product was gained as white powder (14 mg, 3.9 µmol, 7.8% yield) and analyzed by UPLC (method B; rt.: 7.34 min).

HRMS: m/z: 1019.5471 $[M+3H]^{3+}$ (calc. 1019.5881 m/z).

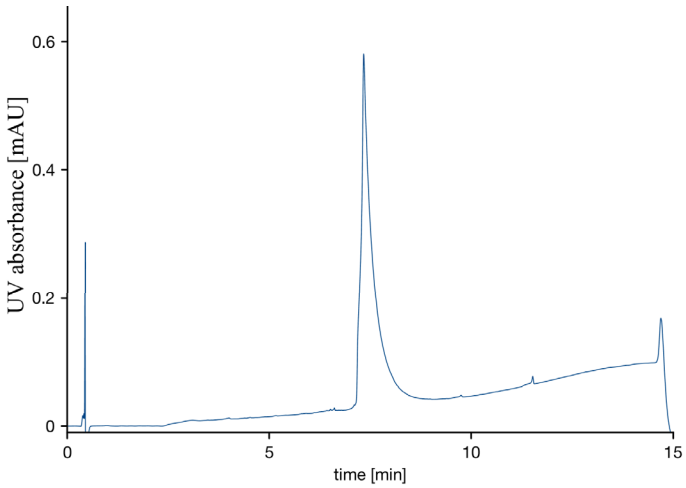

Figure 8.28: UPLC-UV chromatogram of **39**.

FAM-BCL9-Nle-Aha-DCys peptide synthesis (30b-FAM)

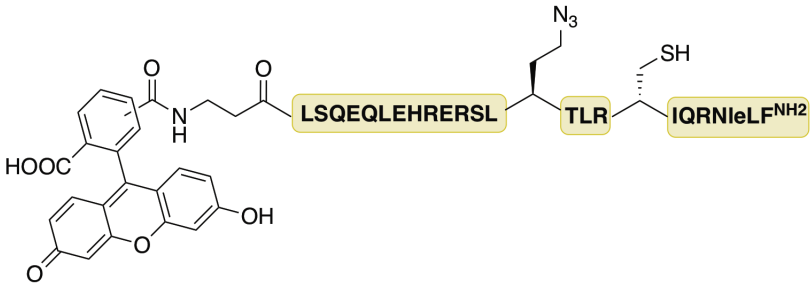

The peptide was synthesized according to general procedure **P4**. After the final regular amino acid coupling and Fmoc-deprotection, Fmoc-β-Alanine (5 eq.) was coupled manually with HATU (5 eq.) and DIPEA (10 eq.) as activating base for one hour. After Fmoc-deprotection 5-(6)-carboxyfluorescein succinimidyl ester (2 eq.) was coupled with DIPEA (3 eq.) as activating base for four hours. Final cleavage from solid support was carried out by incubating the resin with 4 ml of a TFA:TIS:H_2O (95:2.5:2.5) mixture for two hours and precipitated in cold diethylether. The crude peptide was purified by preparative reverse phase C18 HPLC (0-5 min 95/5, water (0.1%TFA)/MeCN (0.1%TFA); 5-60 min 10/90, water

(0.1%TFA)/MeCN (0.1%TFA)). The product was gained as yellow powder (42.0 mg as TFA-salt, 10.2 µmol, 10.2 % yield) and analyzed by UPLC (method B; rt.: 7.20 min).
HRMS: m/z: 1141.5472 $[M+3H]^{3+}$ (calc. 1141.5780 m/z); 856.4244 $[M+4H]^{4+}$ (calc. 856.4355 m/z).

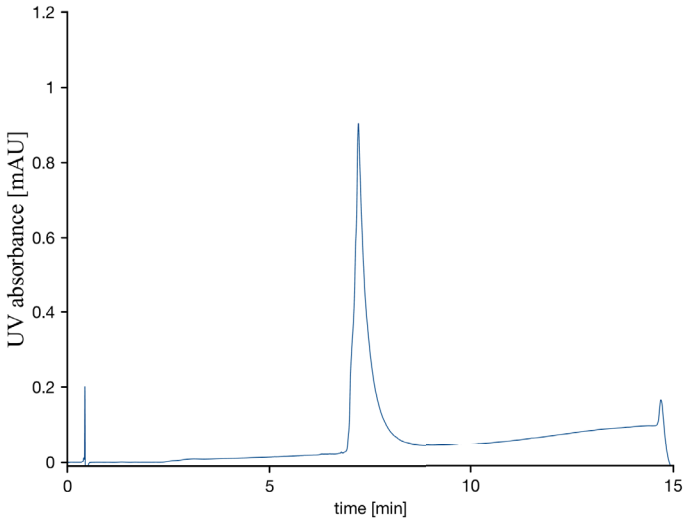

Figure 8.29: UPLC-UV chromatogram of **30b-FAM**.

FAM RCM-BCL9-Nle peptide synthesis (39-FAM)

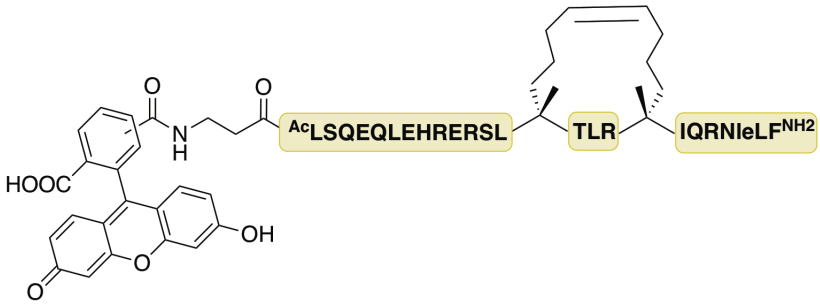

The FAM-RCM-BCL9 peptide was synthesized in a 0.05 mmol scale on a Rink Amide Resin with a loading of 0.78 mmol/g. Until the first olefinic amino acid the synthesis was carried out on a PTI synthesizer with single couplings (5 eq. amino acid for 40 minutes). Olefinic amino acids (2 eq.) were coupled manually with HATU (2eq.) and DIPEA (4 eq.) for two hours and full conversion was checked by trial cleavage. The three amino acids in between the olefinic ones were coupled manually (5 eg. for 40 minutes) all amino acids following the olefinic ones were coupled in double coupling steps with five equivalents for 40 minutes. After the second olefinic amino acids the synthesis was resumed by automated SPPS on the PTI synthesizer and Fmoc-β-Ala was coupled *N*-terminally. To generate the hydrocarbon staple the resin was incubated with a 10 mM solution of bis(tricyclohexylphosphine)-benzylidene ruthenium (IV) (1st generation Grubb's catalyst) in 1,2-dichloroethane for one hour twice. Finally the peptide was fluorescein labeled by

coupling 5-(6)-carboxyfluorescein succinimidyl ester (2 eq.) with DIPEA (3 eq.) as activating base for two hours.

The final cleavage from resin was achieved by incubation with a mixture of TFA:TIS:H_2O (95:2.5:2.5;v:v:v) for two hours followed by precipitation in cold diethylether. The crude peptide was purified by preparative reverse phase C18 HPLC, the product was gained as yellow powder (16 mg, 4.02 µmol, 8.0% yield) and analyzed by UPLC (method B; rt.: 7.86 & 7.95 min).

HRMS: m/z: 1148.5795 $[M+3H]^{3+}$ (calc. 1148.6129 m/z).

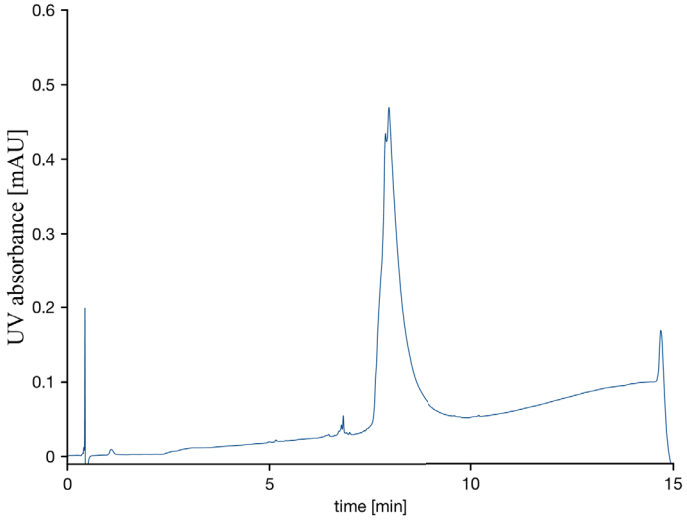

Figure 8.30: UPLC-UV chromatogram of **39-FAM** broad double peak due to diastereomer mixture of fluorescein.

Linear-(R10)-Aha-Cys (41)

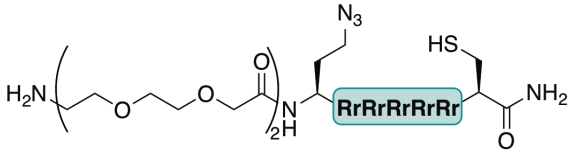

The cyclic-(R10)-azido peptide was synthesized in a 0.1 mmol scale on a Rink Amide Resin with a loading of 0.78 mmol/g. The synthesis was carried out on a PTI synthesizer with double couplings of each amino acid (5 eq. amino acid for 40 min) in DMF apart from Fmoc-azidohomoalanin, which (2eq.) was coupled with HATU (2 eq.) for four hours in presence of NMM (4 eq.) as activating base. SPPS was ending with an Fmoc deprotection step to yield the free *N*-terminal amine. Final cleavage from resin was accomplished in two cleavage steps. First the peptide was cleaved from resin with a mixture of TFA:TIS:H_2O (92:4:4;v:v:v) for 2.5 hours, followed by a second cleavage of not fully cleaved protecting groups with TFA:TIS:DTT:Thioanisole (88:2:2:8;v:v:v:v) for one hour. The crude peptide was purified by preparative reverse phase C18 HPLC (0-5 min 95/5, water (0.1%TFA)/MeCN (0.1%TFA); 5-60 min 10/90, water (0.1%TFA)/MeCN (0.1%TFA)). The product **41** was gained as white

powder (78 mg as TFA-salt, 24.1 µmol, 24.1 % yield) and analyzed by UPLC (method A; rt.: 1.51 min).

HRMS: m/z: 700.0462 $[M+3H]^{3+}$ (calc. m/z: 700.0908).

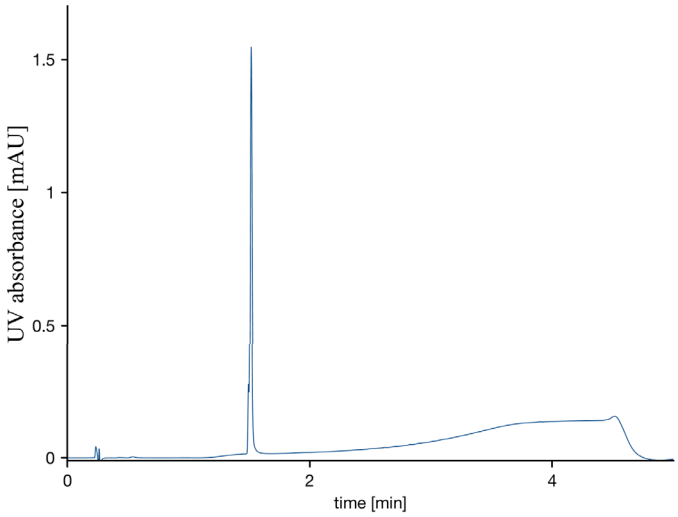

Figure 8.31: UPLC-UV chromatogram of **41.**

8.4.2 Staudinger Phosphonite Reaction

Bisethoxyalkene-phosphonite synthesis (31)

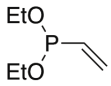

Vinyl magnesium bromide in THF (1 M, 2 ml, 2 mmol, 1 eq.) was cooled to – 78°C in a flame dried schlenk flask and diethylchlorophosphite (0.286 ml, 2 mmol, 1 eq.) was added. The solution was stirred for 10 minutes at – 78°C and let warm to room temperature and stirred for another 90 minutes. The full consumption of starting material was confirmed by ^{31}P-NMR (product at 158.0 ppm; see appendix) and used as crude in the following Staudinger reaction with an azido-peptide. Due to the inherent lability of bisethoxyalkene-phosphonite toward water and air the unprotected compound was not isolated. The correct product formation *via* this reaction however was previously confirmed by Marc-André Kasper in his PhD thesis, by additionally protecting the P(III)-compound with borane, which makes it possible to isolate and characterize the compound.

Bisbenzoylalkene-phosphonite synthesis (36)

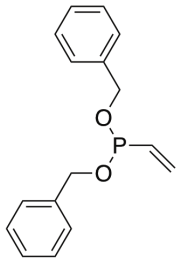

Bis(diisopropylamino) chlorophosphine (267 mg, 1 mmol, 1 eq.) was given into a flame dried schlenk flask and dried under vacuo for 30 minutes. Vinyl magnesium bromide in THF (1 M, 1.1 ml, 1.1 mmol, 1.1 eq.) was added at – 78°C and the reaction mixture was stirred for 10 minutes. Then the reaction was let to warm up to room temperature and stirred for another 30 minutes. First tetrazole in acetonitrile (0.45 M, 5.56 ml, 2.5 mmol, 2.5 eq.) was added to the reaction mixture followed by benzylalcohol (0.26 ml, 2.5 mmol, 2.5 eq.). The reaction was stirred for 16 hours and used further as crude after confirmation of starting material consumption *via* ^{31}P-NMR (product at 164.2 ppm; see appendix). Due to the inherent lability of bisbenzoylalkene-phosphonite toward water and air the unprotected compound was not isolated. Marc-André Kasper showed the successful Grignard reaction followed by exchange of substituents in exactly this reaction cascade previously for a wide range of substituents in his PhD thesis by an additional borane protection step.

General procedure P5 for Staudinger-phosphonite reaction with alkyl azides

Purified azido-peptide was dissolved in DMSO at a 3 mM concentration and dried in a flame-dried flask for one hour prior to adding five equivalents of bisethoxyalkene-phosphonite (volume according to percentage of product determined by NMR). After the reaction mixture was stirred over night at room temperature and full conversion was observed by UPLC-UV/MS, water was added and the reaction mixture directly lyophilized. The crude product was purified by semi-preparative HPLC.

Cyclic-BCL9-Nle-Aha-LCys peptide synthesis (32a)

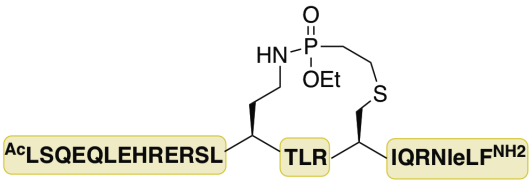

Peptide **30a** (15 mg, 4.16 µmol, 1eq.) was reacted with phosphonite **31** according to the general procedure **P5**. The crude peptide was purified by preparative reverse phase C18 HPLC (0-5 min 95/5, water (0.1%TFA)/MeCN (0.1%TFA); 5-60 min 10/90, water (0.1%TFA)/MeCN (0.1%TFA)). The product **32a** was gained as white powder (7 mg as TFA-salt, 1.89 µmol, 45.4 % yield) and analyzed by UPLC (method A; rt.: 2.93 min).
HRMS: m/z: 1043.1953 $[M+3H]^{3+}$ (calc. 1043.2292 m/z).

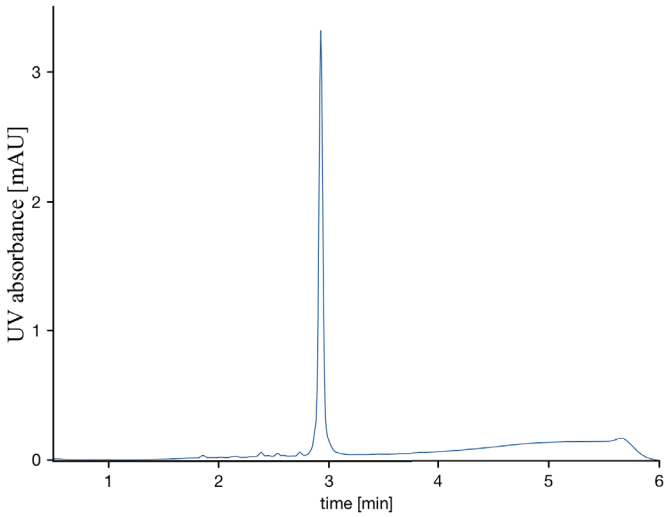

Figure 8.32: UPLC-UV chromatogram of **32a**.

Cyclic-BCL9-Nle-Aha-DCys peptide synthesis (32b)

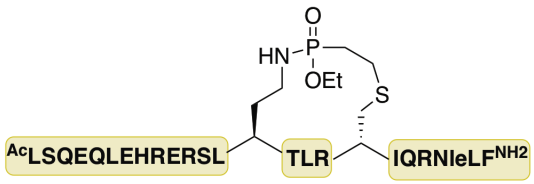

Peptide **30b** (34 mg, 9.43 µmol, 1eq.) was reacted with phosphonite **31** according to the general procedure **P5**. The crude peptide was purified by preparative reverse phase C18 HPLC (0-5 min 95/5, water (0.1%TFA)/MeCN (0.1%TFA); 5-60 min 10/90, water (0.1%TFA)/MeCN (0.1%TFA)). The product **32b** was gained as white powder (15 mg as TFA-salt, 4.06 µmol, 43.1 % yield) and analyzed by UPLC (method B, rt.: 6.41 min).

HRMS: m/z: 1043.2085 $[M+3H]^{3+}$ (calc. 1043.2292 m/z).

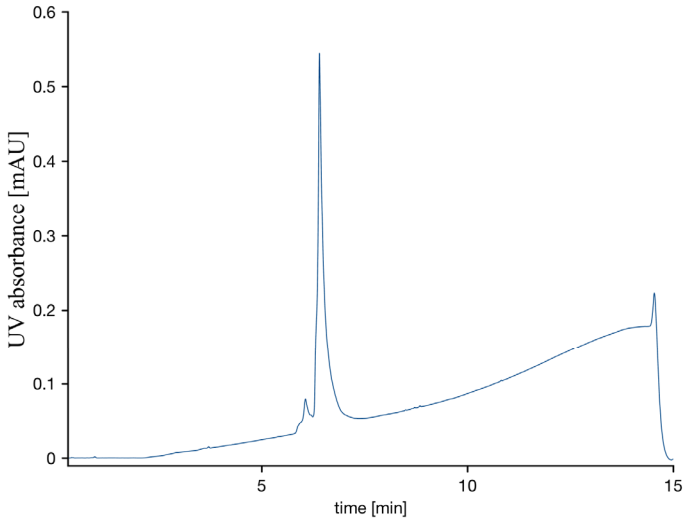

Figure 8.33: UPLC-UV chromatogram of **32b**.

Cyclic-benzoylphosphonite-BCL9-Nle-Aha-DCys peptide synthesis (38)

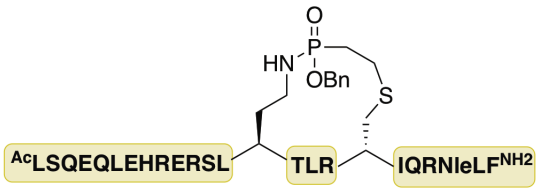

Peptide **30b** (15 mg, 4.04 µmol, 1eq.) was solubilized in DMSO and reacted with **36** (24.2 µmol, 6 eq.) in a final concentration of 10 mM. The reaction mixture was stirred for 16 hours at 40°C and the crude peptide was purified by preparative reverse phase C18 HPLC (0-5 min 95/5, water (0.1%TFA)/MeCN (0.1%TFA); 5-60 min 10/90, water (0.1%TFA)/MeCN (0.1%TFA)). The product **38** was gained as white powder (5 mg as TFA-salt, 1.33 µmol, 32.9 % yield) and analyzed by UPLC (method B; rt.: 6.45 min).

HRMS: m/z: 1063.8917 $[M+3H]^{3+}$ (calc. 1063.9010 m/z).

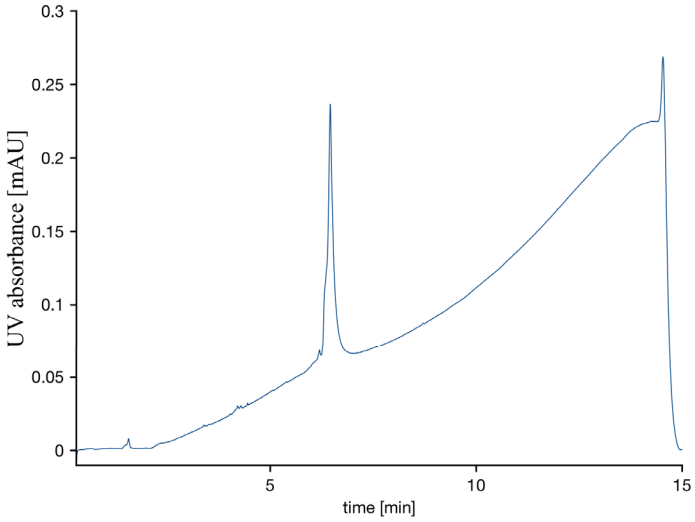

Figure 8.34: UPLC-UV chromatogram of **38**.

Cyclic scrambled-BCL9-Nle-Aha-DCys peptide synthesis (40)

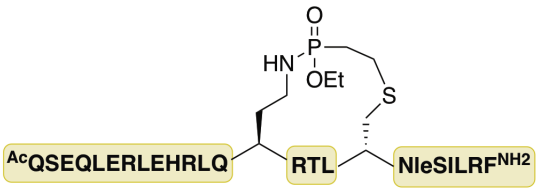

Scrambled-BCL9-Nle-Aha-DCys (7 mg, 1.90 µmol, 1eq.) was reacted with phosphonite **31** according to the general procedure **P5**. The crude peptide was purified by preparative reverse phase C18 HPLC (0-5 min 95/5, water (0.1%TFA)/MeCN (0.1%TFA); 5-60 min 10/90, water (0.1%TFA)/MeCN (0.1%TFA)). The product **40** was gained as white powder (3.2 mg as TFA-salt, 0.87 µmol, 45.8% yield) and analyzed by UPLC (method B; rt.: 6.09 min).

HRMS: m/z: 1043.2217 $[M+3H]^{3+}$ (calc. 1043.2292 m/z).

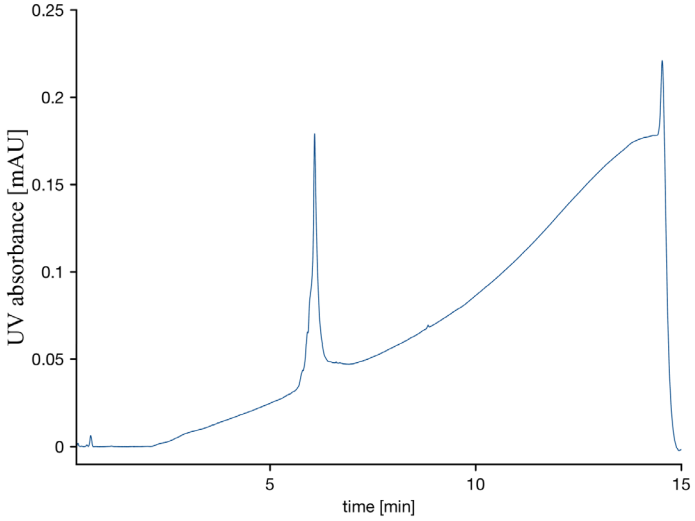

Figure 8.35: UPLC-UV chromatogram of **40**.

FAM labeled cyclic-BCL9-Nle-Aha-DCys peptide synthesis (32b-FAM)

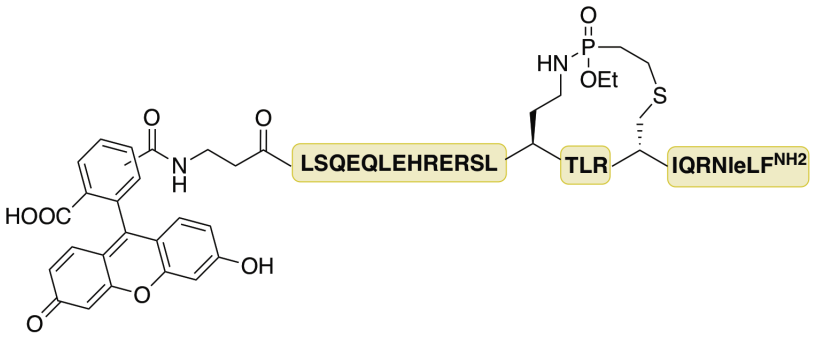

Peptide **30b-FAM** (21 mg, 5.1 µmol, 1eq.) was reacted with phosphonite **31** according to the general procedure **P5**. The crude peptide was purified by preparative reverse phase C18 HPLC (0-5 min 95/5, water (0.1%TFA)/MeCN (0.1%TFA); 5-60 min 10/90, water (0.1%TFA)/MeCN (0.1%TFA)). The product **32b-FAM** was gained as yellow powder (12 mg as TFA-salt, 2.9 µmol, 56.9 % yield) and analyzed by UPLC (method B; rt.: 6.70 min).
HRMS: m/z: 1172.1996 $[M+3H]^{3+}$ (calc. 1171.9222 m/z).

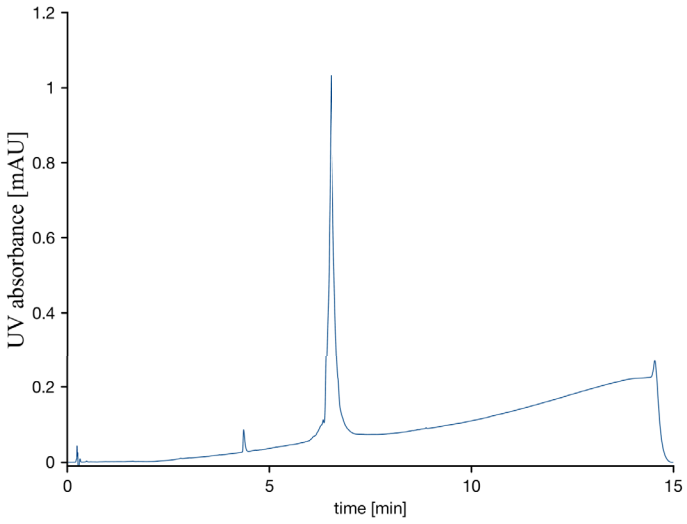

Figure 8.36: UPLC-UV chromatogram of **32b-FAM**.

FAM labeled cyclic-benzoylphosphonite-BCL9-Nle-Aha-DCys peptide synthesis (38-FAM)

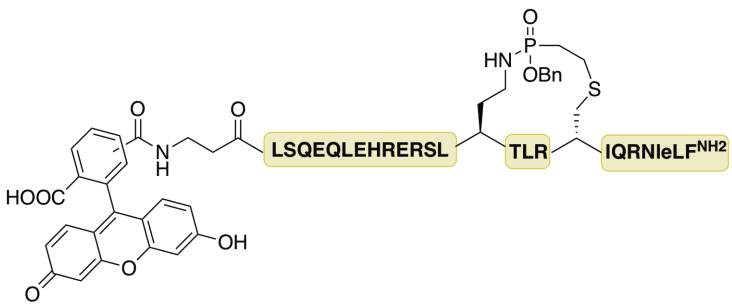

Peptide **30b-FAM** (22 mg, 5.93 µmol, 1eq.) was solubilized in DMSO and reacted with **36** (35.6 µmol, 6 eq.) in a final concentration of 10 mM. The reaction mixture was stirred for 16 hours at 40°C and the crude peptide was purified by preparative reverse phase C18 HPLC (0-5 min 95/5, water (0.1%TFA)/MeCN (0.1%TFA); 5-60 min 10/90, water (0.1%TFA)/MeCN (0.1%TFA)). The product **38-FAM** was gained as yellow powder (3.1 mg as TFA-salt, 0.75 µmol, 12.6 % yield) and analyzed by UPLC (method B; rt.: 6.51 min).

LRMS: m/z: 1193.11 $[M+3H]^{3+}$ (calc. 1192.9258 m/z).

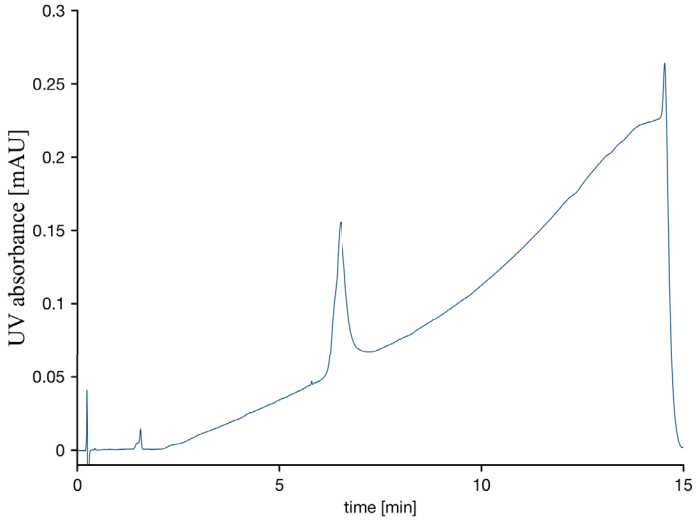

Figure 8.37: UPLC-UV chromatogram of **38-FAM** broad peak due to diastereomer mixture of FAM.

Cyclic-R10-Staudinger-Macrocycle 42

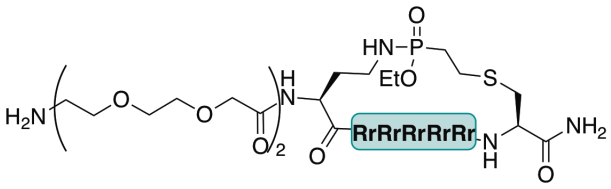

Peptide **41** was reacted with phosphonite **31** according to general procedure **P5** with the deviation that the reaction was carried out at 50°C instead of room temperature. The crude peptide was purified by preparative reverse phase C18 HPLC (0-5 min 95/5, water (0.1%TFA)/MeCN (0.1%TFA); 5-60 min 10/90, water (0.1%TFA)/MeCN (0.1%TFA)). The product **42** was gained as white powder (10.7 mg as TFA-salt, 3.2 µmol, 26.8 % yield) and analyzed by UPLC (method B; rt.: 0.45 & 0.52 min).

HRMS: m/z: 730.7141 $[M+3H]^{3+}$ (calc. 730.7668 m/z).

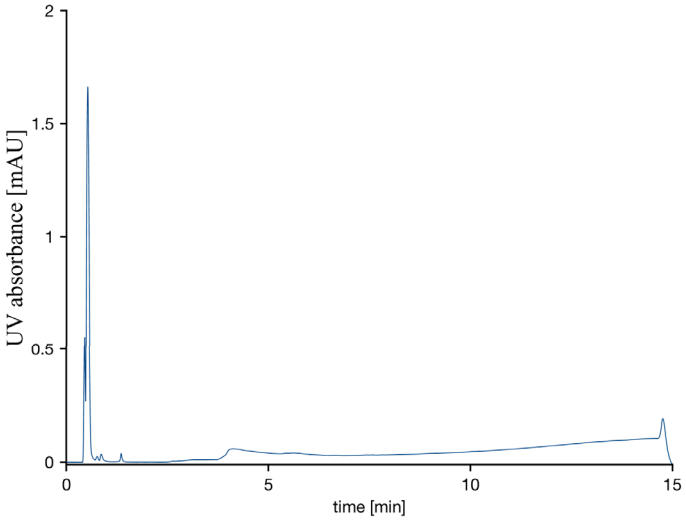

Figure 8.38: UPLC-UV chromatogram of **42**.

Alkyne-Cyclic-R10-Staudinger-Macrocycle 44

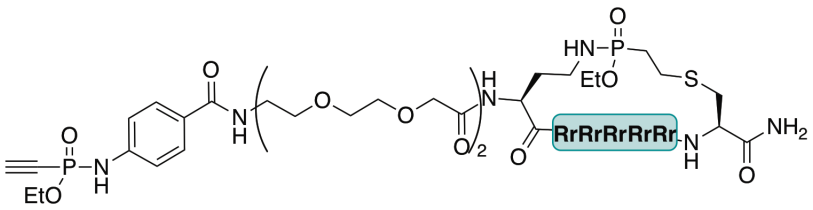

Peptide **42** (20 mg, 6 µmol, 1 eq.) solubilized in DMF (400 µl, c = 15 mM) was incubated with NHS-phosphonamidate alkyne **43** (6.3 mg, 18.0 µmol, 3eq.) in presence of DIPEA (4.68 µl, 26.9 µmol, 4.5 eq.) for one hour. After confirmation of product formation by LC-MS, the crude was diluted with water and purified by preparative HPLC. The product was gained as white poweder (9.8 mg as TFA salt, 2.8 µmol, 46 %yield) and analyzed by UPLC (method A; rt.: 1.64 min).

LRMS: m/z: 809.0552 $[M+3H]^{3+}$ (calc. 809.1134 m/z).

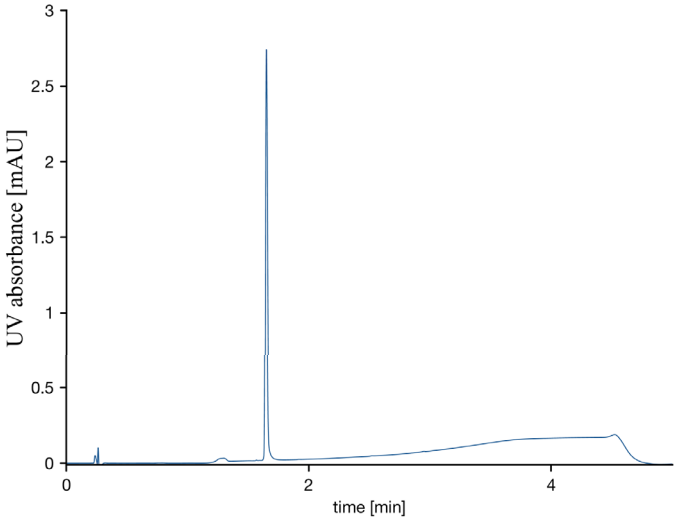

Figure 8.39: UPLC-UV chromatogram of **44** after prep. HPLC purification

8.4.3 Protein Expression

Protein expression β-Catenin-GST

β-Catenin-GST (pGEX-Bcatfl was a gift from David Rimm (Addgene plasmid #24193)) was expressed in *E.coli* BL21 (DE3) with LB medium including 100 µg/ml Ampillicin. Cells were grown at 37°C at 180 rpm until OD_{600} reached 0.73 followed by induction with 0.2 mM IPTG and expression at 18°C at 180 rpm for 16 hours.

The cells were harvested by centrifugation at 4000 g for 15 minutes at 4°C. Cell lysis was carried out in Dulbecco's PBS with a sonicator at 30% for six minutes. Finally debris was centrifugation at 27000 g for 20 minutes. β-Catenin-GST was purified with Bioscale™ Mini Profinity™ GST cartridge (5 ml) on a BioRad NGC system (Binding/Wash buffer: 50 mM Tris HCl pH 8.0/ 150 mM NaCl/ 0.1 mM EDTA; elution buffer: 50 mM Tris HCl pH 8.0/ 150 mM NaCl/ 0.1 mM EDTA/ 10 mM reduced glutathione). After elution the peak fractions were combined and dialysed to Dulbecco's PBS. The protein was aliquoted at a concentration of 0.87 mg/ml, shock frozen and stored at - 80°C.

His-BCL9 (243 – 469)

The cDNA for BCL9 was purchased from biocat (Gene ID 607) in a pCR-BluntII-TOPO vector.

PCR

The Gene region of interest was amplified with BamHI and HindII restriction sites by PCR using complementary primer pairs (for conditions see Table 8.5 and 8.6) (GTAGTGGATCCAACCAGGACCAGAATTCTTC and ATACGAAGCTTTTAC TGCTCGGGAGTCATATGGT) for cloning into the pET28a vector. Two PCRs were done in parallel.

Table 8.5: Reaction mix of PCR.

ddH_2O	13.6 µl
Phu HF buffer (5x) (Thermo scientific, USA)	4 µl
template DNA (1 ng/µl)	1 µl
fwd primer mix (10 µM)	0.4 µl
rev primer mix (10 µM)	0.4 µl
dNTP mix (10 mM each) (Thermo scientific, USA)	0.4 µl
Phusion polymerase (Thermo scientific, USA)	0.2 µl

Table 8.6: Cycle steps in mutagenesis PCR.

step	cycles	temp.[°C]	time
initial denaturation	1	98	30''
denaturation	30	98	10''
annealing		58	30''
extension		72	3'
final extension	1	72	10'
hold		4	∞

Digestion with restriction endonucleases

The PCR product as well as the target vector pET28a was digested with the restriction endonucleases BamHI and HindII for 70 minutes at 37°C. To the vector digestion, 1 µL of FastAP Themosensitive Alkaline Phosphatase (1 U/µl) was added and again incubated at 37°C for 15 minutes.

Table 8.7: Reaction mix of restriction digestion.

	PCR product	vector
DNA	2 x 20 µl	16 µl (1 µg)
FastDigest™ buffer (10x)	5 µl	2
BamHI enzyme (10 U/µl)	1 µl	1
HindII enzyme (10U/µl)	1 µl	1
ddH_2O	3 µl	-

DNA purification

DNA fragments were purified by agarose gel electrophoresis (1% agarose in TAE buffer) at 120 V in 1x TAE buffer for 20 minutes. The samples were mixed with MidoriGreen Direct before loading, for visualization purposes. GeneRuler 1kb Plus DNA Ladder was used as size marker. The target DNA bands were excised from the agarose gel with a clean scalpel and purified with a GeneJET™ Gel Extraction Kit according to the manufacturer's protocol, but was eluted with 20µl ddH_2O contrary to the included elution buffer.

DNA ligation

The Ligation between vector and PCR product was done with T4 DNA ligase (Thermo Scientific USA) and the T4 Buffer (Thermo Scientific USA). The vector to insert ration was

either 1:5 or 1:10 and was calculated according to length of both DNA parts and their respective concentration. The reation mixture was incubated at 16 °C for 16 hours and directly transformed into competent DH5α cells.

Table 8.8: Reaction mix of Ligation.

vector DNA	50 – 100 ng
insert DNA	variable
T4 buffer (10x) (Thermo scientific, USA)	2 µl
T4 DNA ligase (Thermo scientific USA)	1 µl
ddH_2O	adjust to 20 µl

Clones were picked and cultured over night in LB_{Kana} at 37°C; 180 rpm and DNA was isolated with a GeneJET Plasmid Miniprep Kit (Thermo Scientific, USA) according to manufacturer's protocol, but again elution was done in 30 µl ddH_2O. DNA concentration was determined by Nanodrop and send to sequencing. DNA was stored at -20°C.

Protein expression and purification

Finally His-BCL9 (243 – 469) was expressed in *E.coli* BL21 (DE3) with LB medium including 100 µg/ml kanamycin. Cells were grown at 37°C at 180 rpm until OD_{600} reached 0.7 followed by induction with 0.5 mM IPTG and expression at 18°C at 180 rpm for 16 hours.
The cells were harvested by centrifugation at 4000 g for 15 minutes at 4°C. Cell lysis was carried out in Dulbecco's PBS with a sonicator at 30% for six minutes. Finally debris was centrifugation at 27000 g for 20 minutes. His-BCL9 (243 – 469) purified *via* a nickel affinity column. Elution was performed in PBS with 500 mM Imidazole. Elution fractions containing the wanted protein were combined and further purified with a Superdex 75 10/300 GL column on a ÄKTA FPLC system. The product fractions were combined and concentrated with a Vivaspin 20 filter unit (MWCO 10 kDa) then shock frozen and stored at -80°C.

8.4.4 CD measurement

The peptides were measured in 10% acetonitrile in water at a pH of 7.4 and at a concentration of 50 µM. Peptide concentration was determined by BCA assay using a Pierce™ BCA Protein Assay Kit.

8.4.5 Cellular uptake experiments

All cell uptake experiments were carried out with HeLa (ATCC CCL-2) cells cultured in Dulbecco's MEM medium supplemented with 10% FBS and 1% Penicillin Streptomycin. 70 000 cells were seeded in an uncoated glass bottom 8-well µ-slide (Ibidi) 24 hours prior to treatment. The cellular uptake was carried out by gently washing cells three times with DMEM without FBS. The FAM labeled peptides which were solved in DMSO (1 mM stock solution), were added to the medium after the final wash. The cells were incubated for at 37°C in a 5% CO_2 atmosphere for two hours. Then the cells were gently washed with 25 mM HEPES in Dulbecco's MEM supplemented with 10% FKS and cells were rested for 30 minutes at 37°C. The cell nucleus was stained with Hoechst 33342 and cells imaged with a Zeiss 710 confocal microscope. Each uptake experiment was repeated at least three times.

8.4.6 Homogenous time resolved fluorescence assay (HTRF)

The HTRF assay was carried out by Andreas Oder in the FMP screening unit. Betacatenin-GST (3.75 nM) was first mixed with the peptides at different peptide concentrations in PBS with 0.05% Tween 20, followed by addition of BCL9-His (62,5 nM), Anti-GST-Tb (1:200) and Streptavidin-XL665 (1:200) in PBS with 0.05% Tween 20. After mixing on a plate shaker for 15 seconds at 1500 rpm the plate was incubated for one hour at room temperature. The plate was read on an Envision plate reader and data plotted using the prism software. Positive control wells were a mixture of both proteins and both fluorophores. Negative control wells were deprived of betacatenin.

8.5 Diazo-functionalized CPPs for bioreversible esterification of proteins

8.5.1 Peptide synthesis

Synthesis of c(R10)-amine (47)

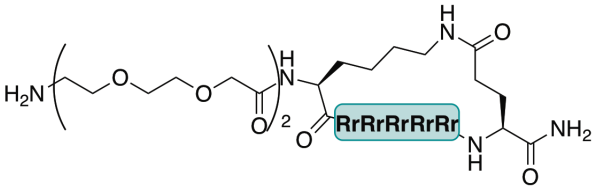

The c(R10) was synthesized in a 0.1 mmol scale on a Rink Amide Resin with a loading of 0.78mm/g. The synthesis was carried out on a PTI synthesizer with double couplings of each amino acid (5 eq. amino acid for 40 min) in DMF. After the final building block coupling the peptide, still Fmoc protected, was treated with $Pd(PPh_3)_4$ (24 mg, 20 µmol, 20 mol%) and phenylsilane (308 µl, 2.5 mmol, 2.5 eq.) in 4 ml dry CH_2Cl_2 for one hour in order to cleave the alloc and allyl protecting groups in one step. After confirmation of full deprotection by test cleavage, cyclization with 2 eq. HATU 4 eq. DIPEA was carried out over night in DMF.

The peptide was then Fmoc-deprotected using 20% piperidine in DMF and the peptide was cleaved from the resin by treatment with 4ml of a TFA:TIS:H_2O (95:2.5:2.5) for three hours and precipitated in cold diethylether. The crude peptide was purified by preparative reverse phase C18 HPLC (0-5 min 95/5, water (0.1%TFA)/MeCN (0.1%TFA); 5-60 min 10/90, water (0.1%TFA)/MeCN (0.1%TFA)).

The product was gained as white powder (18 mg, 5.5 µmol, 5.5 % yield) and analyzed by UPLC (method B; rt.: 3.03 min).

LRMS: m/z: 704.08 $[M+3H]^{3+}$ (calcd. m/z: 703.44).

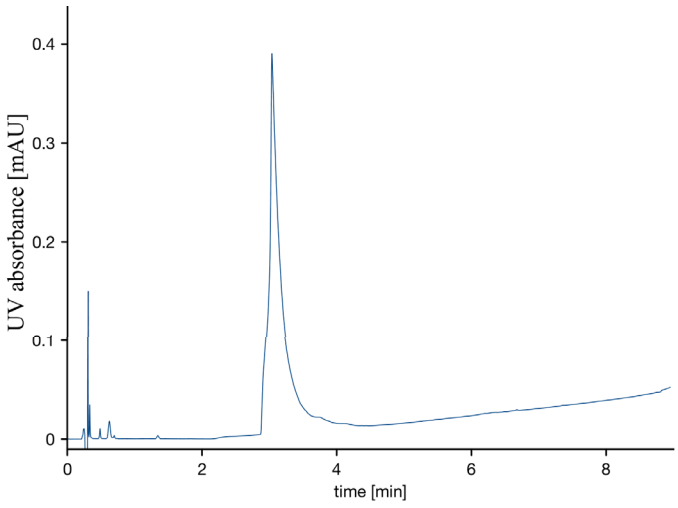

Figure 8.40: LC-UV trace of **47**.

Diazo-c(R10) synthesis (48)

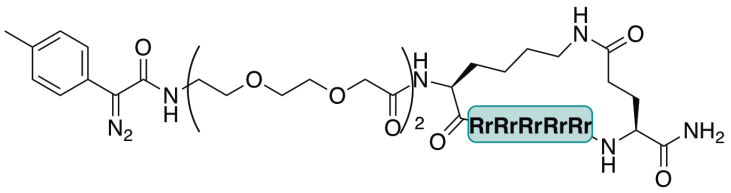

The purified c(R10) (9 mg, 2.8 µmol) and the NHS-diazo building block (1.5 eq.) were solved in 300µl DMF and DIPEA was added (1.5 eq.). The reaction mixture was shaken for four hours and then precipitated in ether.

The product was gained as white powder (8.2 mg, 2.4 µmol, 85.7 % yield, >90% purity) and analyzed by UPLC (method A; rt.: 2.09 min).

LRMS: m/z: 753.44 $[M+3H]^{3+}$ (calcd. m/z: 752.79).

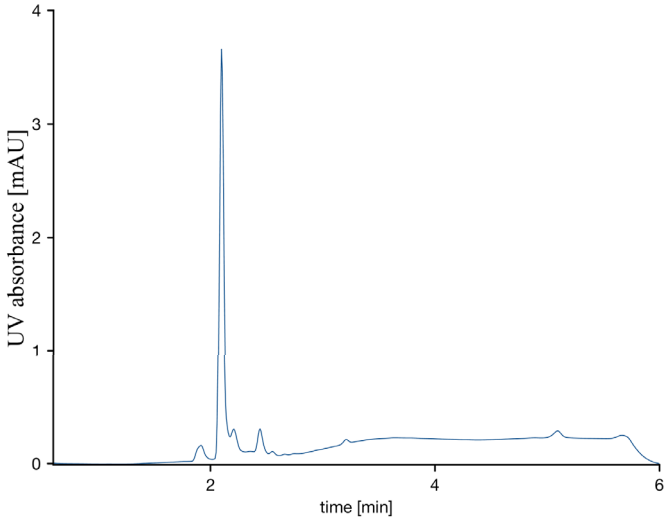

Figure 8.41: LC-UV trace of **48**.

Synthesis of c(Tat)-azide (52a)

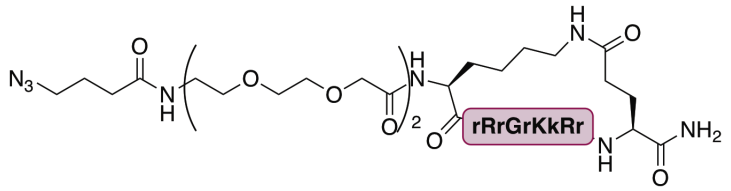

The c(Tat) was synthesized in a 0.1 mmol scale on a Rink Amide Resin with a loading of 0.78 mm/g. The synthesis was carried out on a PTI synthesizer with single couplings of each amino acid (10 eq. amino acid for 40 min) in DMF. After the final building block coupling the peptide, still Fmoc protected, was treated with $Pd(PPh_3)_4$ (24 mg, 20 µmol, 20 mol%) and phenylsilane (308 µl, 2.5 mmol, 2.5 eq.) in 4 ml dry CH_2Cl_2 for 1 hour in order to cleave the alloc and allyl protecting groups in one step. After confirmation of full deprotection by test cleavage, cyclization with 2eq. HATU 4 eq. DIPEA was carried out over night in DMF. After

Fmoc deprotection with 20% piperidine in DMF, azidobutanoic acid (129 mg, 1mmol, 10eq.) was coupled to the *N*-terminus with HATU (390 mg, 1 mmol, 10 eq.) and DIPEA (170µl, 1 mmol, 10 eq.) in DMF for two hours. The peptide was finally cleaved with 4ml of a TFA:TIS:H_2O mixture (95:2.5:2.5) for two hours. After precipitation in ether the crude peptide was purified by HPLC (0-5 min 95/5, water (0.1%TFA)/MeCN (0.1%TFA); 5-60 min 10/90, water (0.1%TFA)/MeCN (0.1%TFA)). The product was yielded as white powder (27.2 mg as TFA-salt, 10.5 µmol, 10.5% yield) and analyzed by UPLC (method A; rt.: 1.87 min).
HRMS: m/z: 636.6921 $[M+3H]^{3+}$ (calc. m/z: 636.7288).

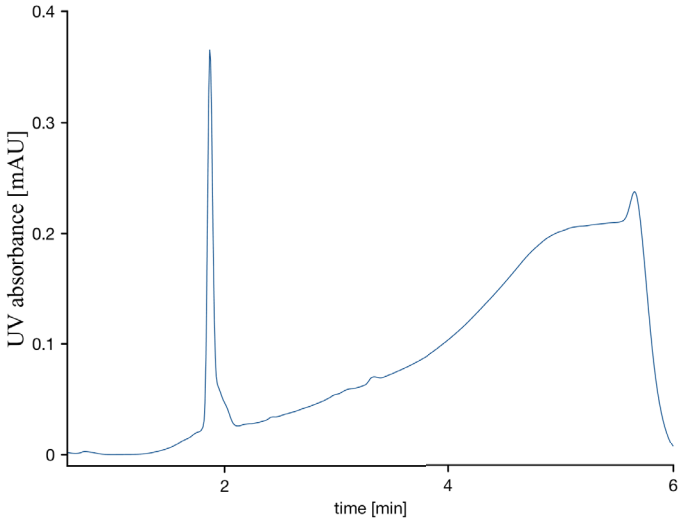

Figure 8.42: UPLC-UV chromatogram of **52a**.

Synthesis of c(R10)-Cy3-azide (52b)

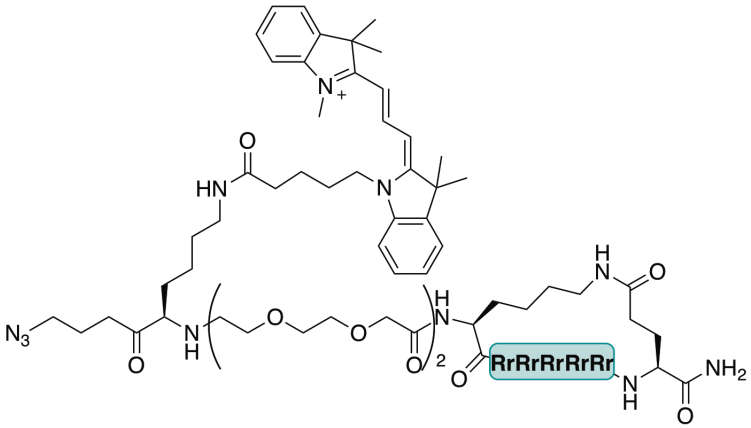

The c(R10) was synthesized in a 0.1 mmol scale on a Rink Amide Resin with a loading of 0.78 mm/g. The synthesis was carried out on a PTI synthesizer with double couplings of each amino acid (5 eq. amino acid for 40 min) in DMF. After the final building block coupling the peptide, still Fmoc protected, was treated with $Pd(PPh_3)_4$ (24 mg, 20 µmol, 20 mol%) and phenylsilane (308 µl, 2.5 mmol, 2.5 eq.) in 4 ml dry CH_2Cl_2 for 1 hour in order to cleave the alloc and allyl protecting groups in one step. After confirmation of full deprotection by test cleavage, cyclization with 2eq. HATU 4 eq. DIPEA was carried out over night in DMF.

The peptide was then Fmoc-deprotected using 20% piperidine in DMF and Fmoc-Lys(dde)-OH was coupled to the *N*-terminus in a standard peptide coupling. After dde removal with 3% hydrazine in DMF (3 x 3min), the Cy3-COOH (1.5 eq) was coupled with HATU (1.5 eq) and DIPEA (3 eq.) for six hours. After final Fmoc deprotection the peptide was finally coupled with 4-azidobutanioc acid (5 eq.), HATU (5 eq.) and DIPEA (10 eq.) and afterwards cleaved from the resin by treatment with 4ml of a TFA:TIS:H_2O (95:2.5:2.5) for 3 hours and precipitated in cold diethylether. The crude peptide was purified by preparative reverse phase C18 HPLC (0-5 min 95/5, water (0.1%TFA)/MeCN (0.1%TFA); 5-60 min 10/90, water (0.1%TFA)/MeCN (0.1%TFA)), product gained as pink powder (20.0 mg as TFA-salt, 5.1 µmol, 5.1% yield) and analyzed by UPLC (method B; rt.: 6.58 min).
HRMS: m/z: 929.2254 $[M+3H]^{3+}$ (calc. m/z: 929.5803).

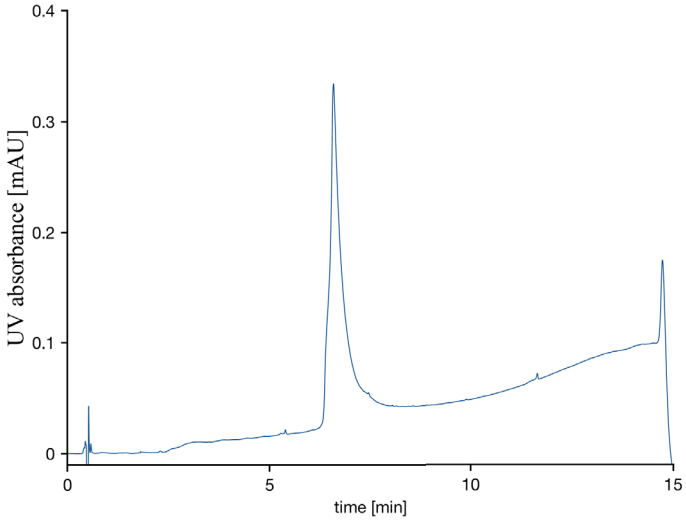

Figure 8.43: LC-UV trace of **52b**.

8.5.2 Esterification with eGFP C70M S143C

General procedure P6 of esterification with diazo-alkyne to generate 51

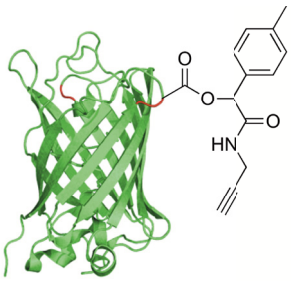

eGFP C70M S143C was rebuffered to 10 mM BisTris Buffer pH 5.8 at a concentration of 50 µM and the alkyne-diazo compound (varying amounts se table 4) in 1% DMF to buffer, was added. The reaction mixture was shaken at 37°C. After 2 – 16 hours (see table 4), the reaction mixture was desalted and rebuffered by a zebaspin column with a MWCO of 7kDa, which also could remove the left over diazo-alkyne. Analysis by MALDI-TOF showed successful alkyne esterification of differing degrees according to incubation time and amount of equivalents (see table 4).

Esterification and CuAAC with 52a to form 53a

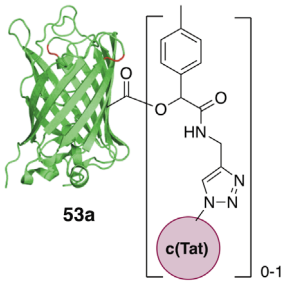

Esterification:

7 nmol eGFP C70M S143C were reacted with 30 equivalents of **50** according to general procedure **P6** for four hours. Analysis by MALDI showed a 1 – 5 fold esterification on GFP **51**.

MALDI TOF:

GFP-alkyne$_{n=1}$ expected Product (in Da): 27948 (M+); found (in Da): 27983 (M+);

GFP- alkyne $_{n=2}$ expected Product (in Da): 28133 (M+); found (in Da): 28170 (M+);

Δ to GFP-alkyne$_{n=1}$: 187 Da (expected 185 Da)

GFP-alkyne $_{n=3}$ expected Product (in Da): 28318 (M+); found (in Da): 28359 (M+);

Δ to to GFP-alkyne$_{n=2}$ 189 Da (expected 185 Da);

GFP-alkyne $_{n=4}$ expected Product (in Da): 28503 (M+); found (in Da): 28546 (M+);

Δ to to GFP-alkyne$_{n=3}$ 187 Da (expected 185 Da);

GFP-alkyne $_{n=5}$ expected Product (in Da): 28688 (M+); found (in Da): 28730 (M+);

Δ to to GFP-alkyne$_{n=4}$ 184 Da (expected 185 Da).

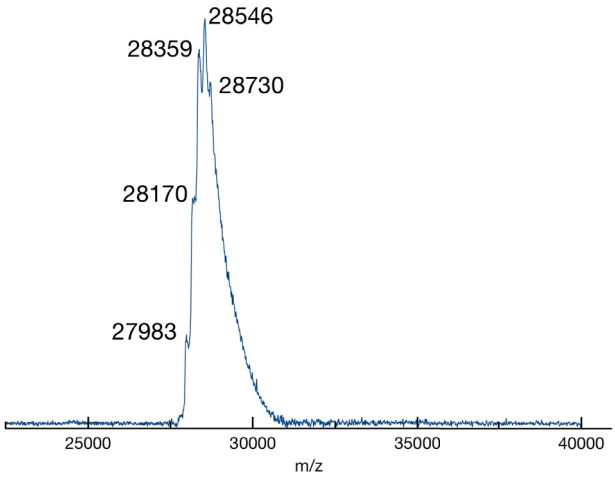

Figure 8.44: MALDI-TOF spectrum of **51** (also found in Figure 42B).

CuAAC:

To the alkyne-functionalized GFP **51** the azido-c(Tat) **52a** (25 eq.) , $CuSO_4$ (10 eq.) and THPTA (50 eq.) were added. The reaction was carried out in PBS supplemented with 10mM Aminoguanidin hydrochloride and 10 mM Sodium ascorbate. The GFP concentration in PBS was 27 µM. The reaction mixture was shaken at 37°C for 16 hours, purified by dialysis and analyzed by MALDI-TOF.

MALDI TOF: mixture of starting material **51** and one times modified **53.**

51: broad peak from 27900 – 28600 Da (from 1 - 5 alkynes)

53: broad peak from 29800 – 30700 Da (one peptide + free alkynes)

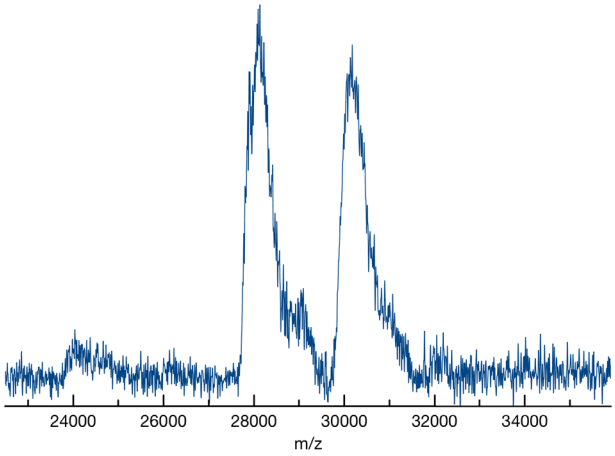

Figure 8.45: MALDI-TOF of **53a** (also found in Figure 42C).

Esterification and CuAAC with 52b to form 53b

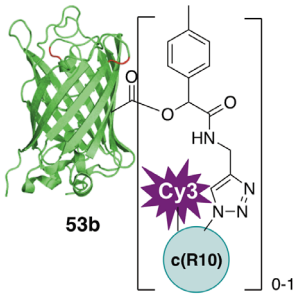

16.2 nmol eGFP C70M S143C were reacted with 20 equivalents of **50** according to general procedure **P6** for four hours. Analysis by MALDI showed mainly a 0 – 2 fold esterification on GFP **51**.

MALDI TOF:

GFP expected Product (in Da): 27764 (M+); found (in Da): 27802.6 (M+);

GFP-alkyne$_{n=1}$ expected Product (in Da): 27948 (M+); found (in Da): 27987.9 (M+);

Δ to GFP: 185.3 Da (expected 185 Da)

GFP- alkyne $_{n=2}$ expected Product (in Da): 28133 (M+); found (in Da): 28170 (M+);

Δ to GFP-alkyne$_{n=1}$: 184.4 Da (expected 185 Da)

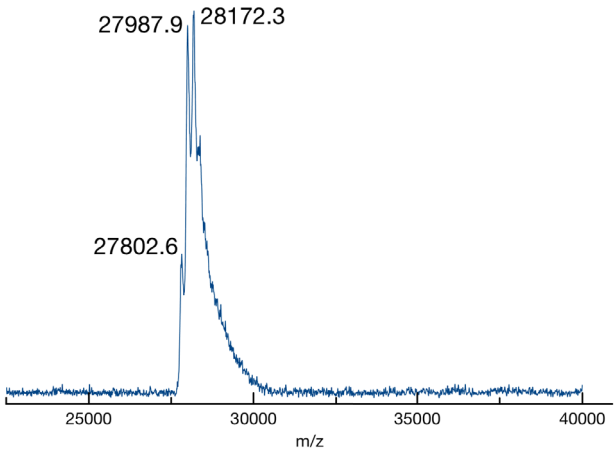

Figure 8.46: MALDI-TOF spectrum of **51** (also found in Figure 42B).

To the alkyne-functionalized GFP **51** the azido-c(Tat) **52b** (1.1 eq.) , $CuSO_4$ (10 eq.) and THPTA (50 eq.) were added. The reaction was carried out in PBS supplemented with 10mM Aminoguanidin hydrochloride and 10 mM Sodium ascorbate. The reaction mixture was shaken at 37°C for 16 hours, purified by size exclusion columns and analyzed by SDS-page. Here **53b** was shown to be gained as mixture consisting of **51** and mainly one peptide modified **53b.**

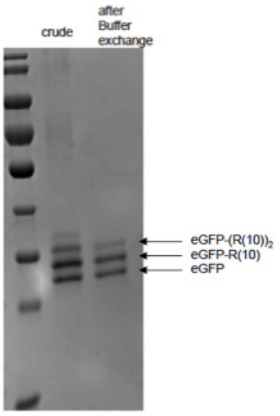

Figure 8.47: SDS-Gel of the reaction on formation of 53 (also found in Figure 42D).

Esterification with Diazo-cR10 (48)

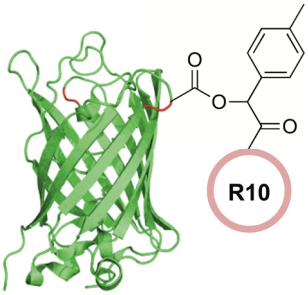

eGFP C70M S143C (18 nmol) was rebuffered to 300µl 10 mM BisTrisBuffer pH 6.5 (100 mM NaCl) and **48** (30 eq.) was added solved in 60µl of the same buffer. The reaction mixture was shaken at 37°C and excess peptide was removed after four hours by desalting with a zebaspin column with a MWCO of 7kDa. Analysis by MALDI-TOF showed a 0 – 2 fold modification of GFP with the cR10-peptide **53**.

MALDI TOF:

GFP expected Product (in Da): 27764 (M+); found (in Da): 27804.1(M+);

GFP-cR10$_{n=1}$ expected Product (in Da): 30001.4 (M+); found (in Da): 30041.4 (M+);

Δ to GFP: 2237.3 Da (expected 2239.4 Da)

GFP-cR10$_{n=2}$ expected Product (in Da): 32240.8 (M+); found (in Da): 32285.9 (M+);

Δ to GFP-cR10$_{n=1}$: 2244.5 Da (expected 2239.4 Da)

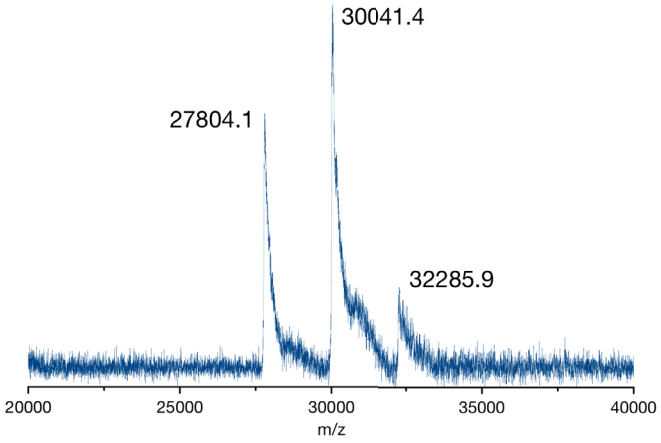

Figure 8.48: MALDI-TOF spectrum of eGFP-ester-cR10.

8.5.3 Cellular uptake experiments

All cell uptake experiments were carried out with HeLa (ATCC CCL-2) cells cultured in Dulbecco's MEM medium supplemented with 10% FBS and 1% Penicillin Streptomycin. 70 000 cells were seeded in an uncoated glass bottom 8-well µ-slide (Ibidi) 24 hours prior to treatment. The cellular uptake was carried out by gently washing cells three times with HEPES buffer pH 7.5 (5 mM HEPES, 140 mM NaCl, 2.5 mM KCl, 5 mM glycine). The peptide-protein conjugate buffered in the same HEPES buffer was added to the cells in 200 µl at respective concentration and incubated for at 37°C in a 5% CO_2 atmosphere. After one hour cells were gently washed with 25 mM HEPES in Dulbecco's MEM supplemented with 10% FKS and cells were rested for 30 minutes at 37°C. The cell nucleus was stained with Hoechst 33342 and cells imaged with a Zeiss 710 confocal microscope.

9 References

(1) Mathews, C. K.; Van Holde, K. E. *Biochemistry*; Benjamin/Cummings series in the life sciences and chemistry; Benjamin/Cummings Publishing Company, Incorporated, 1996.
(2) Bairoch, A. *Nucleic Acids Res.* **2000**, *28* (1), 304.
(3) Sear, R. P. *Phys. Biol.* **2004**, *1* (2), 53.
(4) Kaspar, A. A.; Reichert, J. M. *Drug Discov. Today* **2013**, *18* (17–18), 807.
(5) Fosgerau, K.; Hoffmann, T. *Drug Discov. Today* **2015**, *20* (1), 122.
(6) Behrendt, R.; White, P.; Offer, J. *J. Pept. Sci.* **2016**, *22* (1), 4.
(7) Schumacher, D.; Hackenberger, C. P. R. *Curr. Opin. Chem. Biol.* **2014**, *22*, 62.
(8) Gálvez, A. O.; Schaack, C. P.; Noda, H.; Bode, J. W. *J. Am. Chem. Soc.* **2017**, *139* (5), 1826.
(9) Lau, J. L.; Dunn, M. K. *Bioorg. Med. Chem.* **2018**, No. 26, 2700.
(10) Bodenner, D.; Redman, C.; Riggs, A. *Clin. Interv. Aging* **2007**, *2* (4), 499.
(11) Imam, S. K. In *Glucose Intake and Utilization in Pre-Diabetes and Diabetes*; 2018; 29–44.
(12) McGivern, J. G. *Neuropsychiatr. Dis. Treat.* **2007**, *3* (1), 69.
(13) Callaway, E. *Nature* **2017**, *550* (7675), 167.
(14) Smith, G. P.; Petrenko, V. A. *Chem. Rev.* **1997**, *97* (2), 391.
(15) Smith, G. P. *Science* **1985**, *228* (4705), 1315.
(16) Ng, S.; Tjhung, K. F.; Paschal, B. M.; Noren, C. J.; Derda, R. In *Peptide Libraries: Methods and Protocols.*; Derda, R., Ed.; Springer New York: New York, NY, 2015; 155–172.
(17) Krumpe, L. R. H.; Mori, T. *Expert Opin. Drug Discov.* **2007**, *2* (4), 525.
(18) Baeriswyl, V.; Calzavarini, S.; Gerschheimer, C.; Diderich, P.; Angelillo-Scherrer, A.; Heinis, C. *J. Med. Chem.* **2013**, *56* (9), 3742.
(19) Baeriswyl, V.; Calzavarini, S.; Chen, S.; Zorzi, A.; Bologna, L.; Angelillo-Scherrer, A.; Heinis, C. *ACS Chem. Biol.* **2015**, *10* (8), 1861.
(20) Deyle, K.; Kong, X.-D.; Heinis, C. *Acc. Chem. Res.* **2017**, *50* (8), 1866.
(21) Howell, S. M.; Fiacco, S. V; Takahashi, T. T.; Jalali-Yazdi, F.; Millward, S. W.; Hu, B.; Wang, P.; Roberts, R. W. *Sci. Rep.* **2014**, *4*, 6008.
(22) Song, X.; Lu, L.; Passioura, T.; Suga, H. *Org. Biomol. Chem.* **2017**, *15* (24), 5155.
(23) Jongkees, S. A. K.; Caner, S.; Tysoe, C.; Brayer, G. D.; Withers, S. G.; Suga, H. *Cell Chem. Biol.* **2017**, *24* (3), 381.
(24) Yu, H.; Dranchak, P.; Li, Z.; MacArthur, R.; Munson, M. S.; Mehzabeen, N.; Baird, N. J.; Battalie, K. P.; Ross, D.; Lovell, S.; Carlow, C. K. S.; Suga, H.; Inglese, J. *Nat. Commun.* **2017**, *8*, 14932.
(25) Kawamura, A.; Münzel, M.; Kojima, T.; Yapp, C.; Bhushan, B.; Goto, Y.; Tumber, A.; Katoh, T.; King, O. N. F.; Passioura, T.; Walport, L. J.; Hatch, S. B.; Madden, S.; Müller, S.; Brennan, P. E.; Chowdhury, R.; Hopkinson, R. J.; Suga, H.; Schofield, C. J. *Nat. Commun.* **2017**, *8*, 14773.
(26) Roberts, R. W.; Szostak, J. W. *Proc. Natl. Acad. Sci.* **1997**, *94* (23), 12297.
(27) Young, T. S.; Schultz, P. G. *J. Biol. Chem.* **2010**, *285* (15), 11039.
(28) Morimoto, J.; Hayashi, Y.; Iwasaki, K.; Suga, H. *Acc. Chem. Res.* **2011**, *44* (12), 1359.
(29) Hipolito, C. J.; Suga, H. *Curr. Opin. Chem. Biol.* **2012**, *16* (1), 196.
(30) Taub, R.; Gould, R. J.; Garsky, V. M.; Ciccarone, T. M.; Hoxie, J.; Friedman, P. A.; Shattil, S. J. *J. Biol. Chem.* **1989**, *264* (1), 259.
(31) Williams, W. V.; Kieber-Emmons, T.; VonFeldt, J.; Greene, M. I.; Weiner, D. B. *J. Biol. Chem.* **1991**, *266* (8), 5182.
(32) Levi, M.; Sällberg, M.; Rudén, U.; Herlyn, D.; Maruyama, H.; Wigzell, H.; Marks, J.; Wahren, B. *Proc. Natl. Acad. Sci. U. S. A.* **1993**, *90* (10), 4374.
(33) Memczak, H.; Lauster, D.; Kar, P.; Lella, S. Di. *PLoS One* **2016**, *11* (7), e0159074.
(34) Casset, F.; Roux, F.; Mouchet, P.; Bes, C.; Chardes, T.; Granier, C.; Mani, J. C.;

Pugnière, M.; Laune, D.; Pau, B.; Kaczorek, M.; Lahana, R.; Rees, A. *Biochem. Biophys. Res. Commun.* **2003**, *307* (1), 198.
(35) Lauster, D.; Pawolski, D.; Storm, J.; Ludwig, K.; Volkmer, R.; Memczak, H.; Herrmann, A.; Bhatia, S. *Beilstein J. Org. Chem.* **2015**, *11*, 589.
(36) Kadam, R. U.; Juraszek, J.; Brandenburg, B.; Buyck, C.; Schepens, W. B. G.; Kesteleyn, B.; Stoops, B.; Vreeken, R. J.; Vermond, J.; Goutier, W.; Tang, C.; Vogels, R.; Friesen, R. H. E.; Goudsmit, J.; Van Dongen, M. J. P.; Wilson, I. A. *Science* **2017**, *358* (6362), 496.
(37) Fischer, E.; Fourneau, E. *Berichte der Dtsch. Chem. Gesellschaft* **1901**, *34* (2), 2868.
(38) Bergmann, M.; Zervas, L. *Berichte der Dtsch. Chem. Gesellschaft* **1932**, *65* (7), 1192.
(39) Merrifield, R. B. *J. Am. Chem. Soc.* **1963**, *85* (14), 2149.
(40) Merrifield, R. B. *Angew. Chemie Int. Ed.* **1985**, *24* (10), 799.
(41) El-Faham, A.; Albericio, F. *Chem. Rev.* **2011**, *111* (11), 6557.
(42) Pedersen, S. L.; Tofteng, A. P.; Malik, L.; Jensen, K. J. *Chem. Soc. Rev.* **2012**, *41* (5), 1826.
(43) Pelay-Gimeno, M.; Glas, A.; Koch, O.; Grossmann, T. N. *Angew. Chemie Int. Ed.* **2015**, *54* (31), 8896.
(44) Bullock, B. N.; Jochim, A. L.; Arora, P. S. *J. Am. Chem. Soc.* **2011**, *133* (36), 14220.
(45) Walensky, L. D.; Bird, G. H. *J. Med. Chem.* **2014**, *57* (15), 6275.
(46) Felix, A. M.; Heimer, E. P.; Wang, C.-T.; Lambros, T. J.; Fournier, A.; Mowles, T. F.; Maines, S.; Campbell, R. M.; Wegrzynski, B.; Toome, V.; Fry, D.; Madison, V. S. *Int. J. Pept. Protein Res.* **1988**, *32* (6), 441.
(47) Harrison, R. S.; Shepherd, N. E.; Hoang, H. N.; Ruiz-Gómez, G.; Hill, T. A.; Driver, R. W.; Desai, V. S.; Young, P. R.; Abbenante, G.; Fairlie, D. P. *Proc. Natl. Acad. Sci.* **2010**, *107* (26), 11686.
(48) Shepherd, N. E.; Hoang, H. N.; Desai, V. S.; Letouze, E.; Young, P. R.; Fairlie, D. P. *J. Am. Chem. Soc.* **2006**, *128* (40), 13284.
(49) Shepherd, N. E.; Harrison, R. S.; Fairlie, D. P. *Curr. Drug Targets* **2012**, *13* (11), 1348.
(50) Harrison, R. S.; Ruiz-Gómez, G.; Hill, T. A.; Chow, S. Y.; Shepherd, N. E.; Lohman, R.-J.; Abbenante, G.; Hoang, H. N.; Fairlie, D. P. *J. Med. Chem.* **2010**, *53* (23), 8400.
(51) Shepherd, N. E.; Hoang, H. N.; Abbenante, G.; Fairlie, D. P. *J. Am. Chem. Soc.* **2005**, *127* (9), 2974.
(52) Hill, T. A.; Shepherd, N. E.; Diness, F.; Fairlie, D. P. *Angew. Chemie Int. Ed.* **2014**, *53* (48), 13020.
(53) Taylor, J. W. *Pept. Sci.* **2002**, *66* (1), 49.
(54) Phelan, J. C.; Skelton, N. J.; Braisted, A. C.; McDowell, R. S. *J. Am. Chem. Soc.* **1997**, *119* (3), 455.
(55) Galande, A. K.; Bramlett, K. S.; Trent, J. O.; Burris, T. P.; Wittliff, J. L.; Spatola, A. F. *ChemBioChem* **2005**, *6* (11), 1991.
(56) Bracken, C.; Gulyas, J.; Taylor, J. W.; Baum, J. *J. Am. Chem. Soc.* **1994**, *116* (14), 6431.
(57) Yang, B.; Liu, D.; Huang, Z. *Bioorg. Med. Chem. Lett.* **2004**, *14* (6), 1403.
(58) Jackson, D. Y.; King, D. S.; Chmielewski, J.; Singh, S.; Schultz, P. G. *J. Am. Chem. Soc.* **1991**, *113* (24), 9391.
(59) Leduc, A.-M.; Trent, J. O.; Wittliff, J. L.; Bramlett, K. S.; Briggs, S. L.; Chirgadze, N. Y.; Wang, Y.; Burris, T. P.; Spatola, A. F. *Proc. Natl. Acad. Sci.* **2003**, *100* (20), 11273.
(60) Chen, X.-H.; Xiang, Z.; Hu, Y. S.; Lacey, V. K.; Cang, H.; Wang, L. *ACS Chem. Biol.* **2014**, *9* (9), 1956.
(61) Galande, A. K.; Bramlett, K. S.; Burris, T. P.; Wittliff, J. L.; Spatola, A. F. *J. Pept. Res.* **2004**, *63* (3), 297.
(62) Schafmeister, C. E.; Po, J.; Verdine, G. L. *J. Am. Chem. Soc.* **2000**, *122* (24), 5891.
(63) Blackwell, H. E.; Grubbs, R. H. *Angew. Chemie Int. Ed.* **1998**, *37* (23), 3281.
(64) Kim, Y.-W.; Kutchukian, P. S.; Verdine, G. L. *Org. Lett.* **2010**, *12* (13), 3046.

(65) Shim, S. Y.; Kim, Y.-W.; Verdine, G. L. *Chem. Biol. Drug Des.* **2013**, *82* (6), 635.
(66) Hilinski, G. J.; Kim, Y.-W.; Hong, J.; Kutchukian, P. S.; Crenshaw, C. M.; Berkovitch, S. S.; Chang, A.; Ham, S.; Verdine, G. L. *J. Am. Chem. Soc.* **2014**, *136* (35), 12314.
(67) Walensky, L. D.; Kung, A. L.; Escher, I.; Malia, T. J.; Barbuto, S.; Wright, R. D.; Wagner, G.; Verdine, G. L.; Korsmeyer, S. J. *Science* **2004**, *305* (5689), 1466.
(68) Cromm, P. M.; Schaubach, S.; Spiegel, J.; Fürstner, A.; Grossmann, T. N.; Waldmann, H. *Nat. Commun.* **2016**, *7*, 4.
(69) Kawamoto, S. A.; Coleska, A.; Ran, X.; Yi, H.; Yang, C.-Y.; Wang, S. *J. Med. Chem.* **2012**, *55* (3), 1137.
(70) Cantel, S.; Le Chevalier Isaad, A.; Scrima, M.; Levy, J. J.; DiMarchi, R. D.; Rovero, P.; Halperin, J. A.; D'Ursi, A. M.; Papini, A. M.; Chorev, M. *J. Org. Chem.* **2008**, *73* (15), 5663.
(71) Haney, C. M.; Horne, W. S. *Chem. – A Eur. J.* **2013**, *19* (34), 11342.
(72) Lau, Y. H.; de Andrade, P.; Wu, Y.; Spring, D. R. *Chem. Soc. Rev.* **2015**, *44* (1), 91.
(73) Kumita, J. R.; Smart, O. S.; Woolley, G. A. *Proc. Natl. Acad. Sci.* **2000**, *97* (8), 3803.
(74) Nevola, L.; Martín-Quirós, A.; Eckelt, K.; Camarero, N.; Tosi, S.; Llobet, A.; Giralt, E.; Gorostiza, P. *Angew. Chemie Int. Ed.* **2013**, *52* (30), 7704.
(75) Lau, Y. H.; de Andrade, P.; Quah, S.-T.; Rossmann, M.; Laraia, L.; Skold, N.; Sum, T. J.; Rowling, P. J. E.; Joseph, T. L.; Verma, C.; Hyvonen, M.; Itzhaki, L. S.; Venkitaraman, A. R.; Brown, C. J.; Lane, D. P.; Spring, D. R. *Chem. Sci.* **2014**, *5* (5), 1804.
(76) Fujimoto, K.; Kajino, M.; Inouye, M. *Chem. – A Eur. J.* **2008**, *14* (3), 857.
(77) Jo, H.; Meinhardt, N.; Wu, Y.; Kulkarni, S.; Hu, X.; Low, K. E.; Davies, P. L.; DeGrado, W. F.; Greenbaum, D. C. *J. Am. Chem. Soc.* **2012**, *134* (42), 17704.
(78) Spokoyny, A. M.; Zou, Y.; Ling, J. J.; Yu, H.; Lin, Y.-S.; Pentelute, B. L. *J. Am. Chem. Soc.* **2013**, *135* (16), 5946.
(79) Chu, Q.; Moellering, R. E.; Hilinski, G. J.; Kim, Y.-W.; Grossmann, T. N.; Yeh, J. T.-H.; Verdine, G. L. *Medchemcomm* **2015**, *6* (1), 111.
(80) Bird, G. H.; Mazzola, E.; Opoku-Nsiah, K.; Lammert, M. A.; Godes, M.; Neuberg, D. S.; Walensky, L. D. *Nat. Chem. Biol.* **2016**, *12* (10), 845.
(81) Okamoto, T.; Zobel, K.; Fedorova, A.; Quan, C.; Yang, H.; Fairbrother, W. J.; Huang, D. C. S.; Smith, B. J.; Deshayes, K.; Czabotar, P. E. *ACS Chem. Biol.* **2013**, *8* (2), 297.
(82) Okamoto, T.; Segal, D.; Zobel, K.; Fedorova, A.; Yang, H.; Fairbrother, W. J.; Huang, D. C. S.; Smith, B. J.; Deshayes, K.; Czabotar, P. E. *ACS Chem. Biol.* **2014**, *9* (3), 838.
(83) Tian, Y.; Jiang, Y.; Li, J.; Wang, D.; Zhao, H.; Li, Z. *ChemBioChem* **2017**, *18* (21), 2087.
(84) Stanzl, E. G.; Trantow, B. M.; Vargas, J. R.; Wender, P. A. *Acc. Chem. Res.* **2013**, *46* (12), 2944.
(85) Frankel, A. D.; Pabo, C. O. *Cell* **1988**, *55* (6), 1189.
(86) Green, M.; Loewenstein, P. M. *Cell* **1988**, *55* (6), 1179.
(87) Fawell, S.; Seery, J.; Daikh, Y.; Moore, C.; Chen, L. L.; Pepinsky, B.; Barsoum, J. *Proc. Natl. Acad. Sci.* **1994**, *91* (2), 664.
(88) Brooks, H.; Lebleu, B.; Vivès, E. *Adv. Drug Deliv. Rev.* **2005**, *57* (4), 559.
(89) Schwarze, S. R.; Ho, A.; Vocero-Akbani, A.; Dowdy, S. F. *Science* **1999**, *285* (5433), 1569.
(90) Vivès, E.; Brodin, P.; Lebleu, B. *J. Biol. Chem.* **1997**, *272* (25), 16010.
(91) Zhu, M.; Nie, G.; Meng, H.; Xia, T.; Nel, A.; Zhao, Y. *Acc. Chem. Res.* **2013**, *46* (3), 622.
(92) Rothbard, J. B.; Garlington, S.; Lin, Q.; Kirschberg, T.; Kreider, E.; McGrane, P. L.; Wender, P. A.; Khavari, P. A. *Nat. Med.* **2000**, *6*, 1253.
(93) Wender, P. A.; Mitchell, D. J.; Pattabiraman, K.; Pelkey, E. T.; Steinman, L.; Rothbard, J. B. *Proc. Natl. Acad. Sci.* **2000**, *97* (24), 13003.
(94) Futaki, S.; Suzuki, T.; Ohashi, W.; Yagami, T.; Tanaka, S.; Ueda, K.; Sugiura, Y. *J.*

Biol. Chem. **2001**, *276* (8), 5836.
(95) Vives, E.; Richard, J.-P.; Lebleu, C. R. and B. *Curr. Protein Pept. Sci.* **2003**, *4* (2), 125.
(96) Wadia, J. S.; Stan, R. V; Dowdy, S. F. *Nat. Med.* **2004**, *10*, 310.
(97) Richard, J. P.; Melikov, K.; Vives, E.; Ramos, C.; Verbeure, B.; Gait, M. J.; Chernomordik, L. V; Lebleu, B. *J. Biol. Chem.* **2003**, *278* (1), 585.
(98) Fittipaldi, A.; Ferrari, A.; Zoppé, M.; Arcangeli, C.; Pellegrini, V.; Beltram, F.; Giacca, M. *J. Biol. Chem.* **2003**, *278* (36), 34141.
(99) Ferrari, A.; Pellegrini, V.; Arcangeli, C.; Fittipaldi, A.; Giacca, M.; Beltram, F. *Mol. Ther.* **2003**, *8* (2), 284.
(100) Ziegler, A.; Nervi, P.; Dürrenberger, M.; Seelig, J. *Biochemistry* **2005**, *44* (1), 138.
(101) Tünnemann, G.; Martin, R. M.; Haupt, S.; Patsch, C.; Edenhofer, F.; Cardoso, M. C. *FASEB J.* **2006**, *20* (11), 1775.
(102) Lee, H.-L.; Dubikovskaya, E. A.; Hwang, H.; Semyonov, A. N.; Wang, H.; Jones, L. R.; Twieg, R. J.; Moerner, W. E.; Wender, P. A. *J. Am. Chem. Soc.* **2008**, *130* (29), 9364.
(103) Ter-Avetisyan, G.; Tünnemann, G.; Nowak, D.; Nitschke, M.; Herrmann, A.; Drab, M.; Cardoso, M. C. *J. Biol. Chem.* **2009**, *284* (6), 3370.
(104) Jiao, C.-Y.; Delaroche, D.; Burlina, F.; Alves, I. D.; Chassaing, G.; Sagan, S. *J. Biol. Chem.* **2009**, *284* (49), 33957.
(105) Duchardt, F.; Fotin-Mleczek, M.; Schwarz, H.; Fischer, R.; Brock, R. *Traffic* **2007**, *8* (7), 848.
(106) Brock, R. *Bioconjug. Chem.* **2014**, *25* (5), 863.
(107) Rothbard, J. B.; Jessop, T. C.; Lewis, R. S.; Murray, B. A.; Wender, P. A. *J. Am. Chem. Soc.* **2004**, *126* (31), 9506.
(108) Herce, H. D.; Garcia, A. E. *Proc. Natl. Acad. Sci. U. S. A.* **2007**, *104* (52), 20805.
(109) Herce, H. D.; Garcia, A. E.; Litt, J.; Kane, R. S.; Martin, P.; Enrique, N.; Rebolledo, A.; Milesi, V. *Biophys. J.* **2009**, *97* (7), 1917.
(110) Herce, H. D.; Garcia, A. E.; Cardoso, M. C. *J. Am. Chem. Soc.* **2014**, *136* (50), 17459.
(111) Mishra, A.; Gordon, V. D.; Yang, L.; Coridan, R.; Wong, G. C. L. *Angew. Chemie Int. Ed.* **2008**, *47* (16), 2986.
(112) Chérine, B.; Sandrine, S. *FEBS Lett.* **2013**, *587* (12), 1693.
(113) Perret, F.; Nishihara, M.; Takeuchi, T.; Futaki, S.; Lazar, A. N.; Coleman, A. W.; Sakai, N.; Matile, S. *J. Am. Chem. Soc.* **2005**, *127* (4), 1114.
(114) Sakai, N.; Takeuchi, T.; Futaki, S.; Matile, S. *ChemBioChem* **2005**, *6* (1), 114.
(115) Takeuchi, T.; Kosuge, M.; Tadokoro, A.; Sugiura, Y.; Nishi, M.; Kawata, M.; Sakai, N.; Matile, S.; Futaki, S. *ACS Chem. Biol.* **2006**, *1* (5), 299.
(116) Pujals, S.; Miyamae, H.; Afonin, S.; Murayama, T.; Hirose, H.; Nakase, I.; Taniuchi, K.; Umeda, M.; Sakamoto, K.; Ulrich, A. S.; Futaki, S. *ACS Chem. Biol.* **2013**, *8* (9), 1894.
(117) Murayama, T.; Masuda, T.; Afonin, S.; Kawano, K.; Takatani-Nakase, T.; Ida, H.; Takahashi, Y.; Fukuma, T.; Ulrich, A. S.; Futaki, S. *Angew. Chemie Int. Ed.* **2017**, *56* (26), 7644.
(118) Lättig-Tünnemann, G.; Prinz, M.; Hoffmann, D.; Behlke, J.; Palm-Apergi, C.; Morano, I.; Herce, H. D.; Cardoso, M. C. *Nat. Commun.* **2011**, *2*, 453.
(119) Rothbard, J. B.; Kreider, E.; VanDeusen, C. L.; Wright, L.; Wylie, B. L.; Wender, P. A. *J. Med. Chem.* **2002**, *45* (17), 3612.
(120) Nagel, Y. A.; Raschle, P. S.; Wennemers, H. *Angew. Chemie Int. Ed.* **2017**, *56* (1), 122.
(121) Nischan, N.; Herce, H. D.; Natale, F.; Bohlke, N.; Budisa, N.; Cardoso, M. C.; Hackenberger, C. P. R. *Angew. Chemie Int. Ed.* **2015**, *54* (6), 1950.
(122) Herce, H. D.; Schumacher, D.; Schneider, A. F. L.; Ludwig, A. K.; Mann, F. A.; Fillies, M.; Kasper, M.-A.; Reinke, S.; Krause, E.; Leonhardt, H.; Cardoso, M. C.; Hackenberger, C. P. R. *Nat. Chem.* **2017**, *9*, 762.
(123) Koniev, O.; Wagner, A. *Chem. Soc. Rev.* **2015**, *44* (15), 5495.
(124) Lang, K.; Chin, J. W. *ACS Chem. Biol.* **2014**, *9* (1), 16.

(125) Sletten, E. M.; Bertozzi, C. R. *Angew. Chemie - Int. Ed.* **2009**, *48* (38), 6974.
(126) Brotzel, F.; Mayr, H. *Org. Biomol. Chem.* **2007**, *5* (23), 3814.
(127) D., C. P. M. S.; L., B. G. J.; P., G. P. M. *Angew. Chemie Int. Ed.* **2014**, *53* (40), 10585.
(128) Gilis, D.; Massar, S.; Cerf, N. J.; Rooman, M. *Genome Biol.* **2001**, *2* (11), research0049.1.
(129) Jackson, D. Y. *Org. Process Res. Dev.* **2016**, *20* (5), 852.
(130) Goddard, D. R.; Michaelis, L. *J. Biol. Chem.* **1935**, *112* (6), 361.
(131) Floyd, N.; Vijayakrishnan, B.; Koeppe, J. R.; Davis, B. G. *Angew. Chemie Int. Ed.* **2009**, *48* (42), 7798.
(132) Steiner, M.; Hartmann, I.; Perrino, E.; Casi, G.; Brighton, S.; Jelesarov, I.; Bernardes, G. J. L.; Neri, D. *Chem. Sci.* **2013**, *4* (1), 297.
(133) Saito, F.; Noda, H.; Bode, J. W. *ACS Chem. Biol.* **2015**, *10* (4), 1026.
(134) Shen, B.-Q.; Xu, K.; Liu, L.; Raab, H.; Bhakta, S.; Kenrick, M.; Parsons-Reponte, K. L.; Tien, J.; Yu, S.-F.; Mai, E.; Li, D.; Tibbitts, J.; Baudys, J.; Saad, O. M.; Scales, S. J.; McDonald, P. J.; Hass, P. E.; Eigenbrot, C.; Nguyen, T.; Solis, W. A.; Fuji, R. N.; Flagella, K. M.; Patel, D.; Spencer, S. D.; Khawli, L. A.; Ebens, A.; Wong, W. L.; Vandlen, R.; Kaur, S.; Sliwkowski, M. X.; Scheller, R. H.; Polakis, P.; Junutula, J. R. *Nat. Biotechnol.* **2012**, *30*, 184.
(135) Kalia, D.; Malekar, P. V; Parthasarathy, M. *Angew. Chemie Int. Ed.* **2016**, *55* (4), 1432.
(136) Lyon, R. P.; Setter, J. R.; Bovee, T. D.; Doronina, S. O.; Hunter, J. H.; Anderson, M. E.; Balasubramanian, C. L.; Duniho, S. M.; Leiske, C. I.; Li, F.; Senter, P. D. *Nat. Biotechnol.* **2014**, *32*, 1059.
(137) Kalia, D.; Pawar, S. P.; Thopate, J. S. *Angew. Chemie Int. Ed.* **2017**, *56* (7), 1885.
(138) Jones, M. W.; Strickland, R. A.; Schumacher, F. F.; Caddick, S.; Baker, J. R.; Gibson, M. I.; Haddleton, D. M. *J. Am. Chem. Soc.* **2012**, *134* (3), 1847.
(139) Schumacher, F. F.; Nunes, J. P. M.; Maruani, A.; Chudasama, V.; Smith, M. E. B.; Chester, K. A.; Baker, J. R.; Caddick, S. *Org. Biomol. Chem.* **2014**, *12* (37), 7261.
(140) Jongkees, S. A. K.; Umemoto, S.; Suga, H. *Chem. Sci.* **2017**, *8* (2), 1474.
(141) Maruani, A.; Smith, M. E. B.; Miranda, E.; Chester, K. A.; Chudasama, V.; Caddick, S. *Nat. Commun.* **2015**, *6*, 6645.
(142) Morais, M.; Nunes, J. P. M.; Karu, K.; Forte, N.; Benni, I.; Smith, M. E. B.; Caddick, S.; Chudasama, V.; Baker, J. R. *Org. Biomol. Chem.* **2017**, *15* (14), 2947.
(143) Chalker, J. M.; Gunnoo, S. B.; Boutureira, O.; Gerstberger, S. C.; Fernandez-Gonzalez, M.; Bernardes, G. J. L.; Griffin, L.; Hailu, H.; Schofield, C. J.; Davis, B. G. *Chem. Sci.* **2011**, *2* (9), 1666.
(144) Bernardes, G. J. L.; Chalker, J. M.; Errey, J. C.; Davis, B. G. *J. Am. Chem. Soc.* **2008**, *130* (15), 5052.
(145) Chalker, J. M.; Lercher, L.; Rose, N. R.; Schofield, C. J.; Davis, B. G. *Angew. Chemie Int. Ed.* **2012**, *51* (8), 1835.
(146) Rowan, F. C.; Richards, M.; Bibby, R. A.; Thompson, A.; Bayliss, R.; Blagg, J. *ACS Chem. Biol.* **2013**, *8* (10), 2184.
(147) Nathani, R. I.; Moody, P.; Chudasama, V.; Smith, M. E. B.; Fitzmaurice, R. J.; Caddick, S. *Chem. Sci.* **2013**, *4* (9), 3455.
(148) Vinogradova, E. V; Zhang, C.; Spokoyny, A. M.; Pentelute, B. L.; Buchwald, S. L. *Nature* **2015**, *526*, 687.
(149) Kubota, K.; Dai, P.; Pentelute, B. L.; Buchwald, S. L. *J. Am. Chem. Soc.* **2018**, *140* (8), 3128.
(150) Hoare, D. G.; Koshland, D. E. *J. Am. Chem. Soc.* **1966**, *88* (9), 2057.
(151) Hoare, D. G.; Koshland, D. E. *J. Biol. Chem.* **1967**, *242* (10), 2447.
(152) McGrath, N. A.; Andersen, K. A.; Davis, A. K. F.; Lomax, J. E.; Raines, R. T. *Chem. Sci.* **2015**, *6* (1), 752.
(153) Doscher, M. S.; Wilcox, P. E. *J. Biol. Chem.* **1961**, *236* (5), 1328.
(154) Mix, K. A.; Aronoff, M. R.; Raines, R. T. *ACS Chem. Biol.* **2016**, *11* (12), 3233.

(155) Mix, K. A.; Raines, R. T. *Org. Lett.* **2015**, *17* (10), 2358.
(156) Mix, K. A.; Lomax, J. E.; Raines, R. T. *J. Am. Chem. Soc.* **2017**, *139* (41), 14396.
(157) Roberts, J. D.; Watanabe, W.; McMahon, R. E. *J. Am. Chem. Soc.* **1951**, *73* (2), 760.
(158) Prescher, J. A.; Bertozzi, C. R. *Nat. Chem. Biol.* **2005**, *1* (1), 13.
(159) Xie, J.; Schultz, P. G. *Nat. Rev. Mol. Cell Biol.* **2006**, *7*, 775.
(160) Davis, L.; Chin, J. W. *Nat. Rev. Mol. Cell Biol.* **2012**, *13*, 168.
(161) Lang, K.; Chin, J. W. *ACS Chem. Biol.* **2014**, *9* (1), 16.
(162) Michael, A. *J. für Prakt. Chemie* **1893**, *48* (1), 94.
(163) Huisgen, R. *Angew. Chem.* **1963**, *13* (1938), 604.
(164) Rostovtsev, V. V.; Green, L. G.; Fokin, V. V.; Sharpless, K. B. *Angew. Chemie - Int. Ed.* **2002**, *41* (14), 2596.
(165) Tornøe, C. W.; Christensen, C.; Meldal, M. *J. Org. Chem.* **2002**, *67* (9), 3057.
(166) Himo, F.; Lovell, T.; Hilgraf, R.; Rostovtsev, V. V.; Noodleman, L.; Sharpless, K. B.; Fokin, V. V. *J. Am. Chem. Soc.* **2005**, *127* (1), 210.
(167) Chan, T. R.; Hilgraf, R.; Sharpless, K. B.; Fokin, V. V. *Org. Lett.* **2004**, *6* (17), 2853.
(168) Hong, V.; Presolski, S. I.; Ma, C.; Finn, M. G. *Angew. Chemie Int. Ed.* **2009**, *48* (52), 9879.
(169) Besanceney-Webler, C.; Jiang, H.; Zheng, T.; Feng, L.; del Amo, D.; Wang, W.; Klivansky, L. M.; Marlow, F. L.; Liu, Y.; Wu, P. *Angew. Chemie Int. Ed.* **2011**, *50* (35), 8051.
(170) Li, S.; Wang, L.; Yu, F.; Zhu, Z.; Shobaki, D.; Chen, H.; Wang, M.; Wang, J.; Qin, G.; Erasquin, U. J.; Ren, L.; Wang, Y.; Cai, C. *Chem. Sci.* **2017**, *8* (3), 2107.
(171) Chen, Z.; Meng, H.; Xing, G.; Chen, C.; Zhao, Y.; Jia, G.; Wang, T.; Yuan, H.; Ye, C.; Zhao, F.; Chai, Z.; Zhu, C.; Fang, X.; Ma, B.; Wan, L. *Toxicol. Lett.* **2006**, *163* (2), 109.
(172) Shin, J.-A.; Oh, S.-J.; Lee, H.-Y.; Lim, Y.-G. *Catal. Sci. Technol.* **2017**, *7* (12), 2450.
(173) Worrell, B. T.; Malik, J. A.; Fokin, V. V. *Science* **2013**, *340* (6131), 457.
(174) Wittig, G.; Krebs, A. *Chem. Ber.* **1961**, *94* (12), 3260.
(175) Agard, N. J.; Prescher, J. A.; Bertozzi, C. R. *J. Am. Chem. Soc.* **2004**, *126* (46), 15046.
(176) Baskin, J. M.; Prescher, J. A.; Laughlin, S. T.; Agard, N. J.; Chang, P. V; Miller, I. A.; Lo, A.; Codelli, J. A.; Bertozzi, C. R. *Proc. Natl. Acad. Sci.* **2007**, *104* (43), 16793.
(177) Ning, X.; Guo, J.; Wolfert, M. A.; Boons, G.-J. *Angew. Chemie Int. Ed.* **2008**, *47* (12), 2253.
(178) Debets, M. F.; van Berkel, S. S.; Schoffelen, S.; Rutjes, F. P. J. T.; van Hest, J. C. M.; van Delft, F. L. *Chem. Commun.* **2010**, *46* (1), 97.
(179) Dommerholt, J.; Schmidt, S.; Temming, R.; Hendriks, L. J. A.; Rutjes, F. P. J. T.; van Hest, J. C. M.; Lefeber, D. J.; Friedl, P.; van Delft, F. L. *Angew. Chemie Int. Ed.* **2010**, *49* (49), 9422.
(180) van Geel, R.; Pruijn, G. J. M.; van Delft, F. L.; Boelens, W. C. *Bioconjug. Chem.* **2012**, *23* (3), 392.
(181) Ning, X.; Temming, R. P.; Dommerholt, J.; Guo, J.; Ania, D. B.; Debets, M. F.; Wolfert, M. A.; Boons, G. J.; Van Delft, F. L. *Angew. Chemie Int. Ed.* **2010**, *49* (17), 3065.
(182) McKay, C. S.; Moran, J.; Pezacki, J. P. *Chem. Commun.* **2010**, *46* (6), 931.
(183) Colombo, M.; Sommaruga, S.; Mazzucchelli, S.; Polito, L.; Verderio, P.; Galeffi, P.; Corsi, F.; Tortora, P.; Prosperi, D. *Angew. Chemie Int. Ed.* **2012**, *51* (2), 496.
(184) Temming, R. P.; Eggermont, L.; van Eldijk, M. B.; van Hest, J. C. M.; van Delft, F. L. *Org. Biomol. Chem.* **2013**, *11* (17), 2772.
(185) McKay, C. S.; Blake, J. A.; Cheng, J.; Danielson, D. C.; Pezacki, J. P. *Chem. Commun.* **2011**, *47* (36), 10040.
(186) Huisgen, R. *Proc. Chem. Soc.* **1961**, No. O, 357.
(187) Moran, J.; McKay, C. S.; Pezacki, J. P. *Can. J. Chem.* **2011**, *89* (2), 148.
(188) McGrath, N. A.; Raines, R. T. *Chem. Sci.* **2012**, *3* (11), 3237.
(189) Aronoff, M. R.; Gold, B.; Raines, R. T. *Org. Lett.* **2016**, *18* (7), 1538.

(190) Gold, B.; Aronoff, M. R.; Raines, R. T. *Org. Lett.* **2016**, *18* (18), 4466.
(191) Gold, B.; Aronoff, M. R.; Raines, R. T. *J. Org. Chem.* **2016**, *81* (14), 5998.
(192) Aronoff, M. R.; Gold, B.; Raines, R. T. *Tetrahedron Lett.* **2016**, *57* (22), 2347.
(193) Andersen, K. A.; Aronoff, M. R.; McGrath, N. A.; Raines, R. T. *J. Am. Chem. Soc.* **2015**, *137* (7), 2412.
(194) Blackman, M. L.; Royzen, M.; Fox, J. M. *J. Am. Chem. Soc.* **2008**, *130* (41), 13518.
(195) Devaraj, N. K.; Weissleder, R.; Hilderbrand, S. A. *Bioconjug. Chem.* **2008**, *19* (12), 2297.
(196) Oliveira, B. L.; Guo, Z.; Bernardes, G. J. L. *Chem. Soc. Rev.* **2017**, *46* (16), 4895.
(197) Lang, K.; Davis, L.; Wallace, S.; Mahesh, M.; Cox, D. J.; Blackman, M. L.; Fox, J. M.; Chin, J. W. *J. Am. Chem. Soc.* **2012**, *134* (25), 10317.
(198) Plass, T.; Milles, S.; Koehler, C.; Szymański, J.; Mueller, R.; Wießler, M.; Schultz, C.; Lemke, E. A. *Angew. Chemie Int. Ed.* **2012**, *51* (17), 4166.
(199) Seitchik, J. L.; Peeler, J. C.; Taylor, M. T.; Blackman, M. L.; Rhoads, T. W.; Cooley, R. B.; Refakis, C.; Fox, J. M.; Mehl, R. A. *J. Am. Chem. Soc.* **2012**, *134* (6), 2898.
(200) Devaraj, N. K.; Hilderbrand, S.; Upadhyay, R.; Mazitschek, R.; Weissleder, R. *Angew. Chem. Int. Ed.* **2010**, *49* (16), 2869.
(201) Elliott, T. S.; Townsley, F. M.; Bianco, A.; Ernst, R. J.; Sachdeva, A.; Elsässer, S. J.; Davis, L.; Lang, K.; Pisa, R.; Greiss, S.; Lilley, K. S.; Chin, J. W. *Nat. Biotechnol.* **2014**, *32* (5), 465.
(202) Billaud, E. M. F.; Shahbazali, E.; Ahamed, M.; Cleeren, F.; Noël, T.; Koole, M.; Verbruggen, A.; Hessel, V.; Bormans, G. *Chem. Sci.* **2017**, *8* (2), 1251.
(203) Houghton, J. L.; Membreno, R.; Abdel-Atti, D.; Cunanan, K. M.; Carlin, S.; Scholz, W. W.; Zanzonico, P. B.; Lewis, J. S.; Zeglis, B. M. *Mol. Cancer Ther.* **2017**, *16* (1), 124.
(204) Staudinger, H.; Meyer, J. *Helv. Chim. Acta* **1919**, *2* (1), 612.
(205) Bertozzi, C. R.; Saxon, E. *Science* **2000**, *287* (2000), 2007.
(206) Lin, F. L.; Hoyt, H. M.; van Halbeek, H.; Bergman, R. G.; Bertozzi, C. R. *J. Am. Chem. Soc.* **2005**, *127* (8), 2686.
(207) Saxon, E.; Armstrong, J. I.; Bertozzi, C. R. *Org. Lett.* **2000**, *2* (14), 2141.
(208) Nilsson, B. L.; Kiessling, L. L.; Raines, R. T. *Org. Lett.* **2000**, *2* (13), 1939.
(209) Merkx, R.; Rijkers, D. T. S.; Kemmink, J.; Liskamp, R. M. J. *Tetrahedron Lett.* **2003**, *44* (24), 4515.
(210) Nilsson, B. L.; Kiessling, L. L.; Raines, R. T. *Org. Lett.* **2001**, *3* (1), 9.
(211) Soellner, M. B.; Nilsson, B. L.; Raines, R. T. *J. Org. Chem.* **2002**, *67* (14), 4993.
(212) Soellner, M. B.; Tam, A.; Raines, R. T. *J. Org. Chem.* **2006**, *71* (26), 9824.
(213) Tam, A.; Soellner, M. B.; Raines, R. T. *Org. Biomol. Chem.* **2008**, *6* (7), 1173.
(214) Tam, A.; Soellner, M. B.; Raines, R. T. *J. Am. Chem. Soc.* **2007**, *129* (37), 11421.
(215) Tam, A.; Raines, R. T. *Bioorg. Med. Chem.* **2009**, *17* (3), 1055.
(216) Kleineweischede, R.; Hackenberger, C. P. R. *Angew. Chemie Int. Ed.* **2008**, *47* (32), 5984.
(217) Mühlberg, M.; Jaradat, D. M. M.; Kleineweischede, R.; Papp, I.; Dechtrirat, D.; Muth, S.; Broncel, M.; Hackenberger, C. P. R. *Bioorg. Med. Chem.* **2010**, *18* (11), 3679.
(218) Lemieux, G. A.; de Graffenried, C. L.; Bertozzi, C. R. *J. Am. Chem. Soc.* **2003**, *125* (16), 4708.
(219) Hangauer, M. J.; Bertozzi, C. R. *Angew. Chem. Int. Ed. Engl.* **2008**, *47* (13), 2394.
(220) Serwa, R.; Wakening, L.; Signore, G. Del; Mühlberg, M.; Claußnitzer, I.; Weise, C.; Gerrits, M.; Hackenberger, C. P. R. *Angew. Chemie Int. Ed.* **2009**, *48* (44), 8234.
(221) Bertran-Vicente, J.; Serwa, R. A.; Schümann, M.; Schmieder, P.; Krause, E.; Hackenberger, C. P. R. *J. Am. Chem. Soc.* **2014**, *136* (39), 13622.
(222) Serwa, R.; Majkut, P.; Horstmann, B.; Swiecicki, J.-M.; Gerrits, M.; Krause, E.; Hackenberger, C. P. R. *Chem. Sci.* **2010**, *1* (5), 596.
(223) Nischan, N.; Chakrabarti, A.; Serwa, R. A.; Bovee-Geurts, P. H. M.; Brock, R.; Hackenberger, C. P. R. *Angew. Chemie Int. Ed.* **2013**, *52* (45), 11920.

(224) Nischan, N.; Kasper, M.-A.; Mathew, T.; Hackenberger, C. P. R. *Org. Biomol. Chem.* **2016**, *14* (31), 7500.
(225) Böhrsch, V.; Serwa, R.; Majkut, P.; Krause, E.; Hackenberger, C. P. R. *Chem. Commun.* **2010**, *46* (18), 3176.
(226) Jaradat, D. M. M.; Hamouda, H.; Hackenberger, C. P. R. *European J. Org. Chem.* **2010**, *2010* (26), 5004.
(227) Bohrsch, V.; Mathew, T.; Zieringer, M.; Vallee, M. R. J.; Artner, L. M.; Dernedde, J.; Haag, R.; Hackenberger, C. P. R. *Org. Biomol. Chem.* **2012**, *10* (30), 6211.
(228) Chaturvedi, R. K.; Pletcher, T. C.; Zioudrou, C.; Schmir, G. L. *Tetrahedron Lett.* **1970**, *11* (49), 4339.
(229) Gololobov, Y. G.; Kasukhin, L. F. *Tetrahedron* **1992**, *48* (8), 1353.
(230) Vallée, M. R. J.; Majkut, P.; Wilkening, I.; Weise, C.; Müller, G.; Hackenberger, C. P. R. *Org. Lett.* **2011**, *13* (20), 5440.
(231) Vallée, M. R. J.; Artner, L. M.; Dernedde, J.; Hackenberger, C. P. R. *Angew. Chemie - Int. Ed.* **2013**, *52* (36), 9504.
(232) Vallée, M. R. J.; Majkut, P.; Krause, D.; Gerrits, M.; Hackenberger, C. P. R. *Chemistry* **2015**, *21* (3), 970.
(233) Siebertz, K. D.; Hackenberger, C. P. R. *Chem. Commun.* **2018**, *54* (7), 763.
(234) Russell, R. J.; Kerry, P. S.; Stevens, D. J.; Steinhauer, D. A.; Martin, S. R.; Gamblin, S. J.; Skehel, J. J. *Proc. Natl. Acad. Sci. U. S. A.* **2008**, *105* (46), 17736.
(235) Weis, W.; Brown, J. H.; Cusack, S.; Paulson, J. C.; Skehel, J. J.; Wiley, D. C. *Nature* **1988**, *333* (6172), 426.
(236) Mammen, M.; Choi, S. K.; Whitesides, G. M. *Angew. Chemie - Int. Ed.* **1998**, *37* (20), 2754.
(237) Fasting, C.; Schalley, C. A.; Weber, M.; Seitz, O.; Hecht, S.; Koksch, B.; Dernedde, J.; Graf, C.; Knapp, E. W.; Haag, R. *Angew. Chemie Int. Ed.* **2012**, *51* (42), 10472.
(238) Kingery-Wood, J. E.; Williams, K. W.; Sigal, G. B.; Whitesides, G. M. *J. Am. Chem. Soc.* **1992**, *114* (18), 7303.
(239) Mammen, M.; Dahmann, G.; Whitesides, G. M. *J. Med. Chem.* **1995**, *38* (21), 4179.
(240) Sigal, G. B.; Mammen, M.; Dahmann, G.; Whitesides, G. M. *J. Am. Chem. Soc.* **1996**, *118* (16), 3789.
(241) Papp, I.; Sieben, C.; Sisson, A. L.; Kostka, J.; Böttcher, C.; Ludwig, K.; Herrmann, A.; Haag, R. *ChemBioChem* **2011**, *12* (6), 887.
(242) Haldar, J.; Cienfuegos, L. *Pharm.* **2010**, *27* (2), 259.
(243) Roy, R.; Zanini, D.; Meunier, S. J.; Romanowska, A. *J. Chem. Soc. Chem. Commun.* **1993**, 1869.
(244) Nazemi, A.; Haeryfar, S. M. M.; Gillies, E. R. *Langmuir* **2013**, *29*, 6420.
(245) Hidari, K. I. P. J.; Murata, T.; Takahashi, Y.; Minamijima, Y.; Miwa, Y.; Adachi, S.; Ogata, M.; Usui, T.; Suzuki, Y.; Suzuki, T. **2008**, *18* (10), 779.
(246) Ogata, M.; Umemura, S.; Sugiyama, N.; Kuwano, N.; Kadokawa, J.; Usui, T. *Carbohydr. Polym.* **2016**, *153*, 96.
(247) Hendricks, G. L.; Weirich, K. L.; Viswanathan, K.; Li, J.; Shriver, Z. H.; Ashour, J.; Ploegh, H. L.; Kurt-jones, E. A.; Fygenson, D. K.; Finberg, R. W.; Comolli, J. C.; Wang, J. P. *J. Biol. Chem.* **2013**, *288* (12), 8061.
(248) Wang, H.; Huang, W.; Orwenyo, J.; Banerjee, A.; Vasta, G. R.; Wang, L. X. *Bioorganic Med. Chem.* **2013**, *21* (7), 2037.
(249) Papp, I.; Sieben, C.; Ludwig, K.; Roskamp, M.; Böttcher, C.; Schlecht, S.; Herrmann, A.; Haag, R. *Small* **2010**, *6* (24), 2900.
(250) Reuter, J. D.; Myc, A.; Hayes, M. M.; Gan, Z.; Roy, R.; Qin, D.; Yin, R.; Piehler, L. T.; Esfand, R.; Tomalia, D. A.; Baker, J. R. *Bioconjugate Chem.* **1999**, *10*, 271.
(251) Mangan, D.; Snyder, S. *Br. J. Ind. Med.* **1978**, *35*, 305.
(252) Carlescu, I.; Scutaru, D.; Popa, M.; Uglea, C. V. U. *Med. Chem. Res.* **2009**, *18*, 477.
(253) Gambaryan, A. S.; Tuzikov, A. B.; Chinarev, A. A.; Juneja, L. R.; Bovin, N. V;

Matrosovich, M. N. *Antiviral Res.* **2002**, *55*, 201.
(254) Matsubara, T.; Onishi, A.; Saito, T.; Shimada, A.; Inoue, H.; Taki, T.; Nagata, K.; Okahata, Y.; Sato, T. *J. Med. Chem.* **2010**, *53* (11), 4441.
(255) Jones, J. C.; Turpin, E. A.; Bultmann, H.; Brandt, C. R.; Schultz-Cherry, S. *J. Virol.* **2006**, *80* (24), 11960.
(256) Hüttl, C.; Hettrich, C.; Miller, R.; Paulke, B.-R.; Henklein, P.; Rawel, H.; Bier, F. F. *BMC Biotechnol.* **2013**, *13*, 51.
(257) Hatano, K.; Matsubara, T.; Muramatsu, Y.; Ezure, M.; Koyama, T.; Matsuoka, K.; Kuriyama, R.; Kori, H.; Sato, T. *J. Med. Chem.* **2014**, *57* (20), 8332.
(258) Lauster, D.; Glanz, M.; Bardua, M.; Ludwig, K.; Hellmund, M.; Hoffmann, U.; Hamann, A.; Böttcher, C.; Haag, R.; Hackenberger, C. P. R.; Hermann, A. *Angew. Chemie Int. Ed.* **2017**, *56* (21), 5931.
(259) Kwon, S.; Na, D. H.; Kwak, J. H.; Douaisi, M.; Zhang, F.; Park, E. J.; Park, J.; Youn, H.; Song, C.; Kane, R. S.; Dordick, J. S.; Lee, K. B.; Linhardt, R. J. *Nat. Nanotechnol.* **2016**, No. October, 2.
(260) Vonnemann, J.; Liese, S.; Kuehne, C.; Ludwig, K.; Dernedde, J.; Bo, C.; Netz, R. R.; Haag, R. *J. Am. Chem. Soc.* **2015**, *137*, 2572.
(261) Kapp, T. G.; Rechenmacher, F.; Sobahi, T. R.; Kessler, H. *Expert Opin. Ther. Pat.* **2013**, *23* (10), 1273.
(262) Schumacher, D. **2017** *Site-specific functionalization of antigen binding proteins for cellular delivery, imaging anf target modulation* (Doctoral dissertation)
(263) McCusker, C. F.; Kocienski, P. J.; Boyle, F. T.; Schätzlein, A. G. *Bioorg. Med. Chem. Lett.* **2002**, *12* (4), 547.
(264) Logan, C. Y.; Nusse, R. *Annu. Rev. Cell Dev. Biol.* **2004**, *20* (1), 781.
(265) Clevers, H. *Cell* **2006**, *127* (3), 469.
(266) Klaus, A.; Birchmeier, W. *Nat. Rev. Cancer* **2008**, *8*, 387.
(267) Valenta, T.; Hausmann, G.; Basler, K. *EMBO J.* **2012**, *31* (12), 2714.
(268) Mani, M.; Carrasco, D. E.; Zhang, Y.; Takada, K.; Gatt, M. E.; Dutta-Simmons, J.; Ikeda, H.; Diaz-Griffero, F.; Pena-Cruz, V.; Bertagnolli, M.; Myeroff, L. L.; Markowitz, S. D.; Anderson, K. C.; Carrasco, D. R. *Cancer Res.* **2009**, *69* (19), 7577.
(269) Takada, K.; Zhu, D.; Bird, G. H.; Sukhdeo, K.; Zhao, J.-J.; Mani, M.; Lemieux, M.; Carrasco, D. E.; Ryan, J.; Horst, D.; Fulciniti, M.; Munshi, N. C.; Xu, W.; Kung, A. L.; Shivdasani, R. A.; Walensky, L. D.; Carrasco, D. R. *Sci. Transl. Med.* **2012**, *4* (148), 148ra117.
(270) Ina, W.; Giuseppe, del S.; Wiebke, A.; R., H. C. P. *Synthesis* **2011**, *17*, 2709.
(271) Sakagami, K.; Masuda, T.; Kawano, K.; Futaki, S. *Mol. Pharm.* **2018**, *15* (3), 1332.
(272) Pfaff, M.; Tangemann, K.; Müller, B.; Gurrath, M.; Müller, G.; Kessler, H.; Timpl, R.; Engel, J. *J. Biol. Chem.* **1994**, *269* (32), 20233.
(273) Roller, S.; Zhou, H.; Haag, R. *Mol. Divers.* **2005**, *9*, 305.
(274) Staedtler, A. M.; Hellmund, M.; Mehrabadi, F. S.; Thota, B. N. S.; Zollner, T. M.; Koch, M.; Haag, R.; Schmidt, N.; Schmidt, N.; Haag, R. **2015**.

10 Appendix

NMR spectra

PeB-Series

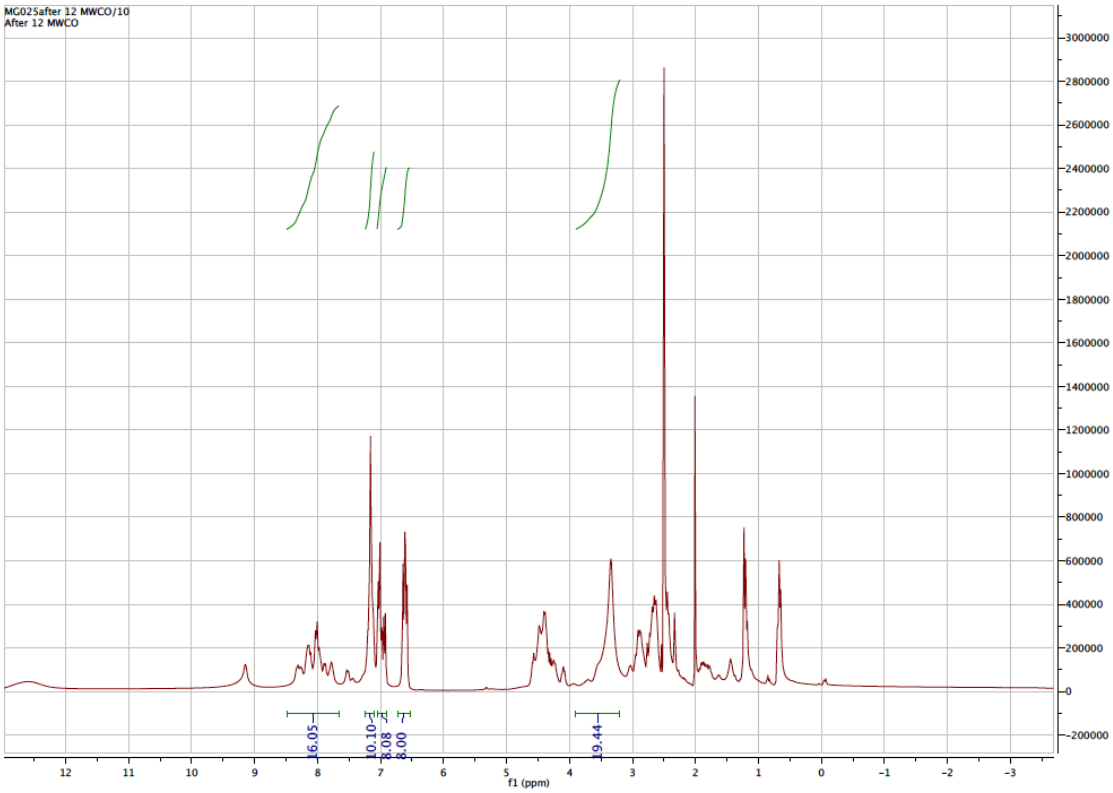

Figure 10.1. ^{1}H-NMR spectra of PG_8PeB_{26} **3b**.

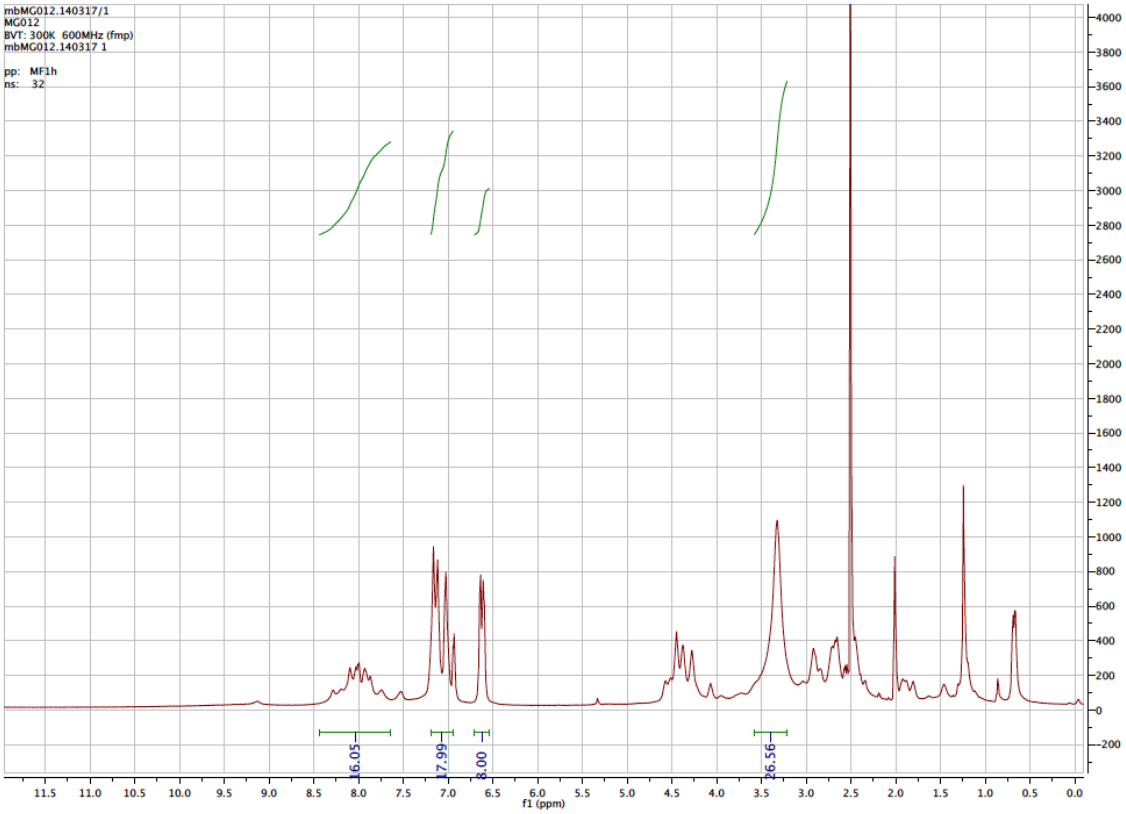

Figure 10.2. ^{1}H-NMR spectra of $PG_{14}PeB_{19}$ **4b**

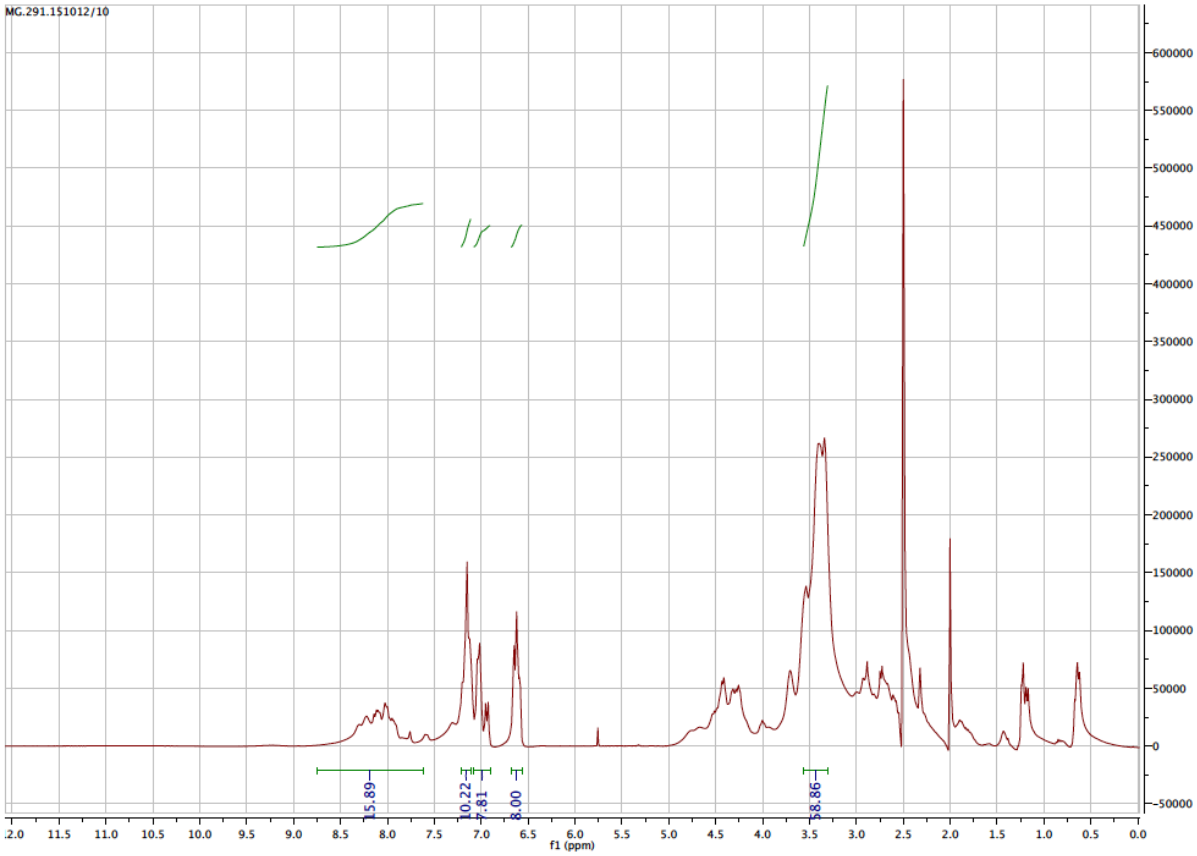

Figure 10.3. ^{1}H-NMR spectra of $PG_{100}PeB_{8}$ **5b**.

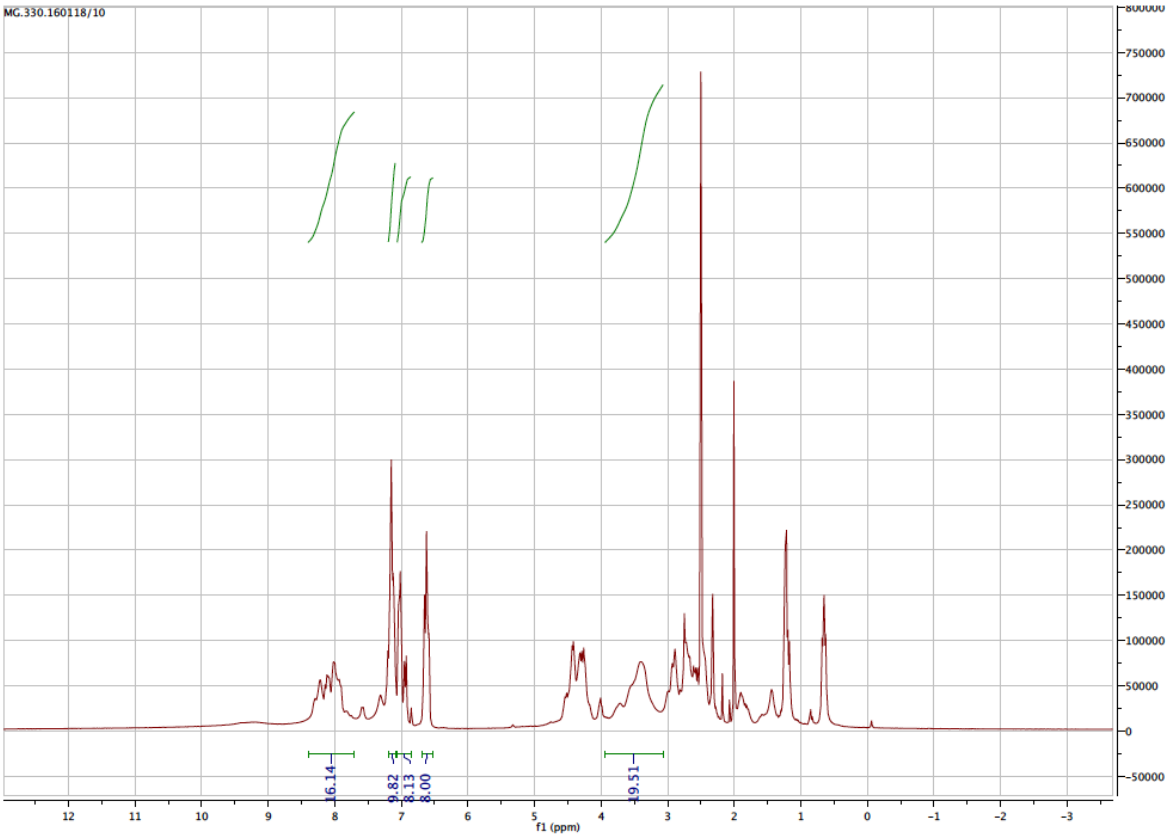

Figure 10.4. ^{1}H-NMR spectra of $PG_{100}PeB_{21}$ **5c**.

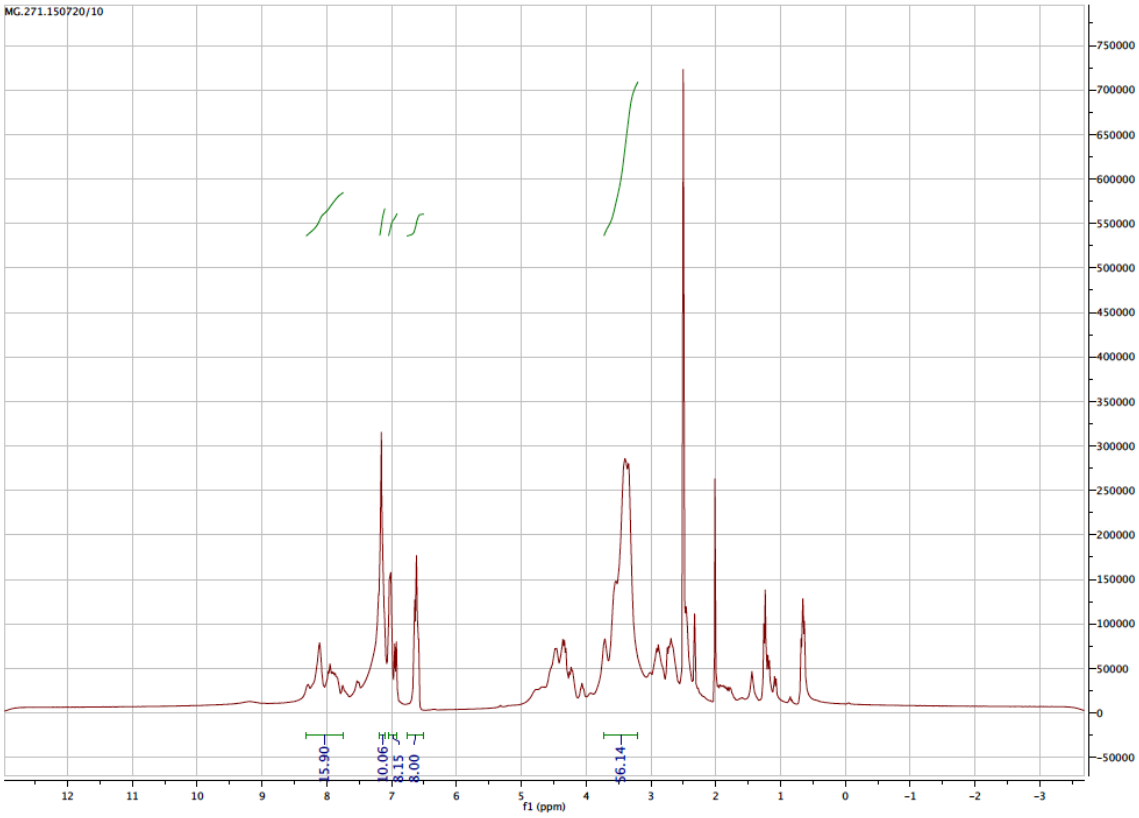

Figure 10.5. ^{1}H-NMR spectra of $PG_{340}PeB_{9}$ **6b**.

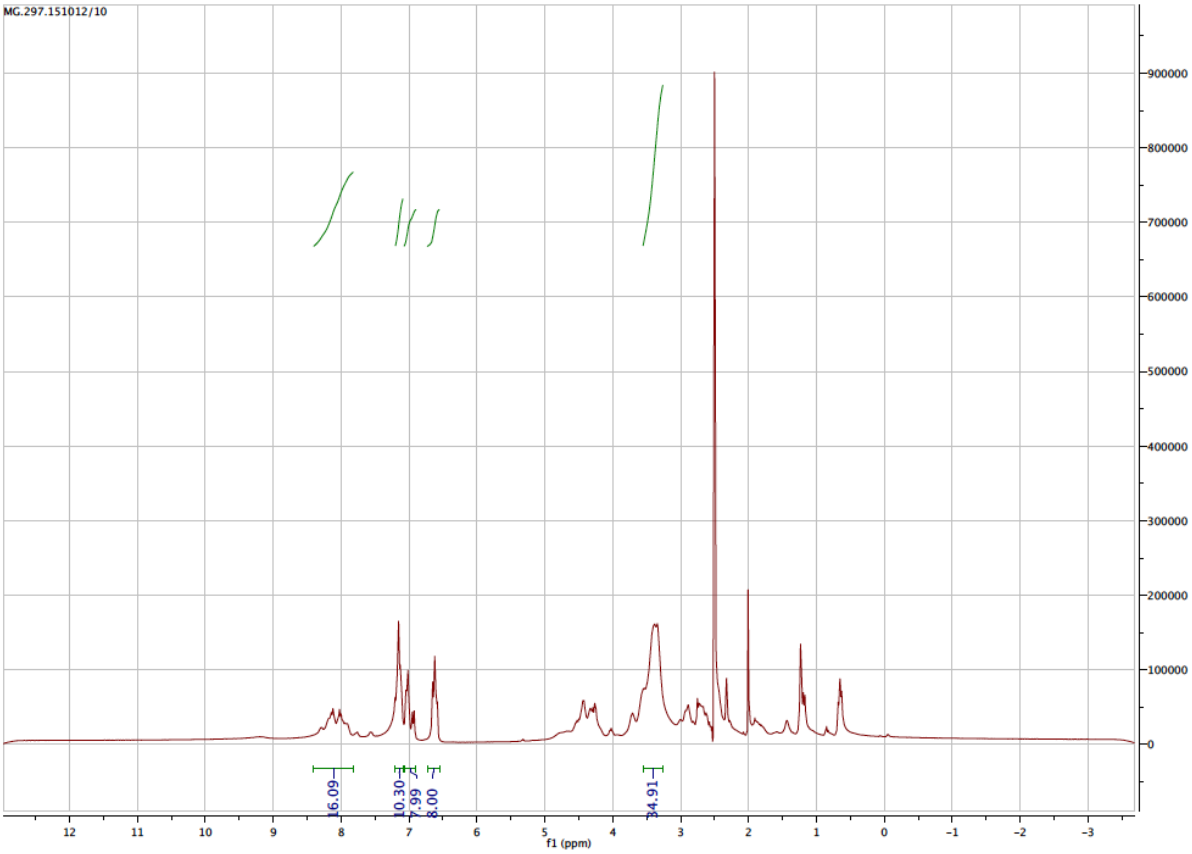

Figure 10.6. ^{1}H-NMR spectra of $PG_{340}PeB_{15}$ **6c**.

PeB^{GF}-Series

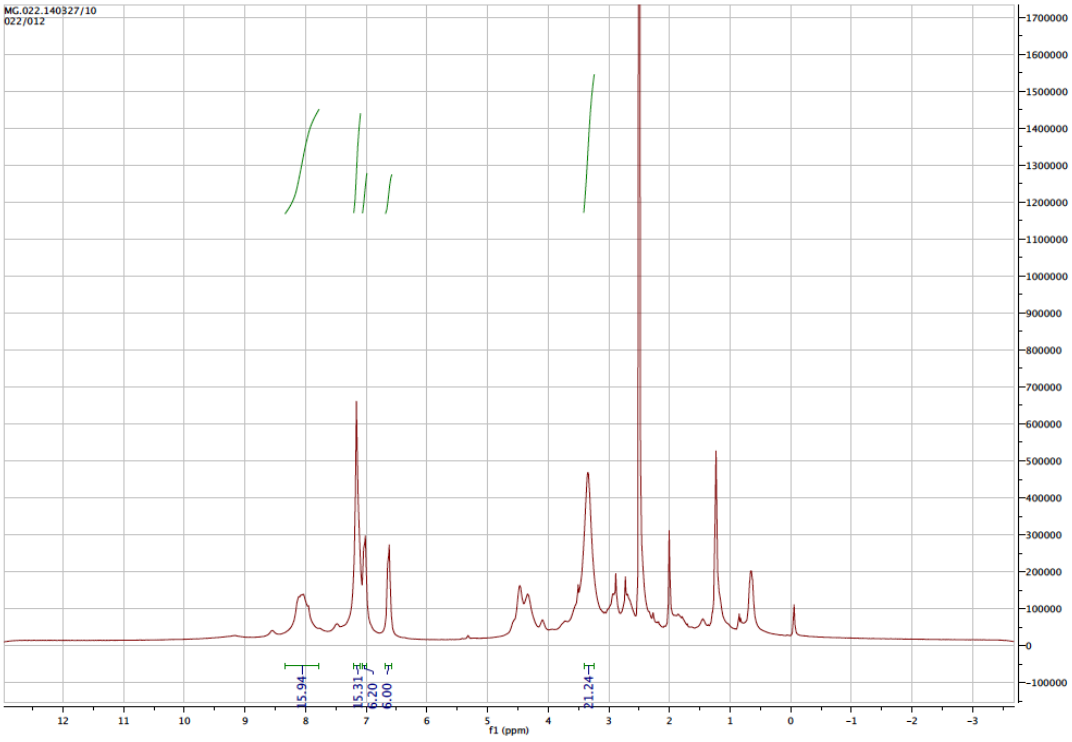

Figure 10.7. ^{1}H-NMR spectra of $PG_{14}PeB^{GF}{}_{19}$ **4c**.

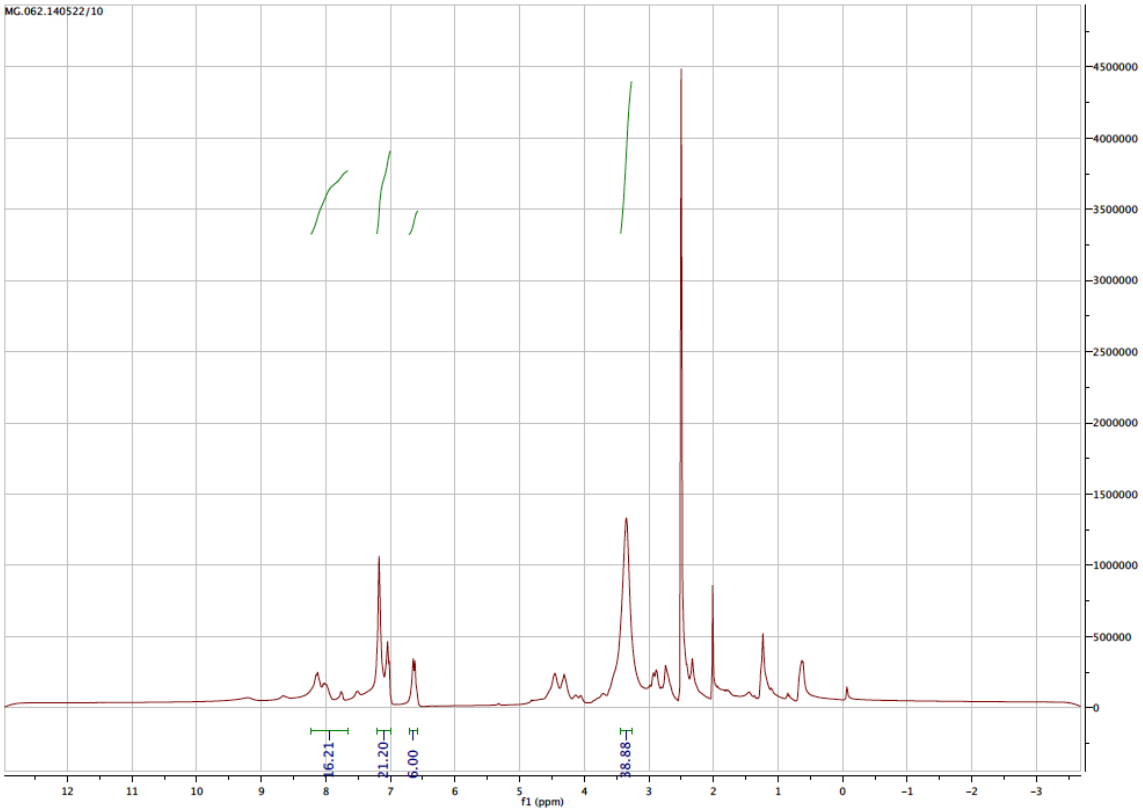

Figure 10.8. ^{1}H-NMR spectra of $PG_{100}PeB^{GF}{}_{10}$ **5d**.

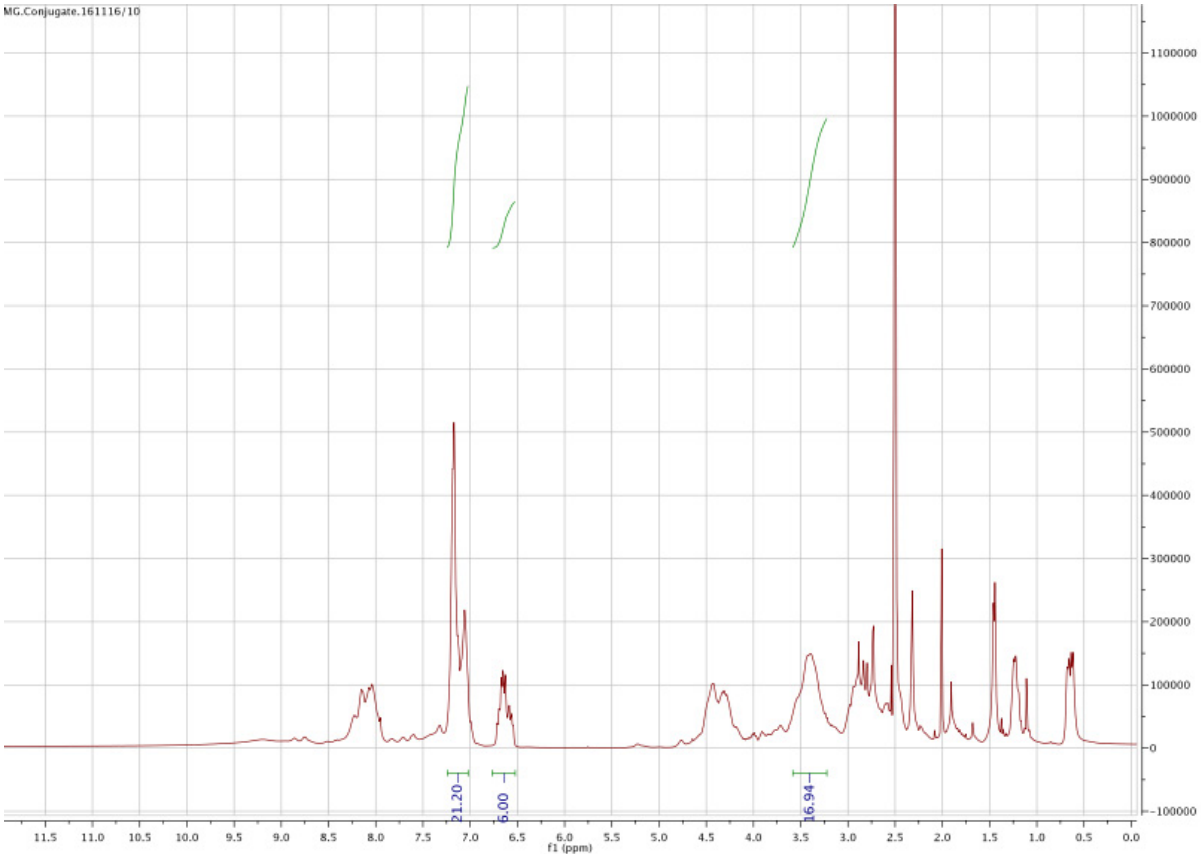

Figure 10.9. ^{1}H-NMR spectra of $PG_{100}PeB^{GF}_{29}$ **5e**.

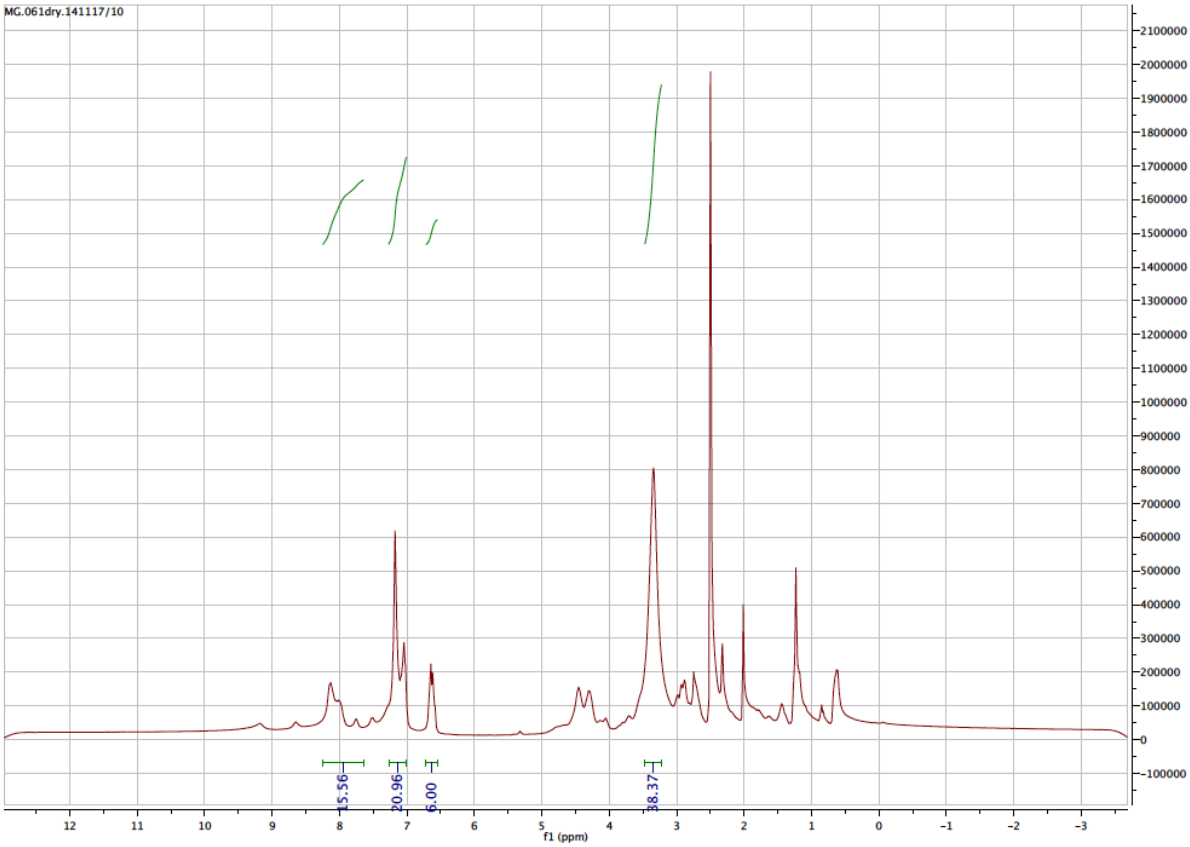

Figure 10.10. ^{1}H-NMR spectra of $PG_{340}PeB^{GF}_{10}$ **6d**.

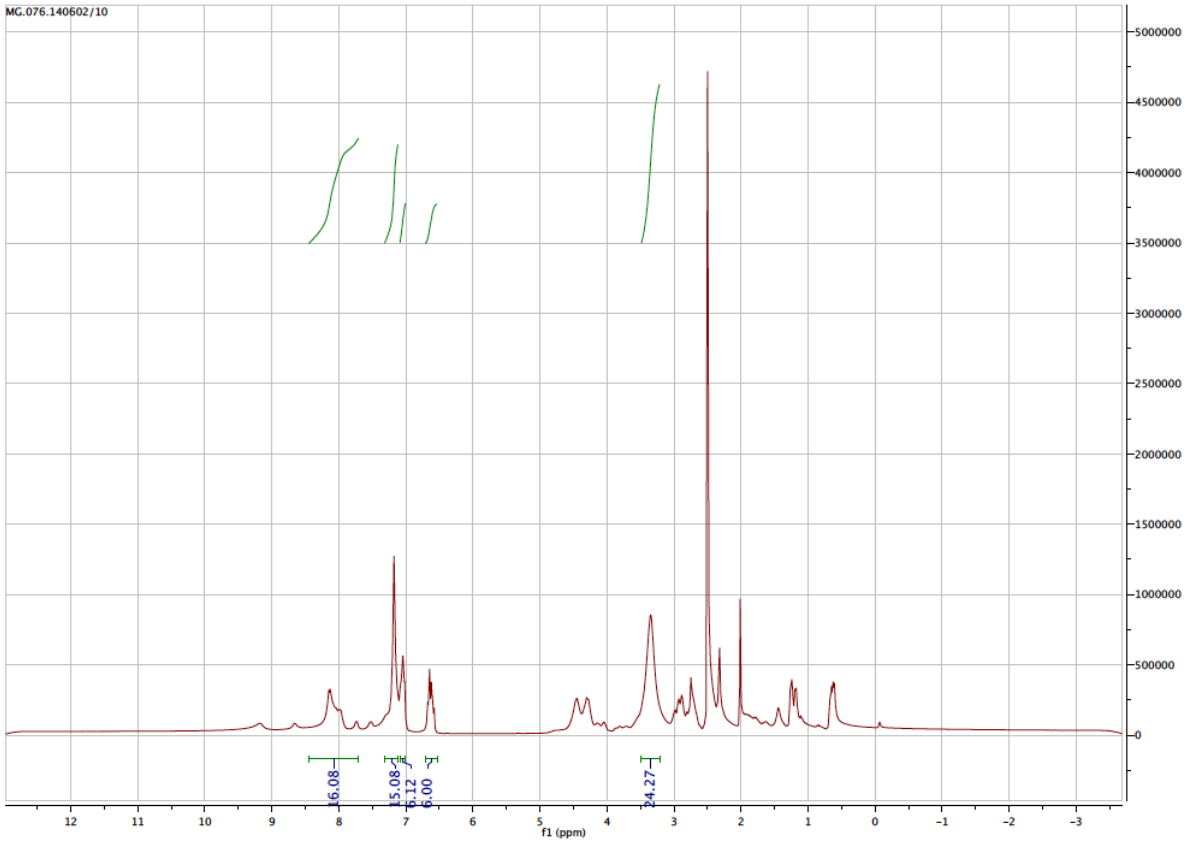

Figure 10.11. ^{1}H-NMR spectra of $PG_{340}PeB^{GF}{}_{16}$ **6e**.

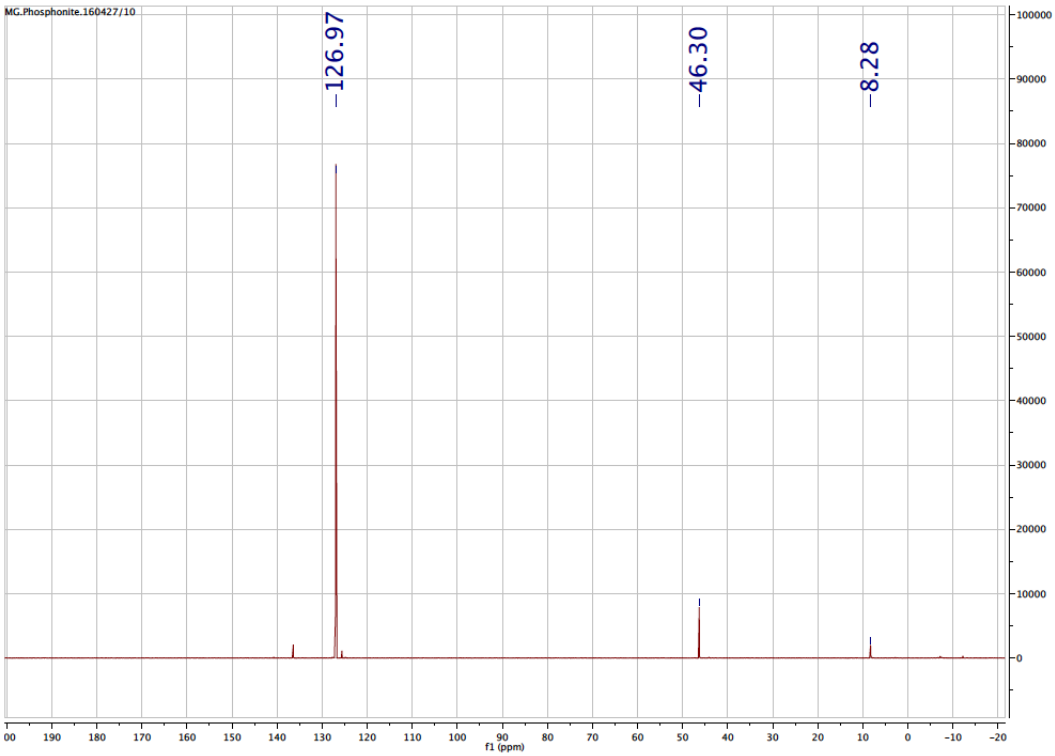

Figure 10.12: ^{31}P-NMR spectra for crude alkyne phosphonite **7.**

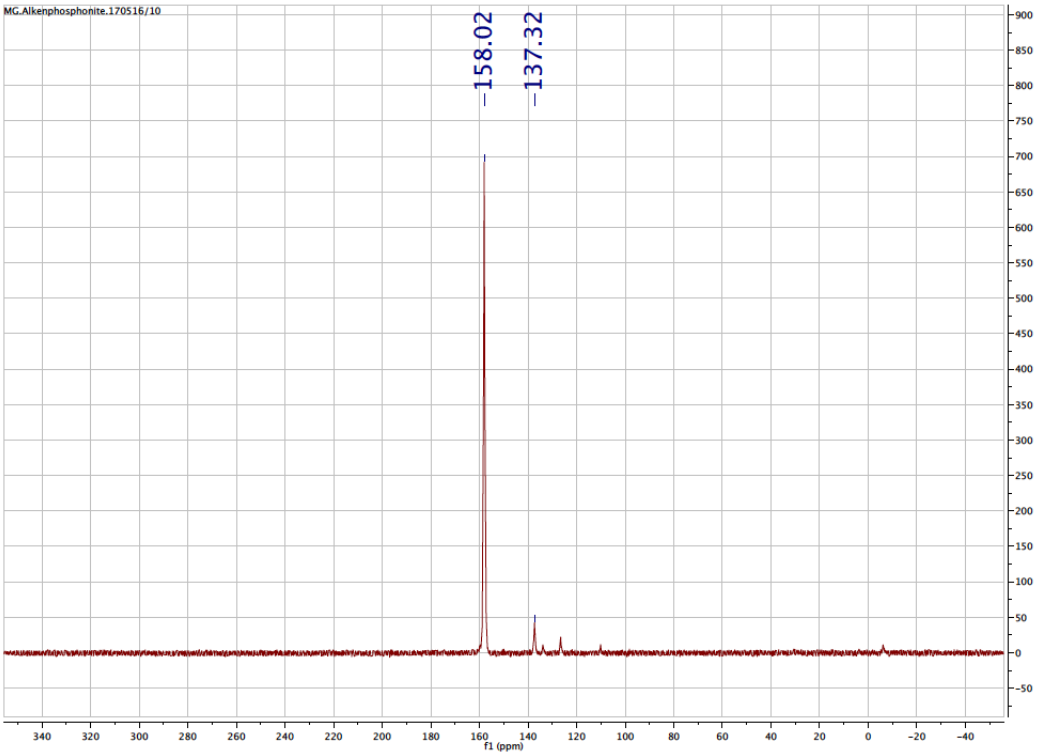

Figure 10.13: ^{31}P-NMR spectra for crude alkene phosphonite **31.**

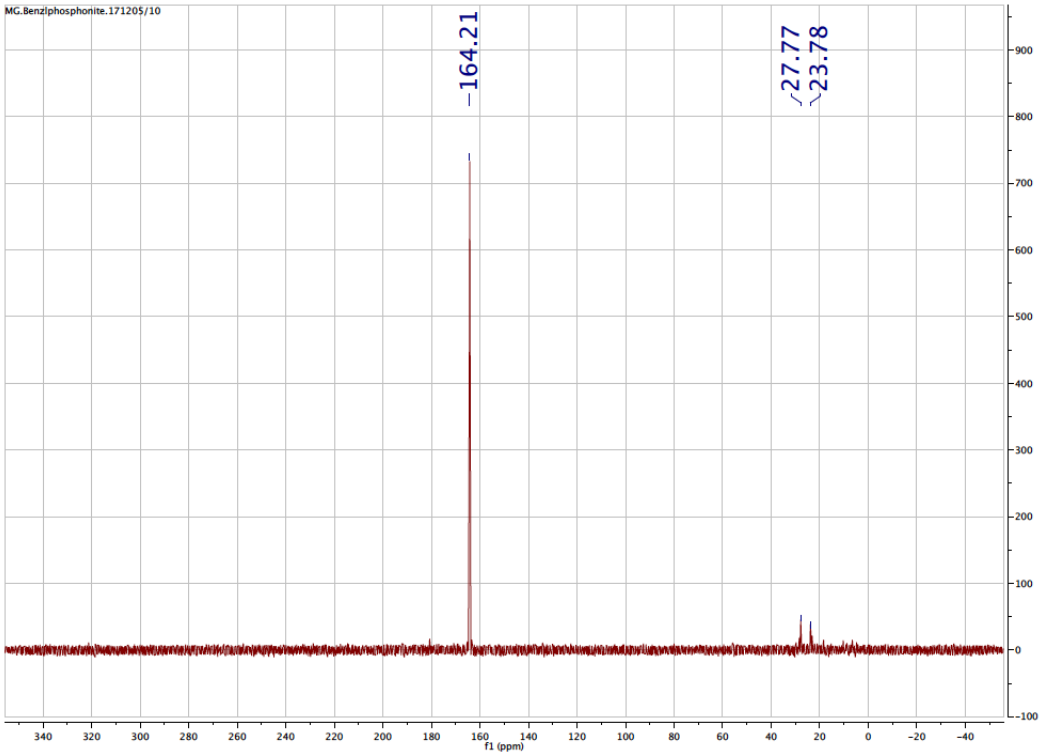

Figure 10.14: ^{31}P-NMR spectra for crude alkene phosphonite **36.**

Cyclic BCL9 peptide **32a**

Figure 10.15: HMBC correlating ^{31}P-NMR and ^{1}H-NMR for **32a.**

Cyclic R10 peptide **42**

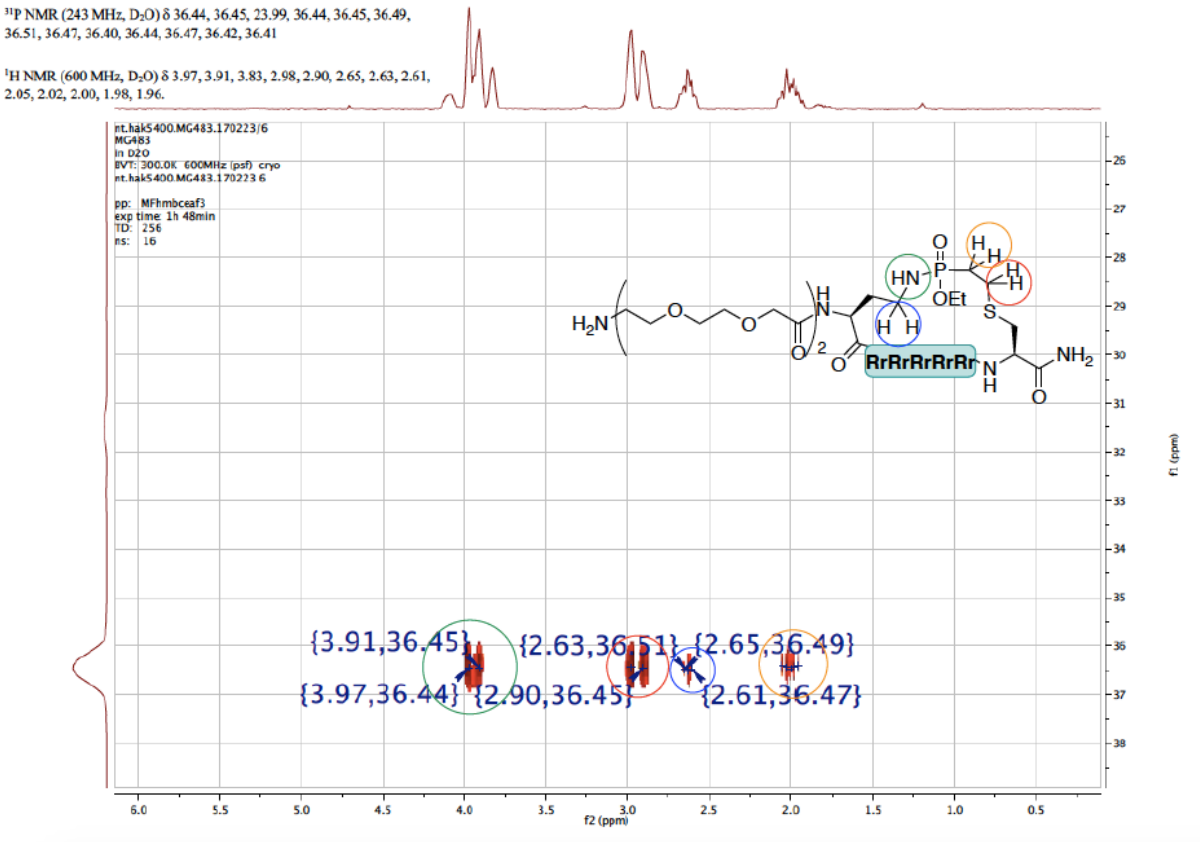

Figure 10.16: HMBC correlating ^{31}P-NMR and ^{1}H-NMR for **42.**